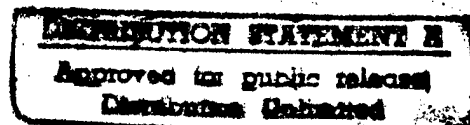# *International Workshop*
on
Ion Beam Surface Technology

May 20-22, 1996

Tomsk, Russia

Professor Gennady Remnëv
Engineering Physical Center
Nuclear Physics Institute
Tomsk Polytechnic University
Russia

Professor Anthony J. Perry
ISM Technologies Inc.
9965 Carroll Canyon Road
San Diego, CA 92131
U. S. A.

19970515 034

DTIC QUALITY INSPECTED 1

DISCLAIMER NOTICE

THIS DOCUMENT IS BEST
QUALITY AVAILABLE. THE
COPY FURNISHED TO DTIC
CONTAINED A SIGNIFICANT
NUMBER OF PAGES WHICH DO
NOT REPRODUCE LEGIBLY.

SUMMARY

The workshop was held May 20-22, 1996, in a resort called 'Blue Cliffs' overlooking the River Tom, located about 10 km from Tomsk. It was attended by about 50 people including a delegation of six from the US, and individual attendees from China, Germany and Poland. Extensive, often humorous, and lively discussions were built around 25 presentations in three major areas:

      Ion Implantation Technology

      Cathodic Arc Technology

      Intense Beam Technology,

followed by a final discussion period. Submitted manuscripts from the presentations are to be published in a special number of the refereed journal *Surface Coatings and Technology*.

The following sections are included in the present report:

- A summary of the visits made by the US delegation prior to the commencement of the workshop
- Summaries of sessions and discussions
- Business Cards of the lecturers in the order presented
- Business Cards of the U.S. delegation
- Business Cards of other Russian colleagues from the workshop and institutes visited
- The program of the workshop
- Copies of all the manuscripts which had been submitted for publication by 24 June 1996
- Technical literature gathered during the visit.

The languages of the workshop were Russian and English with many of the Russians giving their reports and carrying out discussions in fluent English. The workshop attendees were particularly fortunate in having available the services of expert interpreters who could translate very fluently and rapidly in both directions with equal facility. These were Ms. Lubomira Polkovnikova, Ms. Tatiana Litvinova, and Dr. Evgeniy Krastelev. An indication of their extraordinary ability can be gained from one occasion where Lubomira gave a running, two-way, translation of a three-way discussion between a lecturer and chairman speaking Russian on the one hand, and a series of rapid questions from an English speaking attendee on the other.

Following an informal committee meeting in a Russian 'banya', the question of a follow-up workshop in about two years was debated during the final discussion period. One of the US attendees undertook to give his paper in Russian should this re-match take place. It was generally felt that a second workshop was indicated in about two years time. Participation in such a workshop should be expanded to include experts from other countries but without increasing the total participant number. The topics should remain much the same but with coating technology as based on the cathodic arc to be included.

TRIP REPORT ON AMERICAN DELEGATION SITE VISITS
Associated with
THE INTERNATIONAL WORKSHOP ON ION BEAM SURFACE TECHNOLOGY

Dr. Paul Wilbur

Unless noted otherwise, the visits were made on May 19, 1996.

(Any information noted in parentheses denotes uncertainty on the part of the writer and editor, AJP)

Visit to Institute for High-Current Electronics

Prof. Sergei Bugaev (Corresponding Member of the Academy and Director of the Institute) gave outline of Institute. Established 1977. Presently staff of 300 with 150 scientists (15 PhDs and 2 Academicians). Areas of focus are:
Pulsed Power
Z-pinch, X-ray Generators
Gas Lasers
Electron and Ion Sources
Electrical Discharge Plasmas
Much of their work involves cooperative efforts with researchers from other countries.

In the pulsed power area equipment includes megavolt, high-current switches; megavolt fast storage; terawatt, pulsed power generation; and Marx generators (designated GAMMA). Examples of Marx generators include units with the following capabilities - 1 MW. 1.5 MA unit (SNOP-3); 1-2 MV, 2 MA, 2 MJ units (GI-4) [4 ea.]; and 1-2 MV, 6 MA, 4 MJ units (GI-8) [8 ea.]. We also saw a picture of GI-60 which is or will be made up of 60 units. Connections within these units and to the load are made using vacuum coax lines. SINUS, which is an electron accelerator used for microwave generation, was mentioned. It uses a 0.1-2 MV, 1-20 kA, 5 ns generator that operates at up to 200 pulses per sec. BLACKJACK, which is a linear transformer with many primaries and a single secondary was also mentioned as part of this effort.

In the Z-pinch, X-ray generator area pulsed inductive storage with energies to 4 GJ and magnetic fields to 10,000 Tesla (?) were mentioned. There was also mention of a wire array associated with the gas subsystem that provided stability to 70 pulses (?). Much of the work is being done in the area of high power microwaves because this is a source of money from other countries who want to buy equipment. Other applications mentioned involved, Cerenkov radiation, relativistic effects, resonant traveling wave tubes, BWO (?), and a device called an Oratron. Specific units mentioned operated at 3 GW, 3 cm wave length, 20 Hz and at 500 MW, 0.8 cm wavelength and 0.1 Hz. Work that had been done in cooperation with Marconi in England on a 1 GW, 3 cm system to be used for cruise missiles designed to fly at ~100 m altitude was also mentioned.

In the gas laser area a Xe-Cl laser that operated at 10 kW.cm^{-2} in the 126-350 nm wave length regime was mentioned.

In the area of basic research on electrical discharges, topics mentioned included:

Vacuum discharges
High pressure discharges for laser applications
Low pressure discharges from which ions and electrons can be extracted
Electron sources for lasers (electrons flow radially inward through film windows from a 2.5 kV, ~100 A discharge)

The use of Tesla transformers was mentioned for some electron-source applications as were hollow cathode designs for electron beam systems. It appeared that all electron and ion beams being studied were pulsed.

During a general discussion of laboratory operations it was pointed out that:
In the past (i.e. pre Soviet Union breakup)
60% of budget came from state
40% from contracts (industrial & external military grants)
Now
20% from state
50% from foreign customers
30% from ministries of foreign countries.

Twenty five people have gone from this institute compared to as much as 50% of staff in other institutes. For example, in the Atmospheric Optics Institute there were 1000 development and scientific people while there are now only 500. Institute of Strength Physics and Materials Science has grown from 400 to 500. Institute of Oil Chemistry now has 250 compared to 300 before. Most people have gone into businesses, some have gone abroad. The structure of the academic township was mentioned. Novosibirsk is the capital of the Siberian division (55 institutes). Other divisions include the Ural and Far Eastern divisions.

Visited Prof. Dmitry Proskurovsky's laboratory and saw apparatus for electron beam heating. A pulsed electron beam of uniform current density is sought. One systems uses dense electron jets from many metal pins arranged in regular pattern in a ceramic plate. This was described as a plasma-field diode system that has a rarified downstream plasma and a non-propagating double layer at the plate/pins electrode. Operation involves a voltage pulse that first goes positive for a rather short time (to generate plasma) and then negative for a considerably longer time and a greater voltage magnitude (to accelerate electrons through the plasma). Applied voltage magnitudes are of order 10 kV. The e-beam is used to polish (smooth and clean) surfaces. A titanium compressor blade was shown as an example of what can be done and it looked good to me. A new development is

an indium-gallium liquid metal cathode. It appeared to me that one would be used to replace each metal pin and an operating one was shown to us. It runs on 500 kHz pulsed power and can operate at 70 kV although operation at lower voltage is easier. Cathode life is of order one billion pulses.

Visited some of the Marx generator systems (designated GAMMA?) used to supply pulsed power. They are very large. Saw pulsed ion sources suitable for operation on either metal or gas. They operated at ~ 80 keV, delivered 10^{17} ions.cm^{-2} over a 20 cm diameter. in ~30 min. Cathode life is about 40 hr. Metal vapor is derived from an arc discharge and it was suggested that it could operate on most metals (chromium was mentioned specifically). I believe the system includes a 5 ns switch developed with French and Sandia personnel.

Visited low energy electron source that was, as I recall, being sold to China (designated SINUS). It was a 25 kW system that used a trigatron and 50% efficiency was claimed. It deposited 50 J.cm^{-2} operating at 60 A.cm^{-2}. Operating pressure was 0.001 Torr and 10% of the electrons produced were lost. A 3 cm beam diameter was produced and self field induced some compression in this diameter.

Saw a plasma deposition system that used hot cathodes in sources (3 or 4 of them) at a discharge voltage of 20 to 60 V and a discharge current of 10 to 100 A. The system is used for cleaning and activation and it can be operated on reactive gases. Films having good adhesion are applied with the system. Plasma density is 10^{10}.cm^{-3} and electrons consist of two groups, a Maxwellian one with a temperature near 5 eV and a nearly mono-energetic one with an energy in the range 20-30 eV. The system utilizes a magnetic field that serves to filter the output of at least one of the sources.

Saw an IBAD system that used a magnetron and ion implanter combination. It sounded like the two components were operated sequentially to apply metallic coatings that adhere well to ceramic surfaces. Films are applied using lithographic techniques and mention was made metallized regions applied to ceramics so metal elements could be soldered to them.

Visited a facility designated as a technology system. Among other applications, it is used to apply titanium metal coatings to decorative glass plates. The glass was cleaned only with water before it was placed in the system for plasma cleaning. The sources use hollow cathodes in some cases and hot filaments in others. Metal is accelerated through ~60 V sheath onto the surface. The processing rate is about 6-10 sq m.hr^{-1} and coating on a batch basis costs about $40 m^{-2}. Post heat treatment is used to create alternative patterns.

Visit to Institute of Strength Physics and Materials Science

Met initially with Academician Victor Panin. He indicated that the work of the institute is focused on:

Mechanics of Deformable Solids
Materials Science
Strength and Plasticity

He pointed out that TEM has been used to study the motion of dislocations is what is termed the micro-mechanical level (regime). Researchers have worked for decades to relate these findings to mechanical failure characteristics of materials that are observed on the macro-mechanical level (regime). They have been unable to establish significant relationships between measurements made in these two levels. In Tomsk, they have now defined a new level (the meso-mechanical or meso-level) in a solid under load. Their objective is to connect the mechanics of a continuous medium (macro-level) with plasticity physics (micro-level) using this meso-level. They want self-consistent descriptions of motion on the three levels. Ion implantation has a dominant influence on the micro-level where its influence on the behavior of dislocations and slip is well known. On the meso-level, vortical motion of dislocations leading to meso bands is observed. It was argued that fatigue is primarily a meso-scale phenomenon. On the meso-level it is observed that cells separated by bands develop and a few of these cells are involved in plastic deformation, but many are not. Cell rotation is observed on the meso-level. They have reported revealing work on high-nitrogen steel which is unstable to shear loading (see paper given as an attachment to this report). Meso-scale deformation along bands is a precursor to fragmentation. Bands are aligned with directions of maximum shear and its conjugate direction. Understanding meso-level phenomena is important in welding and in the area of wear phenomena. A photograph suggesting a 100 Å meso-band scale was shown. It was indicated that meso-scale sizes are related more to part size that to grain size. Panin has edited a book entitled "Physical Mesomechanics of Heterogeneous Media and Computer-Aided Design of Materials" published by Cambridge Univ. Press (ISBN 1 898326 19 3) that describes these theories in more detail.

We visited a laboratory in which samples could be loaded under a microscope (TEM I believe). Data were shown for a silicon steel sample which had been nitrided to produce a 25 µm thick layer and yielded a 0.5 mm mesoscale dimension. It was pointed out that thicker layers yield a smaller meso-scale dimension and that one usually would want a gradual change in properties at a boundary between a layer and a substrate. If moduli of elasticity are different as they usually are between a layer and a substrate, then oscillating stresses develop along the boundary (this was called an unstable interface). This may determine the meso-scale dimension. We also saw some data on an alumina-aluminum-alumina sandwich sample and a copper sample implanted with Zr (40 nm thick layer).

Next we went with Yurii Sharkeev to see examples of commercial processing being done in a local enterprise that is involved with the institute. We saw blades used to cut synthetic fibers that had been nitrided and circular saw blades that had been hard-faced using an arc discharge process. This visit was cut short to keep on schedule. I believe the

processing had been done at Republican Engineering Center (an enterprise) and we visited there on May 21, 1996 with Sharkeev, Dr. Vladimir Yanovskii and others. That evening we first visited what I believe was Sharkeev's laboratory (the Russian Materials Science Center). It included a TEM, a SIMS system and equipment for applying thin films to metals and ceramics. The laboratory contained three implanters, one that operated on gases, one for metals and one that could implant metals and gases together. The metal implanter used a pulsed metal vacuum arc and operated at voltages ranging to 80 keV and currents ranging to 0.5 A. The laboratory has a charge to investigate the structure of materials. We again saw a circular saw blade that had been electric-spark strengthened (3x to 4x lifetime increase) and knives for slitting and chopping that had been treated. A handout advertising the work is included in the technical literature attachment to this report. Across the street we visited Republican Engineering Center. They claimed the capabilities of treating larger surfaces, applying polymer coatings and coatings for various other purposes. They treat cutting tools and machine parts. It appeared that most of the work involves the application of TiN, TiC and TiO_2 coatings applied at temperatures ranging from ~20 to 50 °C.

Visit to the Nuclear Physics Institute of Tomsk Polytechnic University

Prof. Yuri Usov met with us and mentioned that it was the 100th anniversary of the university and that the institute was established in 1958. He pointed out that the high energy physics equipment all of which is operational includes:

> Electron synchrotron
> Various ion and electron sources driven by pulsed power systems
> Thermal neutron source (10^{14} $cm^{-2}.sec^{-1}$) with a 1 m^3 active volume
> Cyclotron now converted to isotope production uses
> Nuclear reactors (located a short distance out of Tomsk) - now used mostly to transmute Si into P impurities of electronic applications
> High energy ion and electron accelerators

The equipment is used for student training in addition to research. Now there is a problem of survival for the lab which Usov does not attribute to governmental difficulties alone. He felt the most difficult time is over. He finds it more interesting to work with industry. He finds there is more freedom and opportunity to discuss problems openly. The institute did employ 1000 scientists (including students, I believe) but now there are only 350. Previously there were 5000 people employed in total.

Prof. Alexander Ryabchikov showed us his Raduga (Russian for 'rainbow') systems. Most are plasma immersion type systems that employ vacuum arc metal ion sources but some appeared to produce metal ion beams. Cathodes are made of conducting materials and the first four systems are similar but have different cathode and trigger configurations. The cathode(s) are arranged around the centerline and the conical anode expands outward downstream of the cathode(s) and has its axis on the centerline. Rainbow 3 has four

cathodes and their emission spots are controlled using triggers that are positioned between them and that discharge over the surfaces of insulators to the cathodes. Rainbow 4 has two cathodes. These configurations enable multi-element implantation. One can also use cathodes made from compounds. Because these are plasma immersion systems, ion current is not well known but they estimate 10% ion current, 90% electron. At high doses, surface sputtering yields a loss of efficiency and if sample is too close, vapor deposition can cause coating. There is balance situation where coating just balances sputtering and it was suggested this is a good place to operate. They have looked an electron suppression grid around a target to prevent secondary electron currents. Macroparticles continue to represent a problem. Early MEVVA was called Bulat. It sounded like they need to operate for ~1 min to condition the cathodes and get to a stable operating point. They do not see much different in performance as voltage is changed over a significant range, but they generally run at 50 kV. A 10^6 pulse lifetime, which is typical, is limited by coating of the insulator surfaces between the cathodes and triggers. Rainbow 5 uses a MEVVA evaporator and can be operated in steady state usually at a 3 A beam current. This eliminates trigger lifetime problems but macroparticle production is still a problem. This system is very flexible and can be operated in a number of different ways that give it capability to do processing ranging from atomic coating to beam implantation. There are no grids, but a cross magnetic field is applied to impede electron flow while allowing ions to be accelerated. Relative biases between target, chamber and MEVVA source are used to accomplish this. These bias voltages can be pulsed at up to 150 Hz and pulse durations can range to 400 ms. This bias-voltage pulsing enables control of relative vapor deposition and sputtering effects as well as an IBAD operating mode. One has the additional flexibility of adding a background gas flow into the system. Some losses associated with currents going to chamber surfaces were mentioned.

We visited a cyclotron purchased from St. Petersburg in 1972 that is now a workhorse in the lab. It operates at 10 to 30 MeV and 20 microamps and is used to accelerate alpha particles, hydrogen and helium 3. Elastic recoil work is done using it. The location of a nuclear membrane used in some of the work was pointed out.

We saw a synchrotron made in the lab in 1965 to accelerate electrons. It is a 1.3 GeV machine that holds 10^{12} electrons and is fed by a 70 A, 10 keV microtron (?) injector. Concern was expressed about energy usage by the machine.

A membrane treating unit that produces beams of Ar or N ions was shown to us. It is used to produce microchannels in polymers. Near it was a neutron treatment facility used to bombard cancerous tumors in medical patients with 5 to 6 MeV neutrons. It used a Be source that was coupled in with the cyclotron. It this same area was a 20 stage, 1.5 MeV Marx generator made in 1972. It is used with a ring electron gun for microwave generation. This system stores 30 kJ and they are working to concentrate the power and achieve $TW.cm^{-2}$ power densities. There is also another Marx generator system rates at 500 kJ that is used to study plasma switches. Finally, in this part of the lab we saw a Van de Graaff generator system used to generate high energy particles for surface analysis.

Additional information on ion beam capabilities offered by the institute are given in the attached sheet pertaining to the "Charged Particles Analytical Lab."

Dr. Gennady Remnëv next took the group to several "enterprise" facilities where commercial processing is being done. Temp 1 is a pulsed, high-current system that is powered by an oil-filled Marx generator. Each discharge is effected using two voltage pulses with different characteristics; the first yields an "explosive" plasma and the second accelerates the ions from it. The source consisted of a perforated metallic plate separated and isolated from a second graphite electrode. They were contoured on their mating surfaces so the ions would be focused properly on the target surface. Operating conditions were 300 kV, 50 to 200 $A.cm^{-2}$, 50 ns pulse duration and repetition rate of 1 to 0.25 Hz. The Linetron Company is doing processing of cutting tools for railway wheels. The processing involves rapid melt-heating and quenching and it yields a smaller grain size on the surface of the tools which, in turn, yields ~3x increase in lifetime. The fixturing we saw was loaded with 36 cutting tools being processed, but as I recall, the unit could hold 96 tools and they claimed 100,000 tools could be processed each year with 3 hr work days. Other work includes other tools and dies, with WC and ceramic cutting tools being mentioned specifically. Similar processing was suggested to improve bonding of diamond to copper in wheels used for the cutting of glass.

Another enterprise facility involved a system similar to the one in the above paragraph in which metal ions were implanted into semiconductors. The source was made up of an inner cylindrical metal cathode with holes in it and a concentric anode of greater radius. I believe the unit was operated with the same dual-pulse concept in which metal vaporized from the first pulse was ionized and then accelerated through the holes in the cathode to a target surface within the cathode during the second pulse. The objective was to anneal and implant the target surface simultaneously.

The Temp 2 enterprise facility was used to apply thin films to surfaces as large as 10 cm x 20 cm. The films were generated by sputtering a target surface (~4 cm x 0.5 cm) using a high intensity pulsed ion beam. The system was set up so the source could be rotated to achieve complete coverage.

The last facility was one that was used for research but appeared to be planned for eventual commercialization. An ion beam extracted through an annular passage was the end result. It involved injection of a gas pulse into the region upstream of the passage. A high voltage pulse was then applied across an antenna in this region and this induced breakdown of the gas and plasma generation. A high axial electric field and a radial magnetic field of the proper magnitude were applied in the annular passage so an ion beam that was annular in cross section would be extracted but axial electron motion in the annulus would be constrained.

SUMMARY OF SESSION: <u>CATHODIC ARC TECHNOLOGY</u>

Dr. Jesse Matossian

In this session, a total of eight papers were presented. Following the presentation of the papers, a round table discussion was held to identify key points raised during the paper-presentation session.

Three different topics were covered in the presentation section:
- cathodic arc technology for ion implantation and deposition of coatings
- plasma-source ion implantation for novel nitriding of materials
- high-power pulsed ion beams for surface modification of materials.

In this section, we summarize the salient issues presented for each of these topics.

Cathodic-Arc Technology

Dr. Perry presented the first paper on the use of cathodic arc technology with major emphasis on cost, reliability, maintenance, and system efficiency. Conventional MEVVA technology was addressed followed by a new system, referred to as AVIS (Advanced Vacuum-Arc Ion Source) which was designed for large-scale, high-throughput industrial applications. The AVIS system allows for the use of four distinct ion sources with versatile control, long operation without significant maintenance, a larger treatment area than with conventional MEVVA technology.

Dr. Ryabchikov presented a description of the RADUGA system. In this system, the plasma production and ion extraction processes are independently controlled to allow for novel surface treatment capability. The technique allows for reducing self-sputtering of the implanted/deposited ions and improves the retained dose achieved.

Dr. Karpov presented a detailed review of 25 years of the development history of cathodic arc sources. The review included techniques for filtering of macroparticles using plasma optical techniques, as well as magnetic filtering approaches.

No paper was presented by Dr. Sirmnov.

Dr. Guoqing presented a paper describing a an new process called MIBED (metal ion beam enhanced Deposition) which combines the use of a metal ion source and a low-energy ion beam-sputter source to deposit hard coatings on materials. The MIBED process has been used to deposit MoS_2 coatings. A particular strength is that it allows for enhanced adhesion of coatings via interfacial mixing using; Corrosion resistant films of (Ti,Mo)N were prepared using a N-Mo ion beam process.

Dr. Sergeyev presented results on the use of the Diana pulsed ion source for implantation of metallic as well as non-metallic ions for improving the wear resistance of cutting tools.

Plasma-Source Ion Implantation

Dr. Reinhard Günzel presented a paper on the use of plasma-source ion implantation (PSII) for novel nitriding of various steel materials. The sheath dynamics in the PSII process were modeled and used to provide understanding of the PSII process during treatment of materials. A study was conducted of various types of plasma sources (ECR, RF, DC, etc.) to motivate the choice of ECR sources in PSII as providing the best compromise of high plasma density and low gas pressure.

High Power Pulsed Ion Beams

Dr. Shulov presented the use of high-power pulsed ion beams (HPPIB) for improving the surface wear properties of compressor blades. Very deep treated layer depths (200 micron or more) can be achieved using the technology. HPPIB as a treatment technology produces the best combination of improved fatigue life, corrosion resistance, and sand abrasion resistance compared to hard coatings.

Dr. Lopatin presented the use of pulsed ion beams for modifying the properties of dielectric materials. The use of light and heavy ions was demonstrated to achieve changes in the conductivity of materials used in resistors and electric heaters.

Round Table Discussion

Several topics were covered in the discussion session following the presentation of papers. A major concern that was addressed involved a request for more careful documentation of the treatment parameters used by researchers during a treatment of a materiel; the implantation voltage, current density, pulse duration, and treatment temperatures are critical parameters that affect the success of the desired surface treatment.

A critical issue discussed in this regard is what is the dependence of ion energy and current density on the properties of the treated layer for cathodic arc work. One hand, it was regarded that high energy and low energy ion implantation studied should be conducted to identify the advantages and disadvantages. On the other hand, it was also indicated that for industrial applications and simplicity of hardware as well as for safety, implantation at voltage levels of 100 kV are not needed for achieving tribological improvements of materials. Industrial use of ion implantation typically dictates the use of the simplest and most reliable equipment which every researcher should strive to adhere to. A voltage range of 40-70 kV is sufficient for most applications identified using cathodic-arc implantation technology.

SUMMARY OF SESSION: ION IMPLANTATION TECHNOLOGY

Dr. Donald J. Rej

The second day session of the Workshop consisted of eleven talks (7 by Russians, 4 by Americans), and it was chaired by Nikolai V. Pleshivtsev of the Kurchatov Institute Troitsk Laboratory, and Donald J. Rej of Los Alamos National Laboratory. The presentations could be divided into the following five topical areas:

- Beamline Implantation and IBAD Expts   3 papers
- Plasma Immersion Ion Implantation   3 papers
- Low Voltage, High j, Elevated T Implants   2 papers
- Ion Sources   2 papers
- Neutron Capture Induced Implantation   1 paper

The most comprehensive set of results were given by Dr. V. V. Brukhov from the Tomsk Polytechnic University. For more than 20 years, his group performed ion implantation of coupons and manufacturing components. Hardening of cutting tools has been a primary focus. A beamline implanter with Penning ion source was used. Improvements in wear and corrosion lifetimes were observed for an extensive variety of materials and applications. The plasma immersion groups at LANL and Hughes showed similar improvements in materials ranging from tungsten-carbide, high-speed steels, to hard chromium coatings and polymers.

Dr. A. Korotaev and Dr. P. Shanin of the Siberian Physical and Technical Institute in Tomsk gave an extended talk on ion implantation and ion beam assisted deposition research. Both gas and metal (arc) sources were used and a 0.3 - 0.5 A beam was extracted at 80 keV. Deposition was achieved with a 10-100 A, 20-40 V arc source. TiN was deposited onto metallic substrates such as stainless steel. When combined with ion implantation, substantial mixing into the substrate is observed, leading to a functionally graded interface with reduced internal stresses. TiN deposition along with sub-eV ion bombardment also led to reduced imperfections and internal stress.

Dr. Yuri Sharkeev of the Institute of Strength Physics and Materials Science, Tomsk, reported on his understanding of the effect of ion implantation in metals. In particular he systematically examined the defect structures formed in the near surface of several metals (including Fe, Cu, Ni) after ion implantation, microwaves, and plasma bombardment. The defect structure and thickness of the modified layer depend on the treatment process. With ion implantation, the defect structure is observed to be deeper than 10 μm, 100x beyond the range of the implanted ions. With intense ion beams, it extended up to 150 μm.

Results from, to our knowledge, the first immersion ion implantation program in Russia were presented by Piotr Tsygankov from the Bauman State University in Moscow. The work represents Tsygankov's Doctor of Science Thesis research which was performed under the supervision of Professor Vladimir Khvesyuk. They call their process 3D Ion

Implantation or (3DII) and claim the following distinctions from conventional plasma immersion (or plasma source) ion implantation:

- Stationary sheaths (primarily because of relatively long pulses of 300 μs)
- Small sheaths (1 cm or less) with high ion current density
- High efficiency (up to ion/total current ratios of up to 70%)
- No need for magnets or external plasma ion sources

All of these claims can be challenged. In particular, stationary sheaths are often observed (e.g., reported by the ANSTO Group in Australia) for non-supersonic sheaths when the Bohm condition can satisfy ion current continuity. The reported sheath dimension and ion current densities were inconsistent with the Child-Langmuir space-charge limited flow which would predict ion current densities of more than an order of magnitude greater than that reported. The high efficiency seems to imply exceeding low secondary electron emission coefficients. Details of the work by Tsygankov have been relayed to Dr. M. Shamim who works in Professor John Conrad's Group at the U. Wisconsin. Shamim has made comprehensive measurements of secondary emission and should compare results with Tsygankov. The fourth claim is just wrong.

In the second immersion talk, Dr. Jesse Matossian (Hughes) presented some interesting work on positive polarity immersion processing where intense electron bombardment from the plasma heat treats the workpiece surface. In the third talk, Dr. Don Rej of Los Alamos discussed three important issues that should be addressed before wide-scale commercialization of PSII: (1) implant conformality; (2) ion sources; and (3) secondary electron emission.

High current density ion implantation of B into Fe was reported by Dr. Paul Wilbur (Colorado State). The ion current density and workpiece temperature appear to be a more important processing parameter than the ion energy, which can be as low 5 keV. The work at first appears as an extension of thermochemical treatments such as plasma boriding, though substantially different microstructure (e.g., amorphization) may be obtained. Low Energy implantation was also reported by Dr. Igor Churkin from the Nuclear Physics (Budker) Inst., Novosibirsk. At these energies, charge exchange in the ion source and extractor can be high. Consequently, a large fraction of the beam is in the form of energetic neutral atoms which increases flux, efficiency, thereby reducing process time. Carbon was implanted into niobium and titanium at ion current densities of 20 mA.cm^{-2}.

Dr. Nikolai Gavrilov from the Inst. of Electrophysics, Ekaterinburg reported on a simple, robust, high-density plasma source based on the hollow cathode discharge, coupled with a weak magnetic field to enhance confinement of electrons and maximize the number of ionizing collisions. The source has been given the name "reverse magnetron." It consists of a coaxial anode cantilevered from one end and an axial magnetic field. Ions are accelerated by grids and extracted from the ion source. To date, sources of up to 100 cm^2 area have been deployed with pulsed current densities up to 30 mA.cm^{-2} extracted over 1 ms wide pulse lengths and at repetition rates of 3 to 50 Hz. Future work is to include the

development of 1000 cm^2 source. Past ion implantation R&D work focused on C. N. and O implantation into stainless steel, carbon fiber, tungsten carbide, and polymers.

Dr. Nikolai Pleshivtsev of the Kurchatov Institute Troitsk Laboratory reported on another type of broad beam gas ion source developed for neutral beam injection in Tokamak fusion plasmas. The source is capable of supplying 60 A (optimum ion current density of 600 mA.cm^{-2} for H) of H, He, N, Ar or other gases or mixtures at 10-60 keV over pulse widths between 1 μs and 1 sec. The beam cross section varies from 105 cm^2 to 420 cm^2 with a uniformity to within 5% at a distance 1 m from the source. Applications explored to date including hardening and lifetime increases of cutting plates, rolls, woodworking knives, and plow blades.

Finally, Dr. D. Rej of Los Alamos gave a second talk proposing a method for the bulk treatment of polymeric materials. Energetic ions created after capture of a neutron beam by constituent atoms located within the polymer can be used to cause radiation-induced modifications such as cross-linking in the polymer. In contrast to traditional ion implantation, the proposed method enables bulk treatment because of the relatively deep penetration of neutrons. Analytical were given for the 10B(n,α)7Li reaction for the cross-linking and hydrogen depletion of boron-doped polystyrene. Requirements for the polymer composition and microstructure, as well as potential synthesis methods were also discussed.

SUMMARY OF SESSION: <u>INTENSE BEAM TECHNOLOGY</u>

Dr. Michael O. Thompson

The third session of the Ion Beam Surface Technology Workshop focused on the application and generation of intense beams with sufficient energy densities to modify surface properties by the thermal process itself, independent of the actual beam used. The fundamental interactions include rapid melt and solidification, leading to metastable phases and grain structure modification, and shock hardening, which can produce effects well beyond the direct modified range.

The session was opened by Dr. M. Thompson discussing work done in collaboration with the Sandia National Labs group on intense ion beam modification of surface, with a particularly emphasis on enhancing the corrosion resistance of Al and Ti alloys. Using an intense beam of mixed protons and carbon from a flashover diode source, various alloy surfaces showed hardening (slip bands introduced by shock hardening in 304 stainless steel), polishing (by liquid phase transport on Al), enhanced wear resistance (440 stainless steel), and enhanced corrosion resistance (Ti by grain refinement).

The majority of the work involved treatment of thin surface coatings using the ion beam to melt, mix by liquid phase and convection, and solidify into both metastable alloys and complex microstructures. A wide range of transition metal coatings on Al were studied. Mixing was observed in most systems to depths of approximately 5 μm before surface damage became dominant. Si coatings on Al enhanced surface hardness by a factor of 2 with Cr layers similarly enhancing the corrosion resistance. For aluminum alloys, the dominant problems were microcraters left after processing (corrosion sites) and the excessive overheating of Al liquid required prior to melt of the high temperature surface coatings. On Fe substrates, Cr was much more effective and could be mixed to produce surfaces with a corrosion resistance equivalent to stainless steels. In the Ti system, Pt layers were mixed to produce solid solutions of Ti:Pt to concentrations of 8 at.%. The best corrosion resistances were obtained at intermediate Pt thickness where precipitation of second phase intermetallics did not occur.

The second talk, by Dr. G. Remnev, addressed a specific ion treatment system being presently used to routinely treat industrial tools for wear reduction. The accelerators, MAC and TEMP, use a double pulse operation with an initial voltage applied to create a plasma followed by the main extraction pulse to create the energetic ion beam. The MAC accelerator with an Al anode produced a mixed beam with various Al charge states and substantial Cu, C and H components. The TEMP accelerator, using a graphite anode, generated primarily a C and H beam.

Unlike the research beams discussed otherwise, the TEMP accelerator has a considerable history of usage in industrial surface treatment with statistics of benefits. Wear improvements of 2-3 times are observed for various tools such as swirls or fine drills. The

treatment chamber currently hold 96 tools with a total treatment time of approximately 1 hour. Operating lifetime of the accelerator has been 10^6 pulses with weak-link components being the connectors, Marx generator, and the pulse capacitors (through water/oil contamination). The vacuum insulators and the double pulse-forming line, initially expected to be problematic, proved to be reliable. In 4 years of operation, no major repairs except for replacement of the items noted above. On a commercial scale, these results suggest that the technology is sufficiently well developed to be viable.

Currently, Dr. Remnev is designing a larger accelerator, TEMP-4, to increase the throughput of the system. Like TEMP-1, it will be a 300 keV at 50-200 A.cm^{-2} system. Major changes will be an increase in the rep-rate to 1 Hz (from 0.25 Hz) and nearly an order of magnitude increase in the tool holding capacity (to 800 tools). His predictions are that this will reduce the cost of treatment to the $2 per square meter.

Prof. B.A. Kalin, from Moscow State Engineering Physics Institute, in the third talk discussed some of the microstructural origins of the observed material modifications. The incident energy source for his work was the HTTPF accelerator which provided beams of H, D, He, N or Ar at energies of 10-25 keV with fluences of 10-100 J.cm^{-2} in relatively long pulses of 10-50 μs. Up to 100 pulses were used to treat materials. At fluences below 10^6 W.cm^{-2}, only surface heating occurs; from 10^6 to 5 x 10^6, surface melting occurs without damage while above 5 x 10^6 W.cm^{-2}, melt and subsequent boiling of the surface occurs.

Treatment of Ni/Cr alloys yielded cellular microstructures with carbides and nitrides at grain boundaries, and possibly He bubbles, at low energy densities corresponding to recyrstallization. At higher energy densities, dislocations were observed to depths of 50-100 μm, at least an order of magnitude beyond the primary melt zone, forming from either thermal stresses or shock waves following treatment. An interesting experiment with one edge of the sample held pinned during treatment suggests that thermal stresses may be responsible for a substantial part of the hardness improvements. Treatment at higher energy densities in the melt regime also exhibited reduced grain sizes with increasing power density; this is surprising since increased melt dwells should slow solidification and enhance grain growth. However, the longer melt dwells also improve homogeneity leading to kinetically suppressed solidification from dissolved impurities.

Hardness improvements were observed across all steel materials with enhancements of 40-200%. In the thermal only treatment, the maximum hardness improvements were observed below the surface. In the melt regime, the maximum occurred at the surface, though a subsidiary maximum was also observed buried substantially in depth (50-100 μm). The smallest hardness improvements were observed at the highest energy densities in the boiling regime. Commensurate with the hardness improvements was also an increase in the ultimate tensile strength without an increase in the Young's modulus (plasticity). This is potentially very useful for engineering applications.

In addition to increasing hardness, Dr. Kalin's results also showed reduced coefficients of friction to depths well beyond the primary treatment depth. Structural modifications resulting from the thermal shock wave, or thermal expansion mismatch, are likely responsible for these changes as well.

Besides pulsed ion beams, it is possible to effect similar microstructural and materials changes using relatively low energy electron beams. In the fourth talk by Prof. D. Proskurovsky of Tomsk, the development and behavior an intense electron beam was discussed. To limit the energy deposition to the near surface, electron beams must be in the 10-40 keV range, pulse widths between 10^{-7} and 10^{-6} seconds to avoid substrate heating, and total fluences in the 10-40 J.cm^{-2} range. One major advantages of an electron source is that is radiation safe if the energy is kept this low.

The first part of his talk discussed the development of the electron diode. A positive pre-pulse is used to pull electrons from an external plasma into the acceleration chamber and bombard the cathode. Explosive electron emission from the cathode (and/or prepulse) provides the 10^{14} - 10^{15} cm^{-3} plasma density required for the primary beam. The pre-pulse was found necessary only below 25 keV while at higher voltages explosive electron emission was sufficient itself. Once the high density plasma was generated, the double layer propagated at 2 cm.μs^{-1} until shorting out the anode/cathode gap in about 3 μs. The beam fluence as a function of the sample position downstream initially increased (too close and the sample influenced the beam dynamics) before decreasing from beam divergence. At low fluences, it was possible to get excellent uniformity from the beam over distances of 6 cm -- although at higher powers the fluence on axis was substantially higher than outer radii. The design of the anode and gap appear to make this system very competitive with ion beam systems for scale up to manufacturing levels.

Treatment of Fe with the electron beam exhibited similar characteristics to ion beam irradiated Fe. Microstructures were modified both over a 15 micron primary heat affected zone, and over a 300 μm stress wave zone. In contrast to Dr. Kalin minor secondary peak in hardness, Dr. Proskurovsky observed extremely large secondary hardness peaks in depth, nearly as large as observed in the primary heated zone. Total hardened layers in some cases exceeded 300 μm, with 2-3 times improvements in lifetime. Dr. Proskurovsky supports the model that hardening occurs by a stress wave which is amplified as a standing wave upon reflection from the front and back surfaces. Modeling of the heat transport and shock wave generation appear to support, at least qualitatively, this model. (Note: The origin of this deep hardening is one of the major outstanding problems that need to be resolved.)

Other treatments undertaken with this pulsed electron beam include surface cleaning and smoothing of Ti surface layers, increased vacuum breakdown potential on surface (resulting from such smoothing), reduction of polymer wear on Ti (again likely resulting from smoothing), surface alloying of elements in Fe and Ti, and treatment of turbine blades (both polishing and removal of old coatings).

In the afternoon, Dr. Sinebrykhov discussed another application of intense ion beams in the deposition of material by pulsed ablation, similar to pulsed laser ablation but at significantly higher deposition rates. A focused ion beam (cylindrical focusing to focal plane) irradiated a 5 cm radius graphite or tungsten(?) target set at the focal plane. The ablation plume then deposited material onto a Si substrate at a rate of approximately 0.2 µm per pulse. Although the coatings were relatively pure graphite, adhesion was poor and no mechanical properties were measured. The authors indicated that diffraction measurements showed two cubic phases of graphite with lattice constants of 0.428 and 0.369 nm, but this is extremely unlikely since there are no cubic graphite.

The second afternoon talk by Dr. S.P. Bugaev also addressed a novel deposition technique utilizing plasmas, though not pulsed energetic beams as the previous speakers. The basic idea of their system was to use a pulsed high voltage plasma discharge to deposit diamond-like coatings (DLC) from organic precursors in a confined geometry. The plasma characteristics were 15-17 kV source with a 100-200 usec duration repetitively pulsed at about 1 kHz. The estimated energy density during the plasma was 0.01 $J.cm^{-3}$. Various gases were used including methane, ethane and acetylene, all in an hydrogen excess (95%) at flow rates of 3-4 $l.hr^{-1}$.

The growth rate from this pulsed plasma was low for methane (1-2 $µm.hr^{-1}$), increasing substantially for ethane to 60-100 $µm.hr^{-1}$, but dropping again for acetylene. Deposited films were nominally amorphous by TEM and FTIR was used to characterize the sp^2 versus sp^3 bonding fractions. In even the best cases, the $sp^3 : sp^2$ ratio was only 68 : 32 indicating some diamond like bonding but a substantial remnant graphitic bonding. Mechanical properties likewise showed enhancements, but not at the level of DLC deposited by other techniques. Further work is needed before the potential of this deposition technique can be evaluated.

Prof. Langner then presented a paper on a very different technology for creating pulsed ion beams, coupled with a new simultaneous material deposition and annealing technology. In the *Ionotron*, ions are produced by a low pressure, high current electric discharge followed by a delayed high voltage pulse. This unit has two modes of operation: the first, pulse implantation deposition (PID), creates a 1 microsecond pulse of the working gas. The second, DPE, occurs for short delays of the HV and leads to arc erosion of the cylinder giving metal ions. Both modes can be used for surface melting and mixing.

In the current configuration, Prof. Langner added a pulsed metal source coupled with the *Ionotron* operating in PID mode with nitrogen gas. A pulsed Ti source deposits a thin metal layer on the target while the nitrogen from the pulsed ion beam can be set to arrive either before, during, or after the Ti atoms. If the Ti arrives before the nitrogen, no surface melt occurs since the surface is shielded by the Ti plasma. However, with proper delay, the Ti can be designed to reach a target shortly after the nitrogen pulse allowing the Ti to react with a molten surface.

Results were presented for a nitrogen beam at 3.5 - 5 J.cm^{-2} with a 100 μs pulse of Ti, Co or W beam at 120 kA arc current; for mixing, the delay between beams was 75 μs. Films were deposited on 321 stainless steel in either direct mixing mode (5 simultaneous pulses) or deposition mode (5 deposition pulses, 10 separate mixing pulses). Following treatment, surface exhibited 5-10 μm granular morphology with roughness remaining roughly constant at 0.2 μm Ra but increasing with increasing energy density. Although hard to explain, the Ti appeared to penetrate 6 μm while Cr and W reacted to depths of 0.6 and 0.35 μm respectively. In the deposition only mode, it appeared nitrogen was extracted from the bulk into the surface layers.

Finally, the last paper by Dr. Y.D. Korolev discussed theoretical issues involving the extraction of beams from liquid metal sources. Unfortunately, the present reviewer was unable to understand the subtleties of the mathematical models and cannot comment further.

Over the course of the day, several issues recurred in the treatment of materials. One was the problem of microcratering which appears in both ion and electron beam treatments of metal surfaces. Although there was considerable discussion about this problem, it is clear there is no real understanding of the origin. Multiple pulse irradiation, a general direction of all the treatments, appears to reduce this problem but not eliminate it. The relative importance various with substrates being most problematic with low melting alloys like aluminum.

A second issue that arose several times was the specific mechanism responsible for the hardening in depth in beam-treated materials. Both the shock wave proposed by Proskurovsky and the simple thermal stress from expansion mismatch suggested by Dr. Kalin have support in the data.

Throughout the talks there were also some common successes. Beam induced mixing of surface deposited layers is successful on Fe and Ti substrates though more difficult on Al substrates. Corrosion is limited by the microcratering problem, but general mechanical properties such as hardness, wear resistance, and friction can be enhanced considerably by treatment.

The choice of the treatment source is clearly an open target. Although ion beams have been the dominant technology, the high fluence new electron beams appear to hold some advantages if the size can be scaled up without loss of uniformity. Given the present application of treatments in enhancing the wear resistance of industrial tools (Dr. Remnev), it is also now clear that this technology will have some role to play in future industrial processes.

SUMMARY OF GENERAL DISCUSSION

Dr. Anthony J. Perry

The final discussion took place after the last Session on the Wednesday. It focused on the intense beam technologies and was very lively, and remarkably frank and open. There were many interjections during the sometimes lengthy commentaries. The following summarizes the main aspects.

The discussion was opened by Dr. Matossian with the comment that while the applications of many of the technologies are clear, citing the use of intense ion beams (IIB) on turbine blades (which have advantages over hard coatings) and potential use of intense electron beams(IEB), there is overlap with, e.g., the potential use of metal ion implantation. Hence the question to be answered is where does each fit in.

Dr. Shulov commented on the need for an integrated approach because different processes produce different properties, hence the required properties define the process. The benefits of each process need to be known through expertise in a specific field and a good overview. As an example he cited compressor blades where irradiation improves fatigue resistance, with IIB offering the best solution but the IEB will probably prove to be as good. At the present time in Russia, the need is for maximum benefit with minimum development; it is difficult to introduce new technology, and impossible to introduce new equipment -- a situation which he paralleled with France.

Dr. Proskurovsky commented on the competition from the IEB which, in terms of development, is about 5 years behind IIBs. He suggested that it will be the next generation of technologists who will evaluate them, not new technologies but new people who will understand their different strengths! He remarked on the different temperature profiles (see the attached figure) which he believes are sufficiently similar for heating purposes.

Dr. Rej remarked on a significant difference in that IEBs operate with lower voltages so that x-ray generation is less significant, but IIBs can treat greater areas per pulse. He cited the $1000cm^2$ per pulse of the 'Temp' system (of Remnev), contrasting ease of operation with area and treatment economics.

Dr. Thompson brought the discussion back to the question of application, the material to be treated by the beam. He believes that whereas the electron beam has a unique profile at a given energy, an ion beam offers greater flexibility in terms of a choice of the ion used. Better process control is offered as a specific profile can be defined, giving uniformity and reproducibility. He held the opinion that the low cost applications had received too much attention, and, further, that new applications should be sought where there is currently no technology in place rather than continue trying to compete with an existing solution. The drive has to come from applications, the research (the fun part) can follow.

Dr. Kalin broadened the discussion to include his own technology which provides uniformity, eliminates micro-arcs, and offers a wide energy content of the beam. The technique offers, specifically, a good corrosion resistant treatment by putting down a coating then mixing it in via a liquid phase.

Dr. Langner reminded us that in both cases, IIB and IEB, the ion dose is too low to modify the material other than through the thermal treatment. He agreed with the need for both: the thermal effect (melting) and alloying of some 15% down to a depth of over 3" but this is currently without commercial application.

Dr. Kozlov contested the subsidiary nature of research in this field. Regardless of the material properties and the economics, the science behind the different technologies and their effects on materials needs to be understood, or else the real properties cannot be guaranteed. These processes are very science intense because the material being treated are inherently very complex and the energies released are very high. He believes in the usefulness of computer modeling coupled with basic research to define technique and application and resolve the cry of "our technology is best".

Dr. Sharkeev also supported the need for materials research. He pointed out that over the past few years about 80% of papers published have dealt with new sources, and only about 20% with their effect on structural materials being treated. It is the material studies which should define the required technology.

Dr. Karotaev supported the need for materials studies. He pointed out that high power beam techniques, pulsed power in general, cause cratering on the surface of the materials treated. This is not true of plasma treatment methods. He saw the real need for (minimal) collaborative studies on specific materials, their properties and phase states, to compare the respective features.

Dr. Li remarked that there is much technology in China which should be included in such a study to mutual benefit. He also saw the need for computer simulation.

Dr. Brukhov agreed with the need for comparative studies, and added that both high and low energy beams should be studied on real materials.

Dr. Rej effectively summarized the discussion by remarking that we had discussed good science, and good applications as a result of the unique properties generated. The need for collaborative, application oriented comparative studies is clear.

Institute of High Current Electronics
Siberian Division of the Russian Academy of Sciences
4 Akademichesky Ave., 634055 Tomsk, Russia
Phone: (3822)258544 Fax: (3822)259410 E-mail: root@hcei.tomsk.su

Dear Prof. A. J. Perry,

Thank you very much for your e-mail letter where you give a high appreciation of the work of my laboratory and give hope of our possible collaboration with US facility. We would be happy if with your assistance it would be possible to set up such joint project.

As for figure indicating the temperature profiles its history is as following. Temperature profiles of laser and power ion beam we took from article of Dr. Stinnett et al. "Ion Beam Surface Treatment: A New Technique for Thermally Modifying Surfaces Using Intense, Pulsed Ion Beams" published as Stinnett said in Proc. of 10th Pulsed Power Conference, July 10-13, 1995 Albuquerque, NM USA. On my request A. Markov, a scientific worker of my laboratory, who deals with modelling of temperature and stress fields have calculated temperature profile which according to the typical parameters of our beam. It appeared that in comparison with an ion beam we have the same specific energy expenditure, but temperature gradients inside of material are lower and temperature profile is more gently sloping. The last may be attractive for some technologies. I send you this picture. As for our calculation of temperature fields, they have been published, for example, in the following article:

Yu. F. Ivanov, V. I. Itin, S. V. Lykov, et al. "Phase and Structural Changes in Steel 45 under the Action of a Low-Energy High-Current Electron Beam"— Izvestiya Akademii Nauk SSSR, Seriya Metally (IANSM), 1993, No. 3, pp. 130-140.

Besides you likely can read our Reports on Contract AM-2868 implemented for SNL.
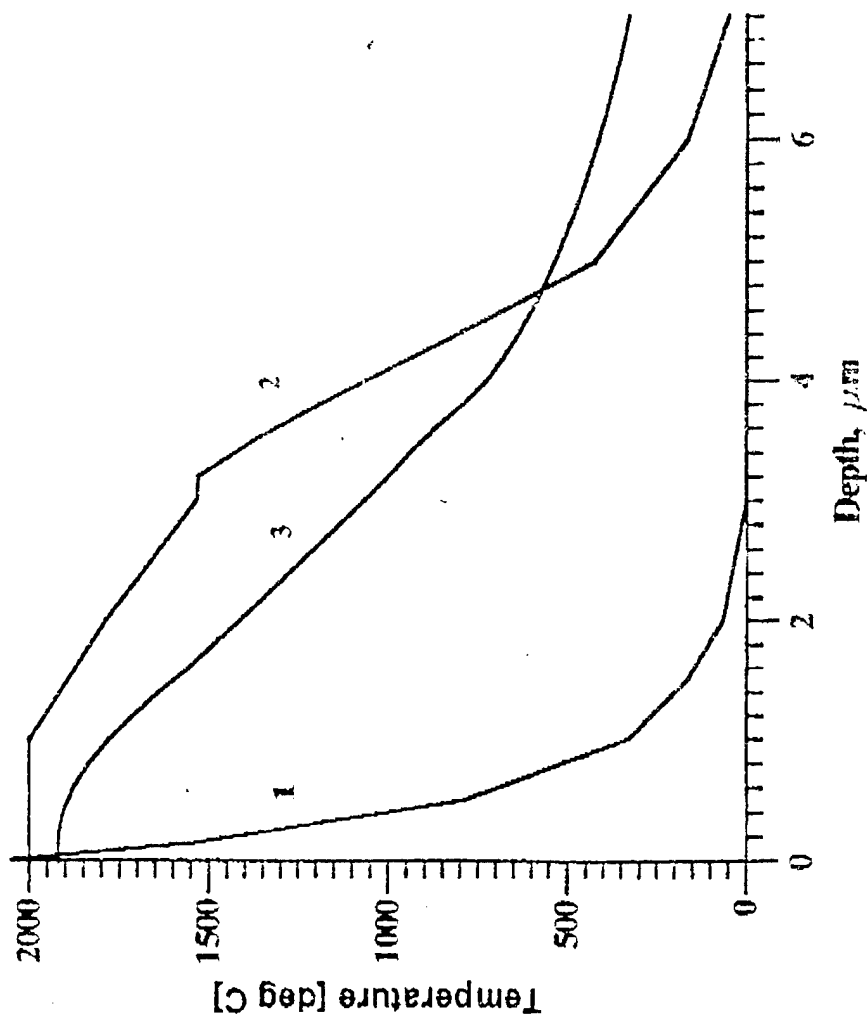
Thank you very much for your credit to me as a scientist and a specialist. If you will be in Prague we can meet there. Besides I would like to came to USA (Berkeley) to take part in ISDEIV.

Hope for future meetings and collaboration.

Yours Sincerely, Dmitry

Prof. D. I. Proskurovsky, D. Sc.

Temperature Profiles in Steel Due to Laser,
Proton Beam , and Electron Beam Heating

1 - Laser Beam, 308 nm,   80 ns, 1.25 J/cm2 [R.V.Stinnett et al.]
2 - Proton Beam, 500 keV, 100 ns, 4.0 J/cm2 [R.V.Stinnett et al.]
3 - Electron Beam, 25 keV, 2000 ns, 4.5 J/cm2   [Our results]

Business Cards of the Presenting Authors
(where available, and in the order of the papers presented)

ISM

ANTHONY J. PERRY, D.Sc., Ph.D.
DIRECTOR, RESEARCH & TECHNOLOGY

ISM Technologies, Inc.

9965 CARROLL CANYON RD.   TEL (619) 530-2332
SAN DIEGO, CA. 92131   FAX (619) 530-2048

NUCLEAR PHYSICS INSTITUTE
TOMSK POLYTECHNIC UNIVERSITY

Alexander I. RYABCHIKOV

Prof., Deputy director in Science,
Head of Physics and Technique of
Ion Beam and Ion Plasma Material
Treatment laboratory

Lenin Str., 2a,   Tel: 3822-440-639, 3822-257-173
Tomsk, 634050,   Fax: 3822-440-100
Russia   E-mail: alex@tsinph.tomsk.su

Research Center Rossendorf Inc.

Dr. Reinhard Günzel

Institute for Ionbeam Physics and
Material Research
                                    260 2762
PF 510119   ☎ 351/5913273
D-01314 Dresden   Fax: 351/5913285
Germany

e-mail: guenzel@fz-rossendorf.de

D.V. Efremov Scientific Research Institute of Electrophysical Apparatus
SCIENCE TECHNICAL CENTRE
"SINTEZ"

DIMITRI A. KARPOV

Doctor Science (Tech.)
Chief of Laboratory

NIIEFA   Ph.: (812) 265-58-22 762-78-22
St. Petersburg, Metallostroy   FAX: (812) 314-33-60 764-76-2
189631, Russia   E-mail: filatov@synthesis1.spb.su
                        karpov@cs.niefa.spb.su

Dalian University of Technology
Dev National Lab. of Materials Modification by
Three Beams

Dr. Li Guo Qing

Professor

City Dalian Province Liao Ning China   Postcode: 116023
Tel: 86–411–4671961   Fax: 86–411–4671009
     86–411–4708384   Telex: 86231 DUT DN
     86–411–470912(H)   Cable: 7108 Dalian

Moscow Aviation Institute
Research laboratory
"Surface layer and service properties
of machine parts" "

professor
Vjacheslav A. Shulov

Russia, 125871,Moscow,Volokolamskoe sh.,4
Tel:(095)-158-44-24 Fax:(095)-158-29-77
E:mail: surface @ k208. mainet. msk. su

Dr. VICTOR SERGEEV

republican   scientific
engineering   director
centre

8/2, Akademicheskii Pr,
Tomsk, 634055, USSR
Phone: 25 84 81, 25 85 91
Telex: 133179 RITC SU
Fax: (382.2) 258863
25.80.32

Los Alamos
NATIONAL LABORATORY
Physics Division Office

Mail Stop D434
Los Alamos, NM 87545

TEL: 505/665-1883
FAX: 505/665-8520
EMAIL: drej@lanl.gov

Dr. Donald J. Rej
Program
Coordinator

Paul J. Wilbur
Professor

Colorado State
University

Department of Mechanical Engineering
Fort Collins, Colorado 80523
(303) 491-8564
FAX: (303) 491-8671
910

HUGHES

DR. JESSE N. MATOSSIAN
Senior Member of the Technical Staff
Plasma Physics Laboratory

Research Laboratories
Loc. MA, Bldg. 250, MS RL57
3011 Malibu Canyon Road
Malibu, CA 90265-4799

(310) 317-5121
FAX: (310) 317-5483
e-mail: jmatossian@msmail4.hac.com

Bauman State Technical University
Power Engineering Institute

Piotr A. TSYGANKOV
senior scientist

ADD.:MSTU, P.O.Box 38, Moscow 107005, Russia
PHONE: 7-(095)-263-6085
E-mail: piotr@khvesyuk.msk.ru

Russian Academy of Sciences
Ural Division
Institute of Electrophysics

Dr. Nikolaj V. GAVRILOV
Head of Particle Beam Laboratory

34, Komsomolskaya,   *phone (3432) 499-185*
GSP-387, 620219,
Ekaterinburg, Russia

Russian Research Centre
Kurchatov Institute

Nikolai V. Pleshivtsev
Senior Research, Doctor of science

Kurchatov sq.1
Moscow 123182
RUSSIA

☎ +7-095-196 9574
☎ +7-095-940 6612 (private)
Fax: +7-095-943 0073
E-mail: nfi@wowa.net.kiae.su

Institute of Strength Physics and Materials Science of RAS

Yurii P. SHARKEEV
Head of Laboratory
"PHYSICS AND TECHNOLOGY OF ION IMPLANTATION"

Russia, 634021,   Phone: (3822) 25 82 45. 90 68 68
Tomsk,   Fax: (3822) 25 95 76
2/1, pr. Akademicheskii Telex: 612854 ROSMC SU
E-mail 1: X.400 (C:USSR. A:SOVMAIL. O:CUSTOMERS. UN:ROSMC)
·E-mail 2: ispms@ispms.tomsk.su

CORNELL
U N I V E R S I T Y

MICHAEL O. THOMPSON
Associate Professor

Dept. of Materials Science &
Engineering
Bard Hall
Ithaca, New York 14853-1501

Telephone: 607 255-4714
Fax: 607 255-2365
E-Mail:mot1@cornell.edu

MOSCOW STATE
ENGINEERING-PHYSICS INSTITUTE
(TECHNICAL UNIVERSITY)

Kashirskoe sh., 31, Moscow, 115409, Russia

Professor
Boris Alexandrovich
K A L I N

Head of the Department of
Physical Problems of Materials Sciences

Tel.:   (7 095) 323-90-43,   (7 095) 324-31-65
Fax: (7 095) 324-21-11,   (7 095) 324-31-65
E-mail: kalin @ phm. mepi. msk. su
              kalin @ ameto. mephi. ru

Andrei A.Sinebryukhov
Head of Laboratory
Institute of Electrophysics
4 Academy ave., 634055
Tomsk, RUSSIA
Phone/Fax +73822 259040/259410
E-mail: aasin@ief.tomsk.su

SOLTAN INSTITUTE FOR NUCLEAR STUDIES
05-400 Świerk n. Warsaw, Poland

JERZY LANGNER, Ph.D.
Deputy Head, Dept. of Thermonuclear Research

Office:
Tel.: /0 48/ 2-779 86 13
Tlx: 813244 IBJS PL
Fax: /0 48/ 2-779 34 81

Private:
Ul. Traktorzystki 11
01-114 Warsaw
Tel.: 36 14 44

Engineering Physical Centre
Nuclear Physics Institute of Tomsk
Polytechnical University

Dr.   GENNADII E. REMNEV
Director

Lenin str., 2a.
634050 Tomsk,
Russia

Tal.: (3822) - 440097
Fax (3822) - 440812
E-mail: REMNEV @ tspu. tomsk SU

Prof. DMITRY I. PROSKUROVSKY

Head of Laboratory
Laboratory of Vacuum Electronics,
Institute of High-Current Electronics,
Russian Academy of Sciences, Siberian Division

4, Akademichesky Av., Tomsk, 634055, Russia
Phone: (3822) 25-97-09, Fax: (3822) 25-94-10
Telex: 128112 PTB SU, E-mail: PDI @ lve.hcei.tomsk.su

Business Cards of the U.S. delegation

JOYCE L. ILLINGER, PhD
CHIEF, MATERIALS SCIENCE BRANCH
EUROPEAN RESEARCH OFFICE

U.S. Army Research, Development and Standardization Group (UK)

USARDSG-UK
PSC 802, BOX 15
FPO AE 09499-1500
DSN: 235-4930
COML: 44-171-514-4930

223 Old Marylebone Road
London NW1 5TH UK
Tel. 0171-514-4930
FAX 0171-724-1433

EMAIL: jillinger@army.ehis.navy.mil

DR. JESSE N. MATOSSIAN
Senior Member of the Technical Staff
Plasma Physics Laboratory

Research Laboratories
Loc. MA, Bldg. 250, MS RL57
3011 Malibu Canyon Road
Malibu, CA 90265-4799

(310) 317-5121
FAX: (310) 317-5483
e-mail: jmatossian@msmail4.hac.com

HUGHES

ISM

ANTHONY J. PERRY, D.Sc., Ph.D.
DIRECTOR, RESEARCH & TECHNOLOGY

ISM Technologies, Inc.

9965 CARROLL CANYON RD.
SAN DIEGO, CA. 92131

TEL (619) 530-2332
FAX (619) 530-2048

Los Alamos
NATIONAL LABORATORY

Physics Division Office

Mail Stop D434
Los Alamos, NM 87545

TEL: 505/665-1883
FAX: 505/665-8520
EMAIL: drej@lanl.gov

Dr. Donald J. Rej
Program
Coordinator

CORNELL
UNIVERSITY

MICHAEL O. THOMPSON
Associate Professor

Dept. of Materials Science &
  Engineering
Bard Hall
Ithaca, New York 14853-1501

Telephone: 607 255-4714
Fax: 607 255-2365
E-Mail:mot1@cornell.edu

Paul J. Wilbur
Professor

Colorado State University

Department of Mechanical Engineering
Fort Collins, Colorado 80523
(303) 491-8564
FAX: (303) 491-8671
910

Business Cards of other Russian colleagues

Russian Materials Science Centre
Institute of Strength Physics and Materials Science
Russian Academy of Science

Jurii R. KOLOBOV

*Prof., Dr Phis. and Math. Science, Head of Department
of Phisics and Technological Problems of Solids Surface*

2/1, pr. Academicheskii,
Tomsk, Russia, 634021

Phone /382-2/ 25-82-45
Fax /382-2/ 25-95-76
E-mail ispms @ ispms. tomsk. su

High Current Electronics Institute
Russian Academy of Sciences

prof.

Yuri D. Korolev

4, Akademichesky ave.
634055 Tomsk
Russia

*head of
Low Temperature
Plasma
laboratory*

Phone: (3822) 254-971
Fax: (3822) 259-410
E-mail: korolev@lnp.hcei.tomsk.su

ФИАН

P. N. Lebedev Physics Institute
Academy of Sciences of Russia

Evgeniy G. KRASTELEV Dr. Sci.

Senior Reseacher

Adress: Leninsky prosp., 53
117924 Moscow, GSP-1
Russia
Telex: 411479 NEOD SU

Tel.: (095) 132 65 35 (office)
(095) 452 47 42 (home)
E-mail: krastele@lpnu.fian.msk.su
Fax: (095) 135 78 80

**High Current Electronics
Institute USSR**

Dr. Nikolay N. Koval

634055, Tomsk Akademichesky Ave. 4
Phone (3822) 259-792 Telex: 128114 TAKT SU Fax (3822) 259-410

State Research Center of Russia
Institute of Strength Physics and Materials Science
Russian Academy of Science, Siberian Branch

Dr. Sc. Alexander I. LOTKOV

*Deputy Director of Science
Head of Shape Memory Alloys Laboratory*

2/1, Av. Academichesky Tomsk, 634048, Russia
Phone (3822) 259696   Fax (3822) 259576
E-mail: ispms@ispms.tomsk.su

Academician

Gennady A. MESYATS

Vice-President
Russian Academy of Sciences

32a, Lenin Ave.
Moscow, B-334, 117334

Phone: (095) 938 18 58
Fax: (095) 938 22 11
E-mail: mesyats@urd.ac.msk.SU

Particle Beam
Laboratory

I ♥ my ...

Institute of Electrophysics,
Ural Division,
Russian Academy of Sciencies

Vladimir N. Mizgulin

Dr. S. (Physics @ Mathematics), Senior Researcher

Office: Komsomolskaya st., 34
Yekaterinburg, 620049, Russia
Tel.: +(3432) 49-93-92
Fax: +(3432)44-50-51
E-mail: mizgulin@ief.intec.ru

Home: Malysheva 131 - 10,
Yekaterinburg,
620049,Russia
Tel.: 44-86-16

High Current Electronics Institute
Russian Academy of Sciences

Prof.

Efim M. OKS

*Leader of
Plasma
Sources
Group*

4, Akademichesky ave, 634055 Tomsk, Russia
Phone: (3822) 258-776, 414-712
Fax: (3822) 259-410
E-mail: oks@hcei.tomsk.su

RUSSIAN MATERIALS SCIENCE CENTRE

RMSC

prof. **Victor E. PANIN**

General Director, academician

2/1, Academichesky pr., Tomsk 634 055, RUSSIA
Fax (3822) 259 576   Phone (3822) 259 481
Telex: 612854 ROSMC SU
E-mail: ISPMS @ ISPMS.TOMSK.SU

Nuclear Physics Institute
of Tomsk Polytechnic Univercity

USOV Yuri Petrovich

Director
Professor, Doctor of Engineering

fax/tel. 3822-440100
tel. home. 3822-415238
e-mail: USOV@tsinph.tomsk.su
teletype: 128271 FOTON RU

Lenin st. 2a,
634050 Tomsk
RUSSIA

Lubomira S. Polkovnikova
Head of Foreign Languages Department,
Tomsk Scientific Center of Siberian Branch of
Russian Academy of Sciences

e-mail: dfl @ miriam. tomsk . su

634012 Tomsk
ul. Elizarovikh, 4–130
Tel: (3822) ~~149744~~ 41-43-29
Fax: 3822 259 713

634055 Tomsk
pr. Akademicheskii, 2
Presidium of TSC, SB RAS
Foreign Languages Department
Tel: (3822) 258 937

Engineering Physical Centre
Nuclear Physics Institute of
Tomsk Polytechnic University

Dr. **RYZHKOV**
Vladislav A.

Senior Researcher,
PhD, Head of Laboratory

Lenina avenue, 2a
Tomsk, 634050,
Russia

Phone: (3822) 440097
Fax (phone): (3822) 440812
remnev@ifc.tiasur.tomsk.su

Institute of Strength Physics and Materials Science
of the Russian Academy of Sciences,
Siberian Branch

Arnold P. SAVITSKII

Professor, Dr.
Head of Powder Metallurgy Laboratory

IFPM
Akademichesky st., 2/1
Tomsk 634021 Russia

Office phone: 7-3822-258-138
Private phone: 7-3822-242-066
fax: 7-3822-259-576

E-mail: ispms@ispms.tomsk.su

REPUBLICAN ENGINEERING CENTRE

Dr. Vladimir
Yanovskii

head
of laboratory

8/2, Academicheskii, Tomsk, 634055, USSR
phone: 25 85 91, telex: 133179 RITC SU,
fax: (382.2) 258863

THE RUSSIAN ACADEMY OF SCIENCES
HIGH CURRENT ELECTRONICS INSTITUTE

Dr. George Yu. YUSHKOV

Laboratory of the plasma emission electronics

4, Akademichesky Ave., Tomsk, 634055, RUSSIA
Ph.: + 7 (382 2) 258 776
Fax: + 7 (382 2) 259 410
E-mail: gyshkov @ hcei.tomsk.su

Workshop Program and Preprints of the Papers submitted

	Workshop Opening		
Section1		**Cathodic Arc Technology**	
		CHAIRS: Anthony J.Perry, USA, *A.I.Ryabchikov, Russia*	
1	Cathodic ARC metal ion implantation systems	James R.Treglio, Robert J.Stinner, Alexander Elkind, **Anthony J.Perry,** *ISM Technologies, Inc., San Diego, CA*	30 min
	Coffee Break		30 min
2	"RADUGA" Repetitive Pulsed Vacuum Arc Ion and Plasma Sources and New Methods of Ion and Ion-Plasma Treatment of Materials	**A.I.Ryabchikov,** *Nuclear Physics Institute,Tomsk*	30 min
3	Utilization of Plasma Source Ion Implantation for Tribological Applications	**R. Guenzel**, J.Brutscher, S. Mueldi, W. Moeller *Research Center Rossendorf, Inc., Institute for Ion Beam Physics and Material Research, Germany*	30 min
4	Cathodic Arc Sources and Macroparticle Filterings	**D.A.Karpov**, D.V.Efremov *Scientific Research Institute of Electrophysic Apparatus, St.-Peterburg*	30 min
~~5~~	~~Technology and Equipment for the Vacuum Ion Beam and Plasma Treatment of the Material Surface~~	~~V.P.Smirnov, V.Ya.Tsarfin, O.I.Obrezkov, B.A.Vershok, V.A.Mayevsky, V.M.Savostikov, S.M.Sergeyev~~ ~~*Moscow Inst. of High Tech., TECHNOKON, Inc., Moscow, TECHNOTRON, Inc, Tomsk*~~	~~30 min~~
	Lunch		60 min
6	The Development of Metal Ion Beam Enhanced Deposition	**Li Guoqing**, Liu Bangzhi, Li Geibin, Ma Tengcai, *Dalian University of Technology, Dalian*	30 min
7	Modification of Aircraft Engine Compressor Blades Properties by Uninterrupted and Pulsed Ion Beams	**V.A.Shulov**, N.A.Nochovnaya, G.E.Remnev, A.I.Ryabchikov, *Moscow Aviation Institute, All-Russian Institute of Aviation Materials, Moscow, Nuclear Physics Institute, Tomsk*	30 min
8	Application of Ion Beam Processing for Improvement of the Operational Properties of Detailes of Machines and Tools	**V.P.Sergeyev**, V.I.Gonchikov, I.K.Zverev, S.M.Chesnokov, V.P.Yanovsky, *Russian Engineering Technical Center, Tomsk*	30 min
~~9~~	~~Ion-Thermal Modification of Structural Dielectric Material Properties~~	~~**V.V.Lopatin**, High-Voltage Institute, Tomsk~~	~~30 min~~
	Coffee Break		30 min
Discussion			90 min

Section 2	Ion Implantation Technology	
	CHAIRS: Donald J. Rej, USA, *N.V.Pleshivtsev, Russia*	
1 Key Issues in Plasma Source Ion Implantation	**D.J.Rej**, R.J.Faehl, J.N.Matossian, *Los* *Alamos National Labs, Los Alamos, Plasma Physics Lab.* *Huges Research Labs.. Malibu*	30 min
2 High-Current-Density, Broad-Beam Boron Ion Implantation	**P.J.Wilbur**, J.A.Davis, D.L.Williamson, J.J.Vajo, r.Wei, *Department of Mechanical Engineering, Colorado State* *University, Fort Collins, Department of Physics, Colorado* *School of Mines. Golden. Huges Research Labs. Malibu*	30 min
3 Plasma-Based Ion Implantation and Electron-Bombardment for Surface Modification of Materials	**J.N.Matossian**, Ronghua Wei, J.D.Williams *Plasma Physics Lab. Huges Research Labs., Malibu*	30 min
4 The Use of a High Voltage Discharge at Low Pressure for Ion Implantation	V.I.Khvesyuk, **P.A.Tsygankov**, *Bauman StateTechnical University, Moscow*	30 min
Coffee Break		30 min
5 High Effective Implantation Method in the Range of the Energy of 0.5keV-10keV	V.I.Volosov, **I.N.Churkin**, *Nuclear* *Physics Institute, Novosibirsk*	30 min
6 Gas Ion Beam Sources on the Basis of the Hollow-Cathode Glow Discharges for Industrial Application	V.V.Bersenev, **N.V.Gavrilov**, G.A.Mesyats, G.V.Radkovsky, *Institute of Electrophysics, Yekaterinburg*	30 min
7 Gas Ion Beam Sources with 60 A Current for Technological Application	N.N.Semashko,V.M.Kulygin, A.A.Panasenkov, **N.V.Pleshivtsev**, *Nuclear* *Synthesis Institute of RSC "Kurchatov Institute", Moscow*	30 min
8 Equipment and Methods of Surface Modification of the Microstructure and Properties of Metals Assisted by Ion Plasma Deposition and Adsorbtion	**P. M. Schanin**, A.D.Korotayev, A.N.Tiumentsev, Yu.P.Pinzhin, N.N.Koval, G.Yu.Yushkov, *Siberian Physical Technical Institute, High Current Electronics* *Institute, Tomsk*	30 min
9 Neutron-Capture-Induced Radiation Treatment of Polymeric Materials	**D.J.Rej**, M.M.Pickrell, D.A.Wrobleski, *Los Alamos National Labs*	30 min
Lunch		60 min
~~**10** 50 A Positive Ion Source and Plasma Jet Formation of Ion Flow~~	~~G.I.Dimov, A.S.Donin, **I.I.Morozov**, V.Ya.Savkin, *Budker*~~ ~~*Nuclear Physics Institute, Novosibirsk*~~	~~30 min~~
11 Defect Structures in Metals Exposed to Irradiation of Different Nature	**Yu.P.Sharkeev**, E.V.Kozlov, A.N.Didenko, *Physical Engineering Institute, Moscow, Institute of Strength* *Physics & Materials Science of RAS, Tomsk State Academy* *of Architecture & Building, Tomsk*	30 min
~~**12** Dimentional Ion Beam Treatment of Diamond Layers~~	~~A.F.Belyanin, **A.P.Semenov**, A.E.Alexeyenko, L.L.Builov,~~ ~~B.V.Spitsyn, *Technological Scientific Institute, Physical*~~ ~~*Chemistry Institute, Moscow, Buryatia Natural Science*~~ ~~*Institute, Ulan-Ude*~~	~~30 min~~
13 Ion Implantation Technology in Mechanical Engineering	**V.V.Brukhov**, *Tomsk Polytechnics University*	30 min
Coffee Break		30 min
Discussion		60 min

Section 3	Intense Beam Technology	
	CHAIRS: M.O.Thompson, USA, G. E. Remnev, Russia	
1	Pulsed Ion Beam Treatment of Metal and Metastable Alloys to Improve Surface Properties	**M.O.Thompson**, T.J.Renk, R.Buchheit, R.Sorensen, K.S.Grabovsky, *Department of Material Science and Engineering, Cornell University, Ithaca, Sandia National Labs, Albuquerque, Naval Research Lab., Washington DC*	30 min
2	High Power Ion Beam Sources and their Industrial Application	**G.E.Remnev**, I.F.Isakov, V.L.Kutuzov, M.S.Opekunov, A.N.Zakoutayev, *Nuclear Physics Institute, Tomsk, SIE "LINETRON", N.Novgorod*	30 min
3	The Use of High-Temperature Pulsed Plasma Fluxes in Technology of Metal Materials' Modification	**B.A.Kalin**, Yu.V.Yakushin, V.I.Vasilyev, S.S.Tserevitinov, *Moscow State Engineering Physics Institute, Moscow, State Research Center of Russian Federation, Troitsk Institute for Innovation and Fusion Research*	30 min
4	Pulsed Electron Beam Eqiupment and Fundamentals of Technology for Surface Treatment of Metalic Material	**D.I.Proskurovsky**, G.E.Ozur, V.P.Rotstein, *High Current Electronics Institute, Tomsk*	30 min
	Coffee Break		30 min
5	Technological Application of High Power Ion Beams: Surface Modification and Thin Film Deposition	V.M.Bystritsky, S.V.Grigoryev, A.V.Kharlov, A.M.Mytnikov, **A.A.Sinebrykhov,** S.N.Volkov, P.V.Burkov,V.P.Grigoryev,*Institute of High Current Electronics, Material Science Institute, Nuclear Physics Institute, Tomsk*	30 min
6	Diamond-like films deposited in the plasma of barrier and surface discharges at atmospheric	**S.P.Bugaev**, A.D.Korotaev, K.V.Oskomov, N.S.Sochugov High Current Electronics Institute, Tomsk	30 min
~~7~~	~~Near - cathode region in a low pressure gas discharge~~	~~Yu.D.Korolev High Current Electronics Institute, Tomsk~~	~~30 min~~
8	Deposition and Mixing of Cobalt, Titanium and Tungsten on the Pulse Melted Surface of Substrates	**J.Langner**, J.Piekoszewski, J.Stanislawski, Z.Werner, *Soltan Institute for Nuclear Studies, Swierk*	30 min
~~9~~	~~Improvement of Hard Alloy Cutting Tool Characteristics by Charged Particle Beam Treatment~~	~~G.I.Gering, D.I.Proskurovsky, I.M.Goncharenko, P.B.Grinberg, G.E.Ozur, P.B.Orlov, S.N.Povoroznyuk, K.N.Poleschenko, V.P.Rotstein, G.M.Fedorov, Omsk State University, High Current Electronics Institute, Tomsk~~	~~30 min~~
	Lunch		60 min
Discussion			90 min
	Coffee Break		30 min
Final Discussion and Close of the Workshop			30 min

ADVANCED VACUUM ARC METAL ION IMPLANTATION SOURCE

James R. Treglio, Robert J. Stinner, Alexander Elkind and Anthony J. Perry

ISM Technologies, Inc., 9965 Carroll Canyon Road, San Diego CA 92131, USA

ABSTRACT

The economics of using standard semiconductor-type, mass separated ion beams, for non-electronic, industrial applications are prohibitive. Over the last nine years a major effort has gone into development of direct metal ion implantation systems, using the cathodic arc process to generate a pure metal ion plasma. In the design of industrial systems a number of factors beyond beam current are important. These include system cost, beam profile, maintenance schedules, reliability and system efficiency. In this paper a new cathodic arc ion implantation system designed specifically for industrial applications will be presented. The system, termed *Hydra* by ISM, features multiple cathodic arc ion sources powered by a single power supply and pre-programmed and controlled by computer.

As in MEVVA systems, the new system uses the pulsed cathodic arc for its source of metal plasma. Unlike any other system ever built, this new advanced vacuum arc ion source (AVIS) system operates with four separate ion sources, all driven simultaneously from a single power supply and computer control system. Each ion source is capable of a time average current in excess of 100 mA, has a rectilinear beam spot 0.5 by 1 m at 2 m from the

source, and six cathodes. The operator can choose which of 24 cathodes (6 per source) to operate, arranged in up to three sequences. The system will then fire the cathodes sequentially until a sequence preset level is achieved, then switch to the next sequence. This process can be repeated in incremental steps to facilitate multi-element implants. A further unique feature of the advanced vacuum arc ion sources is that the cathodes are connected to step motors. During operation, the computer feeds the cathodes continuously, allowing the system to operate for extended periods.

1. INTRODUCTION

The development of direct metal ion implantation systems, required by simple economic considerations [1], has enabled expansion into many non-electronic applications at the industrial production level. The advantages include ease of operation, good economy, and high throughput when compared with systems using mass separation methods necessary in the semiconductor industry. Currently, the largest ion source available, based on the metal vapor vacuum arc [2,3], is designated the MEVVA IV 80-50 where the designators define the features as follows. The designation IV was used by Lawrence Berkeley National Laboratory, and has been adopted by ISM Technologies, Inc., and Nippon Steel Corporations for ion sources using a multiple cathode carousel, typically with up to 12 cathodes. This increase in cathode capacity significantly increases operating time of the machine and permits multi-element implantations without breaking vacuum. The ion source is capable of producing circular beams of 300mm diameter at a distance of 1000mm from the source. At an accelerating voltage of 80 kV and a 50mA power supply the ion current, typically of chromium ions, is 25 mA as described elsewhere [4-7]. The ion source has been used for several years for commercial surface modification as well as for development projects employing metal ion beams. One successful application is in the implanting of cutting tools and tool inserts with the so-called *ToolPeen®* process, developed by ISM, which utilizes a dual Ti and Ni implant at 70kV to a total dose of 10^{17} ions.cm^{-2} [8]. At the lower end of the scale a laboratory system, termed a MEVVA IIC 80-5, generates a typical ion beam approximately 150 mm in diameter at a distance of 1200 mm from the source with an chromium ion current of 2mA.

The existing systems are quite adequate for process development and small scale production, but they are inadequate when large areas or high numbers of parts have to be implanted. Many industrial applications require the implantation of large size work pieces, such as dies and molds, or very large surface areas, such as rolled metal sheets. Thus there is a requirement for a ion source generating a broader uniform ion beams the geometrical shape of which, for incorporation into a production line, is dictated to be rectangular.

In this paper we present the design and characteristics of a new cathodic arc metal ion source, termed the advanced vacuum arc ion source (AVIS), which has been developed at ISM for large scale industrial application. The novel features of this ion source are discussed and compared with the existing MEVVA IV 80-50 with some of the significant system parameters noted in Table I. The source has been mounted on a commercial ion implantation system and had been run regularly in production at ion beam currents of 100mA for more four hours. In a recent test the system was run continuously at 80kV and over 75mA average beam current for Cr implantation for a period of 24 hours without breaking vacuum.

2.   THE ION IMPLANTATION SYSTEM

The major innovative feature of the new system, in contrast to any existing system, is the operation of four separate AVIS ion sources, each with a nominal average ion current of 75mA, via a single, computer controlled, power supply. This system is termed *Hydra* by

ISM. The total average ion current produced by the system is 300 mA at an accelerating voltage 80 kV. In practice, the four ion sources are mounted on the top of a vacuum chamber, as indicated schematically in Fig. 1, and oriented to produce vertical beams. The beams are combined to cover a rectangular area 2000mm x 1000mm at a distance 2000mm below the sources. All four sources are water-cooled with deionized water and share a common lead enclosure for an X-ray retention suitably designed to bring the power leads to the sources.

In the current arrangement the ion implantation system has four AVIS sources each mounted with six arc cathodes. The sequencing and firing is pre-programmed and then computer controlled. The computer is programmed to control the sequencing of 24 arc cathodes but their distribution of the is flexible, e.g., they can be mounted separately and located in specified positions on an implantation chamber wall, or mounted in groupings other than the current six per AVIS source.

2.1. Ion Source

As shown schematically in Fig. 2, the ion source of the AVIS system is of the classical MEVVA type comprising the arc plasma source, the drift tube through which metal plasma expands and drifts to the extraction area, and the ion extraction and acceleration system. The source is fitted with a water cooled heat shield, made of oxygen-free high conductivity copper, and is mounted on a 300mm x 300mm square, 110mm high voltage insulator base.

The vacuum arc cathode is rod-shaped, with trigger ring and trigger insulator. In contrast to the single cathode MEVVA design, an innovation in the AVIS is the use of an assembly of six cathodes mounted in each ion source. These cathodes can be fitted with any desired cathode material, and can be computer programmed to fire independently and in any desired sequence. The anode configuration is a plate with a set of six annular openings coaxial with the cathodes. The arc discharge is initiated by a high voltage (20 kV) pulse applied between the trigger ring and the cathode, then sustained by the arc power supply (80 V open circuit voltage, 150 A arc current) in the region between cathode and anode. The highly ionized metal vapor generated drifts to the ion extraction system.

The configuration has an inherent drawback because a fraction of the ionized metal vapor and the macroparticles which are inherent in cathodic arc evaporation condense out as a metallic film on the edge of the anode annular opening. This build-up reduces the diameter of the opening blocking the plasma drift (and decreasing the performance of the source) and may eventually become thick enough to short circuit the anode-to-cathode gap. In practice, this imposes a limit on the operating time of the system, which has to be determined experimentally as different metals behave differently, making it necessary to shut down the system and break vacuum for servicing the source by mechanically removing the metal build-up on the anode. An electrical short circuit between anode and cathode can lead to damage of the electrical components in the power supply systems.

Two further innovations were introduced to maximize the continuous running time of the system. First, an anode plate was developed for the system which can be step-rotated around an axis off-set from the axis of the cathode assembly (Fig. 3) of the

multiple cathode unit. Several sets of holes (each set aligned with the set of cathodes) were cut into the anode plate and located symmetrically around the axis of rotation. Each step brings a new set of the anode holes directly under the cathodes to replace the used set. In the initial experiments eight such sets of anode holes were employed. Second, a cathode feed feature was added to the system which mode of operation can be understood as follows. In the existing MEVVA ion sources the cathode rod is held fixed so that, after an integrated charge of some 10 - 15 kC per cathode depending on the material, the cathode would stop firing because of material consumption and uneven wear, then requiring source servicing to advance the cathode rod. In the AVIS source the cathodes are connected to stepper motors, which are computer controlled to advance the cathode during implantation. The feed rate and increments are set on the computer for each cathode depending on the specific properties of the material.

The ion extraction and acceleration system was designed to deliver an ion beam with a uniformity of better than $\pm 15\%$ when entering the chamber through the insulator duct. It is a conventional three electrode system comprising extractor (80 kV), suppresser (-5 kV) and ground grids. The extraction system has 369 circular apertures arranged on a 170mm x 210mm rectangle. The spacing between extractor and suppresser is 20 mm and between suppresser and ground grid 4 mm. The high voltage across a given accelerator gap for metal ion sources is usually lower than for a gaseous source because of the metal macroparticles which are always present in the arc discharge and was taken into account in the present settings.

2.2. Power Supply

The power supply system to the arc source consists of separate power supply units for the triggers, and single supply for the arc currents mounted in a Faraday cage on high voltage insulators. They are controlled through a fiber-optic connector because these systems are brought to high voltage during operation. The high voltage power supply for the ion beam includes the 100 kV capacitor bank (total capacitance is 4.8 mF), and a high voltage regulator based on the tetrode tube. The feedback control circuit allows the regulator to turn off the high voltage during breakdowns to protect the ion source grids from damage. All the components of the high voltage power supply are rated at 100 kV, 20 kV above the ion source rating. The power supply for the suppresser electrode is adjustable up to -5 kV and connected in parallel with a high voltage diode stack to protect the system if a breakdown occurs between the extractor and suppresser electrodes. The Faraday cage door and the lead shield enclosure are interlocked with a Kirk key system such that they cannot be open without the power supply turned off and grounded.

2.3. Control System

The computer control system based on a 486-33 processor was integrated into the design to allow an easy and flexible operation of the whole system. In defining a specific implantation sequence, an operator can designate up to three firing sequences for the six cathodes in each source (and the total of 24 cathodes in the whole implantation system). Each sequence can be set for the specific element to be implanted with predetermined optimal parameters such as the arc current, repetition rate and pulse length. The system

then fires the cathodes following the defined sequence until a pre-set implant dose level is achieved, and then switches to the next pre-programmed sequence. This process can be repeated in incremental steps. The computer is programmed to analyzes the data on the integrated arc current per cathode in real time mode and send the appropriate signal to the control board of the stepper motors to feed the cathodes during the implantation process. Further, the computer stores the information on the status of each cathode used in the current implantation and maintains in files the data for previous implantations.

3.   EXPERIMENTAL

The AVIS array of four ion sources is designed for mounting onto any vacuum system for ion implantation in production facilities. In the present experiments a single source was used to determine the characteristics of the ion source. The initial experiments were carried out with the ion source mounted on a cylindrical steel vacuum chamber 1.8m in length and 1.2m in diameter with nickel plated walls and fitted with a 16" Varian cryopump and a vacuum ion gauge. The base pressure in the chamber was 10^{-5} Torr, which is relatively poor for a conventional ion implanting system. This allowed the system to be tested under the vacuum conditions likely to be met in industry where the cost of the vacuum chamber and pumping station are significant considerations. The chamber was fitted with a water-cooled table made from a low outgassing aluminum alloy. The table was fitted with flexible water-cooling connections, and wheels which ran on rails in the bottom of the chamber, all designed to provide convenient loading of heavy and large size samples.

Following the first series of experiments studying and optimizing the ion source parameters under industrial conditions, a second chamber was installed for further studies under higher vacuum. This was made of stainless steel with water-cooled walls and was more compact, 980mm x 550mm x 500mm. Using the same pumping system as before this chamber reached a vacuum of better than 3×10^{-6} Torr in 1 hour.

3.1. Beam diagnostics

Two methods were used for the measurement of the ion beam current profiles. First, a Faraday cup was used with a 4 mm diameter opening which had magnetic secondary electron suppression and an optional biased collector to measure the ion current. An array of 6.35mm diameter current collectors was designed to determine the relative ion current profile and was arranged in a cross-like form over a rectangular plate 300mm x 500mm located 500mm below the ion source. The collectors on the array were made of aluminum with high temperature ceramic insulators to withstand the ion beam power. During the tests it was found unnecessary to use the optional Alnico permanent magnets to suppress secondary electrons. The signal received on the collectors was calibrated at the center of the ion beam and on the periphery before using the array to obtain the distribution of the beam current. Second, samples were places at specified points at different distances from the beam center on the base-plate. A Portaspec model 2501 portable X-ray fluorescence (XRF) analyzer was used to compare the implanted dose in the samples. In these tests Cr ions were implanted to a dose of approximately 2×10^{17} ions/cm^2 into Al, Si and graphite samples.

4. RESULTS AND DISCUSSION

4.1. Regimes of operation

The single ion source was tested in two operating regimes.

In the first regime, the high voltage on the ion source was maintained continuous with the arc current pulsed. In this regime all the ions from the plasma created by the arc discharge are accelerated through the extractor-suppresser gap, and the length of the ion current pulse is determined by the length of the arc current pulse.

- In the second regime, the high voltage on the ion source is also pulsed so that the length of the ion current pulse is now controlled by the high voltage regulator. This can be set to any value within the time period that the arc current is on, thus changing the ratio t_{arc}/t_{HV}, ($t_{arc} > t_{HV}$) where t_{arc} is the arc current pulse length, and t_{HV} is the length of the high voltage pulse. Thus, the second regime permits a combination of ion implantation with metal film deposition. Typical oscilloscope traces for the arc current and ion extractor current are shown in Fig. 4. During these experiments, it was found in this regime that there was a reduction in the amount of high voltage breakdowns between pulses, thus improving the efficiency of the system.

4.2. Metal plasma and perveance studies

The metal plasma distribution was first studied at different distances from the anode plate with a single cathode prototype unit. The results indicated that the drifting distance

can be selected between 220mm and 300mm. As a next step an optimal plasma density was determined for selected parameters of the ion extraction/acceleration system. This was done by adjusting the value of the arc current, and thus the amount of ionized metal vapor, which delivered metal ions to the extraction area as shown in Fig. 6. However, it should be noted that using high values of the arc current (for most metals this is set above 135 A) can cause an increased rate of macroparticle production, and a higher rate of erosion of the cathode and trigger insulators. Consequently, a comprehensive series of experiments was carried out to find an optimal combination of arc current, plasma drift distance and extraction system parameters for the beam perveance without sacrificing the uniformity of the beam. Typical perveance curves are shown in Fig. 7. The optimal plasma density for each value of the high voltage was found by comparing the extractor I_{ext} and suppresser I_{sup} current signals on a digital oscilloscope. The ratio I_{sup}/I_{ext}, averaged over all six cathodes, has to be less than 0.1 to maintain optimal conditions at the ion extraction system. During the experiments in the larger chamber the ratio was observed to be greater than 0.1. It was considered that this phenomenon was the result of the chamber pressure being higher than 2×10^{-5} Torr. Further experiments showed that ions were hitting the edges of the insulator duct of the ion source mounting flange, in other words, the ion beam with its desired spread was unavoidably interfering with the duct. This geometric effect was taken into consideration during the design of the second chamber, where the ratio I_{sup}/I_{ext} was measured as 0.04.

4.3. *Extraction system design and beam uniformity*

The relationship between the uniformity of the plasma from the arc discharge and the uniformity of the ion beam was a significant issue during the design and testing stages of the system. The measurements were carried out at the distance of 500mm from the source using the methods described above. The Faraday cup was mounted together with the current profile measurement array for the initial calibration of the ion current signal. The array was then used for determining the relative distribution of the beam current across the rectangular field. The distribution of the ion current along the short Y-axis of the rectangle was expected to be Gaussian and our experiments confirmed this. As noted above, the desired distribution along the X-axis was a uniformity of $\pm 15\%$. Most experiments were conducted with the accelerating voltage set at 80 kV, with some data additional data taken at 50 kV and 70 kV to confirm the current profile at lower voltages. The suppresser voltage in all the experiments was kept constant at -5 kV. No significant changes were observed in the ion current distribution, but there was a tightening effect when the edges of the beam cross-section became sharper at higher voltages. The distribution of the beam current along the X-axis measured at an accelerating voltage of 80 kV is shown in Fig. 8. The results returned by the current profile array were in acceptable agreement with the XRF measurements.

In the attempt to simplify the structure of the ion source and to improve the current distribution further we carried out an experiment with a two electrode arrangement, e.g. with ground grid assembly removed. Such configuration is used to broaden the beam and, in this case, the lines of equipotential of the electrical field between suppresser and grounded elements of the chamber work as a decelerating structure for the ion beam [9].

This modified structure significantly broadened the beam. However, further experiments showed that a better uniformity could be obtained, without spreading the edges of the ion beam, by removing only the grounded grid, keeping the ground cup assembly in the source.

Many commercial implantations have been carried out with the system since the experimentation was completed. These have included high dose Cr implantation for corrosion resistance, and a number of Ti-Ni *ToolPeen®* dual metal ion implantations of large batches of cutting tools. The time of implantation for both these processes with an average beam current of 12-15mA is approximately 1 hour to reach the dose of 1×10^{17} ions.cm^{-2}. The system has also been tested at far higher ion beam currents of 100 mA average current for more than four hours with a coarse vacuum of $2\text{-}3 \times 10^{-5}$ Torr to demonstrate that indeed the system has a rugged design and is suitable for operating under industrial conditions. Finally, the system has been run continuously at 80kV and over 75mA average beam current for Cr implantation for a period of 24 hours without breaking vacuum.

5. CONCLUSION

An advanced vacuum ion implantation source (AVIS) for metal ion implantation has been developed with enhanced capabilities as based on experience with several generations of MEVVA type metal ion sources. The AVIS source features six cathodes, and its versatility of the was significantly enhanced by integrating into it a sophisticated computer control system which allowing multi-element implantations to be implemented in

preprogrammed sequences. Further innovations have increased the operating time of the source without breaking vacuum, extended cathode lifetime with a feed mechanism, and raised the arc current efficiency. Several AVIS sources can be controlled at one time from the single computer and power supply, with the system termed *Hydra* by ISM. The system has a rugged design and is suitable for operation in industrial conditions.

REFERENCES

1.   J.R. Treglio, A.J. Perry and R.J. Stinner, *Surf. Coat. Technol.*, 65, 184 (1994)

2.   I.G. Brown, J.E. Galvin and R.A. MacGill, *Appl. Phys. Lett., 47* (1985) 358

3.   I.G. Brown, J.E. Galvin, B.F. Gavin and R.A. MacGill, Rev. Sci. Instrum., 57 (1986) 1069.

4.   I.G. Brown, J.E. Galvin, R.A. MacGill and R.T. Wright, Status on the MEVVA high current metal ion source, *1987 Particle Accelerator Conf., Washington, DC, March, 1987.*

5.   J.R. Treglio, *Nucl. Instrum. Methods B, 40-41* (1989) 567

6.   B.L. Gehman, G.D. Magnuson, J.F. Tooker, J.R. Treglio and J.P. Williams, *Surf. Coat. Technol.,* 41 (1990) 389

7.   J.R. Treglio, G.D. Magnuson and R.J. Stinner, *Surf. Coat. Technol.*, 51, 546 (1992)

8.   J.R. Treglio, A. Tian and A.J. Perry, *Surf. Coat. Technol.*, 62, 438 (1993)

9.   A.T. Forrester, *Large ion beams,* Wiley-Interscience, New-York, 1988

Table 1.

Parameter	MEVVA IV 80-50	AVIS
Average current	25 mA	100 mA
Accelerating voltage	80 kV	80 kV
Beam size	0.018 m^2	~ 0.50 m^2
Shape of the beam	Circular	Rectangular
Source to substrate distance	1200 mm	1600 mm
Number of cathodes	12	6
Cathode feed option	No	Yes

Figure captions.

Figure 1. Schematic diagram of a *Hydra* system featuring the advanced vacuum ion implantation source (AVIS) for metal ion implantation showing: 1 - vacuum chamber, 2- cryopump with gate valve, 3 - ion sources, 4 - high voltage cable duct, 5 - Faraday cage, and 6 - X-ray shield enclosure.

Figure 2. Schematic diagram of the ion source assembly showing: 1 - arc source with cathode drive; 2 - drift tube; 3 - high voltage insulator assembly ; containing the ion extraction system; 4 - ground cup assembly.

Figure 3. Schematic diagram of the AVIS arc source: 1 - cathode drive; 2 - water-cooled flange; 3 - cathodes; 4 - anode plate; 5 - arc source flange; 6 - ratchet mechanism.

Figure 4. Typical oscilloscope traces of the extractor current (upper trace) and arc current (lower trace) for: (a) pulsed high voltage and pulsed arc current, and (b) DC high voltage and pulsed arc current.

Figure 5. Extractor current and suppresser current from a single cathode as a function of arc current at 40 kV accelerating voltage.

Figure 6.   Extractor current at optimum perveance for the six (chromium) cathodes as

a function of extractor voltage with the suppresser voltage U_{sup} set at -4.7 kV).

Figure 7.   Ion beam current profile at a distance of 500mm from the AVIS ion source

as measured by X-ray fluorescence.

(FARADAY CAGE)

Fig. 1

TOP OF CHAMBER

EXTRACTED ION BEAM

Fig. 2

Fig. 3

a)

b)

Fig 4

Extractor and suppressor currents as a function of arc current for single cathode at 40 kV

Fig 5

Extractor current at optimum perveance for different cathodes, Cr

Fig 6

Beam Current Profile (XRF) at 50 cm from the ion Source

Distance from the center (mm)

Fig. 7

REPETITIVELY PULSED VACUUM ARC ION AND PIASMA SOURCES "RADUGA 1-5" AND NEW METHODS OF ION AND ION-PLASMA TREATMENT OF MATERIALS

A.I.Ryabchikov

Nuclear Physics Institute, 634050 Tomsk, Russia

A btief reveiw is presented of the "Raduga 1-5" repetitively pulsed vacuum arc ion sources. Their operation principles and functional ranges are described. The Raduga ion sources provide single- and multi-element implantation. These advantages are achieved by using not only pure single-element or mixed ion beams, but also pulsed beam sequences with controllable composition and energy of each ion species. Another feature of the ion sources is their ability to generate a sequence of ion beam and plasma stream pulses. Switching between ion implantation and plasva deposition can be done from pulse to pulse, within each pulse, or after accumulation of a required dose. "Raduga 5" ion and plasma source operates in a d.c. mode of plasma forvation and repetitively pulsed mode of ion beam generation.

I. INTRODUCTION

In recent years sources of accelerated ions as a tool for modifying the physical and chemical surface properties of different materials have become of great interest. Numerous fields of application of ion implantation for improving the surface properties of metals, alloys, and other construction materials have required a substantial increase of irradiation dose, up to 1017-1018 ions/cm2, resulting in the development of high intensity ion sources. Among the range of existing and developed kinds of ion sources, the repetitively pulsed vacuum arc ion source ranks high [1-9]. These sources can produce high intensity beam of metal ions as well as metal and gases together. The Raduga ion sources can provide beams of composition- and energy-controlled ion beam for single- and multi-element implantation. The high concentration implantation operation, with surface ion sputtering compensation using deposition of plasma and neutral atoms, is of special interest. In this mode of operation, any concentration of dopants in different materials can be obtained with a simultaneous substantial reduction of irradiation time[10-12]. The operation of repetitively pulsed vacuum arc sources under ion/plasma conditions allows the performance of plasma deposition of coatings under ion beam mixing.

II. PRINCIPLES OF ION BEAM FORMATION IN RADUGA SOURCES

Ion beam production in ion and ion/plasma Raduga sources is accomplished by use of the repetitively pulsed vacuum ars discharge. To initiate the discharge positive voltage is applied to a trigger electrode. As a result a cathode spot is formed on the cool cathode because of breakdown across the surface of a ceramic insulator placed between the cathode and trigger electrode. The expanding plasma of the cathode spot approaches the anode. The arc discharge burns in the vapor

of the cathode material between the anode and cathode. The species of the accelerated ions is determined by the cathode material.

In Raduga sources, a three-electrode ion extraction and acceleration system is generally used. A voltage is fed to one of the electrodes to prevent plasma electrons from streaming from the on beam drift into the accelerating gap.

Any version of "Raduga" ion source can produce single-component and multi-component beams (but not controlled in composition) based on single-element cathodes or cathodes of complex composition.

To generate multi-component ion beams which are controllable in composition, three approaches have been proposed and are in use now: (a) a set of cathodes which are different in their element composition and a system of controllable triggering electrodes[13], (b) a directed motion of the cathode spot along the working surface of the composite cathode[13,14], (c) repetitive variation of the functional duties of the ion source electrodes[15].

III. THE FEATURES OF ION AND ION/PLASMA SOURCES "RADUGA 1" - "RADUGA 5" AND METHODS OF ION BEAM AND ION/PLASMA TREATMENT OF MATERIALS.

In the source Raduga 1 the pulse duration and current of the vacuum arc discharge can be varied over the range 20-500 ms and 10-100 A by variation of the circuit elements and the discharge voltage[16,17].

The accelerating voltage is provided by a pulse transformer. Simplicity and reliability of the supply system combined with a good cooling system allows high repetition raty operating conditions of Raduga 1. The main parameters of the source are presented in Table I. Because of the high pulse repetition rate the source can provide both ordinary ion implantation and also

3

implantation in combination with plasma coating deposition. In particular, if the accelerating voltage is formed by a pulse transformer and connected to the target, various methods of ion/plasma treatment can be used, dependent on the relationship of pulse durations (arc discharge and accelerating voltage) and the system geometry.

A distinctive feature of the ion source Raduga 3 is its power supply system, which is desighed with a single pulse transformer only by using an extrahigh-voltage transformer with both triggering and arc discharge windings[10-20].

A system of multiple self-triggering of the arc discharge in case of its spontaneous quenching is ised to increase the efficiency of the ion source at low discharge currents (Ic~10-20 A). In Raduga 3 source the accelerating voltage is adjusted by the initial charging voltage fed from a three-phase autotransformer to the pulse forming line. The lower limit of the accelerating voltage (20 kV) is determined by the need to form a voltage (on the extrahigh-voltage winding of the pulse transformer) sufficient for breakdown across the insulator surface separating the cathode and trigger electrode. Increase of the accelerating voltage is simultaneously accompanied by an arc current increase, as well as by beam current of the accelerated ions. The main parameters of the ion source "Raduga 3" are shown in Table I.

Within the ion source Raduga 2 four cathodes with different element composition are mounted to form multicomponent, composition-controlled, ion beams. Each of the cathodes has an independent trigger electrode. In one version of the cathode assembly the cathodes are in the form of a cylinder of 10 mm diameter. Within each cathode a ceramic tube and trigger electrode of 2 mm diameter are inserted. The thickness of the ceramic tube is 0.5 mm. All cathodes are electrically mounted on the same cathode holder. In another version additional elements are placed on the end surface of the cylindrical cathode, each having an individual trigger electrode.

Each trigger electrode has its individual supply system. To initiate the discharge, a high voltage pulse of 2-10 kV amplitude and 2-10 mks duration is applied between the trigger electrode and cathode. A given pulse is produced by discharging a charged capacitor into the primary winding of a suitable pulse transformer. The circuit switching for each transformer is perfomed by a thyristor block. After breakdown over the insulator surface, the generated plasma expands toward the anode. At this moment, a discharge occurs between the cathode on which the cathode spot was formed and the anode. The duration of this discharge is determined by the parameters of the pulse forming line[13,14]. The main parameters of the ion source "Raduga 2" are shown in Table I.

Control of the repetitive formation of the spot on the cathode surfaces combined with controlled ion acceleration provide several ways of carrying out material treatment:

(1) Four variants of single-component implantation.

(2) Multi-element ion implantation (two to four elements with various sequences of component).

(3) Coating deposition with single-element and compound multi-element composition (without accelerating voltage).

(4) Combination of plasma deposition and ion implantation processes.

The Raduga 4 ion/plasma source can generate two-element compound ion beams with varying composition during implantation and with ion current up to 0.7 A within the pulse[21-23]. The cathode of the source is desighed to be compound, and each of the two cathode elements has a system of independent trigger electrodes. The anode of the source is a cone with a 20-cm-diam base and with apex directed to the cathode. The formation of pulse voltages for the arc discharge supply and ion acceleration is accomplished using 3 pulse transformers. The primary windings of each transformer are fed from the corresponding pulse-forming LC lines.

Under convertional repetitively pulsed conditions, the ion source forms a beam of accelerated ions of the conducting material. Pure metals and alloys as well as gas-containing compounds may be used as cathodes. The mean energy of the accelerated ions is determined by the accelerating voltage and the mean ion charge state. The latter depends, in turn, on the cathode material and varies from 1 to 3 [4]. The pulse duration of the accelerated beam in the Raduga 4 can be varied over the range 50-200 mks. The source control system allows the irradiation dose ratio to be adjusted for different ion species. Using this method, both the ion implantation of metals and metal and gas implantation may be carried out. In the second case one of the cathodes is manufactured from a compound, gas-containing, conducting material. Subsequently, by combining the different distribution profiles of the different dopants, or from other conditions, the required source operation regime is defined.

The regime of high-concentration implantation is accomplished using ion sputtering compensation by plasma and neutral atom deposition [10,11]. This can be done by combination of ion implantation and plasma deposition, i.e., ion/plasma operation conditions of the source. Plasma deposition occurs when the accelerating field is not switched on, and the freely expanding plasma is deposited onto the target. According to the specific task or the need to form an implantation distribution profile with high concentration of dopants below the surface (at the ion range depth) or near the surface for sputtering compensation of the surface layer, plasma deposition is used with composition coinciding with the target material or the implanted ion species. In the latter case, additional doping from the surface is done by recoil implantation. Then the source operating conditions for high-concentration repetitively pulsed implantation can be varie*d from ionic to plasma after a given irradiation dose, from pulse to pulse or within a pulse. In the latter case, the pulse duration of the arc discharge exceeds that of the accelerating voltage. The excess is defined by the geometric parameters of the source, such as the distance to the target,

6

the degree of ionization of the cathode material, and the coefficient of target ion sputtering. The arc discharge duration in the source can be adjusted from 50 up to 1000 mks, while the pulse duration of the accelerating voltage is controlled over the range of 50-200 mks.

Thin film deposition mode can be accomplished by single- and multi- element operation of the source, without accelerating voltage.

Thin film deposition with ion mixing can be accomplished when the repetitively pulsed deposition for coating exceeds that of surface ion sputtering under implantation[24].

The further development of the idea of the ion and plasma operation regimes resulted in creation of an ion/plasma source "Raduga 5" [25]. The main feature of this source lies in continuous regime of generating plasma by a vacuum arc. Due to the d.c. mode of the vacuum arc several problems connected with creation of highly intensive ion implanters on the basis of the vacuum arc are solved. The first problem is concerned with a limited period of operating an arc-initiating system. This problem can be divided into two parts. The first part of the problem is that of failure of the ceramic insulator which separates the cathode and the keep-alive electrode. The second one is due to necessity for initiating the cathode spot of the vacuum arc immediately on the cathode working surface. As the cathode is depleted the initiation of an arc becomes unstable.

The second problem of the vacuum-arc ion sources of conducting materials is connected with duration of pulses in plasma generation. The pulse duration applied in reality range from a hundred to several hundreds of microseconds. Such duration are inhibitory to constructing highly intensive ion sources with a large area of the cathode working surface. The period of continuous operation of the source is limited by a high-speed depletion of a small cathode.

A continuous regime of generating plasma removes the above problems. Initiation may be even single with a subsequent prolonged work.

7

Originally the cathode spot may be initiated on the non-working surface with its subsequent transfer to the working surface of the cathode. Thus, with such an approach to the task the cathode sizes may be large and the operating period of the source may amount to hundreds of hours.

Already at the stage of generating highly intensive beams of accelerated metal ions, with the vacuum arc operating in pulse regimes, the problem of a microparticle fraction in the plasma flux became of high priority. It is well known that the share of the microparticle fraction grows sufficiently if low-melting-point cathodes are used instead of refrectory ones.

Working under continuous regimes of generating plasma by the vacuum arc the ploblem of the microparticle fraction makes the realization of a highly intensive ion implanter practically impossible.

To clear the vacuum-arc plasma from the microparticle fraction the authors studied and developed a shutter system whose schematic view projection is shown in Fig.1[26]. In the simplest case the system represents a set of plates through which current is passed. The current generates the magnetic field arround in the vicinity of each plate. Additionally, a positive bias voltage is applied to the plates. The latter are placed so that the straihgt-line transit of microparticles from any point of the cathode surface into the working volume of the vacuum chamber should be cut off.

While the electric-arc evaporator is in operation the plasma flux is moving towards the shutter system. When plasma is approaching the electrodes it is influenced by both the electric and magnetic fields. The magnetic field around the electrodes ensures partial or total magnetization of the electron component of plasma, reduces plasma conductivity and, consequently, makes it possible to keep the positive potential on the electrodes of the system.

The near-electrode potential drop existing due to the potential difference of electrodes and plasma as well as the finite conductivity of plasma influences the ion component of the plasma

flux [27]. Depending on the near-electrode potential drop the plasma flux ions possessing a directed velocity in their initial state may, in overcoming this barrier, deposit on the electrodes or change the path of their motion. For example, if an ion approaches the electrode surface at the angle of α, it has an energy component

$$E_o = E_{zo} \cdot \sin \alpha + kT_i \qquad (1)$$

which is influenced by the near-electrode potential barrier. It means that if

$$Ze(\varphi_e - \varphi_p) > E_{zo} \cdot \sin \alpha + kT_i \qquad (2)$$

an ion will be elastically reflected by the anode side surface and continue its motion in plasma, being involved in the total flux ions and, consequently, plasma passing through the clearing system.

At the same time the microparticles flying from the cathode along straight-line paths always collide with the shutter of the plasma filtering sistem.

The results of the experimental investigations into the efficiency of passing through the filter and cleaning the plasma from the microparticles showed the following: in the experiments with the system of shutters where each one was made of two separate plates 15 mm wide, the efficiency of passing plasma essentially depends on the amount of current passing through each plate. Fig.2 presents the results of the ion current measurements of a collector installed at the output as a function the current passing through the plates. It follows from the Fig. that already at small magnetic fields amounting to several tens of gauss the efficiency of passing plasma reaches saturation.

The dependences of passing plasma through the microparticle filter on the angle of plasma incidence and the bias potintial on the shutters for the same geometric conditions as is the case in Fig.2 are shown in Fig.3.

It follows from Fig.3 that the efficiency of passing plasma is reduced with increase of the shutter inclination angle with respect to the system's axis. When the angle of the shutter turn slewing is increased a maximum efficiency is obtained at high bias potentials. At the slewing angle b=15 which ensures a straight-line transit cut-off of the path for microparticles, the maximum efficiency is 70%. Decrease in efficiency with increase in the bias potential is explained by reflecting the low-energy ion component of the plasma flux from the longitudinal component of the electric field available in this system. It should be noted that unlike other plasma optical systems for microparticles plasma filtering [28,29] the described system is simple, compact and highly effective.

The efficiency of clearing plasma from microparticles can be seen well if the pictures (obtained in the optical microscope under 400-fold multiplication) of the surfaces of the deposited Ti coatings are compared (Fig.4a ,b).

The application of the developed microparticle filtering system in the ion/plasma source "Raduga 5" removed practically all the problems in the process of constructing a multi-functional installation, which is promising to realize new ion and ion-plasma technologies not only in the laboratory conditions but also in the commercial scales.

Up to the present time the following parameters were obtained:

regime of vacuum arc plasma formation	d.c.
regime of ion accelaration	repetitively-pulsed
acceleration voltage , kV	up to 50
pulse duration, mks	200-400
pulse repetition rate, p.p.s.	up to 200
ion beam current in a pulse, A	0,1-3

average ion beam current, A	up to 0,12
ion beam area, cm2	100-500
speed of plasma deposition of coatings, mkm/h	up to 5

It should be noted that by taking this approach the problem of maximum ion beam current depends only on the power of the accelerating voltaqe generator. The power of the ion beam may be easily increased due to increase in ft of a generator, i.e., at the expense of both the increase in the pulse freqnency f and the increase in the pulse duration t of the accelerating voltage.

Consider briefly the technological advantages of the ion/plasma source "Raduga-5". The simplest regime is that of the plasma deposition of coatings in this case no accelerating voltage generator is used. Obviensly there is no reason for expecting good properties of coatings only due to clearind plasma from micropartieles.

The second regime is intended for the plasma deposition of adhesively strong and even ion-modified coatings at the same time. In this case the source generates an alternating sequence of pulsed beams of accelerated ions and plasma fluxes. If an accelerating vdltage with the pulse duration t and the pulse repetition rate f is appleid to the source, the ratio of ion beams in the plasma to the accelerated beam at output of the source may be determined in the first approximation as

$$\Phi = (1/(ft)-1) \qquad (3)$$

The correction of ratio (3) may be done on the basis of the experimental data. The cause for this may be the fact that the efficiency of passing the plasma through the plasma filter will be somewhat lower than in case of the ion acceleration. The latter is due to the partial penetration of the accelerating field into the filter-electrode space of the filter system.

By introducing the correction coefficient K > 1 ratio (3) takes the form

$$\Phi = (1/(Kft)-1) \qquad (4)$$

It follows from condition (4) that the ratio on the target may be controled within wide limits by changing the pulse frequency or pulse duration. At the same time there is another powerful instrument making it possible to control this correlation. If a specimen under treatment is placed not near the source but at some distance L from it one should take into account that, depending on the distance, the current density of the accelerated ion beam and the plasma density decrease according to the different law. Decrease in the density of the ion beam current depends on its angle divergence and usually is not very significant. At the same time in case of the lack of the driving magnetic field the plasma density becomes lower according to the law close to $1/L2$. Thus, placing the target at some distance one may solve the technological problems of the plasma deposition of coatings and effective ion mixing of the target - coating interface as well as modifying the properties of the coating itself at the expense of ion implantation.

The regime of high - concentration implantation is also easily realized due to choice of the corresponding parameters of f, t, the accelerating voltage and the distance from specimens. Increase in the rate of the retained doze withont additional heating of specimens will be in this case attained due to both compensating the effect of ion sputtering of a specimen surface and to additional doping of the surface by the recoil implantation .

The "Raduga-5" may be used as an ordinary highly powerful implanter. In the first version this may be realized at a considerable distance from the source, e.g., L ~ 1 m. In the second version the problem may be solved by cutting off the plasma stream, e.g., by a magnetic field. Obviously, the magnetic field does not considerably influence the beam of accelerated ions

REFERENCIES

1. A.A.Plyutto, V.N.Ryzhkov, and A.T.Kapin, Sov. Phys. JETF 20, 328 (1965).

2. G.P.Bagenov, S.P.Bugaev, G.P.Erohin et. all. V Simposium po Silnotochnoi Electronike. Tez. Dokl. Tomsk (Russia), V.2, 93 (1984)

3. A.N.Didenko, Ya.E.Krasik, A.I.Ryabchikov, and S.N.Volkov, Piasma Zh. Tekh. Rhys.(Russia) No. 4, 112 (1984).

4. I.G.Brown, J.E.Galvin, and R.A.MacGill, Appl. Phys. Lett. 47, 358 (1985).

5. R.Adler and S.Picreau, Nucl. Instrum. Methods B 6, 123 (1985).

6. L.K.Len, C.Burhart, G.W.Cooper, S.Humphris, Jr., M.Savage, and D.M.Woodall, IEEE Trans. Plasma Sci. PS-14, 256 (1986).

7. Z.Hiaoji, Z.Fengsheng, Z.Huixing et al., Rev. Sci. Instrum. 63, 2431 (1992).

8. S.P.Bugaev, A.G.Nikolaev, E.M.Oks et al., Rev. Sci. Instrum. 63, 2422 (1992).

9. J.R.Treglio, A.Tian and A.J.Perry, Surf.Coat. Technol. 62 ,438 (1993)

10. A.I.Ryabchikov and R.A.Nasyrov, Rev. Sci. Instrum. 63, 2428 (1992).

11. A.I.Ryabchikov and R.A.Nasyrov, Poverhnost. Physika Himia, Mehanika (Russia) 3,98 (1992).

12. A.I.Ryabchikov, R.A.Nasyrov, and A.A.Kompaniets, Proceedigs of the International Conference on Ion Implantation and Ion Beam Equipment, Elenite, Bulgaria, 1990, p. 377.

13. A.I.Ryabchikov, Rev. Sci. Instrum. 61, 641 (1990).

14. N.M.Arzubov, S.V.Dektjarev, and A.I.Ryabchikov, Prib. Techn. Exp. (Russia) 1,171 (1991).

15. A.I.Ryabchikov, N.M.Arzubov, and R.A.Nasyrov, J. Tech. Fis. (Russia) 60, 106 (1990). 16. N.M.Arzubov, G.P.Isaev, and A.I.Ryabchikov, Prib. Tech. Exp. (Russia) 5,28 (1988).

17. N.M.Arzubov, G.P.Isaev, and A.I.Ryabchikov, Izvest. Vusov. Fis. (Russia) 8,68 (1989).

18. A.I.Ryabchikov, I.B.Stepanov, and S.V.Dektyarev, Abstracts of the 5th International Conference of Ion Sources, Beijing, China, 1993, p.44.

19. A.I.Ryabchikov and I.B.Stepanov, 3 konferentsia po Modificatsii Svoistv Konstruksionych Materialov Puchkami Zarjashenych Chastitz, Tez. Dokl., Tomsk (Russia) 1, 112 (1994).

20. A.I.Ryabchikov, N.M.Arzubov, and E.I.Lukonin, 1 Konferentsia po Modificatsii Svoistv Konstruktsionych Materalov Puchkami Zarjashenych Chastits, Tez. Dokl., Tomsk (Russia) 1, 17 (1988).

21. A.I.Ryabchikov, N.M.Arzubov, N.A.Vasilyev et al., Proceedings of the International Conference on Ion Implantation and Ion Beam Equipment, Elenite, Bulgaria, 1990, p. 327.

22. A.I.Ryabchikov, N.M.Arzubov, N.A.Vasilyev et al., Nucl. Instrum. Methods Phys. Res. B 59/60, 124 (1991).

23. A.I.Ryabchikov and R.A.Nasyrov, Nucl. Instrum. Methods. Phys. Res. B 61, 48 (1991).

24. A.I.Ryabchikov, E.I.Lukonin, and D.A.Karpov, 9 Simposium po Silnotochnoi Electronike. Tes. Dokl. Ekaterinburg (Russia) 3,86 (1992).

25. A.I.Ryabchikov, S.V.Dektyarev, IV Konferentsia po modificatsii Svoistv Konstruktsionnych materyalov Puchkami Zarjashennych Chastits, Tez. Docl., Tomsk (Russia) 93 (1996).

26. A.I.Ryabchikov, I,B.Stepanov (see ref. 25) 29 (1996)

27. A.I.Ryabchikov, S.V.Dektjarev and I.B.Stepanov. Rev. Sci. Instrum. v.65, N 10, 3126 (1994).

28. A.I.Morozov. Dokl. Akad. Nauk (Russia), v.163,1363 (1965).

29. I.S.Abramov, V.A.Andreev, V.T.Barchenko et.all, Izvestiya Vuzov Fizika (Russia), 3,121(1994).

30. I.I.Aksenov, V.A.Belous, V.G.Padalka and V.M.Khoroshikh, Fiz.Plazma 4, 758 (1978); Sov. J. Plasma Phys. 4, 425 (1978).

TABLE I. Characteristies of the different Raduga ion sources.

Parameter	Raduga 1	Raduga 2	Raduga 3	Raduga 4
Cathode material	Any conducting material, single element or complex			
Mean ion charge state	1-3	1-3	1-3	1-3
Beam diameter (mm)	up to 100	up to 200	up to 200	up to 200
Mean ion energy (keV)	up to 180	up to 160	up to 300	up to 300
Pulse length (mks)	20-500*	50-400*	100-400	50-200
Ion current (mean, mA)	up to 25	up to 14	up to 40	up to 14
Ion current (pulse, A)	0,1-0,5	0,2-0,7	up to 1	0,2-0,7
Pulse rep. rate (pps)	up to 200	up to 50	up to 100	up to 100

*Plasma is generated when the acceleratind voktage is switched off.

FIGURE CAPTIONS

Fig. 1. Schematic view of the plasma filtering system.

Fig. 2. Dependence of the ion current to the collector on the current in the electrodes.

Fig. 3. Ratio of the input ion current in the plasma filtering system to the output ion current as a function of the bias potential on the shutters at different angles of the shutter inclination to the direction of the plasma flux.

Fig. 4.

Fig. 1

Collector ion current I(mA)

Electrode current I(A)

H=10 mm
L=30 mm
α=30°

U=5 V
U=10 V
U=15 V
U=20 V
U=25 V
U=30 V

Fig. 3

Fig 4

Utilization of Plasma Source Ion Implantation for

Tribological Applications

R. Günzel, J. Brutscher, S. Mändl, and W. Möller

Research Center Rossendorf Inc., Institute for Ion Beam Physics and

Materials Research, P.O. Box 51 01 19, D-01314 Dresden, Germany

Plasma source ion implantation (PSII) has been developed as an alternative technique to circumvent the limitations of conventional ion implantation, like the requirements of a complicated target handling and beam raster system for a uniform ion implantation of 3-dimensional samples. By applying negative high voltage pulses, positively charged ions are accelerated to and implanted into the target. The plasma sheath expansion and ion doses, calculated with a theoretical model, are in good agreement with the experimentally obtained data. As the analytical model describes sufficiently the experimental data, it is used to discuss design specifications for PSII systems. Furthermore, the possibility of implanting ions into large, 3-dimensional samples is discussed based on the predictions of the analytical model. The results of nitrogen PSII treatment of planar shaped samples are shown. Wear and hardness of the implanted and not implanted flat steel samples with a high chromium content were measured. An increased hardness as well as a decreased wear was obtained.

1. Introduction

Conventional ion implantation can be used for modifying surface properties of different materials, thereby enhancing, for example, corrosion resistance, hardness, friction coefficient, and wear behavior [1]. However, high costs and a sophisticated system for target movement when implanting 3-dimensional workpiece limit the technological applications. PSII was developed as an alternative technology to circumvent these restrictions [2,3]. The sample in the treatment chamber is immersed in a plasma and by applying negative high voltage pulses to the sample, positively charged ions are extracted from the plasma through the plasma sheath and implanted into the surface.

During the voltage pulses the plasma sheath, separating the plasma and the workpiece, is expanding and the implanted ions are accelerated through this sheath to the target. Various models for the analytical description of the sheath dynamics are shortly discussed in section 2. Furthermore, a procedure for simulating PSII in targets with rotational symmetry was developed on the foundations of the sheath dynamic [4]. In section 3 simulation results for the ion fluxes are compared with ion doses measured with RBS. PSII treated steels with a high chromium content are investigated in section 4. It is well known that their wear behavior can be indeed improved by conventional plasma nitriding, albeit the institution of chromium nitride formation at temperatures above 500°C persistently degrades the corrosion resistance [5,6]. PSII allows an efficient nitriding of stainless steels at temperatures sufficiently below the formation temperature of Cr-N compounds, leading to improved tribological properties and retained corrosion resistance. Finally, conclusions are drawn in the last section.

2. Plasma Sheath Dynamics

In contrast to the conventional beam line ion implantation, the current of the implanted ions cannot be measured reliably in PSII. However, for technological application information about

the ion flux, the angle of incidence and the energy distribution of the implanted ions must be available. All these parameters are determined by the dynamics of the plasma sheath and thus a series of models for this process was published in the literature.

A first approach employs an ion matrix sheath [7,8], assuming a homogenous plasma of density n_o with cold ions in the plasma and thermal electrons, obeying the Boltzmann distribution

$$n_e = n_o \exp\left(\frac{-\phi}{kT_e}\right) \qquad (1)$$

with kT_e the electron temperature, and ϕ the spatially varying potential in the plasma. For voltage rise times slower than the inverse electron plasma frequency but faster than the inverse ion plasma frequency $1/\omega_i$, the electrons are considered inertialess. The width of the initial ion matrix sheath can be calculated for a voltage U_o and planar geometries to

$$x^{ini} = \sqrt{\frac{-2\varepsilon_o U_o}{en_o}} \qquad (2)$$

with the dielectric constant ε_o and the elementary charge e. This width is the minimum distance of the plasma sheath edge to the target for a given implantation voltage and plasma density, albeit not observable for implantation voltages larger than 5 kV due to rise times of some microseconds [9].

Next, models describing the plasma-plasma sheath-surface [10,11] were modified and adapted for the context of PSII [12,13]. However, most of these models assume a current to the wall supplied only by the sheath edge moving into the plasma. For long pulses this results in a non-stationary sheath edge in contradiction to experimental data.

A more realistic description is obtained when the presheath, where the ions with the mass m_i are accelerated to the ion acoustic sound or Bohm's speed $v_B = (kT_e/m_i)^{1/2}$, is included [14,15]. It is not only valid for a stationary sheath edge but also for a sheath edge moving with

constant velocity [16]. Again the ions are considered as cold in the bulk plasma, whereas the electrons obey Boltzmann's equation (1). The ions are accelerated in the presheath to the velocity [17]

$$v_s = \sqrt{v_B^2 - \dot{d}^2}$$

(3)

with $\dot{d}$ the velocity of the moving sheath edge. Assuming a collision-free transit through the sheath, where the ions are accelerated to the implantation energy eU_o, allows the description of the sheath by the Child-Langmuir law [18]. For planar geometries the space charge limited current can be written as

$$j_{CL} = \frac{4\varepsilon_o(-U_o)^{3/2}}{9d^2}\sqrt{\frac{2e}{m_i}} .$$

(4)

This current is supplied by the ion current passing the moving sheath edge, as we have shown in Ref. [17]:

$$j_{CL} = \begin{cases} en_o v_B \exp\left(\dfrac{\dot{d}^2 - v_B^2}{2v_B^2}\right) & \dot{d} < v_B \\ en_o \dot{d} & \dot{d} > v_B. \end{cases}$$

(5)

The pair of eqns. (4) and (5) can be solved numerically with $d(t)$ describing the time evolution of the plasma sheath.

Equation (5) is strictly valid only for $\dot{d}$ = constant. However, the characteristic time constant $\tau = L/v_B$ of a presheath with a length L [15] is large compared to the inverse ion plasma frequency, so that the presheath can be assumed to be constant. As the plasma sheath is expanding in the first microseconds with supersonic speed even for voltages of a few kV (see Fig. 1), instead of the model of a variable presheath, described here, a model with a constant presheath is used by other authors [19]. There, the Child-Langmuir current in eqn. (4) is

supplied by ions accelerated to v_B in the presheath independent of the edge velocity and by the ions uncovered by the moving sheath edge:

$$j_{CL} = 0.6en_o\left(\dot{d} + v_B\right) \tag{6}$$

Both models yield sufficiently precise results for practical applications in PSII processes, e.g. current density and edge velocity, as can be seen in Fig. 1. A better approximation of the sheath dynamics is achieved when the model of a variable presheath is changed so that the time constant of the presheath is included, leading to a delayed reaction of the presheath to the moving sheath edge. Here work is in progress and a detailed description will be published [20].

Both models – constant presheath and variable presheath – yield a stationary solution for a d.c. high voltage, which describes the maximum extent of the sheath

$$x^{max} = \frac{(-U_o)^{3/4}}{(ekT_e)^{1/4}} \sqrt{\frac{\varepsilon_o}{n_o}}, \tag{7}$$

giving a lower limit for the size of the vacuum chamber. At the same time, the parameter space for the plasma density and working pressure at a given implantation voltage U_o is restricted [21,22], leading to a predetermined sheath expansion and ion flux. The upper boundary of the plasma density and, correspondingly, lower limit for the sheath width is given by the maximum allowed electric field E^{max} without arcing. E^{max} is approximately 10 kV/mm for lower pressures [23], depending among others on the specific geometry, i.e. field enhancement at edges or protrusions from the workpiece, and surface properties. For an initial matrix sheath the maximum field can be calculated to be

$$E^{max} = \left|\left(\frac{dU}{dx}\right)_{x=0}\right| = \sqrt{\frac{-2U_o en_o}{\varepsilon_o}}. \tag{8}$$

This dielectric breakdown occurs at the beginning of the voltage pulse, as the sheath width is minimal and concurrently the electric field at the target maximal. When the plasma parameters

are determined, the current density of the ions, accelerated from the plasma sheath edge, can be calculated from the eqns. (4) and (5). For the determination of the power density of the high voltage pulser this current density has to be multiplied with the secondary electron coefficient [24,25] and the total area of the workpiece and sample holder.

3. Implantation in 3-D Workpieces

Even the first publications on PSII elaborate on the possibility of homogeneous implantation in 3-dimensional targets [2,3]. For sheath widths of the order of 10 cm and inhomogeneities in the plasma on the same length scale, this implies limitations for the homogeneity of implantations in large targets or workpieces with curved surfaces. The ions are accelerated perpendicular from the sheath edge, an equipotential surface, by the electric field in the sheath. The field lines are also perpendicular to the surface for metallic workpieces. During the transit through the sheath, the momentum of the ions increases, resulting in a trajectory deviating from curved field lines near the surface and dose inhomogeneities on the target surface and different angles of incidence of the ions. These qualitative considerations were validated by experimental investigations for different test pieces [26,27]. Experiments for determining the dose distribution are very complicated so that computer programs for simulating the implantation were developed. A self-consistent 3-dimensional calculation of the sheath dynamics and ion current is prohibitively time consuming which results in most programs calculating the dose distribution only for the case of an initial ion matrix sheath [28,29]. The sheath dynamic for planar geometry, as given by eqns. (4) and (5) can be extended for cylindrical and spherical geometries [2].

The dose distribution was calculated and measured with Rutherford backscattering spectroscopy (RBS) for a three dimensional object. A cylindrical target with a height of 37 mm and a diameter of 8 mm, representing an M8 drill was used in the experiment. A detailed

description of the simulation procedure, the experimental details, and results is presented in [4].

For obtaining the dose distribution for a given voltage pulse, the sheath expansion is calculated for the known plasma parameters for cylindrical symmetry. Then the contour of the sheath edge, corresponding to the voltage $\varphi = 0$, around the 3-dimensional workpiece with rotational symmetry is determined by solving Poisson's equation with a constant charge density n_c in the sheath, using a set of finite-difference equations solved with the successive over-relaxtion method [30]. This density n_c is adjusted so that the sheath width obtained in the simulation corresponds with the width calculated with the theoretical model for a selected region with cylindrical symmetry around the target. The obtained potential and field distribution is then used for determining ion trajectories and the angles of incidence at the surface. Finally, the flux distribution is calculated from these trajectories using eqns. (4) and (5). Figure 2 shows the calculated edge contour around a target with cylindrical symmetry, representing a drill on a holder, for three times ($t = 0^+$, 3.5, and 8 μs) with a plasma density of $n_o = 6 \times 10^{15}$ m^{-3} and an electron temperature of $kT_e = 2$ eV for a 10 μs rectangular voltage pulse of $U_o = 30$ kV. The calculated flux for the top and the side wall, areas 1 and 2 – 5 in Fig. 2, respectively, is depicted in Fig. 3. For the conditions in our PSII experiments it is sufficient to use the sheath expansion at three discrete times during the voltage pulse for obtaining good agreement between calculated and measured flux distribution. The experimentally observed doses vary by 50%.

The conditions for implantations in a flat target with an 8 mm diameter hole are totally different. The walls of the hole, as expected for sheath widths of several cm, are nearly not implanted as the ions enter the hole nearly vertical and, due to the displacement of the electric field out of the small hole and the large momentum at the end of the trajectory, are hardly deflected.

At the used voltage of $U_o = 30$ kV, the ion trajectories near the target are only slightly modified when a constant charge density is used instead of a charge density according to the Child-Langmuir law. This approximation and the use of discrete snapshots instead of the self-consistent evolution lead to a substantially reduced computing time. It is possible to calculate the flux distribution for workpieces with cylindrical symmetry on PCs which is essential for applications. Convex shaped objects can be implanted by PSII for tribological applications as the measured dose variation is here acceptable in contrast to semiconductor applications.

4. Tribological Properties of Steel

Stainless steels with their excellent corrosion properties have a very broad application range. It extends from food and chemical industry over medicine technology into the private sector. The low hardness of stainless steels, being of the order of $200 - 300$ kp/mm^2 and the large wear in abrasively stressed parts hinder the use of these steels in farther areas, which could be exploited with improved tribological properties and retained corrosion resistance.

Apart from coating methods that are not considered here, it was shown that hardness and wear of stainless steels can be substantially improved with plasma nitriding [6]. Unfortunately comparatively high temperatures are needed in this process, leading to the formation of chromium nitrides at temperatures above 450°C, which bind chromium from the solid solution, and therewith lower the corrosion resistance [6,31]. Nitriding of stainless steel must therefore occur below 400°C, which can be done with PSII.

Four different steels with a high chromium content, 210Cr46, X5CrNi18.10, 42CrMo4, and X20C13, were treated with nitrogen PSII at 350°C for one hour and a dose of 10^{18} cm^{-2}. All samples were treated with 5 µs pulses at a repetition rate of 1 kHz and 40 kV, and the temperature was checked with a pyrometer. Figure 4 shows their relative hardness increase, i.e. hardness after implantation relative to the untreated value, as measured with a

nanoindenter. As can be seen, a substantial hardness increase was observed for all samples for depth up to several micrometer, extending below the maximum depth which could be measured with the available equipment. The observed hardness increase concurs with a substantial wear reduction of the treated samples as shown in Fig. 5. All implantations were repeated with the same dose at a lower repetition rate, yielding a lower temperature of 150°C. Hardness as well as wear exhibited no significant improvement compared to the untreated samples. Glancing angle XRD measurements show that in all samples only a small fraction of the chromium was bound as CrN [32]. Therewith, in spite of the considerable improvement of the tribological properties, the high corrosion resistance of these steels remains [33,34].

A several μm thick very hard layer is found in nitrided steels below the implanted surface region, called "expanded austenite", depending on the treatment time and temperature [35]. Expanded austenite is a metastable phase with nitrogen supersaturation in a solid solution, leading to the increased hardness and reduced wear. A more detailed overview on mechanisms for expanded austenite formation and a discussion of its properties can be found in the work of Williams et al. [36]. For the samples implanted at 350°C the hardness is increased for depths up to several micrometer which is in contrast to the mean projected range of approximately 20 nm for N_2^+ ions. The elevated treatment temperature of 350°C is responsible for the enhanced diffusion. On the other hand at 150°C the diffusion is neglible, resulting in no improvement of the tribological properties for these samples.

The depth of the "expanded austenite" layer is obviously determined by the incorporated amount of nitrogen at sufficiently high doses. For practical applications of PSII the most favorable acceleration voltage has still to be found. An argument for a voltage as high as possible ($\approx$ 30 kV) is the maximum in the sputter yield near an energy of 1.5 keV [37], which leads to an increased material removal and reduced retained dose. On the other hand higher

plasma densities can be used at 2 kV which reduces the sheath width and enables the implantation of smaller structures than at 30 kV [22].

5. Conclusions

PSII has several advantages compared to conventional beam line implantation, e.g. less expensive setup and shorter implantation times. Substantial wear reduction and hardness increase was obtained with PSII at elevated temperatures for steels with a high chromium content. No complicated target handling system is necessary for implantation of three dimensional workpieces, although implantation in small holes, especially in the side walls is still not feasible. The maximum surface area is limited by the size and hence the peak current of the pulse generator. For higher voltages and larger areas local implantation and target manipulation may become again essential.

References

1   G. Dearnaley, *Surf. Coat. Technol., 65* (1994) 1.

2   J. Conrad, J.L. Radtke, R.A. Dodd, F.J. Worzala, and N.C. Tran, *J. Appl. Phys., 62* (1987) 4591.

3   J. Tendys, I.J. Donnelly, M.J. Kenny, and J.T.A. Pollock, *Appl. Phys. Lett., 53* (1988) 2143.

4   S. Mändl, N.P. Barradas, J. Brutscher, R. Günzel, and W. Möller, *Comparison of Measured and Calculated Dose for Plasma Source Ion Implantation in 3-D Objects*, to be published.

5   P.A. Doarnley, A. Namvar, G.C.A. Hibbort, and T. Bell, in E. Broszeit, W.D. Münz, H. Oechsner, K.-T. Rie, and G.K. Wolf (eds), *Proc. 1st Int. Conf. on Plasma Surface Engineering*, Garmisch-Partenkirchen, Sept. 1988, Vol. 1, Deutsche Gesellschaft für Metallkunde, Oberursel, 1989, p. 219.

6   E. Rolinski, *Surf. Eng. 3* (1987) 35.

7   V. Vahedi, M.A. Liebermann, M.V. Alves, J.P. Verboncoeur, and C.K. Birdsall, *J. Appl. Phys., 69* (1991) 2008

8   T.E. Sheridan, *J. Appl. Phys., 74* (1993) 4903.

9   J. Brutscher, *Rev. Sci. Instrum.*, (1996) in press.

10   The Collected Works of Irving Langmuir, edited by C.G. Smits, Pergamon, New York, 1961, Vol. 4, pp. 1-98.

11   M. Widner, I. Alexeff, W.D. Jones, and K.E. Lonngren, *Phys. Fluids, 13* (1970) 2532.

12   M. Shamim, J.T. Scheuer, and J.R. Conrad, *J. Appl. Phys., 69* (1991) 2904.

13   M.A. Lieberman, *J. Appl. Phys., 66* (1989) 2926.

14   D. Bohm, The Characteristics of Electrical Discharges in Magnetic Fields, ed. A. Guthry and R.K. Wakerling, MacGraw-Hill, New York, 1949, p. 77.

15   K.-U. Riemann, *J. Phys. D: Appl. Phys.*, *24* (1991) 493.

16   F. Chen, Introduction to Plasma Physics, Plenum, New York, 1974, p. 244.

17   J. Brutscher, R. Günzel, and W. Möller, *Plasma Sources Sci. Technol.*, *5* (1996) 54.

18   C.D. Child, *Phys. Rev.*, *32* (1911) 492.

19   W. En and N.W. Cheung, *J. Vac. Sci. Technol.*, *B 12* (1994) 833.

20   S. Mändl, J. Brutscher, R. Günzel, and W. Möller, *Sheath and Presheath Dynamics in Plasma Immersion Ion Implantation,* to be published.

21   S. Mändl, J. Brutscher, R. Günzel, and W. Möller, *E-MRS Spring Meeting 1995*, Straßbourg, France.

22   S. Mändl, J. Brutscher, R. Günzel, and W. Möller, *J. Vac. Sci. Technol.*, in press.

23   J. Brutscher, Ph.D. Thesis, Johann Wolfgang Goethe-Universität Frankfurt/M., 1993.

24   G.A. Collins, R. Hutchings, K.T. Short, J. Tendys, and C.H. Van Der Valk, *9th Int. Conf. on Surface Modification of Metals by Ion Beams*, San Sebastian, Spain, 1995, to be published in *Surf. Coat. Technol.*

25   J.P. Blanchard, *J. Vac. Sci. Technol.*, *B 12* (1994) 910.

26   J. Hartmann, W.Ensinger, R.W. Thomae, H. Bender, A. Königer, B. Stritzker, and B. Rauschenbach, *E-MRS Spring Meeting 1995*, Strasbourg, France.

27   S.M. Malik, D.E. Muller, K. Sridharan, R.P. Fetherston, N. Tran, and J. Conrad, *J. Appl. Phys.*, *77* (1995) 1015.

28   T.E. Sheridan, *Appl. Phys. Lett.*, *68* (1996) 1918.

29   M.W. Kissick, M.P. Hong, M.M. Shamin, J.D. Callen, J.R. Conrad, and G.A. Emmert, *J. Appl. Phys.*, *76* (1994) 7616.

30   Los Alamos Accelerator Code Group, The Poisson/Superfish group of codes, LA-UR-87-115, LANL (1987).

31   Z.L. Zhang and T. Bell, *Surf. Eng.*, *1* (1985) 131.

32   C. Blawert, *private communications*.

33   M.E. Chabica, O.L. Williamson, R. Wei, and P.J. Wilbur, *Surf. Coat. Technol., 51* (1992) 24.

34   M. Samandi, B.A. Shedden, D.I. Smith, G.A. Collins, R. Hutchings, and J. Tendys, *Surf. Coat. Technol., 59* (1993) 261.

35   M. Samandi, B.A. Shedden, T. Bell, G.A. Collins, R. Hutchings, and J. Tendys, *J. Vac. Sci. Technol., B 12* (1994) 935.

36   O.L. Williamson, O. Ozturk, R. Wei, and J.P. Wilbur, *Surf. Coat. Technol., 65* (1994) 15.

37   J. Bohdansky, *Phys. Res., 32* (1984) 587.

Figure Captions

Figure 1: Voltage pulse shape and sheath expansion for a planar target. The simulation results with the models for variable [17] and constant [19] presheath are shown for comparison (plasma density $n_o = 1.5 \times 10^{10}$ cm^{-3}, electron temperature $kT_e = 2$ eV).

Figure 2: Sheath contour around an 8 mm cylinder, representing a drill, for three different times 0^+, 3.5, and 8 μs after the start of the pulse. The numbers 1 to 5 indicate the positions where the dose was measured with 1 at the top and 2 – 5 at the side wall [4].

Figure 3: Calculated flux and dose measured with Rutherford backscattering spectroscopy for different points along the surface of the cylinder depicted in Fig. 2 [4].

Figure 4: Relative hardness increase for different steels after 1 hour treatment at an applied voltage of 40 kV.

Figure 5: Specific wear reduction with PSII treatment. The wears test were performed with an oscillating ball-on-disc tribometer, and the volume of the wear tracks is normalized to the total distance. The hatched column of each pair corresponds to the unimplanted and the unhatched column to the implanted state (Note the logarithmic scale).

Fig. 1

Voltage (kV)

Sheath width (mm)

Time (μs)

■ measured data
―― constant presheath
- - - variable presheath

Fig. 2

Fig. 3

Fig. 4

X axis: Depth (μm) — 0.0, 0.5, 1.0, 1.5, 2.0, 2.5, 3.0, 3.5, 4.0

Y axis: Hardness improvement — 1.4, 1.6, 1.8, 2.0, 2.2, 2.4, 2.6, 2.8, 3.0

Legend:
.... 210Cr46
————— X5CrNi18.10
– – – – 42CrMo4
–·–·–· X20Cr13

Fig. 5

Fig. 5

Application and Simulation of Metal Ion Beam Enhanced Deposition

Li Guoqing ,Zhang Tao, Liu Bangzhi , Li Guibin, Ma Tengcai

The Key National Laboratory of Materials Modification , Dalian University of

Technology, Dalian 116023, China

Abstract

The equipment for metal ion beam enhanced deposition is introduced. this is composed of an all-element gas-solid ion source and low energyion sputtering source. The process of metal ion beam enhanced deposition and multi-ion beam enhanced deposition was studied,for examples, pure Ag film on Si plate was prepared by Ag ion beam enhanced deposition , corrosion resistant film (Ti,M)N was prepared by N ion and (M) metal ion beam enhanced deposition and metal-MoS_2 films was studied.

the results show that the pure and alloy films can be prepared on varieous substrates at low temperature and the adhesion of the films to substrates is higher because of a wide mixed interface .

A model of multicomponent ion beam enhanced deposition was presented to simulate the deposition procedure, the relationship between the calculated composition of the film and the atomic arrival ratio has been established, the simulated composition profile of film is in good agreement with experimental results

1. Introduction

Ion beam enhanced deposition (IBED), which is also called ion beam assisted deposition, the bombardment of a thin film with a beam of energetic particles during deposition, provides a powerful technique for modifying the microstructure and properties of thin films and coatings. The earliest description of an ion beam enhanced deposition system appears to be in 1976 [1]. The basic motivation for development of the IBED process in the need for independent control of the major process variables-vapour flux., ion flux, ion energy, system pressure and substrate temperature.[2] At present, by combining evaporation or sputtering .process with ion beam implanting process, a variety of IBED processes were developed,which have the advantages of both processes. High quality films and coatings with high adhesion can be prepared with it.[3]

The so called all-element ion beam enhanced deposition system here is the combination of all-element ion implanter with ion beam sputtering source. Its structure is shown in Fig.1. The all-element ion implanter is capable of extracting gas or metal ion beams simultaneously or seperately, its extracting voltage is about 10-80 kV, the ion current for gas and metal is about 0.25 A and 0.5A respectively. The implanter works in pulse mode, the repetion frequence of which is 10,20 Hz, and the pulse width is 0.4 ms. By combination with ion beam sputtering source, the system not only have the fuction of traditional process of gas ion beam enhanced deposition but also have the function of metal ion beam enhanced deposition and gas-metal multi-ion beam enhanced deposition processes.

Recently, the nanometer magnetic film, metal-MoS₂ composite films, multicomponent alloy films of TiN and the metallization of diamond for preparing heat sink materials were investigated.

Fig. 1 The **MIBED** equipment , including the all-element gas-solid ion implantation system, low energy sputtering deposition system, vacuum system and rotating water-cooled work table

2. Application of metal ion beam enhanced deposition

2.1 Metal-MoS₂ films

Sputtered MoS₂ films are widely used in vacuum and spacecraft as a solid lubricant, but in many cases their wear life and moisture resistance are insufficient. Many studies on overcoming these disadvantages were completed, the matal (Au or Ni) co-deposition with MoS₂ can not only improve its tribological properties, but also enhance its moisture resistance; our recent research indicated that modification of MoS₂ film by metal ion implantation (Ag ion implantation or Mo-S simultanneous ion implantation) is a effective way to improve properties, in fact, the wear life and moisture resistance were increased by a factor over 8 times because implanted Ag impedes the oxidation of of sputtered MoS₂ films in a humid atmosphere and Mo-S implanted can elevate the S/Mo ratio of sputtered MoS₂ film to 1.8.

In consideration of the effects of metal elements, we design a new metal-MoS₂ films solid lubricant, for example, Ag-MoS₂ or (TiMo)N-MoS₂ solid lubricant deposited on bearing steel 9Cr18. It is well known that Ag element is insoluble in Fe substrate and the Ag film is difficultly deposited on bearing steel at low or room temperature.In this paper, the Ag film was firstly deposited on 9Cr 18 steel by Ag ion beam enhanced deposition ,the acceleration voltage of Ag ion was 40kV, the Ag atom sputtered by Ar ion ,whose acceleration voltage was about 2kV and beam current was about 200mA; then the MoS₂ film was deposited with JS-450 rf sputtering system under following conditions: target-substrate distance 4 cm, Ar pressure 6.7×10^{-4} Pa, rf. voltage 2.5kV, d.c. bias voltage 80V, the thickness of the deposited film ranged from 0.8 to 1 μm; at last the films was modified by Ag ion implantation at dose 2×10^{16}cm^{-2}. The microstructure is shown in Fig. 2,. The tribological test in vacuum or air conditions express that the wear life of MoS₂ film

modified by Ag ion implantation were increased 6-8 times; the wear life of Ag-MoS₂ films modified by Ag ion implantation was increased over 20 times compared with that of as-deposited MoS₂ film.

Fig. 2 cross-sectional micrograph (8000 ×) and EDS of Ag-MoS₂ films
modified by Ag ion implantation

2.2 Ag film deposited by MIBED

Silicon plates are widely used in electronic and sensor industry, the sealing technique between Si plates became a hot project. We try to do a test to mount a sensor at low temperature 550-750 ℃. Metal ion beam enhanced deposition was used to prepare Ag film on Si plate and sealing Ag -Ag facing each other at different temperature in vacuum .

Pure Ag film was deposited on Si substrate by Ag ion beam enhanced deposition, the accelerating voltage of Ag ion was 50 kV, beam current was 0.3 A per pulse; the Ar ion beam accelerating voltage of sputtering source was 1.8 kV , its current was 180 mA.The thickness was about 0.5μm.

The adhesion of Ag film to Si substrate was measured by CRS-01 scratch tester, the critical load shown in Fig. 3 is as high as 1500 gf, the analyses results of AES shown in Fig.4 and X-ray shown in Fig.5 express that there is a mixed interface of about 500 Å between the film and the substrate, which is the main factor contributing to the enhanced adhesion. The sealing stress of samples sealing at different temperature 500,600,700,800 ℃ were tested and is shown in Fig.6. The best process can be selected from above tests.

Fig.3 the adhesion of Ag film to substrate   Fig.4 composition profile of AES analysis
measured by CRS-01 scratch tester, critical   mixed interface about 500Å
load was about 1500 gf

Fig.5 the analysis result of X-ray
samples

Fig. 6   the sealing stress analyses of

at different temperature

2.3 Multi-ion beam enhanced deposition

As the gas-solid source can generate gas ions and metal ions simultaneously, when both the gas ions and metal ions bombard the specimens while a film is being formed on the specimens by ion sputtering, a multielement film is prepared by multi-ion beam enhanced deposition. The metal ions,gas ions and the sputtering target can be chosen as required. Different films for different purposes can therefore be prepared in this way.

To prepare corrosion-resistant and wear- resistant films, both an N ion beam and a metal ion beam was used to bombard the specimen during Ti film deposition by ion sputtering. The ratio of N ions to metal ions can be regulated by the voltage of the gas arc and metal arc. In this paper TiN, (TiMo)N, (TiCr)N, (TiZr)N, (TiY)N and (TiNi)N were prepared, the content of metal ion in films was controlled as less as 10%, the analyses results of XRD express that the alloy elements were all soluble in crystal of TiN as shown as Fig.7.

Fig.7 XRD analyses results

Table 1 lists the hardness, adhesion and corrosion resistance of films, the hardness were measured by DMH-21S micro hardness tester, loading 5gf; the adhesion of films was measured by a CSR-01 scratch tester, the loading speed used was 5000 gf min^{-1}; the anode polarization of films in 0.5 M H_2SO_4 were tested .

Table 1 the properties of hardness,adhesion and corrosion resistance

Films	Hardness	Critical load gf	Self-corrosion E mV	Self-corrosion I $\mu A/cm^2$
TiN	1620	2150	-141.4	1.01
(TiMo)N	1580	3150	-300.42	1.95
(TiCr)N	1540	2350	304.8	0.04
(TiZr)N	1560	2400	279.4	0.13
(TiY)N	1490	2100	306.0	0.07
(TiNi)N	1510	2500	-176.5	3.21

It can be seen that there are different behaviors of films , in which, the adhesion of film deposited by multi-ion beam enhanced deposition is superior to that of film deposited by IBED, specially, (TiMo)N is of the best adhesion to substrate because of Mo ion with higher charge and energy and because the radius ratio of nitrogen Vs Mo is equivalent to that of nitrogen Vs Ti ; the films of (TiCr)N, (TiZr)N,(TiY)N have better corrosion resistance in 0.5 M H_2SO_4 solution.

The process of multi ion beam enhanced deposition is a multifuctional process which makes it possible to prepare films with special properties and is widely used to workpieces with low tempering temperature.

3. Dynamic Monte Carlo simulation for multi-ion beam enhanced deposition

The process of two kinds of ions implanting into the deposition film need to be considered in view of understanding full and effectively controlling the process of multi-ion beam enhanced deposition. In this paper. a dynamic Monte Carlo simulation program is introduced and a model of dynamic target is used to simulate the concentration change of the target.

The multi-ion beam enhanced deposition process is actually a simultaneous and continuous process of implantation and deposition. To simulate the process, implantation and deposition are treated as being alternatively carried out, and the deposition film is subdivided into layers thin enough to approximate to the actual continuous process. The number of implanting ions of one group are decided according to the deposition rate and ion dose. The effect of gas absorption on the film growth is considered also in the model. The sticking speed of nitrogen molecular on the substrate surface is evaluated by using the following formula:

$$ \beta = \frac{\delta a^2}{2} \left(\frac{h^2 + k^2 + l^2}{2 \pi M K T} \right) \cdot \eta_{hkl} \cdot \rho \cdot t $$

where δ is a constant, a is the lattice constant of substrate, η_{hkl} is the coefficient of gas molecular sticking to the (hkl) facet, T is gas temperature, K is Boltzmen constant, M is gas mars. Under our experiment condition, the time order for covering a half of the substrate surface is estimated by 10^{-2} sec. There fore, the sticking speed is comparatively fast and the nitrogen content of the film mainly come from gas surface adsorption, the part provided by N^+ ion implantation is small comparatively.

Like wise, the substrate was also subdivided into layers to compute the constituents across the interface. The density and content of one layer is rearranged according to the number of every kinds of atoms in the layer after the simulation of ion implantation into one layer is finished.

Fig. 8 shows the program organization of the simulation of N, Mo ions implanting into Ti film deposition onto Fe substrate. The parameters are present

according to the experiment condition . Accelerating voltage of ion beam is 40 kV, the film and the target are subdivided into layer of 4nm thickness. 12 psedoprojectiles per layer for Mo ion and N ion each for a total dose of 1.2×10^{16} ions cm^{-2} each in the study. The deposition rate of Ti atoms is 100 A min^{-1} . The ratios of different ion charge state of Mo element and N element are

$$Mo^+ : Mo^{2+} : Mo^{3+} : Mo^{4+} = 2 : 6 : 3 : 1$$
$$N^+ : N_2^+ = 8 : 4$$

Fig. 9 shows the simulation results of profile content distribution, the amount of N in the film is relatively high, which is in agreement with the analysis result of experiment. It can be also seen that across the interface there are quotation of N atoms and Mo atoms, it results from the cascade collision between incident ions and target atoms leading to the mixing between film and substrate.

Fig.8 program organization

Fig.9 simulation results and AES analysis of (TiMo)N film
simulation: ....N, ----Fe, _._Mo, — Ti
AES : : o Ti, △ Fe, ● Mo

4. Conclusion

The equipment for and process of metal ion beam enhanced deposition is multifunctional and efficiently used to prepare films with special properties, in which the wear life of metal-MoS2 solid lubricant was increased over 20 times compared with that of rf.deposited MoS2 film; the Ag film deposited by Ag ion beam enhanced deposition was used for mounting technique of sensor, its sealing stress can be get to 8 MPa; a model of multi ion beam deposition was presented to simulate the deposition procedure, the relationship between the calculated composition of the film and the atomic arrival ratio has been established, the composition profile obtained by computer simulation is in good agreement with the experimental results, this is significant for ion beam processing of film composition and structure.

References

1.D.K.Sood and G. Dearnaley. Inst. Phsy. Conf. Ser. 28 (1976)

2 A.A.Galska. J. C. UHT and P. M. Adaias, J. Vac.Sci. Technol. A, 6(1)(1988)99.

3 Guoqing Li,Xiaowei su and et al, Surf.and Coat. Technol. 66(1994)350-354

4 G. Dearnaley, Nucl. Inst. and Meth.Phys. Research,B 50 (1990) 358-367

5 Huiwen Liu and et al, Wear 173 (1994) 145-149

Fig 1

gas

metal ion source
metal ion beam
sputter target
Ar ion beam
gas
sputter source

work table   atom beam

Application
and simulation
of MIBGD

Fig 2

0 CH1   10340 EV   20 EV/CHAN
Link Systems 860 Analyser   27/16 85

Si Ag MoS$_2$

Si Ag MoS$_2$

Si

Mo(L)
S

Cu

Ag

Fe

Au

Mo(K)

0.1   05 76   20.0
KLM MARKERS FOR Z =   0 <   5

Fig 3

Fy [gf]

150
100
50
0

0   600   1200   1800   2400

Fz [gf]

Fig 4

At %

100

50

0

Si

Ag

0   200   400   600

TIME(sec)

Fig 5

Si[220]

Ag[220]

Ag[311]

2θ

Fig 6

sealing at 800°C

sealing at 700°C

sealing at 600°C

sealing at 500 C

stress [MPa]

Fig 7

TiN

(TiMo)N

(TiCr)N

(TiZr)N

(TiY)N

(TiNi)N

TiN(220)

TiN(200)

TiN(111)

2θ

Intensity

preset parrameters

simulation of N ion induced cascade collion process

is it the end of N ion implantation into one layer — N

simulation of Mo induced cascade collion process

is it the end of Mo ion implantation into one layer — N

rearrange the density of target

rearrange the content of target

deposit one layer of Ti atoms

Is It the last layer of the film — N

END

Fig 9

COMPOSITION At.%

DEPTH (Å)

Formation of Nanometer Magnetic Iron Nitride Films by IBED

Li Guibin, Li Guoqing , Lei Minkai and Liu Bangzhi

Key National Laboratory of Materials Modification, Dalian University of Technology
Dalian, 116023, China

Abstract

A series of magnetic iron nitride films in nanometer scale were synthesized by Ion Beam Enhanced Deposition(IBED) method. The composition and structure of the Fe-N films were assessed by TED,TEM and XRD, the magnetic properties were verified using Vibrating Sample Magnetometer(VMS),. The results shown that it was possible to prepare films containing α''-$Fe_{16}N_2$ phase which possesses a high Ms value by IBED. The films consist of α-Fe, α''-$Fe_{16}N_2$, γ'-Fe_4N and ε-$Fe_{2,3}N$ phase or mixture of these phases under different deposition parameters, the magnetic properties dramatically depended on the phase structure and composition of films.

1. Introduction

In recent years, Ion Beam Enhanced Deposition (IBED) is widely used in the preparation of magnetic films as a new surface modification and optimization technique in which ion implantation and film deposition were combined perfectly. IBED method has several advantages to synthesize films, namely the independent control of atom deposition and ion implantation parameters, the possibility of forming thick film of consistent composition; the possibility of growing film at room temperature and the possibility of forming metastable phase [1].

Iron nitride films present several magnetic properties that make them good candidates of magnetic recording heads and media. In the Fe-N system, there exist many phases including γ-austenite, α'-martensite, α''-$Fe_{16}N_2$, γ'-Fe_4N, ε-$Fe_{2,3}N$ and η-Fe_2N. Among these, α'-martensite, γ'-Fe_4N and ε-$Fe_{2,3}N$ exhibit ferromagnetism at room temperature, especially, the a''-$Fe_{16}N_2$ nitride displays a saturation magnetization more higher than pure iron. Besides the magnetic properties the iron-nitrides exhibit also good corrosion durability, surface hardness and wear resistance [2,3]. Some work have been done on the magnetic properties of iron nitride films prepared by the IBED technique[1,4,5,6]. For different IBED equipment, the relationship between deposition parameters and phase formation and the influence of phase formation on magnetic properties is quite different. Almost all IBED equipment have ion sources to extract N-ions. If the energy and the dose of N-ions extracted from ion sources are controlled appropriately, metastable compounds which can not be produced by thermochemical processes can be synthesized. Few researcher, however, have studied high-energy(>10kV) N-ion bombardment in the processing of Fe-N films by IBED.

We report here on the preparation of a series of nanometer scale magnetic iron nitride film by using an all-element IBED system which possesses an ion source of high extraction

voltage. The influence of N-ion dose and substrate temperature on the phase formation were investigated and the magnetic properties of the film were measured.

2. Experimental Details

Experiments were performed in a IBED system consisting of an all element gas-solid ion source, low energy ion sputter source, vacuum system and rotating water-cooled work table etc., as shown in Fig. 1 [7]. To prepare the films, an energetic Ar ion beam extracted from sputter source bombards the iron sputtering target, and the Fe atoms deposit onto the surface of substrate. Simultaneously, the N-ions extracted from the ion source bombard the deposited iron film.

Fig. 1. The IBED system , including an all element gas-solid
ion source,a low energy ion sputter source, vacuum system
and rotating water-cooled work table.

The extraction voltage of the ion source is about 10-80 KV, the N-ion current is about 0.1-0.2 μA, the pulse repetition is 10 Hz, the pulse width is 400 μs. The accelerating voltage of the low energy ion sputtering source is 1.2-2 KV, the beam current is 100 mA, the deposition rate is about 0.15 Ås^{-1} for Fe atom.

A base pressure of 8×10^{-3} Pa of the vacuum system was achieved by using a turbomolecular pump. The partial pressure of N_2 gas (99.999%) was 2×10^{-2} Pa with the ion source operating, the purity of the iron target is 99.95%. Film thickness is 700-1000 Å. Table 1 lists the experimental conditions for sample preparation.

The single crystal Si and GaAs wafer were selected as substrates. Before the deposition, the substrates was bombarded by the N-ions for about 10 minute in order to clear the impurity on the substrate surface.

The structure and composition of the film were assessed by X-ray diffraction (XRD), transmission electron diffraction (TED) and transmission electron micrographs (TEM). The magnetic properties were studied at 5 KOe using vibrating sample magnetometer(VMS) which was calibrated with a standard nickel sample

TABLE 1   Experimental conditions for film preparation

Sample No.	Substrate	N-ion Energy (keV)	N-ion Dose (10^{17} cm^{-2} h^{-1})	Temperature (℃)	Film Thickness (Å)
1	Si	0	0	RT	700
2	Si	40	0.38	RT	700
3	Si	40	1.3	RT	700
4	Si	40	2.5	RT	700
5	Glass	40	1.4	250	700
6	GaAs	15	2.5	300	1000

3. Results and Discussion

3.1 Phase

3.1.1 The Phase Formation at Room Temperature

Fig.2 shows the XRD data and Fig.3 indicates TED patterns and TEM micrographs taken at room temperature (RT) for the four films under different doses of N-ion(I_{N2}).Not all the phases seen with XRD are also seen with TED. This shows that XRD or TED alone sometimes is not sensitive enough for phase identification and may explain some of the confusion in previous works attempting to clarify the magnetic properties of Fe-N films. At I_{N2}=0, XRD shows that α-Fe with a (110) preferential orientation is observed. With the bombarding of N-ions , iron nitrides were found in the film. At I_{N2}=3.3 × 10^{17} cm^{-2} h^{-1}, the diffraction data show two phases α-Fe and α''-Fe$_{16}$N$_2$, and possibly from the very weak (103), (110) lines of a very small amount of ε-Fe$_{2.3}$N phase. The two x-ray diffraction peaks present at the 2 θ position of 28.5°and 42.7° (Fig.2 b) correspond to the (002) and (220) family planes of α''-Fe$_{16}$N$_2$ phase, a rough estimation from XRD intensities indicate that the fraction of α''-Fe$_{16}$N$_2$ phase in the film is over 40 vol%. At I_{N2}=1.3 × 10^{17} cm^{-2} h^{-1} the phases in the sample were mainly ε-Fe$_{2.3}$N with small amount of α-Fe phase. At I_{N2}=2.6 × 10^{17} cm^{-2} h^{-1}, the dominant phase is the lattice-expanded ε-Fe$_{2.3}$N with the increasing nitrogen content, the retained α-Fe phase is still observed.

Fig.2. X-ray diffraction data for the Fe-N films formed at room temperature(RT) (a) I_{N2}=0. (b)I_{N2}=0.38 × 10^{17}cm^{-2}h^{-1} (c) I_{N2}=1.3 × 10^{17}cm^{-2}h^{-1} (d) I_{N2}=2.5 × 10^{17}cm^{-2}h^{-1} (e) additional N-ion implantation of (d) with dose 1.3 × 10^{17}cm^{-2}

Fig.3. TED electron diffraction patterns and TEM micrographys for the Fe-N films formed at room temperature(RT) (a) I_{N2}=0. (b)I_{N2}=0.38 × 10^{17}cm^{-2}h^{-1} (c) I_{N2}=1.3 × 10^{17}cm^{-2}h^{-1} (d) I_{N2}=2.5 × 10^{17}cm^{-2}h^{-1}

To further investigate the dependence of phase formation on N-ions dose,for the sample of I_{N2}=2.6 × 10^{17} cm^{-2}h^{-1}, an additional 40kV N-ion implantation with dose of 1.3 × 10^{17} cm^{-2} h^{-1} was carried out . The results shows that not only ε-Fe$_{2.3}$N transformed into η-Fe$_2$N, but also some amount of γ'-Fe$_4$N and α''-Fe$_{16}$N$_2$ phase were formed after implantation (Fig.2 e).Apparently, γ'-Fe$_4$N and α''-Fe$_{16}$N$_2$ was transformed from the retained α-Fe phase in the film.

The above results indicate that it was an effective method to fabricated iron nitride film containing α''-$Fe_{16}N_2$ metastable phase with low dose and high energy N-ion bombardment by IBED. With the increase of I_{N2}, it is almost impossible to form α''-$Fe_{16}N_2$ metastable phase furthermore due to strong thermal spike and shift spike effects[1]. The TED patterns and micrographys(Fig.3) show that the grain grows with the increase of N content in the films. It proved that grain growth is proportional to dose for IBED[1]. However, for the same sample, the grain size of ion nitride is homogeneous in the film with 10-20 nm sizes. Therefore, the typical nanometer polycrystalline iron nitride films were synthesized by our IBED system.

3.1.2 The Phase Formation During Heating Process

Compared to the phase formation at room temperature, the phase composition is quite different as the substrates is heated. At T=250°C,I_{N2}=1.42 × 10^{17} cm^{-2}h^{-1}, the phases were ε-ε-$Fe_{2.3}N$ and γ'-Fe_4N(Fig.4.a)(process: after N-ion implantation of 0.94 × 10^{17} cm^{-2}, the substrate was being heated while the film deposition continue, the heating time is about 30 minutes). At T=300°C, I_{N2}=2.5 × 10^{17} cm^{-2} h^{-1}, the main phases is α-Fe and γ'-Fe_4N, in addition, a small amount of ε-$Fe_{2.3}N$ was found (fig.4 b).

Fig.4 . X-ray diffraction data for the Fe-N films formed during heating process
(a) I_{N2}=1.4 × 10^{17}cm^{-2}h^{-1}, T=250°C (b)I_{N2}=2.5 × 10^{17}cm^{-2}h^{-1} , T=300°C

These results show that substrate temperature is very important to the phase formation of the film. As it is well know, IBED is a nonequilibrium and dynamic mixing process. Heating substrate not only changes the film deposition but also increase the disabsorption of N atom [1].In contrast with the films deposited at room temperature, γ'-Fe_4N, which has less N content than ε-$Fe_{2.3}N$, is formed more easily on the heated substrates. Concerning with the structure of ion nitrides, γ'-Fe_4N phase exhibits f.c.c structure while ε-$Fe_{2.3}N$ is h.c.p. structure , it seemed that heating process are more suitable for the formation of f.c.c. structure.

3.2 Magnetic Properties

The value of Ms vs I_{N2} is shown in Fig.5. At I_{N2}=0, Ms equals to 202 emu/g, within experimental error equal to the bulk room temperature value for α-Fe of 212 emu/g. As I_{N2} increases, Ms increases reaching a maximum of 245 emu/g at I_{N2}=0.37 × 10^{17} cm^{-2} h^{-1}. The increase is ascribed to the effects of α''-$Fe_{16}N_2$ phase formation. From the estimation of XRD intensities, the calculated value of α''-$Fe_{16}N_2$ is 310 emu/g which is in good agreement with the measured value of 315 emu/g [8]. For I_{N2}>1.3 × 10^{17} cm^{-2} h^{-1}, Ms decreases dramatically

and drops to 65 emu/g at I_{N2}=1.3 × 10^{17} cm^{-2} h^{-1} and 61 emu/g at I_{N2}=2.5 × 10^{17} cm^{-2} h^{-1} due to the formation of ε-Fe$_{2.3}$N phase.

Fig.5.The *Ms* value of films vs I_{N2} (a) I_{N2}=0.
(b)I_{N2}=0.38 × 10^{17}cm^{-2}h^{-1} (c) I_{N2}=1.3 × 10^{17}cm^{-2}h^{-1}
(d) I_{N2}=2.5 × 10^{17}cm^{-2}h^{-1} (e) additional N-ion
implantation of   (d) with dose 1.3 × 10^{17}cm^{-2}

However, for the sample of I_{N2}=2.5 × 10^{17} cm^{-2} h^{-1}, *Ms* increases suddenly to 215 emu/g after additional N-ion bombardment. *Ms* also increases near to Fe when the substrate was heated at I_{N2}=2.5 × 10^{17} cm^{-2} h^{-1}. These changes in observed *Ms* can also be correlated with the structure data. Fig.4(b) shows that the retained α-Fe has been converted to the γ'-Fe$_4$N and α''-Fe$_{16}$N$_2$. This explained the increased *Ms* after additional *N*-ion bombardment. The film prepared on a heated GaAs substrate atI_{N2}=2.5 × 10^{17} cm^{-2} h^{-1} was mainly composed of α-Fe and γ'-Fe$_4$N and as expected the measured *Ms* has a slight change within the experimental error compared with α-Fe.

4. Conclusion

In summary, nanometer scale iron nitride magnetic films have been synthesized by an all-element IBED system.α''-Fe$_{16}$N$_2$ phase was formed in the films under bombardment with low dose and high energy N-ion. The dose of N-ions and substrate temperature have a strong influence on the phase formation of ion nitride films while the magnetic properties dramatically depend on the phase structure.

Acknowledgements

Reference

1. F.A.Smidit, Inter. Mat. Rev. 1990 Vol. 35 No.2, 61-128

2. M.Naoe, M. Nagokubo and T. Yamamoto, J. Appl. Phys. 64(1988) 5449

3. K.Umeda, E. Kite and A. Tasaki, IEE Trans. Magn. MAG-22(1986) 591 .

4. D.H. Mosca, P.H. Dionisio, W.H. Schreiner, I.J.R. Baumvol and C.Achete, J. Appl. Phys. 67(1990)7514

5. R.Hübler, S.R. Teixeira, W.H. Schreiner and I.J.R. Baumvol, Nucl. Instr. and Meth. B 80/81 (1993)1392-1396

6. Hai Jiang, Kun Tao and Hengde Li, J. Phys. Condens. Matter 6(1994) L279-L286

7. Guoqing Li, Xiaowei Su, Zexiang Gong, Bangzhi Liu, Xueya Wen and Tengcai Ma, Surface and Coatings Technology, 66(1994) 350-354

gas

metal ion source
metal ion beam
sputter target
Ar ion beam
gas
sputter source

Fig.1

work table atom beam

intensity

a

α-Fe(110)

b

α-Fe(110)

α"-Fe16N2 (220)

α"-Fe16N2 (002)

α-Fe(211)

c

ε-Fe2,3N(101)

ε-Fe2,3N(020,210)

α-Fe(110)

ε-Fe2,3N(102)

α-Fe(211)

d

ε-Fe2,3N(101)

ε-Fe2,3N(020,210)

ε-Fe2,3N(102)

α-Fe(211)

e

η-Fe2N(211)

γ'-Fe4N (111)

η-Fe2N(112)

α"-Fe16N2 (220)

α"-Fe16N2 (002)

η-Fe2N(321,230)

η-Fe2N(022,212)

20   30   40   50   60   70   80   90 95

2θ

Fig.2.

α-Fe(110)

α-Fe(211)
ε-Fe2,3N(103)
ε-Fe2,3N(110)
α-Fe(200)
α-Fe(110)
α"-Fe16N2 (220)
α"-Fe16N2 (002)

α-Fe(211)
ε-Fe2,3N(103)
ε-Fe2,3N(110)
ε-Fe2,3N(102)
α-Fe(110)
ε-Fe2,3N(101)

α-Fe(211)
ε-Fe2,3N(103)
ε-Fe2,3N(110)
ε-Fe2,3N(102)
ε-Fe2,3N(101)

Fig.3. TED electron diffraction patterns and TEM micrographys for the Fe-N films formed at room temperature(RT) (a) I_{N2}=0. (b)I_{N2}=0.38 × 10^{17}cm^{-2}h^{-1} (c) I_{N2}=1.3 × 10^{17}cm^{-2}h^{-1} (d) I_{N2}=2.5 × 10^{17}cm^{-2}h^{-1}

Fig.4.

Fig. 5

MODIFICATION OF AIRCRAFT ENGINE COMPRESSOR BLADES PROPERTIES BY UNINTERRUPTED AND PULSED ION BEAMS *

V. A. Shulov[a], N. A. Nochovnaya[b], G. E. Remnev[c], A. I. Raybchikov[c]

[a] Moscow Aviation Institute, 4, Volokolamskoye shosse, 125871, Moscow, Russia

[b] All- Russian Institute of Aviation Materials, 17, Radio Street, 107005, Russia

[c] Nuclear Physics Institute, 2a, Lenin Street, 634050, Tomsk, Russia

Abstract

The influence of uninterrupted and arc- pulsed ion implantation, high- power ion beam treatment and final annealing dregimes on chemical composition and phase- structural state of surface layers and on surface properties of gas turbine engine compressor blades manufactured from refractory alloys was investigated. Long- term full- scale tests of the production and irradiated compressor blades in gas turbine engine operating conditions were carried out. After completing tests the physical- chemical state of the blades was studied.

Keywords: Ion beam: Refractory alloys: Service properties

1. Introduction

The elaboration of the most advanced technological methods for surface processing of gas turbine engine parts manufactured from refractory alloys is one of the important problems of the aviation material science. It is attributed by high cost and great responsibility of these parts exposed to simultaneous force of constant and cyclical loads, gas oxidation and sulphidization at high temperature, particle and hydro- abrasive erosion. Exactly the turbine and compressor blades determine the duration of gas turbine engine operation. The ion- beam treatment is the most advanced method for surface processing of machine parts. There are ion implantation by uninterrupted beams (IIUB) [1], arc- pulsed implantation (API) [2] and high power pulsed ion beams (HPPIB) treatment [3]. The perspectives of IIUB, API and HPPIB application in aircraft building industry were analyzed in [4-6] on the base of experimental results obtained by surface state researches of refractory alloys model samples irradiated by ion beams.

+ Corresponding author. Fax: 197095 158 29 77, e- mail: surface @ k208. mainet. msk. su

In this connection the arm of the present paper is the investigation of ion- beam treatment influence on the surface condition of aviation engine compressor blades and on their properties including discussion of the long time engine tests results.

2. Experimental

The blades of gas turbine engine compressor (3,7,8 and 9th stages) were manufactured from refractory alloys (VT9- $\alpha+\beta$- titanium alloy; VT25U- pseudo-α- titanium alloy; EP866sh- carbide strengthened steel; EP718ID- nickel- iron alloy [4-6]).The uninterrupted rotating blades have been irradiated by the C, N, B, La, La and B (LaB$_6$), Sm and Hf- ions employing the following accelerators: ILU-4, DELTA, Raduga [7] and Temp [8]. The irradiation regimes (Table 1) have been chosen according the results of ion- beam treatment optimal regimes determination as it was made using the thermodynamical methods [5] and generalizing from the experimental data published in [4-6] for model samples. Surface conditions of the initial and irradiated blades have been studied by Auger electron spectroscopy (AES), scanning electron microscopy (SEM), X- ray diffraction analysis, optical microscopy and exo- electron emission (EEE). Furthermore, roughness and microhardness of the blade surface have been measured (R$_a$, H$_\mu$). The total set of these researches has repeated after the final annealing (P= 10^{-1} Pa, T= 450- 650 ^{0}C, τ= 2 hours). Then the blades passed long- term full- scale tests in gas turbine engine operating conditions (Table 1).After completing of these tests the surface layers of the blades were investigated by the EAS, SEM, X- ray analysis methods and there were determined the following properties: fatigue strength (σ_{-1}, Mpa, loading frequency- f= 1800- 3000 Hz, temperature- T= 450- 600 ^{0}C, air,the base of tests- 2×10^7 cycles), oxidation resistance (h$_0$- thickness of oxidized layer), erosion resistance (Δm/ S$_{er.}$, quartz sand- d= 80- 120 μm, speed of particles- V= 200 m s^{-1}, sand load- p= 20 mg mm^{-2}, angle of impact- α= 90^0)*. The eroded surfaces of the blades and the fatigue cracks have been studied by the SEM- fracture method [8,9].

3. Results

Some results of investigations and tests are presented in Tables 2 and 3 and in Fig. 1-5. Comparing these data with the results published in [4-6] the following conclusions can be made: (i) the usage of low current ion beams (j~10 μA cm^{-2}) allows to alloy surface layers with thickness from 30 nm (heavy ions) to 0.3 μm (light elements) besides the processes of phase formation (fine dispertional precipitations of carbides, borides, oxides

* The blades irradiated by the B, LaB$_6$, Sm and Hf- ions were not tested in gas turbine engine.

and nitrides are formed) and defect formation (concentrations of point and linear defects change) take place in the near surface layer with thickness h~ 1 μm during ion implantation and final heat treatment; (ii) the most homogeneous state in surface layers is formed in the process of the light ions IIUB at high values of current density (j>1 mA·cm^{-2}) and doses (D>10^{19} ion·cm^{-2}), in addition a depth of ion penetration into a matrix achieves ~6 μm and an amorphous state is formed in this layer (in this case the blades were heated up to 600- 700 $^{\circ}$C in spite of their compulsory water- cooled); (iii) the distinction between IIUB and API shows itself by formation of near surface zones had great concentrations of implanted components (more 70 at.%) and impurities (C, O), if the pulsed regime of implantation is used, and by the increase of the more thick modified layers (h~1-4 μm). Most likely, the latter was connected with the thermal effects took place during high current irradiation in a pulse (j~0.2-0.5 mA·cm^{-2}); (iv) HPPIB treatment of the compressor blades in the melting regimes (j≤ 60 A·cm^{-2}) and the final annealing allow: to decrease roughness considerably (up to R$_a$= 0.06 μm); to eradicate micro- defects of surface that it is important for parts having the sharp edges; to increase the strength of material in account to the fine dispertional carbide precipitations formation in the layer with thickness of 0.2 μm and at the expense of the defect composition increase as a result of shock waves spreading into a matrix (h~100 μm); to form a homogeneous stable structure in surface layer (the average grain size of the titanium alloy blades surface layers was equal to 40-60 μm [6]; to seek a considerable decrease of the interplate distance during the annealing.

The variations of the blades surface layer physical- chemical state have determined the operation behavior of these blades in the process of their tests in gas turbine engine.

Using the prolonged machine test results it was shown that the following service properties of the blades (7,8 and 9th stages) can be improved by the IIUB (La, B) despite a small thickness of modified surface layers: σ$_{-1}$- (by 10-40 %); h$_0$ (more than 2 times); Δm/ S$_{er}$- (by 40-200 %).This effect is attributed to a lack of erosion force on the surface of the compressor last stage blades in the course of the tests. As a result the thin surface layers modified by ion beams have been preserved all the running time. The changes of these properties, however, were caused by the next reasons: a variation of fatigue crack formation mechanism from "surface "
(Fig. 5a) to "under surface "(Fig. 5b) or a decrease of the fatigue furrows step during a passage of the fatigue crack through a grain; formation of the La$_2$O$_3$ and CrN- barrier layers preventing diffusion of oxygen into a matrix; formation of residual compress stresses in the thin surface layer (h~1 μm) that ensures the increase of incubatory period during the erosion fracture.

At the same time the test results of the compressor third stage blades, for which the erosion force became the main factor of fracture ever at first of operation, showed that ion implantation can not ensure the statistic

significant improvement of blade properties. Furthermore, even some decrease of operating characteristics of the third stage titanium alloy blades treated by uninterrupted ion beams took place (Table 3). The latter caused the fracture of the thin strengthened layer in the beginning of tests (particularly, erosion load is a great in the zones of the blade entrance edges, Fig. 6). As a result over a long period of operation already the under surface layer have been exposed to a load where the residual tensile stresses were formed during irradiation [6,8,9]. The data obtained after the tests of titanium blades irradiated by HPPIB allow to conclude that ion- beam treatment must be carried out at low values of ion current density (j=60 $A \cdot cm^{-2}$). In this case the HPPIB treatment enables to improve: σ_{-1} - by 30%; $\Delta m/S_{er.}$ - more than 2 times; h_0 - more than 9 times. At the same time the irradiation at high values of ion current density leads to a great decrease of the service properties level. It was caused by the micro- heterogeneities having a form of craters (diameter- 5-100 μm; a depth- 0.5-2 μm) during the HPPIB treatment at high values of ion current density. The formed craters are surface concentrations of stresses and it leads to formation of micro- cracks (or even a crack net) during irradiation or operation of the blades. The reasons and mechanisms of crater formation are presented in [11,12].

4. Conclusion

It was shown using the prolonged engine tests and the researches of irradiated blades surface layer state that the usage of uninterrupted and arc- pulsed implantation allows to improve the service properties of these parts dramatically if the erosion force is absent during operation. The HPPIB treatment has the better perspectives of application in aircraft engine building in comparison with ion implantation because the usage of high power ion beams ensures the modification of more thick surface layers and formation of record low values of surface roughness.

References

[1] G.K. Hirvonen, Ion Implantation, Moscow: Metallurgy, 1985. p.391.

[2] A. I. Ryabchikov and R. A. Nasyrov, Nucl. Instr. and Meth., in Phys. Res., B61(1991) 48-51.

[3] K. Yatsui, Laser and Particle Beams, 7(1989)4, 733-741.

[4] G. E. Remnev and V.A.Shulov, Laser and Particle Beams, 11(1993)4, 707-731.

[5] V. A. Shulov, Universities News. Physics (in Russian), 6(1994)72-91.

[6] V. A. Shulov, N. A. Nochovnaya, G. E. Remnev, F. Pellerin, 9th Int. Conf.on SMMIB, San-Sebastian- Spain, September 4-8, Abstracts, p. 69.

[7] A. I. Ryabchikov and N. M. Arzubov, Rev. Sci. Instrum., 63(1992)1, 2428-2430.

[8] V. A. Shulov and A. E. Strygin, Problems of Strength (in Russian), 11(1990) 40-46.

[9] V. A. Shulov, A. E. Strygin, A. M. Sulima, Wear and Friction (in Russian), 11(1990) 1030-1038.

[10] Ronghua Wei, 9th Int. Conf.on SMMIB, San-Sebastian- Spain, September 4-8, Abstracts, p. 48.

[11] V. A. Shulov, G. E. Remnev, N. A. Nochovnaya, Surface (in Russian), 12(1993) 110-121.

[12] V. A. Shulov, G. E. Remnev, N. A. Nochovnaya, Surface (in Russian), 6(1995) 77-91.

Fig. 1. The element distributions in the surface layer of the blades manufactured from the VT9 alloy after ion

implantation of B (D= 2×10^{17} ion cm^{-2}) and annealing (500 ^{0}C, 2 hours, vacuum):

Δ- Ti; ●- C; O- O; □- Al; ×- B.

Fig. 2. The element distributions in the surface layer of the blades manufactured from the VT9 alloy after ion

implantation of Sm (D= 5×10^{17} ion cm^{-2}) and annealing (500 ^{0}C, 2 hours, vacuum):

Δ- Ti; ●- C; O- O; □- Al; ×-Sm.

(a)

(b)

Fig. 3. SEM micrographs of the VT25U titanium alloy blades surface: a- production blades; b- the blade after HPPIB treatment (j= 60 A cm^{-2} ; n= 20 pulses).

(a)

(b)

Fig. 4. SEM micrographs of the VT9 alloy blades surface after the prolonged tests in gas turbine engine: a- HPPIB treatment (j= 160 A cm^{-2}); b- HPPIB treatment (j= 60 A cm^{-2}).

(a)

(b).

Fig 5. SEM micrographs of fatigue fracture surface of the EP718ID alloy blades after the prolonged tests in gas turbine engine: a- production blade; b- the blade irradiated by N.

Fig. 6. SEM micrograph of the VT9 alloy blade surface in the zone of the entrance edge after the prolonged tests in gas turbine engine.

№	Material of blades, stage	Ion	E keV	j µA·cm^{-2}	f Hz	τ µs	D ion·cm^{-2}	n pulses	Running time t, %
1	VT9, 3	B	40	20	-	-	10^{17}	-	-
2	VT9, 3	B	40	20	-	-	2×10^{17}	-	-
3	VT9, 3	B	40	20	-	-	3×10^{17}	-	-
4	VT9, 3	N	40	20	-	-	2×10^{17}	-	850
5	EP866sh7	N	40	5×10^3	-	-	2×10^{19}	-	600
6	EP866sh7	La	30	20	-	-	10^{17}	-	600
7	EP718, 8	N	40	20	-	-	10^{17}	-	600
8	EP718, 9	N+La	40+30	5×10^3+20	-	-	10^{19}+10^{17}	-	600
9	VT9, 3	Sm	63	2×103	10	200	5×10^{16}	-	-
10	VT9, 3	Sm	63	2×10^3	10	200	8×10^{16}	-	-
11	VT9, 3	Sm	63	2×10^3	10	200	10^{17}	-	-
12	VT9, 3	Sm	63	2×10^3	10	200	5×10^{17}	-	-
13	VT9, 3	Hf	87	2×10^3	10	200	10^{16}	-	-
14	VT9, 3	Hf	87	2×10^3	10	200	5×10^{16}	-	-
15	VT9, 3	Hf	87	2×10^3	10	200	8×10^{16}	-	-
16	VT9, 3	Hf	87	2×10^3	10	200	10^{17}	-	-
17	VT25U,4	La+B	66+30	2×10^3	30	200	4×10^{17}	-	-
18	VT9, 3	C+p	300	60±10	0.2	0.05	-	3	850
19	VT, 3	C+p	300	160±20	0.2	0.05	-	3	850

Table 1. The irradiation regimes and the running time.

№	Materal of blade	Rp nm	X_{max}^0 at.%	h_{max} nm	(hkl)	$\Gamma_{1/2}$, grad ±0.06	H_μ, Mpa p=0.5N	R_a, μm ±0.01	I_{eee} pulse·s^{-1}
1	VT9	-	3±1	200±20	201	0.77	400±30	0.13	120±20
2	VT9	70±10	6±1	220±20	201	0.83	430±30	0.12	180±40
3	VT9	30±5	12±3	220±20	201	0.84	450±30	0.15	220±40
4	VT9	40±5	4±1	150±30	201	0.85	430±30	0.14	200±30
5	EP866sh	-	6±1	(6±1) 10^3	211	-	460±20	0.19	420±20
6	EP866sh	10±3	20±5	25±5	211	1.11	360±40	0.21	240±50
7	EP718ID	30±5	10±3	140±20	311	0.85	450±30	0.21	50±10
8	EP718ID	20 / 9	10 / 15	120 / 20	311	0.83	480±30	0.20	800±100
9	VT9	15±4	23±3	40±5	201	0.81	440±40	0.15	210±20
10	VT9	20±5	32±4	43±5	201	0.89	460±40	0.15	120±30
11	VT9	20±5	39±5	43±5	201	1.00	400±40	0.15	120±30
12	VT9	10±3	68±5	80±10	201	0.82	560±40	0.15	45±10
13	VT9	4±3	10±5	35±5	201	0.78	530±50	0.15	70±20
14	VT9	15±5	23±4	30±4	201	0.87	580±30	0.15	250±50
15	VT9	14±5	30±5	33±4	201	0.90	520±50	0.15	200±40
16	VT9	17±5	38±5	40±5	201	0.93	500±50	0.15	110±30
17	VT25U	12 / 100	25 / 8	32/ 220	201	0.95	460±50	0.14	120±20
18	VT9	-	-	-	201	0.61	420±30	0.06	140±20
19	VT9	-	-	-	201	0.65	400±20	0.10	250±20
20	VT9, *	-	-	-	201	0.79	380±30	0.16	60±5
21	VT25Y,*	-	-	-	201	0.78	400±30	0.15	45±5
22	EP866,*	-	-	-	211	1.02	360±30	0.20	150±20
23	EP718,*	-	-	-	311	0.71	420±20	0.21	210±30

Table 2. The influence of ion- beam treatment regimes on the concentration profile characteristics (Rp-projective running; x_{max}^0 - concentration of implanted element in a depth of Rp; h_{max}- thickness of ion alloyed layer), microhardness, roughness, exo- electron emission and a half- width of X-ray lines (hkl). *- production blades.

№	Material of blade, stage	H_μ, Mpa p=0.5N	σ_{-1}, Mpa ± 10	$\Delta m/S_{er.}$, mg·mm^{-2} ± 0.005	h_0, μm ± 5	R_a, μm ± 0.01
4	VT9, 3	840±100	510	0.075	80	0.29
5	EP866sh, 7	650±30	270	0.060	50	0.25
6	EP866sh, 7	460±30	320	0.080	25	0.24
7	EP718ID, 8	440±30	355	0.060	35	0.23
8	EP718ID, 9	440±30	360	0.065	25	0.23
18	VT9, 3	420±40	580	0.025	6±1	0.06
19	VT9, 3	860±30	420	0.070	60	0.34
20	VT9, 3	650±70	540	0.065	55	0.23
21	EP866sh, 7	600±50	270	0.090	50	0.26
22	EP718ID, 9	620±50	295	0.090	70	0.25

Table 3. Service properties of the blades after the prolonged engine tests (the regimes of treatment are presented in Tables 1 and 2).

Imployment of the multi-element ion beam treatment technology of a machine parts and tools for an operation properties improvement.

V.P.Sergeev[1], V.P.Yanovsky, S.M.Chesnokov
Republican Engineering Technical Centre of the Russian Academy of Science, Siberian Branch, Tomsk, 634055, Russia

Abstract
Ti+B, Mo+B, Cr+B, Al+B ion pulse beam implantation effects on the microhardness and wear resistivity of the surface layer of M2, D2, W1-9½ and 52100 steels were researched. According to the obtained data the multi-element ion beam implantation of a machine parts and tools was fulfiled and the industrial test results were shown.

Keywords: steel, implantation, microhardness, wear resistivity.

1. Introduction

Ion beam treatment of a machine parts and tools researches over the two last decades achieved the considerable results on the operation properties improvement. The most studing [1-3] is the ion beam of a single-element composition treatment of a structural and tool steels. The perspective for these purposes of the multi-element ion beams employment was shown at the last years. The more efficient modification of the structure-phase state and, accordingly, physical-chemical properties of the surface layer at least expose dose compared with single-element ion implantation is an advantage of this method [4-6].

This work aims to investigate the effect of ion simultaneous inculcation of boron and metals formed with boron the very hard and wear resisting chemical compounds, into surface layer on the microhardness and wear resistivity of a certain industrial steels with purpose of the machine part and tool operation property improving.

2. Experimental

The irradiation of a steel specimens and machine parts and tools was carried out using the pulse vacuum arc ion source "DIANA-12". The schematic diagram of DIANA-12 source is shown in Fig.1 DIANA-12 source consists of the ion accelerator (I), the high-voltage transformer unit (II) and the vacuum chamber (III). The high-voltage insulator 5 removes the vacuum part of the ion source from contact with the high-voltage transformer unit that fills with a transformer oil.

The vacuum chamber has the 200 mm diameter opening for joining with the ion source. Residual pressure in vacuum chamber during implantation process was maintained $1 \cdot 10^{-3} \div 3 \cdot 10^{-4}$. The DIANA-12 source work thus. A breakdown between cathode (6) and ignitor electrode (4) is due to voltage applied to the transformer Tr1. The discharge plasma of the vacuum arc cathode spot disperse in the expander - anode (2) and short -circuit the secondary winding of the transformer Tr2. Rectangular potential pulse applied to the primary winding of the transformer Tr2 allowed the arc discharge with a current $10 \div 50$ A and duration 300 µs. Simultaneously the voltage pulse applied to the transformer Tr3 that the produced high voltage pulse of the amplitude $20 \div 90$ kV and such duration. Ions of the cathode spot plasma come up to the emitter grid are accelerated that voltage. Its pass through the extracting electrode grid (1) with the transparence 95% and get at the specimen holder (7) that earth through resistor (8).

[1]Corresponding author: Fax: 7 382 22 258 032, e-mail: root@ritc.tomsk.su

The negative potential is applied on the grid (1) to suppress of a secondary elektrons. The irradiated specimens or machiny parts and tools are put in the holder (7). The resistor (8) signal is feeded at the control unit for irradiation dose measuring. The pulse dicrete frecuency 5, 10, 25, 50 Hz, the beam current amplitude 0,1-0,6A, the accelerating voltage 20-90 kV.

The beam element composition forming cathode of DIANA-12 ion source is a tablet with diameter 15 mm and thickness 5 mm that are manufactured of the pressing of a powder compound particles with the dimensions 10-20 µm and solid-phase sintering in the vacuum furnace. The chemical composition of the used cathodes are shown in Table.1. The research of the ion beam mass-charge composition formed compositional cathodes was shown beam composition had ions of all elements that contained cathode [8].

The microhardness and wear resistivity of the multi-element ion beam treatment specimens manufactured with the following steel grade; High Speed Steel ASTM A600 M2 regular "C", Die Steel AISI D2, Carbon Tool Steel ASTM A686 W1-9½ and Bearing Steel ASTM A295 52100 were studied.

The preparation of a research specimens included the heat treatment at a standard method for the showed steel grade, disk grinding, fine polishing and electrochemical polishing achieve the surface roughness R_a=0,10 - 0,08 µm.

The microhardness is determined by PMT-3 instrument with the measuring of the 0,5 N loading diamond indenter impression diagonals. The wear test diagram is shown in Fig.2. The wear tests conducted in the pin-in-disk geometry by the SMT-1 tribotester at the normal load in pin 150N, the disk speed of rotation $1s^{-1}$ and the measurement duration 600 s. The disk of diameter 50 mm made from the research steel and the pin of diameter 2,4 mm was from the hardening bearing steel 52100 with the Rockwell hardness HRC64. The wear was determined by measuring the wear track depth with a surface profilometer K-296.

3. Results

Table2 show that the wear resistivity of M2 steel icreases in 80-90% at the (Mo+B), (Cr+B),(Al+B) ion implantation and 28% at the (Ti+B) ion implantation. The wear resistivity of D2 steel icreases in 20% at the (Mo+B) ion implantation and 29% at the (Ti+B) ion implantation, W1-9½ steel - in 45% at the (Cr+B) ion implantation and 77% at the (Ti+B) ion implantation, 52100 steel in 42% at the (Ti+B) ion implantation.

Microhardness of M2 steel icreases in 50% at the (Cr+B) and (Mo+B) ion implantation and 18% at the (Ti+B) ion implantation, W1-9½ steel - in 45% at the (Cr+B) ion implantation and 28% at the (AL+B) ion implantation, 52100 steel - in 30% at the (Ni+B) ion implantation.

The most considerable effect simultaneosly both wear resistivity and microharness was shown (Cr+B) and (Mo+B) ion beam in M2 steel, (Mo+B) ion beam in D2 steel, (Cr+B) ion beam in W1-9½ steel, (Ti+B) ion beam in 52100 steel.

The obseved changes of the research steel surface properties under the influence B+(Ti, Mo, Cr, Al) ion beams can been bound with a precipitation high concenration titanium, molibdenium, chromium, aluminium borides and carbides into a martensite plates and with a remaining austenite transformation in the alloing martensite. This explanation can following at early TEM and microdifraction observations [5] of a structure-phase composition of a steel surface layer at (Mo+B), (Ti+B), (Cr+B) ion beam implantation.

The multi-element ion beam implantation of the machine parts and tools was carried out on the basic of the obtained experimental data. The industrial tests were

done in a production conditions on the Russian plants. In Table 3 is list industrial test results icluded average values of 100 separate measurements.

The thin disk milling cutters and drills and dies were shown the most commercial results in the life duration increase under the influence of the multi-element ion beam implantation.

4. Conclusions

The wear resistivity and microhardness changes of M2, D2, W1-9½, 52100 steels at (Ti+B), (Mo+B), (Cr+B), (Al+B) ion beam implantation with DIANA-12 ion source and compositional powder cathodes were studied. The most considerable action on these properties has (Mo+B) ion beam in M2 and D2 steels, (Cr+B) ion beam in M2 and W1-9½ steels and (Ti+B) ion beam in 52100 steel. The industrial tests of multi-element ion beam irradiated machine parts and tools were caried out. The thin disk milling cutters and drills and dies were shown the most results.

References

1. G.D.Lempert. Surface and Coat. Technjl. 1988. 34, n2, p.185-207
2. J.K.Hirvonen. //Annu.Rev.Mater.Sci. 1989, 19, p.401-417
3. F.F.Komarov. Ion implantation in metals. Moscow. Russia, 1990.
4. Haolin Lu, Huigin Su, Chen Mei (eds). // Vacuum, 1989, 39, n.2-4, p.187-189.
5. Sergeev V.P., V.P.Yanovskii, Yu.P.Scarkeen (eds). Modification of properties of construction materials by beams of charge particles. //Materials of Proc.2nd Rus.Conf., Sverdlovsk, Russia, 1991, 4, p.99-100.
6. L.N.Puchkareva, O.B.Lodijenskii, V.G.Durakov. // Phisika e Himiya obrabotki materialov, 1995, 6, 5-11.
7. F.I. Aksenov, S.P.Bugaev, V.I.Emelyanov (eds). // Pribori e Tehnika Experimenta, 1987, 3, 139-142.
8. G.P.Bajenov, G.G.Vasiljeva, G.P.Erohin, S.M.Chesnokov. Modification of properties of contruction materials by beams of charge particles. //Materials of Proc.3nd Rus. Conf., Tomsk, Russia, 1994, 1, p.31-33.

Fig.1. Schematic diagram of DIANA-12 ion source.

   I - ion accelarator

  II - high-voltage transformer unit

III - vacuum chamber

   1 - extracting elektrode grid

   2 - expander-anode with emitter grid

   3 - cathode holder

   4 - ignitor electrode

   5 - high-voltage insulator

   6 - cathode

   7 - specimen holder

   8 - ion beam current control resistor

Tr1 - adapter pulse are ignitor transformer

Tr2 - adapter pulse are transformer

Tr3 - high-voltage pulse transformer

  V_b - bias voltage for suppres of secondary electron
     emission

  I_b - ion beam current

Fig.2. Wear test diagram at sliding with pin-on-disk geometry.

   1 - specimen-disk

   2 - cylinder counterface

  F - normal load 150N

  d - cylinder counterface diameter 2,4 mm.

  D - specimen-disk diameter 50 mm.

Table1. Chemical element composition cathode, wt%

Cathode	Ti	Mo	Cr	Al	B
Ti+B	75	-	-	-	25
Mo+B	-	85	-	-	15
Cr+B	-	-	85	-	15
Al+B	-	-	-	70	30

Table2. Microhardness H_v(MPa) and wear groove depth h (μm) measured before and after ion beam treatment of steel samples. V_b=70kV, D=2·10^{17}cm , f=50Hz, j_b=0,4mA/cm² for 52100 and W1-9$^1/_2$ samples and j_b=1,0 mA/cm² for others

Sample	Species ion beam	Hv,MPa before	Hv,MPa after	h, μm before	h, μm after
M2	Ti+B	7300	7300	0,36	0,28
	Cr+B		11500		0,19
	Mo+B		10700		0,19
	Al+B		7400		0,20
D2	Ti+B	5500	6500	1,02	0,79
	Mo+B		8200		0,85
W1-9	Ti+B	4900	4800	1,54	0,87
	Cr+B		7100		1,06
	Al+B		6300		1,55
52100	Ti+B	7100	9300	0,92	0,38

Table3. Russian plant test results of tools and machine parts. V_b=70kV, f=50Hz, j_b=0,4 mA/cm² for 52100 and w1-9½ steels and j_b=1,0 mA/cm² for others

Tool or machine part	Materials of tool or machine part	Material of connected machine part or machined material	Species ion beam and implantation dose, cm	In crease of amount tool and machine partuse
1. Disk milling cutter Ø 20× 0,5mm	W1-9½	Brass	Ti+B 2·10^{17} Cr+B 2·10^{17} Al+B 2·10^{17}	5 10
Ø40× 2mm	M2	Brass	Mo+B 2·10^{17} Al+B 1,7·10^{17}	4 6
2. Milling cutter	M2	Carbon steel Aluminium alloy	Ti+B 2·10^{17} Mo+B 2· 10^{17}	2 2
3. Reamer	M2	Aluminium alloy	Mo+B 2·10^{17}	2
4. Drill Ø2mm	M2	Stainless	Ti+B 2· 10^{17} Ti+B 4· 10^{17}	2 3
5. Die	M2 D2 52100	Carbon steel for GeneralPurposes Heat-Treatable steel Brass	Ti+B 2·10^{17} Mo+B 2· 10^{17} Cr+B 2·10^{17}	3 3 3
6. Hot stamping punch of nut	M2	Carbon steel for General Purposes	Mo+B 3·10^{17}	2
7. Nail die	D2	Carbon steel for General Purposes	Mo+B 3·10^{17}	3
8. Press tool die	D2	Power chemical mixture	Ti+B 2·10^{17}	3
9. Convyer belt for planishing of stone	W1- 9½	Ruby	Cr+B 1·10^{17}	2
10. Ball race	52100	52100	Ti+B 2·10^{17}	3

I_B

V_B

1 2 3 4 I Tr1 Tr2

III 8 7 6 5 II Tr3

KEY ISSUES IN PLASMA SOURCE ION IMPLANTATION

D. J. Rej, R. J. Faehl

Los Alamos National Laboratory, MS-D434, Los Alamos, NM 87545, USA

J. N. Matossian

Hughes Research Laboratory, 3011 Malibu Canyon Rd., Malibu CA 90265, USA

ABSTRACT

Plasma source ion implantation (PSII) is a scaleable, non-line-of-sight method for the surface modification of materials. In this paper, we consider three important issues that should be addressed before wide-scale commercialization of PSII: (1) implant conformality; (2) ion sources; and (3) secondary electron emission. To insure uniform implanted dose over complex shapes, the ion sheath thickness must be kept sufficiently small. This criterion places demands on ion sources and pulsed-power supplies. Another limitation to date is the availability of additional ion species beyond B, C, N, and O. Possible solutions are the use of metal arc vaporization sources and plasma discharges in high-vapor-pressure organometallic precursors. Finally, secondary electron emission presents a potential efficiency and x-ray hazard issue since for many metallurgic applications, the emission coefficient can be as large as 20. Techniques to suppress secondary electron emission are discussed.

I. INTRODUCTION

Ion implantation[1] is a well-developed technology used to modify material surface proper-
ties, *e.g.*, for manufacturing semiconductor junctions and oxides, and for production of high-
strength, light-weight, corrosion-resistant metals. A limitation to more widespread use of
implantation for large-area, high-dose applications is the time, expense, and complexity
associated with conventional line-of-sight, accelerator-based techniques. Plasma source ion
implantation[2-4] (PSII) is a scaleable, non-line-of-sight, batch process that has the potential of
overcoming many of these limitations. In PSII a negative high-voltage pulse, typically ranging
between 10 and 300 kV and over a period between 1 to 40 μs, is applied to an electrically
conducting workpiece immersed in a plasma. The plasma usually consists of a weakly ionized
discharge created from a gaseous precursor admitted into a vacuum chamber. Plasma ions are
accelerated by the applied electrical potential and are implanted into the surface of the
workpiece. Implant times are short when compared to beamline techniques since high-current,
pulsed-power supplies compatible with this process can provide nearly two orders of
magnitude higher average currents than conventional accelerators. Since large areas can be
implanted concurrently, ion current densities to the workpiece can be kept low to avoid
overheating problems sometimes encountered in beamline implants. In this paper, we consider
three issues which must be addressed before wide-scale commercialization of PSII: (1) implant
conformality; (2) ion sources; and (3) secondary electron emission.

II. IMPLANT CONFORMALITY

An attractive feature of PSII is that it is non-line-of-sight. Cumbersome workpiece
manipulation fixtures and beam rastering are unnecessary. System efficiencies are high since

the perpendicular trajectories into the workpiece eliminate the need for masking. However, implants conform around complicated shapes as long as the plasma sheath dimensions remain small compared to the workpiece feature sizes. For certain applications, this condition may not be easily attained because of hardware limitations.

The evolution of supersonic ion sheaths has been discussed in detail elsewhere.[4-7] In brief, following application of the pulsed negative voltage V, plasma electrons near the surface of the workpiece are rapidly repelled (in a few ns) to uncover a region of uniform ion density. This region is known as the ion matrix sheath and has a thickness s_o for planar geometries of[5]

$$s_o = \sqrt{\frac{2\varepsilon_o V}{en_o}} \qquad (1)$$

where n_o = the initial plasma density, $\varepsilon_o = 8.9 \times 10^{-12}$ farad/m is the electric permittivity of free space, and $e = 1.6 \times 10^{-19}$ coul per unit charge is the elemental charge constant. On a longer time scale ($\sim \mu s$) ions are accelerated across the sheath by the applied electrical field and are driven into the workpiece surface. As ions are implanted, charge imbalance repels more electrons away from the workpiece, thereby forcing the sheath to expand outward from the workpiece to uncover more ions For planar geometries the sheath thickness s(t) expands at rate[6]

$$s(t) = s_o \sqrt[3]{\frac{2}{3}\omega_{pi}t + 1} \qquad (2)$$

where $\omega_{pi} = [n_o e^2/\varepsilon_o M]^{1/2}$ and M is the ion mass. The pulse length and the ion density are usually adjusted so that the sheath conforms to the workpiece and remains contained inside the vacuum chamber, and so that sheath overlap between adjacent workpieces is avoided. For a

given average power, a smaller sheath is achieved with higher n_o accompanied by higher pulsed currents, and lower repetition rates; moreover, a lower repetition rate allows more time for plasma ions to diffuse back into the depleted sheath region between pulses.[8] However, for a given V, n and s, the ion current is fixed and is given by the Child-Langmuir equation which for planar geometry is

$$j_i(t) = \frac{4\varepsilon_o}{9} \sqrt{\frac{2e}{M}} \frac{V^{3/2}}{[s(t)]^2} \tag{3}$$

The corresponding electrical resistance R_{pl} of the plasma load for an expanding planar sheath is obtained by combining Eq. 3 with Ohm's law,

$$R_{pl} = \frac{9}{4\varepsilon_o} \frac{s^2}{A(\gamma+1)} \sqrt{\frac{M}{2eV}} \tag{4}$$

where A is the workpiece area, and γ is the secondary electron emission coefficient. In PSII the high-voltage pulser must be capable of driving R_{pl} which can be rather small. For example, for a 50 kV N^+ implant with s=10 mm, A= 5 m^2 and γ=7, R_{pl} is 0.76 Ω (corresponding to a total pulsed current of 65 kA). Most pulsers are incapable of driving this load, so users are often forced to compromise by implanting with larger s.

Insight into conformality issues is gained from the computer simulation shown in Fig. 1 and 2 which are from electromagnetic particle-in-cell (PIC) calculations[9] to model the self-consistent evolution of PSII of two automobile pistons.[10-11] The numerical methodology in PIC simulations is that the full set of Maxwell's equations, including displacement currents, is solved at each time step on a regular Eulerian mesh. In these cylindrical (r,z) calculations, the radial and axial resolution is 2 and 1.5 mm, respectively, which is sufficiently smaller than s(t)

which ranges between 16.5 and 105 mm in this series of calculations. The plasma is modeled by an array of 26,000 electrons and 26,000 $C_2H_2^+$ acetylene ions, which are initially cold with a uniform density n_o of either 2.5×10^{14}, 10^{15}, or 10^{16} ions/m^3.

Each workpiece has a gross outer diameter of 82 mm and length of 50 mm. They are electrically connected to an external voltage supply by a cantilevered rod and surrounded by a 318-mm-diam concentric vacuum chamber. In the calculation, the voltage is fed through a 65.8-Ω coaxial line, and has a pulseshape consisting of a 50 ns linear rise followed by a 20 μs flattop. However, calculations are carried out to only 1 μs. For the magnitude of the ion current which is being drawn, the load impedance R_{pl} is much greater than the line feed impedance. The operating point of this circuit is, therefore, essentially twice the source voltage. Calculations are conducted for a bias voltage of 25.3 kV, while secondary electron emission (*cf.* Sec. IV) is neglected.

The calculations yield the self-consistent expanding sheath position $s(r,z)$ as a function of time (Fig. 1) which has both qualitative and quantitative implications. For $n_o = 10^{16}$ m^{-3}, we find $s_o = 17$ mm which reveals conformality during early times. At 2.5×10^{14} m^{-3}, however, s_o is 105 mm, indicative of poor conformality at all times. For all cases, as the sheath grows, its form changes from an approximately cylindrical to spherical shape, while the ion current decreases consistent with the Child-Langmuir scaling.

Quantitative information extracted from the simulations includes the time-integrated average energy E, implanted dose D_i, and mean angle of incidence θ of implanted ions along the surface of the workpiece as a function of time. The plots in Figure 2 are for t=80, 180, and 480 ns. The time t= 80 ns corresponds to a time shortly after the ion matrix phase has

been established. Relatively few, low-energy ($\leq$ 7 keV) ions have reached the workpiece by this time, especially at low n_o. By t=180 ns, the ion matrix is becoming depleted at the low n_o, but has not yet reached the Child-Langmuir equilibria. Integrated ion energies rise to $\leq$ 14 keV, though this number still includes contributions from the early-time, low-energy ions. By t=480 ns, the ion matrix has been depleted in all cases and Child-Langmuir flow has begun, and E rises to $\leq$ 19.5 keV. This cannot be directly collated to the snapshot of the particle distributions in Fig. 1 since ion transit times are comparable to this time. At t= 980 ns, the instantaneous flux is characterized by energies of 22.7-23.2 keV. E does not reach the full bias voltage because of the finite expansion of the sheath during one transit time.[8] The time elapsed between ion entry into the sheath edge and implantation in the object is of order ω_{pi}^{-1} or about 450-500 ns for the $n_o = 10^{15}$ m^{-3} case. As ions accelerate through the potential well, the well changes both in magnitude and shape. Ion energies are therefore distributed with different energies as one scans along the surface of the object. As the plasma density is increased, so does the dose at any given elapsed time. The increase in dose scales less than linearly with n_o. Also, we find that E at a given time, is slightly greater at higher n_o. Finally, we note that higher n_o leads to more nearly normal ion flow incidence. At later times, this difference begins to relax. This situation is roughly what we expect, based upon the higher degree of conformality which is seen when comparing higher to lower density calculations. Much later in time, as all sheaths lose conformality, we expect this difference to be diminished.

D_i varies by almost 25% along the surfaces. This is due to what might be termed "spherical convergence." Although the exact details depend on the geometry of the implanted object, much of this effect results from intersecting a spherically converging flow with a

cylindrical object. While it does not account for the exact dose pattern, it is useful and generic in understanding dose distributions in long cylindrical arrays of objects. It should be noted, however, that the high density "spikes" at corners of the workpieces are mostly numerical artifact. At a corner, the numerical diagnostic "counts" all ions entering a cell, not just those crossing the outer surface. The retained dose D_r is a more relevant parameter for characterizing implantation than total absorbed dose. D_r depends upon both E and θ. $\theta(z)$ profiles are plotted in Fig 2. The profile and retained dose is estimated with the *Profile Code*[12] for $D_i = 2 \times 10^{17} cm^{-2}$, E=12 keV implants of C into Al. From the results in Fig. 3, shallower profiles and lower D_r are observed as θ increases, because of the geometric spreading of the incident ion flux and increased sputtering.

A final point about the electron and ion distributions in Fig. 1 should be noted. Large "holes" can be seen at the axial end-faces at later times. These evacuated regions reflect that all of the initial plasma in our numerical chamber has been exhausted. In a physical chamber with the same dimensions, the same phenomenon will occur. Increasing the axial length of the chamber will delay the onset of plasma exhaustion. Simple estimates indicate that a sufficiently long voltage pulse can lead to complete plasma usage in even large PSII chambers. Addressing this issue quantitatively, however, requires considerations of the strength of the plasma source and the bias voltage, which are beyond the scope of the present paper. The process of plasma exhaustion in small chambers can be a real effect and should be evaluated when designing a PSII process.

III. PLASMA SOURCES

PSII requires the generation of a plasma with sufficient density n_o and uniformity around complex-shaped workpieces. As discussed in Sec. II, the value of n_o depends on the required sheath thickness s and implant voltage V, while s depends on several job-specific factors such as workpiece geometry, area, feature size, the process time, and the high-voltage pulser characteristics. Ion species composition is another factor that influences the choice of a plasma sources. With molecular gases, one often creates multiple species, *e.g.*, N_2^+ and N^+ with a N_2 fill; consequently, heavier molecules are accelerated to lower velocities and are implanted into shallower depths than lighter ones. For many metallurgical applications, a mixture of ion species is tolerable (and even desirable) to distribute ions more uniformly into the workpiece surface layer. In general, however, one usually prefers to fully dissociate molecular ions to maximize ion velocity, thereby maximizing implant depth and minimizing sputter losses.

Typical experiments are operated with n_o between 10^{14} and 10^{18} ions/m^3, created in a gas fill density between 10^{19} and 3×10^{20} atoms/m^3 (0.3 to 10 mTorr). Plasma sources utilizing biased filaments and radio frequency electric fields are routinely used. To date, a limitation to more wide-spread use of PSII technology is the availability of additional ion species beyond B, C, N, and O. Two possible solutions are the use of filtered metal arc vaporization sources[13-15] and the use of plasma discharges in high-vapor-pressure organometallic precursors.[16] The principal advantage of the metal arc is atomic control of the ions produced and the ability to create multiply-ionized charge states. Vacuum arc sources have been developed for a wide range of metals and are used in beamline implants. Their use in PSII systems is more suited to higher doses ($>10^{17}$ cm^{-2}) and lower energies (tens of keV) than the usual ranges in

conventional metal ion implantation.[15] The advantage of organometallic precursors is their high volatility, which translates into high fill pressures and high plasma densities, which in turn allow for high ion currents and implantation rates. While several precursors currently exist, their use in PSII systems remains to be validated.

IV. SECONDARY ELECTRON EMISSION

Secondary electron emission is another important feature of PSII. As each ion is implanted, electrons are liberated from the workpiece and are rapidly accelerated through the sheath potential. The energetic secondaries stream along essentially collisionless trajectories until they strike and are stopped by grounded objects such as the vacuum chamber walls. For many of the envisioned metallurgic applications, the secondary emission yield γ is large, often ranging between 5 and 20.[17] Therefore, uncontrolled secondary emission could reduce PSII system efficiencies to as low as 5%. Furthermore, the bremsstrahlung x-rays produced by energetic electron bombardment of the chamber walls pose a potential safety hazard.

Lead-shielding is a conventional technique used to provide x-ray shielding in PSII facilities. For implantation voltage up to 100 kV, and total average secondary electron currents of 1 A, lead thicknesses of 7 mm surrounding a vacuum chamber vessel is sufficient to maintain low x-ray flux levels that usually will comply with safety regulations. For many applications, however, implantation voltages well in excess of 100 kV are desirable. For these voltage ranges, the use of lead shielding becomes impractical, since as the implantation voltage is increased from 100 to 300 kV, the x-ray absorption cross section for lead drops by approximately a factor of 20. The lead shielding thickness increase required to accommodate this reduction in absorption becomes

impractical. Therefore, there is a need for methods to reduce or minimize x-ray production in a PSII system.

A technique used to suppress secondary x-ray generation and possibly increase system efficiency, is illustrated in Fig. 4.[18] The technique is based on electrostatic confinement of the secondary electrons. Secondaries are trapped within a metal enclosure supported from the vacuum chamber walls, which is biased to the same electrical potential as the workpiece. A remote plasma source produces a plasma near ground potential. A plasma sheath forms around the part, as well as along the entire surface of the enclosure. When voltage is applied to the workpiece, it also is applied to the entire enclosure. The applied voltage develops across the sheath between the plasma and the workpiece, and also between the plasma and the enclosure. Therefore, ions are implanted into both the workpiece and the enclosure. Secondary electrons emitted from the workpiece and the enclosure are repeatedly reflected within the interior of the enclosure, and they are prevented from impacting the grounded vacuum chamber walls. The only grounded surface available for x-ray production is the plasma source, whose area can be minimized. The secondary electrons may dissipate their energy into the plasma during reflections from the enclosure walls, possibly aiding in the production of additional plasma. This could increase the efficiency of the PSII system by transferring secondary-electron energy into the plasma production process.

Recent experiments using this technique at the Hughes Research Laboratory at 50 kV voltage levels have reduced the unshielded x-ray level from 20 mrad/hour to a level below the minimum detection limit (< 0.2 mrad/hour). At 80 -kV operation, the unshielded x-ray level is reduced by a factor of four. Experiments were conducted with an enclosure constructed from the

same material as the workpiece to ensure that the secondary electron yield for all surfaces was the same. PSII was conducted with N_2^+ ions with and without the enclosure in place, ensuring that the total average current from the high-voltage pulser was maintained constant. This ensured that the total incident ion current to all the interior surfaces of the enclosure was the same. X-ray dosimeter readings at an unshielded glass window located at the front of the vacuum chamber are shown in Table I. Uniform D_r of $1\times10^{17}cm^{-2}$ have been confirmed with secondary ion mass spectroscopy on implanted 6×6 mm stainless steel coupons affixed at various locations to the workpiece and enclosure walls during the PSII experiments.

There exist other proposed (but unproven) techniques for suppressing secondary electrons. One method involves using negative ions and positive accelerating voltages. Negative ion sources have been developed for high-energy particle accelerators. The extrapolation of these sources to supply the large average currents demanded by PSII remains a challenge; furthermore, maintaining a high negative ion to electron density ratio will be essential to minimize unwanted primary electron currents and x-ray emission. A second method uses multiply-charged ions which will reduce the required acceleration voltage, bremsstrahlung generation, and shielding requirements. Indeed vacuum arc sources are well known for their ability to produce multiply-charged species.[14] However, with multiply-charged ions come increased secondary electron yields which must also be contended with and accounted for. A third method uses an externally applied magnetic field.[19] Secondary electrons are trapped in the field to form a virtual cathode layer near the workpiece surface where the local electric field is substantially reduced. Subsequent electrons that are emitted can then be reabsorbed by the workpiece. The magnitude of B is chosen so that secondary electron trajectories are greatly

altered, while ion motion is only slightly perturbed. With this technique, care must be taken in using it in conjunction with magnetic workpieces (such as steel components or dies) which can alter the magnetic field being used for secondary-electron trapping, or may itself become permanently magnetized during the process.

V. CONCLUSION

The appeal of PSII is that it enables one to apply the well-known benefits of ion implantation in a quick and cost-effective manner to complex shapes. However, to take full advantage of the non-line-of-sight property of PSII, it is important to maintain sufficiently small sheath thickness to insure a uniform implant. In some cases, this can not be easily accomplished because pulsed power supplies are incapable of driving the relative low load impedance that results from small sheaths. As a compromise, additional fixturing or multiple workpiece configurations should be implemented to eliminate edge field phenomenon that affect implant uniformity. Another limitation at the present time is the availability of additional ion species beyond B, C, N, and O. Both vacuum arc and volatile organometallic ion sources have been developed to enable PSII with metallic ions. Finally, substantial secondary electron emission often accompanies PSII, limiting electrical system efficiencies. While the suppression of secondaries remains an ongoing part of current research, virtually all PSII devices are operated without any secondary electron control. Consequently, adequate x-ray shielding is an important part of any PSII machine. It should be noted, however, that cost projections[20] for commercial PSII indicate that the poor efficiencies caused by secondary electron losses do not dramatically alter the overall expenses since the additional capital and utility costs for the high-voltage pulser system are a relatively minor part of the total expense.

ACKNOWLEDGMENTS

REFERENCES

[1] Nastasi M and Meyer J W 1996 *Ion Solid Interactions: Fundamentals and Applications* (Cambridge Univ. Press, 1996)

[2] Conrad J R, Radtke J L, Dodd R A, Worzala F J and Tran N C 1987 *J. Applied Physics* **62** 4591-6

[3] Conrad J R 1988 *U. S. Patent 4,764,394*

[4] Rej D J, in *Handbook of Thin Film Technology,* edited by D. Glocker and I. Shah (supplement 1, Inst. of Physics Publishing, in press).

[5] Andrews J G and Varey R H 1971 *Phys. Fluids* **14** 339-43

[6] Scheuer J T, Shamim M and Conrad J R 1990 *J. Appl. Physics* **67** 1241-5

[7] Kissick M W, Hong M P, Shamim M M, Callen J D 1994 *J. Appl. Phys.* **76** 7616-18.

[8] Wood B P 1993 *J. Appl. Phys.* **73** 4770-8

[9] Faehl R J, DeVolder B and Wood B 1994 *J. Vac. Sci. Technol.* **B12** 884-8

[10] Nastasi M, Elmoursi A A, Faehl R J, Hamdi A H, Henins I, Malaczynski G W, Mantese J V, Munson C P, Qui X, Reass W A, *et al.,* 1996 *Proc. Mat. Res. Soc.* (in press)

[11] Malaczynski G W, Qiu X, Mantese J V, Elmoursi A A, Hamdi A H, Wood B P, Walter K C and Nastasi M A 1995 *U.S. Patent 5,458,927*

[12] The *Profile Code*™ is available from Implant Sciences Corp., Wakefield, MA 01880.

[13] Adler R J and Picraux T 1985 *Nucl. Instrum. Methods Phys.* **B6** 123-8

[14] Brown I G and Washburn J 1987 *Nucl. Instrum. Methods Phys.* **B21** 201-4

[15] Brown I G, Anders A, Anders S, Dickenson M R and MacGill R A 1994 *J. Vac. Sci. and Technol.* **B12** 823-827

[16] Healy M D and Smith D C 1993 *Materials Technology* **8**, 149-52

[17] Shamim M M, Scheuer J T, Fetherston R P and J. R. Conrad J R 1991 *J. Appl. Phys.* **70** 4756-9

[18] Matossian J N 1996 U.S. Patent (pending)

[19] Rej D J, Wood B P, Faehl R J and Fleischmann H H 1994 *J. Vac. Sci. Technol.* **B12** 861-6

[20] Rej D J; Alexander R B 1994, *J. Vac. Sci. Technol.* **B12** 2380-2387.

Table I. Effect of electrostatiuc confinement on PSII x-ray emission

V (kV)	Total current to plasma (mA)	Enclosure used?	Dosimeter reading (mRad/hr)
50	20	No	20
50	20	Yes	$\ll 1$
75	15	No	85
75	15	Yes	20

FIGURE CAPTIONS

Fig. 1   Particle-in-cell simulations of PSII into two automotive pistons for initial plasma $C_2H_2^+$ densities n_o of (a) 2.5×10^{14}, (b) 10^{15}, and (c) 10^{16} ions/m^3. Positions of electrons (red) and ions (blue) are plotted for times $t=$ 80, 180, and 480 ns into the PSII pulse.

Fig. 2   Time-integrated average energy E, implanted dose D_i, and mean angle of incidence θ of implanted ions along the outer surface of the pistons for initial plasma $C_2H_2^+$ densities n_o of (a) 2.5×10^{14}, (b) 10^{15}, and (c) 10^{16} ions/m^3 at times $t=$ 80, 180, and 480 ns.

Fig. 3   (a) Computed profiles for a $D_i = 2\times10^{17}$ cm^{-2} implant of 12 keV carbon into aluminum with angle of incidence $\theta = $ 0, 20, 40, and 60°. (b) Retained dose D_r as a function of θ.

Fig. 4   Control of secondary electrons by a biased enclosure.

t = 80 ns

t = 180 ns

t = 480 ns

Fig. 1

Fig. 2

(a)

(b)

Figure 3

REMOTE PLASMA SOURCE

VACUUM CHAMBER

$-V_0$

+   -

METAL
ENCLOSURE
AT SAME
POTENTIAL
AS PART

PLASMA

+ -

e^-

e^-

+

e^-

PART

$-V_0$

$-V_0$

REFLECTED
ELECTRON
PATH

PLASMA
SHEATH
AT PART AND
ENCLOSURE

Fig. 4

HIGH-CURRENT-DENSITY, BROAD-BEAM
BORON ION IMPLANTATION

P.J. Wilbur[1], J.A. Davis[1], D.L. Williamson[2], J.J. Vajo[3], and R. Wei[3]

Department of Mechanical Engineering
Colorado State University, Fort Collins, CO 80523, USA[1]

Department of Physics
Colorado School of Mines, Golden, CO 80401, USA[2]

Hughes Research Laboratories
3011 Malibu Canyon Rd, Malibu, CA 90265, USA[3]

ABSTRACT

Characteristics of iron discs implanted with boron using a high-current-density, broad-beam system with a rapid processing capability are examined. The effects of ion implantation temperature (150-900 °C), energy (7-50 keV) and current density (200-1000 $\mu A/cm^2$) on the microstructures and thicknesses of layers implanted with B are examined using Auger electron spectroscopy, X-ray diffraction and conversion electron Mössbauer spectroscopy. Boron condensation on a surface is observed during implantation unless the combination of energy and temperature are sufficiently great to prevent it. The microstructures observed when conditions enable B penetration are amorphous, Fe_3B and Fe_2B. It is argued that the relative balance between the rate of B implantation into and temperature-controlled diffusion out of the ballistic layer determine the microstructure that forms. Preliminary wear tests show a layer containing Fe_2B in an α-Fe matrix that was formed at the highest temperature investigated (900 °C) yields the most wear-resistant surface.

INTRODUCTION

Nitrogen and carbon ion implantation have been shown to offer effective tribological treatments on ferrous surfaces particularly when the implantation occurs under high current density, elevated-temperature conditions where the treatment is rapid and the resulting surface layers are relatively thick [1,2,3]. The processing is also attractive because it can be carried out at low implantation energies using inexpensive equipment and, compared to the competing nitriding and carburizing processes, it affords great improvements in the control of final surface properties [2]. Low implantation energies are also attractive because they mitigate implantation temperature control problems at the high current densities where rapid processing is realized.

Boronizing, a diffusion process that is similar to nitriding and carburizing, yields a very hard, wear-resistant surface on ferrous materials. In fact comparative tests reported by Budinski [4] have shown that boronized surfaces exhibit adhesive and abrasive wear rates that are one-fifth to one-seventh of those observed with nitrided, carburized or carbonitrided surfaces. Companies offering boronizing services also claim dramatic increases in the resistance of boronized low-alloy iron and austenitic steel surfaces to acid attack [5]. An additional attractive feature of a boronized surface relates to the tendency for boron on a tribological surface to combine with the moisture in air and form boric acid. This acid has a layered crystal structure that makes it an effective solid lubricant [6]. In spite of the attractive characteristics of B-rich surface layers, boronization of ferrous surfaces has not achieved widespread acceptance apparently because of the high treatment temperatures required (900 -1100 °C) and because the resulting boride surface layers are frequently brittle

2

and, therefore, susceptible to failure [7]. Studies have shown that brittleness develops when the boride phases Fe_2B and FeB are both present in the layer and that Fe_2B is the preferred phase [5,7]. It is difficult to control the boronizing process so only the Fe_2B phase forms, however, because the diffusion rate of B through Fe_2B is slow and B tends to be released from a boronizing compound packed next to a surface so rapidly that FeB forms [5,8]. Other shortcomings of boronization relate to problems with contamination and the control of stresses in the treated layer.

Boron ion implantation represents an attractive alternative to boronization because implantation temperature, which determines the B diffusion rate, and implantation current density (which determines the B supply rate) can be controlled independently with good precision. Hence, it should be possible to control the concentration of B in the surface layer and produce a specific microstructure, presumably Fe_2B for tribological applications. The objective of this paper is to demonstrate the extent to which the microstructure of a boron-implanted surface layer can be controlled. This control should be realized through the proper selection of the implantation parameters; which are surface temperature, ion energy, ion current density and implantation time or implanted-ion dose.

APPARATUS AND PROCEDURES

Pure α-Fe (99.5%) in a fully annealed state was selected as the substrate material for this initial study because the microstructures being produced are not masked by alloying elements that are present in steels. Test specimens were 4.8 cm diam. discs that were polished to a mean roughness (R_a) of 0.015 μm. Boron was implanted using a metal ion implanter [9] that employs a cylindrical, graphite discharge chamber in which electron bombardment of gas-phase, atomic boron is employed to produce B ions. The resulting ions are accelerated to implantation energies in an electric field maintained between two plates located on one end of the chamber. The ions, which are extracted through aligned holes in the plates, are directed at a target (disc) surface with an energy determined by the potential difference maintained between the chamber and the surface. The current density in the extracted ion beam, which is ~5 cm in diam. at the target location, is maintained by controlling the intensity of the electrical discharge in the chamber. The gas-phase boron required is vaporized from solid B in a crucible in the chamber at a rate that is controlled by the product of the crucible potential and the electron current drawn to the crucible from the chamber plasma. The chamber itself is maintained at a sufficiently high temperature so B condensation on chamber walls will be minimized.

The implanter can be operated at current densities ranging from 100 to >1000 μA/cm^2 and, if changes in the configuration of the ion extraction plates are made, at ion energies over the range from 2 to 50 keV. Temperatures are measured during implantation using a thermocouple located near the surface of each disc during processing. Temperatures are controlled by balancing the rate at which heat is being lost by conduction

4

and radiation from the discs against the input thermal power from the beam. The rate of heat loss is controlled, in turn, by using an appropriate level of electrical resistance heating or chilled-water cooling of a plate on which the discs are mounted.

Auger electron spectroscopy (AES) was used with elemental sensitivity factors to determine concentration depth profiles in implanted discs. Sputtering between measurements was accomplished using a 4 keV, Ar+ ion beam at 55° from normal. Profilometric measurement of a typical crater indicated the mean sputtering rate was about 0.025 μm/min. Significant oxygen and carbon AES signals were measured within ~0.1 μm of the surfaces of some discs; their effect is to depress the B concentration in this region. Microstructures present in the discs were determined using conversion electron Mössbauer spectroscopy (CEMS) for near-surface regions (~0.1 μm) and x-ray diffraction (XRD) in the standard Bragg-Brentano geometry with Cu-K$_\alpha$ radiation over a greater depth (~1 μm)[10].

Implanted and unimplanted disc surfaces were wear tested using an oscillating pin-on-disc tribometer designed to wear a relative large surface uniformly [11]. This tribometer has been found to be particularly well suited to the measurement of wear rates when treated layers are thin. For these tests a boundary lubricant (10 volume % oleic acid in kerosene) was flushed over the disc and this resulted in friction coefficients near 0.1. In all cases unimplanted α-Fe pins having hemispherical heads with a 0.32 cm radius of curvature and a mean roughness R_a < 0.02 μm were used as the counterfaces. The pins were oscillated radially inward and outward at 0.2 Hz to wear a 1-cm-wide band on the discs at a mean sliding speed of 13 cm/sec and a normal load of 5 N (corresponding to an initial Hertzian stress of 1.1 GPa). Disc wear depths were determined by removing and weighing the discs

with a balance accurate to ± 10 μgm. Weight losses were divided by the density of the disc

material and the areas of the worn regions to obtain the wear depths.

RESULTS

The B concentration depth profiles measured using AES on four discs implanted under different conditions are shown in Fig. 1. They show B concentrations that range to ~40 at.% and depths estimated using the AES system sputtering rate (~0.025 μm/min) to be as much as 0.4 μm. The disc implanted at the lowest temperature (300 °C) and 40 keV yields the profile expected for ballistic implantation (i.e. with negligible thermal diffusion). As the implantation temperature is increased to 550 and then 700 C°, the data suggest thermal diffusion effects are sufficient to cause the layer depths to grow to ~0.25 and ~0.4 μm, respectively. For these three discs the implantation energies were relatively high (>40 keV) and comparison of the implanted doses (i.e. the current density-time products) and the retained doses (integrated values from Fig. 1 curves) show substantial fractions of the implanted B ions are retained in the layers (~50 to 80%). When the energy is reduced to 7 keV, however, the other data set in Fig. 1 shows a low B concentration is realized, even at the greater temperature of 700 °C and a high dose level (~8×10^{18} B^+/cm^2). The retained dose in this case is estimated on the basis of the AES data in Fig. 1 and complimentary secondary ion mass spectrometric data to be less than 10%. This low retention is considered to be caused by a high B vaporization temperature which facilitates B condensation on surfaces being implanted if the energy and/or temperature are too low. The relationship between the temperature and energy where condensation occurs is uncertain, but the Fig. 1 data indicate 7 keV is marginal at 700 °C and another test showed condensation occurred at 20 keV when the temperature was 150 °C. In contrast, thick N-rich layers are produced at energies and temperatures as low as 1 keV and 400 °C [1] because N doesn't condense. The

7

condensation effect is also observed during C implantation where diamondlike-carbon

coatings are formed if temperatures and energies are low [12].

The microstructures formed at the 300 °C, 40 keV implantation condition are

indicated by the XRD and CEMS data given in Fig. 2. Figure 2a shows XRD peaks

associated with bcc α-Fe and this suggests it is the only crystalline material in a 1-μm-thick

surface layer. De-convolution of the CEMS data of Fig. 2b, which characterize a thinner

($\sim$0.1 μm) surface layer, yields the α-Fe signature and a broad signal designated "a" that is

suggestive of an amorphous material rather than distinct boride phases. The amorphous

phase is characterized by the hyperfine field probability distribution shown in Fig. 2c. This

plot shows a broad distribution that is again typical of amorphous materials rather than the

sharp peaks that characterize crystalline ones. Boron-induced amorphization of α-Fe has

been observed previously under lower temperature conditions at about the same dose levels

that yielded the data of Fig. 2 [13].

Increasing the implantation temperature to 550 and 700 °C yielded the CEMS

spectra given in Figs. 3 and 4. Both show the crystalline Fe_2B microstructure is dominant

within 0.1 μm of the surface; 61% and 82% of the CEMS signal comes from this phase at

the 550 and 700 °C implantation conditions, respectively. The greater signal strength for the

700 °C processing is consistent with the greater layer thickness shown in Fig. 1. The non-

magnetic Fe-B-O signal shown on Fig. 3 is indicative of oxygen contamination near the

surface of the 550 °C disc. This contamination, which was also observed in the AES data

for this disc, is the cause of the dip in B concentration apparent in the Fig.-1 data at

sputtering times $\lesssim$ 3 min. It is postulated that this oxygen contamination comes from water

that is adsorbed on the boron in the crucible when it is exposed to the atmosphere. It appears this contamination has been controlled in other discs by heating the crucible to drive off the water before implantation is initiated.

Figure 5 shows CEMS data from a disc implanted at a still greater temperature (900 °C) at an energy and current density of 24 keV and 600 μA/cm^2, respectively, for 30 min. This energy-temperature combination is sufficient to assure the B did not coat on the surface. The data suggest a thin ($\sim$ 0.1 μm) layer that is a mixture of α-Fe (67%) and iron borides (33% - mostly Fe$_2$B). This signal could be coming from either a layer of iron boride on an α-Fe substrate or a mixture of the borides in an iron matrix.

X-ray diffraction data, which reveal microstructures present in the surface layers extending to $\sim$ 1 μm, are shown in Fig. 6. The three spectra at the bottom suggest with some ambiguity that the dominant microstructures observed in the CEMS data are confirmed by the XRD measurements. The bottom plot (the 300 °C-40 keV data reproduced from Fig. 2a) shows only the α-Fe signal indicative of a substrate covered by a thin amorphous layer. The next two spectra (for 550 and 700 °C both at 50 keV) suggest Fe$_2$B is dominant with the 700 °C one yielding the stronger signals expected from the thicker layer. The disc implanted at 700 °C and 7 keV has not been examined by CEMS, but it has an XRD spectrum indicative of Fe$_3$B and this is consistent with the relatively low B concentrations shown in Fig. 1 for this disc. Finally, the upper spectrum (900 °C, 24 keV), shows a strong Fe$_2$B signal indicative of a substantial concentration of this phase extending to 1 μm on the disc. Taken together with CEMS results, this suggests a layer of Fe$_2$B in an α-Fe matrix was produced in this disc.

9

The sliding wear behaviors of two of the implanted discs are compared to that of an unimplanted α-Fe disc in Fig. 7. The unimplanted disc shows a wear rate (slope) that is high initially and drops to a steady value after the surface has work hardened (~ 10 hr). All B-implanted discs that have been tested to date show initial wear rates that are lower (similar to that shown in Fig. 7 for the 300-°C-40-keV disc with the amorphous layer). This disc wears at a lower rate for about 10 hr and then the rate approaches the terminal rate for the unimplanted discs. The mass loss at the point where the rate appears to change (~ 1 mg) corresponds to wear removal of a layer with a thickness approximately equal to the ballistic depth of the implanted ions (i.e. the depth of the layer from Fig. 1 which is ~ 0.1 μm). It is noteworthy that a CEMS measurement made after the treated layer had been partially worn away suggested the strength of the amorphous signal decreased as the wear progressed and indicated that the layer was being removed quite uniformly. The disc implanted at 900 °C shows a substantially lower wear rate that the amorphous one and it is comparable to those achieved with implanted C and N [3]. The CEMS and XRD data indicated this layer contained Fe_2B precipitates in an iron matrix and the precipitation hardening that this would induce could explain the low wear rate it exhibits.

DISCUSSION

The data of Fig. 1 show that B implantation at elevated temperatures enables growth of the treated layer, but the combination of energy and temperature must be sufficient to prevent B condensation on the surface. It is postulated that the particular microstructure that forms is determined by the relative balance between the rates at which B is supplied (implanted) and lost from the ballistic region by diffusion. If the supply rate is low either because the implantation current density is low or the ions are unable to penetrate a surface barrier like a condensed-B coating, a layer rich in Fe (e.g. Fe_3B) tends to form. At energy/temperature conditions where no surface barrier formed and current densities were moderate (200 $\mu A/cm^2$) Fe_2B formed over the temperature range from at least 550 to 700 °C. At a greater current density (600 $\mu A/cm^2$) and temperature (900 °C) the Fe_2B precipitated in the α-Fe matrix thereby forming a very wear-resistant surface. Thus, the microstructure preferred for boronizing (Fe_2B) is formed quite readily by implanting B. It has also been shown that an amorphous layer is produced when low doses and temperatures are used and the energy is sufficient to enable penetration. Taken together, these results suggest that essentially any preferred microstructure can be produced in a treated layer by controlling implantation conditions. Wear test results must be considered preliminary at this point, but they suggest all of the B implantation of α-Fe improves its wear resistance, but the precipitation-hardened surface is most beneficial.

ACKNOWLEDGEMENT

REFERENCES

1.   R. Wei, B. Shogrin, P.J. Wilbur, O. Ozturk, D.L. Williamson, I. Ivanov and E. Metin, *J. Tribology* 116 (1994) 870.

2.   R. Wei, Low-energy, High-current-density Ion Implantation of Materials at Elevated Temperature for Tribological Applications, in press *Surf. and Coat. Technol.*

3.   P.J. Wilbur and B.W. Buchholtz, *Surf. and Coat. Technol.* 79 (1996) 1-8.

4.   K.G. Budinski, *Wear* 162-164 (1993) 757-762.

5.   W. Fichtl, N. Trausner and A. Graf von Matuschka, "Boronizing with EKabor," Trade Publication of Elektroschmelzwerk Kempten GmbH, Munich, Germany.

6.   A. Erdemir, C. Bindal and G.R. Fenske, *Appl. Phys. Lett.* 68 (1996) 1637, and A. Erdemir, G.R. Fenske, F.A. Nichols, R.A. Erck, and D.E. Busch, "Self-lubricating Boric Acid Films for Tribological Applications," Proceedings of the Japan International Tribology Conference, Nagoya (1990) 1797-1802.

7.   W. Liliental, "Wear Resistance and Brittleness of Diffusion Boride Layers on Steels," Proceedings of the International Conference on Wear of Materials, Reston, VA, April 11-13, 1983, Amer. Soc. Mech. Engrs., 556-563.

8.   J. Pelleg and M. Judelewicz, *Thin Solid Films* 215 (1992) 35-41.

9.   P.J. Wilbur and R. Wei, *Rev. Sci. Instrum.* 63 (1992) 2491.

10.   O. Ozturk and D. Williamson, *J. Appl. Phys.* 77 (1995) 3839.

11.   R. Wei, P.J. Wilbur, W.S. Sampath, D.L. Williamson, Y. Qu and L. Wang, *J. Tribology* 112 (1990) 27.

12.   A. Erdemir, M. Switala, R. Wei and P.J. Wilbur, *Surf. and Coat. Technol.* 50 (1991) 17-23.

13.   B. Rauschenbach, *Nucl. Instrum. Methods B*, B80/81 (1993) 303-308.

14.   R. Wei, J.N. Matossian, J.J. Vajo, D. Clark, P.J. Wilbur, J.A. Davis, "A Preliminary Study of High-current-density Ion Beam Carburizing and Nitriding of Steels, 16th ASM Heat Treating Conf. & Exposition, Mar. 19-21, 1996, Cincinnati, OH.

LIST OF FIGURES

700 °C
50 keV
200 $\mu A/cm^2$
9 min

550 °C
50 keV
200 $\mu A/cm^2$
9 min

300 °C
40 keV
200 $\mu A/cm^2$
8 min

700 °C
7 keV
1000 $\mu A/cm^2$
21 min

BORON CONCENTRATION (at %)

40

30

20

10

5

10

15

20

SPUTTERING TIME (min)

a)

b)

c)

550 °C
50 keV
200 μA/cm^2
9 min

Fe

Fe$_2$B

Fe-B-O

700 °C
50 keV
200 μA/cm^2
9 min

Fe

Fe$_2$B

α-Fe DISC v. α-Fe PIN
5N NORMAL LOAD
13 cm/s SLIDING SPEED
LUBRICATED

UNIMPLANTED

300 °C
40 keV
200 μA/cm²
8 min

900 °C
24 keV
600 μA/cm²
30 min

MASS LOSS (mg)

WEAR TIME (hrs)

COVER SHEET

Title of Paper:

Plasma-Based Ion Implantation and Electron-Bombardment for Large-Scale Surface Modification of Materials

Name of Authors (in same sequence as listed on title page):

Jesse N. Matossian, Ronghua Wei, and John D. Williams

Full Name of Principal Author to Receive All Correspondence:

Jesse N. Matossian

Full Mailing Address of Principal Author:

Jesse N. Matossian
Power Technologies Laboratory
Hughes Research Laboratories
3011 Malibu Canyon Road
Malibu, CA 90265 USA

Telephone Number: (310) 317-5121

Telefax Number: (310) 317-5483

e-mail address: jmatossian@msmail4.hac.com

Keywords for Paper (maximum of four):

Plasma, ion implantation, electron bombardment, pulse modulation

PLASMA-BASED ION IMPLANTATION AND ELECTRON-BOMBARDMENT FOR LARGE-SCALE SURFACE MODIFICATION OF MATERIALS

Jesse N. Matossian, Ronghua Wei, and John D. Williams
Hughes Research Laboratories
3011 Malibu Canyon Road, Malibu, CA 90265 (USA)

ABSTRACT

In this paper we present the use of plasma-based ion implantation (PBII) and plasma-based electron bombardment (PBEB) for large-scale surface modification of materials that has been under development at Hughes Research Laboratories (HRL). In PBII, a part to be implanted is immersed in a gaseous- or metal-ion plasma and pulse biased to a high, negative potential (20-250 kV) to implant positively-charged ions omnidirectionally and simultaneously over the part surface. In PBEB, the polarity of the pulse-bias is reversed to bombard negatively-charged electrons omnidirectionally and simultaneously over the part for surface or bulk heating. Both PBII and PBEB have been conducted at 100-kV, 100-kW levels in a 1.2-m-diameter × 2.4-m-long vacuum chamber to achieve novel surface hardening, bulk hardening, as well as surface alloying and brazing of large-scale objects. Major emphasis of the PBII process is in the development of hard-coatings for wear resistance of tools, dies and molds used in automotive and aerospace applications. As examples, we show the use of PBII to achieve an 8× improved wear life of TiN-coated cutting tools subjected to multiple regrinds under actual gear-manufacturing wear conditions. TiN-coated foundry-mold blocks post implanted via the PBII process demonstrate a >2.5× improved wear life under high-compression, sand-abrasion manufacturing wear conditions. TiN-mixed layers prepared with the PBII process achieve a 3× times reduced wear of steel die materials subjected to accelerated laboratory wear conditions. Major emphasis of the PBEB process is in developing advanced heat-treatment techniques for automotive and aerospace components. As examples, we show the use of the PBEB process to normalize and surface-harden pinion gears in a faster, more efficient manner than achieved using conventional heat-treat techniques. Other uses of PBEB will be discussed, including brazing and melting of materials for surface-alloying applications.

INTRODUCTION

There are three types of surface treatments that can be conducted to improve the tribological (friction and wear) properties of materials; the surface can be coated, heat treated, or implanted. In each of these techniques, plasmas have been used to enhance conventional surface-treatment processes. For example, in plasma-assisted chemical-vapor deposition (CVD) and physical vapor deposition (PVD), hard coatings for wear resistance can be deposited onto large-scale, complex surfaces at lower temperatures and at faster rates than in conventional CVD or PVD alone.[1] In plasma-based nitriding or carburizing of steels for wear improvement, a faster, more uniform heat treatment can be conducted compared to conventional gas nitriding and carburizing.[2] In plasma-based ion implantation (PBII)[3] the treatment capabilities of conventional ion-beam implantation can be extended to allow for larger-scale, faster, and potentially more cost-effective implants of objects. Finally, in plasma-based electron bombardment (PBEB),[4] the capabilities of conventional electron-beam or laser-beam hardening[5] can be extended to faster and more uniform treatment of larger size parts, or the simultaneous treatment of larger numbers of small-scale parts. In this paper, we describe the physics and technology of PBII and PBEB for improving the tribological properties of tools, dies, and components. We first present a process description of the two technologies followed by a description of experimental hardware. We then present recent results of the use of the two technologies for improving the tribological properties of tools, dies, and components used in the automotive and aerospace industries.

Process Description of PBII

Detailed reviews of the PBII process can be found in separate publications.[6-8] Here we present a discussion of the salient features of the PBII process to serve as a basis for later considering the PBEB process.

In PBII, part is placed in a vacuum chamber that is filled with a plasma containing ions to be implanted. The plasma can be comprised of metal or gaseous ions. For gaseous ions such as nitrogen, partially-ionized (0.1-10%) plasmas are typically produced, in a neutral-gas operating pressure range of 10^{-5} - 10^{-3} Torr, with plasma densities in the range of 10^8 - 10^{11} cm^{-3}. For metal

ions, fully-ionized plasmas are typically produced with similar plasma densities as for gaseous ions. The plasma density affects the degree to which the plasma sheath can conform to the surface features of the part — with higher values of the plasma density conforming better than lower densities. The pulse modulator biases the part to a high, negative potential (typically ranging from 20-100 kV) using short-duration (10-30 μsec), repetitive (100-2000 Hz) voltage pulses which develop across the sheath surrounding the part. Plasma ions undergo collisionless acceleration across the sheath and are implanted omnidirectionally and simultaneously over the entire surface of the part. This allows for implantation of part sizes not previously possible or practical using conventional ion-beam implantation. The implantation of ions into the part surface causes the emission of secondary-electrons, which are then re-accelerated across the plasma sheath and impact the chamber walls with the full pulse-bias energy, causing x-ray production that must be shielded for safety.

Figure 1 shows a sample of PBII technology capabilities that have been developed for tribological applications at several facilities throughout the world, plotted as implantation voltage vs. pulse-modulator power. PBII has been demonstrated to be routinely conducted[9,10] at implantation voltages up to 100 kV. Recent advances[11] have also established the feasibility to extend the voltage capability to as high as 250 kV. Continuous, total pulse-modulator power levels of 100 kW at 100 kV have also been demonstrated. Pulsed ion-current densities from 0.1-10 mA/cm^2 have been achieved at 100 kV with total average currents of 1 A. Vacuum chamber sizes used in PBII range in volume from 0.5 m^3 to 8 m^3 to explore scaling issues[12-14] in the treatment of parts. Key issues in PBII technology related to packing density of parts, plasma conformity requirements, and x-ray issues, are addressed in a separate publication.[15]

Process Description of PBEB

In PBEB, a part to be heated via electron bombardment is placed in a vacuum chamber that is filled with a plasma. This chamber may be the same as that used in PBII. The plasma can be comprised of any gas such as nitrogen or argon, since the only essential issue is the production of plasma electrons. The neutral gas pressure is kept below 10^{-4} Torr, and plasma densities can range

from 10^8 - 10^{11} cm^{-3}. The neutral gas pressure is kept below 10^{-4} Torr to minimize current runaway (leading to arcing) during a single pulse.[4] The plasma density allows the part to be enveloped by a sheath that conforms to its general features. The pulse modulator biases the part to high, positive potential (typically ranging from 20-100 kV), using short-duration (10-30 μsec), repetitive (100-2000 Hz) voltage pulses. Electrons are accelerated into the part to heat it omnidirectionally and simultaneously. This allows for uniform surface heating of part sizes not previously practical using conventional electron-beam or laser-beam heating techniques. The bombardment of plasma electrons into the part surface in PBEB does not cause secondary electron emission. Instead, x-ray production occurs due to the direct impact of the plasma electrons into the part surface. Therefore, x-ray shielding is still an issue that must be contended with for safety. When conducting PBEB for heat treatment of parts, it is important that the surface area of the parts be small compared to the surface area of the chamber. This prevents perturbation of the plasma potential and allows the applied pulse bias to accelerate plasma electrons across a plasma sheath that surrounds the part.[16,17] The actual sheath dynamics in PBEB have not been studied in detail and will be the topic of a future publication.

PBEB can be conducted in two different modes of operation. The first mode is a rapid, high-power, burst-train mode (interaction or treatment time of 0.5-5 sec), which is used to achieve rapid and preferential surface heating of a part without significantly heating the part interior. The second mode consists of a low- or high-power, continuous-train mode (interaction of treatment time of 1 min-2 hrs), which is used to achieve uniform surface and bulk heating of the part. In either mode, a separate forced-quenching technique (such as high-pressure gas or oil quenching) can be used to assist in the desired treatment process. PBEB has been demonstrated at the 100-kV, 100-kW power levels to conduct both modes of operation, with and without forced quenching. In the burst mode, pulsed-electron current densities as high as 4 A/cm^2 at 100 kV voltage levels have been used for self quench-hardening of gears, as well as brazing and melting. In the continuous heating mode, normalizing, brazing, and melting have been demonstrated.

Compared to conventional convection, radiation, and conduction heating techniques, the PBEB process is more efficient in that every electron that is accelerated into the part surface contributes to the heating process. It also allows for larger-area treatment capabilities of many small-scale parts, or a larger-scale, single part subject however to the surface-area requirements of the part and the vacuum chamber as discussed previously. Figure 2 summarizes[18] the intended range of application of present PBEB technology (for single-pulse and burst-mode operation) compared to conventional electron- and laser-beam treatment techniques.

EXPERIMENTAL HARDWARE DESCRIPTION

PBII and PBEB experiments were conducted using the Hughes Research Laboratories implant/heat-treat facility. This facility consists of a 1.2-m-diameter × 2.4-m-long stainless steel vacuum vessel and a 100-kV, 100-kW pulse modulator. A detailed description of the vacuum chamber and pulse modulator performance can be found in previous publications.[9-12,19,20]

Figure 3a shows the schematic of the pulse modulator and the vacuum chamber configuration used to conduct PBII experiments. Negative polarity voltage pulses are produced by modulating the voltage of the capacitor using the Crossatron switch. By using a separate double-pole, single-throw, high voltage switch (not shown), the capacitor and Crossatron switch can be interchanged, as shown in Figure 3b to produce positive-polarity voltage pulses used in PBEB.

Figure 4 shows examples of the actual time-phased current and voltage waveforms that result during an actual implant in PBII (Figure 4a) and during an actual heat treatment in PBEB (Figure 4b) using the pulse modulator circuitry shown in Figure 3. In both cases, near-square voltage waveforms are produced with a near-instantaneous (less than 1 μsec) rise time compared to the pulse duration. The current waveforms in both cases exhibit a sharp rise followed by a gradual decay to a near steady-sate value.

EXPERIMENTAL TECHNIQUES DESCRIPTION

In the next two sections, we present recent demonstrations of the use of PBII and PBEB for achieving tribological improvements of tools, dies and components. We first consider examples of PBII technology followed by PBEB treatment of materials.

Treatment Techniques Using PBII

In previous publications, we reported on the use of the Hughes PBII facility to conduct 100-kV implants of a 1362 kg polymer die,[11,12] to extend the wear life of Co-cemented WC drill bits used in printed wiring board fabrication,[21] and to extend the wear life of TiN-coated cutting tools.[12] Major emphasis at HRL is now being placed on using PBII technology to assist in hard-coating development and performance for improving the wear performance of tools, die and molds used in automotive and aerospace applications. Three areas are being pursued; post-treatment, pre-treatment, and *in-situ* treatment of hard-coatings using PBII. As a post-treatment technique, we describe new additional results in the use of PBII to increase TiN-coated, cutting-tool wear performance, as well as for extending the wear life of TiN-coated foundry-mold blocks. As a pre-treatment technique, we present results describing the use of PBII for interfacial mixing of TiN prior to hard-coating deposition. Finally, as a *in-situ* treatment technique, we describe facility upgrades presently under way to develop PBII-assisted deposition of low-temperature coatings of TiN via magnetron sputtering.

Post PBII Treatment of TiN-Coated Cutting Tools

Ion-implantation is known to improve the wear properties of TiN-coated cutting tools.[22,23] Depending on the dose and the energy used for the implant, the surface hardness can be either increased or decreased resulting in variations in wear performance. We implanted molecular nitrogen ion at 100 kV (dose of 2×10^{17} cm^{-2}) into 5-μm-thick, TiN-coated cutting tools.

The cutting tools were coated with TiN by Balzers and Multi-Arc Corp., and the tools were then used by two major manufacturers of gears in the automotive and aviation industries. We found a 2$\times$ decrease in the surface hardness as inferred from nano-indentor hardness measurements penetrating

20-80 nanometers into the coating surface. The tools were evaluated for wear after 300 parts had been produced by measuring the amount of flank wear experienced on select teeth. The tools were then re-sharpened (or re-ground) and placed back into production. The procedure was repeated several times to conduct a thorough evaluation of the effect of implantation on the wear performance of TiN-coated cutting tools used in the two industries. Figure 5 shows the wear vs. re-grind data for the Balzers-coated (Figure 5a) and Multi-Arc-coated (Figure 5b) tools. The Balzers TiN-coated tool (Figure 5a) experiences 24 mil of wear after 300 parts are produced. With PBII treatment, the TiN coated tool wear is reduced to less than 1 mil after 300 parts are produced. After the first re-grind, the tool wear experienced is 2 mil as shown. Multiple re-grinds on two different tools indicate an average 8x reduced tool wear following PBII treatment. An average 6× reduced wear is shown in Figure 5b for Multi-Arc TiN-coated tools.

Post PBII Treatment of TiN-Coated Foundry Blocks

Foundry parts such as patterns and molds used in the automotive and aerospace industries are subject to sand abrasion wear. In many applications, a compact of SiO_2 sand (100-500 μm size) is compressed (several hundred PSI) against stainless steel patterns and molds for casting of parts and components. Wear of the stainless steel limits the lifetime of the pattern or mold; therefore, the part must be replaced or repaired. Typically, a hard coating of TiN (about 3-5 μm thick) is used to reduce surface wear. We post implanted nitrogen into TiN-coated (Balzers Corp.) foundry blocks (10 cm in size) via the PBII process to extend the wear performance of the TiN coating itself. Molecular nitrogen ions were implanted at a voltage of 100 kV and a dose of 2×10^{17} cm^{-2}. Upon implantation, the normally gold-colored TiN coating transformed[22,24] to a deep purple color. We demonstrated that the wear process could be monitored visually by the change in the color of the coating as the implanted layer was worn through. The implication on the manufacturing process in improving the wear performance of a hard coating and simultaneously coloring the surface for wear monitoring is discussed in a separate publication.[24] The five implanted blocks (as well as five un-implanted blocks) were evaluated for foundry wear under actual manufacturing wear conditions by mounting all ten blocks onto a large-scale (1.2 × 1.2 m size) automotive-component pattern. The

blocks were placed at benign locations on the pattern to allow the blocks to experience the same wear condition as the pattern, but without interfering in the actual manufacturing process. Even though the estimated ballistic implantation depth was about 0.1 µm; (very shallow compared to the 3-5 µm thick TiN), each implanted block demonstrated more than 2.5 times longer wear life compared to un-implanted blocks.

PBII-Assisted Hard Coating Deposition

For automotive steel dies used in metal forming applications, chrome plating is typically used to provide a hard, wear-resistant surface to extend die life. We evaluated whether TiN could be used to replace chrome for select applications. Many of the die materials used are temperature sensitive and cannot be heated above 300°C without tempering the die material. Therefore conventional PVD coating technologies to deposit hard TiN cannot be used. We therefore began to develop a PBII-assisted, low-temperature TiN-deposition process. The process first utilizes high-energy PBII as a pre-treatment technique to achieve interfacial mixing of TiN, and then uses low-energy PBII as an *in-situ*, assist to magnetron-sputtered, TiN film growth. In our first set of experiments, we sputter deposited 300-400 Å of Ti onto the identified steel die material and then achieved interfacial mixing of a TiN coating using molecular nitrogen ions implanted at a voltage of 100 kV and a dose of 2×10^{17} cm^{-2}. Auger analysis verified a mixed layer of stoichiometric TiN. We evaluated the wear of the treated steel sample using an oscillating pin-on-disk wear apparatus and then compared it to the wear of conventional chrome-plating. The 0.03-µm-thick TiN-mixed layer was found to have a 3× reduced wear compared to a thick (25 µm) chrome-plated coating. Our second set of experiments dealing with *in-situ* growth of hard coatings are in progress. We have recently installed a 1.2-m-long, magnetron sputter target in our PBII chamber to deposit µm-thick TiN onto the mixed TiN using PBII for *in-situ* growth assist. We plan to evaluate coatings experiment by September of 1996.

Treatment Techniques Using PBEB

The PBEB process can be used as a stand-along technique to conduct heat treating of materials, or it can be used as a combination with PBII for thermally enhanced implantation, or in combination with conventional quenching and heat-treatment techniques.[4] In the sections below, we present experimental results describing the use of the PBEB process in four main areas: normalizing, surface-heating for self-quenching, bulk heating and quench hardening, and brazing/melting.

Normalizing

Normalizing is a heat-treatment process in which a ferrous alloy is heated to a temperature above the austenitic transformation range, and then cooled to produce a uniform structure containing ferrite and pearlite. We sought to conduct normalizing of automotive pinion gear blanks made of type 5130 steel using the PBEB process described in this paper. Each gear blank had a diameter of 5.1cm (2 inches), a 2.54 cm-diameter bore (1 inch), and weighed about 0.5 kg (one pound) each. Nine gear blanks were simultaneously normalized using the PBEB operating parameters shown in Table I, The normalizing temperature of 900°C was achieved in less than 5 minutes using an applied voltage pulse level of 30 kV, a pulse duration of 10 μsec, and a pulse repetition rate of 200 Hz. The gear blanks were maintained at temperature for 15 minutes and then cooled at the rate required for normalizing type 5130 steel. Figure 6 shows a photograph of the nine gear blanks heated in the vacuum chamber. The figure also shows the corresponding fine lamelar microstructure obtained from three of the nine gear blanks upon conducting a microstructural analysis to verify adequate normalizing of the gear blanks, suitable for automotive applications.

Surface Heating for Self Quenching

Self quenching using electron-beam or laser beam hardening processes is a heat-treatment process that is commercially available.[5] The surface of a part is rapidly heated to the austenitic transformation temperature level using a finely-focused, high-energy density (about 10 kW/cm^2) electron or laser beam. Hardening of the treated area is achieved by moving the electron or laser beam in a manner that allows the heated area to rapidly cool via heat transfer into the bulk of the

part. This self-quenching technique is widely used in Europe[5] to conduct selective quench-hardening of automotive gears. We sought to conduct a PBEB self-quenching treatment experiment to duplicate this type of result and demonstrate large-scale processing capability.

Automotive gears made of type 5130 steel were cut into samples having an area of about 25 cm^2. A single sample was placed in the PBEB vacuum vessel to be treated via the rapid burst mode using the operating parameters shown in Table 2. With an argon-gas backfill pressure of 3 × 10^{-5} Torr, we applied a burst of pulses for 1 sec to the part, each pulse having a voltage of 70 kV and pulse duration of 10 μsec, which resulted in a power density on the surface of the part of about 1.5 kW/cm^2. During the one burst of pulses, the surface of the part reached 1000°C and then self cooled to 750°C in less than 0.25 seconds. Temperature measurements were obtained using an infrared, optical pyrometer having a response time of 0.1 seconds. Figure 7 shows the typical time phased voltage and current waveforms used during the burst-mode surface heating. In addition, a strip-chart recording of the surface temperature is also presented. Experiments on actual gears having surface areas of 100 cm^2 are planned during 1996.

Bulk Heating and Forced Quench Hardening

We used the PBEB process in conjunction with a novel quenching technique called solid/gas jet (SGJ) quenching[4] to conduct quench-hardening experiments of gears. The quenching process will be discussed in detail in a forthcoming publication. Briefly, the process consists of spraying solid carbon dioxide (CO_2) onto heated parts. The solid CO_2 sublimes from the heated surfaces, carrying away heat in the form of evaporated, gaseous CO_2. We used the SGJ quenching process following rapid and efficient heating of six pinion gears using the PBEB process.

Each of the six pinion gears (having the same dimensions and weight as the gear-blanks used for normalizing) were heated separately using PBEB. A total of six different treatment temperatures were selected to explore hardness vs, temperature for the gear-material composition. The PBEB process was used to heat and maintain the temperature of each gear at a selected set point. The PBEB heating process was then interrupted and the part was cooled using the SGJ quenching processes. Each gear was sectioned for microstructure and hardness measurements. Through-

hardening of each gear was validated. Table III shows the relationship between process temperature and hardness that was achieved for each set point. Figure 8 shows the cross-section microstructure for gear 2 (Figure 8a) and gear 5 (Figure 8b) treated at 1800 and 2000°F respectively. At 2000°F, there is undesirable grain growth, despite the higher hardness. The microstructure of sample No. 2 was judged to have the fine-grained martensitic structure and hardness that is preferred for automotive gears made of type 5130 steel.

Brazing / Melting

When used the rapid burst mode or the slow, continuous operating mode, PBEB can be used for vacuum brazing and melting of materials. In preliminary experiments, we were able to conduct preferential surface heating experiments for novel brazing and melting applications. Cu-brazing of stainless steel components have been performed with good success. In addition, we have also demonstrated melting and alloying of metals for select metallurgical applications.

SUMMARY

We have presented a description of plasma-based ion implantation (PBII) and plasma-based electron bombardment (PBEB) for large-scale surface modification of materials. In PBII, negative-polarity voltage pulses (20-100 kV) provide for omnidirectional and simultaneous implantation of positively-charged ions into a part that is immersed in a plasma. In PBEB, positive-polarity voltage pulses (20-100 kV) provide for omnidirectional and simultaneous bombardment of negatively-charged electrons into the surface of a part that is immersed in a plasma. Both PBII and PBEB can be used as stand alone process or they can be used in combination with other heat-treat technologies. At Hughes, the PBII process is being applied primarily to enhance the performance of hard-coatings. PBII can be used to improve the wear life of TiN-coated cutting tools by 8×, as well as the wear life of TiN-coated foundry blocks by > 2.5×. Presently, a facility upgrade is underway to combine PBII with magnetron sputtering for low-temperature deposition studies of hard, TiN coatings. The PBEB process has been used to normalize and quench-harden small batches of automotive gears. The process can also be used to achieve large-scale self quench-hardening of

gears. The PBEB process also has potential for surface melting, alloying, and brazing over larger areas than that which is possible using conventional electron- or laser-beam techniques.

ACKNOWLEDGMENTS

REFERENCES

1. Handbook ofDeposition Technologies for Films and Coatings, *Science Technology and Applications*, 2nd Edition, Edited by R. Bunshah, Noyes Publications, Park Ridge, New Jersey, 1994.

2. ASM Handbook, Vol. 4, Heat Treating, Edited by J.R. Davis, et. al., 1991.

3. J.R. Conrad, U.S. Patent No. 4,764,394, Issued August 16, 1988.

4. J.N. Matossian, J.D. Williams, and W. Krone-Schmidt, "Heat Treatment by Plasma Electron Heating and Solid/Gas Jet Cooling", Hughes Research Laboratories, Patent Pending, filed 1992.

5. S. Schiller, S. Panzer, and B. Furchheim, "Electron Beam Surface Hardening", ASM Handbook, Volume 4, Heat Treating, pp. 297-311, ASM International, 1991.

6. J.R. Conrad and K. Sridharan, Editors, Papers From the First International Workshop on Plasma-Based ion Implantation, August 4-6, 1993, University of Wisconsin-Madison, Madison, Wisconsin, Journal of Vacuum Science and Technology B, Vol. 12, No. 2, 1994.

7. G.A. Collins, K. Short Editors, Proceedings of the Second International Workshop on Plasma-Based Ion Implantation, February 12-15, 1995, Australian Nuclear Science and Technology Organization (ANSTO), Sydney, Australia, Surface Coatings and Technology, in preparation.

8. D.J. Rej, "Plasma Immersion Ion Implantation", in Handbook of Thin Film Process Technology, D.A. Glocker and S.I. Shah, Editors, Institute of Physics, in Press.

9. J.N. Matossian and R.Wei, "Operating Characteristics of a 100-kV, 100-kW, Plasma Ion Implantation Facility", Proceedings of the Second International Workshop on Plasma-Based Ion Implantation, February 12-15, 1995, Australian Nuclear Science and Technology Organization (ANSTO), Sydney, Australia, Surface Coatings and Technology, in preparation.

10. J.N. Matossian and D.M. Goebel, "Design Characteristics of a 100-kV, 100-kW, Plasma Ion Implantation Facility", Proceedings of the Second International Workshop on Plasma-Based Ion Implantation, February 12-15, 1995, Australian Nuclear Science and Technology Organization (ANSTO), Sydney, Australia, Surface Coatings and Technology, in preparation.

11. J.N. Matossian and R. Wei, "Challenges and Progress Toward a 250-kV, 100-kW Plasma Ion Implantation Facility", Proceedings of the Second International Workshop on Plasma-Based Ion Implantation, February 12-15, 1995, Australian Nuclear Science and Technology Organization (ANSTO), Sydney, Australia, Surface Coatings and Technology, in preparation.

12. J.N. Matossian, J. Vac. Sci. and Technol. B, Vol. 12, No. 2, March/April, 1994, pp. 850-853.

13. B.P. Wood, I. Henins, R.J. Gribble, W.A. Reass, R.J. Faehl, M.A. Nastasi, and D.J. Rej, J. Vac. Sci. Technol.,B, Vol. 12, No. 2, Mar/Apr 1994, pp. 870-874.

14. C. Munson, R.J. Faehl, I. Henins, M. Nastasi, W.A. Reass, D.J. Rej, J.T. Scheuer, K.C. Walter, and B.P. Wood, "Recent Advances in Plasma Source Ion Implantation at Los Alamos National Laboratory", 22nd International Conference on Ion Beam Modification of Metals (IBMM), San Sebastian, Spain, 1995.

15. D.J. Rej, F.J. Faehl, and J.N. Matossian, "Key Issues in Plasma Source Ion Implantation", this workshop.

16. J. Pelletier, Y. Arnal, R. Debrie, L. Pomathiod, and R.C. Rifflet, Rev. Sci. Inst., Vol 55, No. 10, October 1984, pp. 1636-1638.

17. I. Alexoff, and W.D. Jones, Phys. Rev. Lett., Vol. 15, 286, 1965.

18. Taken from C. Charissoux, P. Bonnin, J.N. Calvert, and M. Contre, "Review of Laser and Electron Beam Processes in the Nuclear Field", pp. 145-159, in R. Bakish, Editor, Proceedings of the Conference, The Laser vs. the Electron Beam in Welding, Cutting, and Surface Treatment, State of the Art, 1987, Bakish Materials Corporation, Engelwood, N.J., 1987.

19. D.M. Goebel, J. Vac. Sci. Technol. B12(2), March/April, 1994, pp. 838-842.

20. D.M. Goebel and W.A. Reass, "Crossatron Modulator Designs and Performance for Plasma Based Ion Implantation Systems", 21st International Power Modulator Symposium, Westin South Coast Plaza, Costa Mesa, CA., June 27-30, 1994.

21. J.N. Matossian, J.J. Vajo, J. A. Wysocki, and M.E. Bellon, Surf. Coat. Technol., **62**, 595 (1993).

22. R. Monory, L.J. Liu, D.KL. Sood, Z.M. Shaw, C.Kylner, and M. Braun, Surf. Coat. and Techn., 70 (1994) 1-7.

23. R.J. Culbertson, F.C. Burns, W. Franzeu, L.J. Lowder, J.J. Ricca, and A. Gonzales, Nucl-Instrum. Methods, B56/57, (1991). 652.

24. J.N. Matossian, P.H. Mikula, J.L. Bartelt, "Evaluation of the Extent of Wear of Articles", U.S. Patent No. 5,303,574, issued April 19, 1994.

FIGURE 1

FIGURE 2

SHOCK HARDENING

SPECIFIC ENERGY J/cm²

10^0 10^2 10^4 10^6

RAPID
SURFACE
ALLOYING
SINGLE PULSE PBEB
MELTING
DRILLING
WELDING & CUTTING
CLADDING & SURFACE MELTING
BURST MODE PBEB
TRANSFORMATION
HARDENING

POWER DENSITY (W/cm²)

10^{10} 10^9 10^8 10^7 10^6 10^5 10^4 10^3

10^{-8} 10^{-6} 10^{-4} 10^{-2} 10^0

INTERACTION TIME (seconds)

FIGURE 3

9512-15-063

2.4 m

PLASMA
SHEATH   OBJECT

8455H
CROSSATRON

10 kΩ   0.5 µf   10 Ω

100 kV
POWER
SUPPLY

5 kΩ

1.2 m

(a)

PULSE MODULATOR   VACUUM CHAMBER

9512-15-063b

2.4 m

PLASMA
SHEATH   OBJECT

8455H
CROSSATRON

10 kΩ   10 Ω

100 kV
POWER   0.5 µf
SUPPLY   5 kΩ

1.2 m

(b)

PULSE MODULATOR   VACUUM CHAMBER

FIGURE 4

18 KV/DIV

(a)

300 A
100 KV

100 A/DIV

0

5 μ SEC/DIV

9312-15-318

(b.)

V = 90 kV

V

I

I = 20 A/div

5 μsec/div

(a)

(b)

FIGURE 6

100X   100X   100X

FIGURE 7

70 kV

100 A

f = 1 kHz
t_{ON} = 1 sec

5 µsec/div

PULSE BURST OFF

SURFACE TEMPERATURE (°C)

TIME (sec)

FIGURE 8

9312-15-133

(a)

9312-15-134

(b.)

TABLE I. Normalizing of Gear Blanks Via PBEB

PBEB Operating Parameter	Parameter Value
Applied Voltage, V (kV)	30
Average Pulsed Current, Ip (A)	150
Average DC Current, I_{AVG} (A)	0.25
Pulse Repetition Rate, f (Hz)	200
Pulse Duration, PD (μsec)	10
Working Gas	Argon
Working Gas Pressure, P (Torr)	3×10^{-5}
Normalizing Temperature, T (°C)	900

TABLE II. Self Quenching Via PBEB Process

PBEB Operating Parameter	Parameter Value
Applied Voltage, V (kV)	70
Pulse Duration, PD (μsec)	10
Burst Time, t (sec)	1.0
Total Number of Pulses in Burst, N	500
Average Power Density, P_{AVG} (kW/cm^2)	1
Working Gas	Argon
Working Gas Pressure, P (Torr)	3×10^{-5}
Pulse Repetition Rate, f (kHz)	1

TABLE III. Quench-Hardening of Gear Blanks Via PBEB

Gear No.	Treatment Temperature (°F)	Rockwell Hardness (R_A)	Surface Composition
1	1700	69	
2	1800	71	Definite Martensite. Good Grain Size
3	1900	72	
4	2000	75	
5	2000	75	Definite Martensite. Large Grain Size
6	2000	74	
7 Untreated	N/A	50-51	

The Use Of A High Voltage Discharge At Low Pressure For 3-D Ion Implantation

Vladimir I. Khvesyuk,

Professor,

Bauman State Technical University, P.O.Box 38, Moscow 107005, Russia

Piotr A. Tsygankov,

Senior Scientist,

Bauman State Technical University, P.O.Box 38, Moscow 107005, Russia

Abstract

A high voltage pulse gas discharge burning on the left branch of the Paschen curve is used as a base for the three dimensional ion implantation (3DII). 3DII technique uses a scheme where target is the cathode and vacuum chamber filled with working gas is the anode. An external characteristics of the gas discharge are described. Results of probe investigation of the main discharge parameters are presented. It is found that gas discharge has a quasi stationary spatial structure with thin layer (less than 1cm) of the cathode fall where all voltage applied to electrodes drops. Ions effectively accelerate in cathode fall in a collisionless mode. The Auger profile of implanted atoms proves treatment by monoenergetic ions flux. High energy ions current density on the cathode surface is measured. Possible mechanisms of generation of ions flux on the cathode are discussed. It is shown that the near-anode plasma is not a general supplier of ions on the cathode. The main measured parameters and discharge features make it possible to use 3DII technique for technological applications.

1. Introduction

First non-line-of-sight technique called plasma source ion implantation (PSII) have been proposed by J.R.Conrad [1,2]. In PSII target to be implanted is placed directly in a preliminary generated plasma and then pulse biased to a high negative potential (up to 100 kV and more) in regard of the chamber walls. A plasma sheath forms around the target and ions accelerated across plasma sheath bombard the whole target surface from all sides simultaneously. The main advantage of PSII in comparison with conventional line-of-sight technique is that it makes redundant target manipulation and ion beam guns with rastering system. PSII is smaller, simpler to maintain and operate. It is also more reliable.

Serious disadvantage of PSII is that ion-matrix sheath surrounding the target is non-stationary: during pulse time it expands. Quality treatment (normal angle of ion accidence, monoenergetic ion flux, implantation dose uniformity) of complex shape workpieces requires a thin sheath surrounding workpiece where ions accelerate on target. The term thin sheath means that it should be thin enough to follow the unevenness of the surface of the workpiece.

The three dimensional ion implantation (3DII) technique are presented in this paper. Target is placed in grounded vacuum chamber and then as in PSII pulse biased by high negative potential in repetion mode. Working gas is led into the vacuum chamber. Quasi stationary form of high voltage self-sustain gas discharge starts up under conditions conform to the left Branch of Paschen curve. The important feature of this kind discharge is a thin layer of cathode fall where all voltage applied to electrodes drops [3,4]. Electrons emitted from cold cathode (non-thermoemissive) are accelerated in this region. The technological electron guns producing monoenergetic electron beam based on the intensive mode of these discharges is known [5].

2. Three dimensional ion implantation device

The scheme of 3DII device and configuration of the discharge volume are shown on Fig. 1. A grounded stainless steel vacuum chamber 650mm in high and $\varnothing$510mm in diameter is the anode. The cathode $\varnothing$70mm×30mm is separated from anode by ceramic (Al_2O_3) insulator. Cathode temperature is controlled by water-cooling system in case of necessity. Unlike PSII 3DII does not use the array of permanent magnets surrounding the vacuum chamber. It does not require unit for preliminary ionization of the working gas to operate the device.

High voltage pulse power supply provides discharge voltage from 10kV to 80kV and average power up to 1kW. The pulse length may range from 80μs to 500μs. The pulses frequency is from 10Hz to 50Hz. A special circuit prevents from arcing mode. Cathode is connected to HV pulse power supply by flexible current feed through.

Vacuum is provided by turbomolecular pump system with a pumping rate of 0.72m^3/s in the pressure range (10^{-2}-10^{-4} Pa).

Working gas is led into vacuum chamber through a system allowing to control taken gas pressure.

3. Results of preliminary experiments with 3DII device

The typical voltage curve applied to electrodes is shown in Fig. 2. The HV pulse power supply generates a negative voltage impulse of relatively rectangular form having a bell-like peak on the rise front due to the current cable capacity. The typical dependencies of discharge current on time for different applied voltages and pressure conditions are also presented in Fig.2, where p1<p2<p3. The discharge current appears without preliminary ionization of gas in the chamber volume with a delay in regard of the voltage rise front depending on the working gas pressure for applied voltage of more than 30kV. A marked plateau is apparent between 80μs and 230μs from discharge

start up. Therefore corresponding dependencies of collected current I(t) and target bias U(t) are essentially different for 3DII and PSII. PSII is marked with a peak of I(t) [6]. It is connected to the following feature of discharge dynamics: surrounding cathode plasma sheath expands at ion acoustic velocity of 0.25cm per μs. Therefore initial current increase changes to a decrease due to the restriction of Child-Langmuir equation:

$$j(t) = \frac{4\varepsilon_0}{9}\left(\frac{2e}{M}\right)^{1/2}\frac{U^{3/2}}{s(t)^2}$$ (1)

where s(t) is the time-dependent sheath thickness.

In 3DII current is independent of time excluding initial pulse rise time and current cut-off. This result points out that plasma sheath is motionless during the whole pulse length, i.e. the discharge under consideration acts in a quasi stationary mode .

Fig. 3 presents the measured increasing current-voltage characteristics of gas discharge and working pressure field vs. applied voltage. Conditions for the existence of a gas discharge correspond to the left branch of Paschen curve (pd is less than $(pd)_{min}$), where d is a distance between electrodes and p is pressure in the vacuum chamber. The start up voltage and the burning voltage are approximately equal for this kind discharge [3]. Discharge starts up only on fixed working gas pressure defined by electrode geometry, applied voltage, cathode materials, etc. These features are illustrated in Fig.3 by the ignition curve marked I_{ign} and a curve p_{ign} in pressure-voltage axes corresponding to it. It is possible to vary discharge current in the range I_{min} and I_{max} after ignition by changing pressure from p_{min} to p_{max}. In case when pressure $p > p_{max}$ gas break-down occurs and discharge converts to the arcing mode, the case $p < pmin$ is that of gas isolation.

Further the results of measurements of Auger depth profile are considered. We used most often nitrogen as a working gas in our experiments (we have also operated

the device with argon and xenon). Our experiments have demonstrated that 3DII is capable of implanting ions to concentrations and depths required for surface modification. For example in Fig. 4 we show Auger profile data of the concentration profile nitrogen ions implanted into a silicon sample during treatment in the discharge at 40kV. The important feature of these dependencies is that we obtain reasonable agreement with data of numerical codes for penetration of monoenergetic (energy is approximately equal to voltage between the cathode and the anode) flux of molecular nitrogen ions [7,8]. This fact indicates that, firstly, the thickness of the ion acceleration region is smaller than the charge exchange free pass length ($d_u < \lambda_{i-a}$, $\lambda_{i-a} \approx$ 3-5cm for discharge conditions) and, secondly, that practically all potential difference falls on this region.

Several series of testing experiments have been carried out to measure microhardness and wear resistance. Generally, the results are in agreement with other data of ion implantation modification [9].

4. Plasma parameters in the gas discharge

The distribution of plasma density and electron temperature and electrical potential along vertical axis of discharge have been determined. The special Langmuir probe has been used to take the main plasma measurements. The point is that high energy (10...80keV) electron beam propagates from the cathode to the anode and the probe collects part of this beam current. In order to minimize collected electron beam current and to provide area sufficient for low density measurements the special shape Langmuir probe is used: hollow cylinder with height 5mm, diameter $\varnothing$35mm and thickness 0.1mm. Vertical axes of gas discharge and the Langmuir probe coincide to provide minimal electron beam current signal. The measured values of plasma density are checked by probe with convenient configurations such as standard cylindrical

geometry in the discharge areas where electron beam effect is negligible to take into account form factor correctly.

In Fig.5 are presented typical results of measurements of electron density, electron temperature and plasma potential along vertical discharge axis. These investigations were carried out for a discharge in a nitrogen with copper cathode and stainless steel vacuum chamber walls (anode). Applied negative pulse voltage was 40kV with repetition rate 25Hz to prevent overheating of cathode. The amplitude of discharge current is maintained equal to 0.4A.

Plasma is found out near anode. Discharge structure builds up to 20-30μs from the appearance of the discharge current. Concentration rises during pulse, but variations are in a 30% interval for times greater than 50μs. Fig.5 illustrates this feature. The plasma density increases from anode surface and achieves maximum $n=9 \cdot 10^{14} cm^{-3}$ about 23cm from the cathode surface and the density steeply drops to $n=10^{14} m^{-3}$ about 18cm from the cathode surface. Electron temperature in the plasma "body" is equal to approximately 0.7eV and increases sharply at the anode plasma boundary ($z \approx 18cm$). The plasma potential is always higher than anode potential to prevent a slow electrons diffusion on the chamber walls. Plasma with a density higher than the threshold for probe investigation ($\sim 5 \cdot 10^{12} m^{-3}$) is not found in the space between the cathode surface and the near-anode plasma boundary, but it should be mentioned that the Langmuir probe measurements are impossible in the near-cathode area ($z=1-3cm$) due to a breakdown on the measuring circuit. Dependencies of plasma parameters and spatial structure from applied voltage, working gas and cathode materials are not discussed in details in this paper. Just note that the replacing cathode material with titanium results in decrease of maximum level of plasma concentration to $4.2 \cdot 10^{14} m^{-3}$, but density distribution behavior and location plasma boundary are approximately the same.

The region between the cathode and the plasma boundary is identified as a cathode layer. A high impedance "floating" probe has been used to investigate the cathode layer [4,5]. In the area with charged particles motion and with no plasma it acts as an indicator of cathode fall region: an abrupt rise of signal from the probe corresponds to the beginning of the cathode drop. Investigations based on this method reveal very thin thickness of the cathode fall where just all applied to electrodes voltage drops. Estimates showed that cathode fall thickness d_u is less than 0.5cm, i.e. it amounts to several Debay length. Optical investigations and geometry of electron beam propagation not presented here prove this feature.

These results make it possible to select two typical fields in discharge structure:

- near-anode plasma with density $n=(1...10)\cdot10^{14}m^{-3}$;

- cathode layer with thin cathode fall region.

5. High energy ion current to the cathode

Probe measurements near the cathode surface have proved impossible, therefore direct measurements of the ion current density at the cathode surface were carried out. The importance of such measurements is in particular based on the fact that they make it possible to understand the mechanism of the ion current generation.

Two alternative mechanisms have been discussed. In accordance with the first supposition the near-anode plasma boundary is the source of the ion current passing to the cathode surface: the ions are extracted from the anode plasma surface, are accelerated in the layer with a very low degree of ionization and then bombard the cathode penetrating into the surface.

In accordance with the second supposition a plasma region with a relatively high degree of ionization is formed in the cathode layer and it is there where the ion current to the cathode is generated.

The method of determining the ion current at the cathode surface is based on experimental measurements of integral dose of atoms absorbed by the cathode surface layers. The measurements are carried out in the following order. After the cathode is treated in a discharge by nitrogen ions, Auger measurements of the nitrogen concentration profile at different locations of its surface are carried out. Then the dose of the absorbed particles is determined by integrating the relationships obtained. Using the total time of treatment (exposure under ions flux) we can calculate the ion current density per pulse average during treatment time:

$$j^+ = 0.5D_N \cdot \frac{1}{\tau \cdot f \cdot t} \qquad (2)$$

where D_N is dose of the implanted nitrogen atoms;

τ is discharge current pulse duration;

f is pulse repetition rate;

t is treatment time.

The above method provides sufficient accuracy if the following conditions are met.

First, the thickness of cathode surface layer sputtered by the ions h_s should be considerably less than the average depth of the ion penetrating into the material R_p, $h_s \ll R_p$. This imposes an upper limit on the time of the cathode exposure in the discharge. But on the other hand implant ions dose must be sufficient for reliable registration by spectrometer. Note that if sputtering is significant measured ions current by Auger will be less than the real ions current.

Second, all the ions bombarding the cathode, are molecular, N_2^+. This is connected with a very low value of the possibility of two successive events, namely, dissociation of molecules and ionization of one of the resulting atoms.

Third, ion current to the cathode should have constant density during the impulse time. This is demonstrated sufficiently accurately by the measurements of relationships I(t) Fig.2.

Forth, effect of thermodiffusion processes is negligible because the temperature of the cathode surface is controlled during treatment and does not exceed 80°C.

The above measurements were carried out using a copper and titanium cathode for different locations along the generating line of the cathode profile (along the flat surfaces radius of the cathode and along the length for the cylindrical surface). These results are present in Fig.6.

The results obtained may be used to answer the question which was asked at the beginning of this section. What is the mechanism of the ion current generation at the cathode surface. The corresponding estimates are mainly based on the application of Bohm relationship for the ion current from plasma extracted to the surface on the flat electrode having a negative bias potential:

$$j_{calc}^+ \approx 0.5en\sqrt{\frac{2kT_e}{M^+}} \tag{3}$$

Calculation of the value of the ion current from the anode plasma surface where the density of charged particles is about $(5...10)\cdot10^{14}m^{-3}$ shows that the measured value j^+ is approximately 100 times higher than the calculated value j_{calc}^+. From this we can conclude that near-anode plasma is not a general supplier of ions to the cathode.

It is suggested that a thin plasma region is formed near the cathode surface and the density of charged particles in the region is approximately two order of magnitude higher than in the anode plasma. Nitrogen ions generating in this region are then accelerated in the collisionless mode through the cathode fall to bombard the surface like a monoenergetic flux.

The above result is supported by one more calculation result. Suppose that the measured value of the ion current is in some way extracted from the anode layer surface. Calculations using Child-Langmuir equation show that the corresponding potential difference (40kV) cannot provide the transport of current of such high density across the distance 15-20cm between the boundary near-anode plasma and the cathode. The size of the gap between the emitter and the collector assumed in accordance with Child-Langmuir for the above conditions is less than 5cm.

Thus, the results of direct measurements of the ion current demonstrate the existence of a thin plasma region with a relatively high degree of ionization in the vicinity of the cathode. It is obvious that problems connected with generation of such a plasma and its containment near the cathode surface require special consideration.

5. Conclusions

In this paper we have presented some results of the investigation of 3DII process based on a high voltage gas discharge burning on the left branch of Paschen curve. This discharge has a thin (less than 1cm) cathode fall layer where all applied voltage drops, thus this feature provides:

1) simultaneous modification of the whole complex surface;

2) normal angle of ion accidence on treated surface;

3) monoenergetic high energy ion flux.

Experimental investigation shows that density of high energy ions current on the cathode surface are in a several miliampere range during discharge pulse, that is enough for consideration of this discharge as a base for ion implantation device for technological application.

Plasma structure of gas discharge is complex and demands detail experimental investigation and numerical simulation, especially considering the mechanism of ion generation in the vicinity of the cathode surface.

Acknowledgments

LIST OF REFERENCES

1. J.R.Conrad, "Method and apparatus for plasma source ion implantation",
   U.S.Patent No. 4 764 394 (August 16, 1988).

2. J.R.Conrad, "Plasma source ion implantation: a new approach to ion beam
   modification of materials", Material Science and Engineering, V.116A, pp. 197-203
   (1987).

3. *in Russian:*

   А.С. Покровская-Соболева, Б.Н. Клярфельд, "Зажигание высоковольтной
   формы разряда в водороде при больших разряжениях", Журнал технической и
   экспериментальной физики, Т.32 (5), сс. 993-1000 (1957).

   translation in English:

   A.S.Pokrovskaya-Soboleva and B.N.Klarfeld, "The ignition of a high voltage
   discharge at low pressure of hydrogen", Russian Journal of Applied Physics, V.32
   (5), pp.993-1000 (1957).

   and in transcription:

   A.S.Pokrovskaya-Soboleva and B.N.Klarfeld, "Zazhiganie vysokovoltnoi formy
   razriada v vodorode pri bolshich razriazheniach", Zhurnal technicheskoi i
   experimentalnoi fisiki, V.32 (5), pp.993-1000 (1957).

4. G.W.McClure, "High voltage glow discharge in D_2 gas. Diagnostic measurements",
   Physical Review, V.124, No.4, pp.969-982 (1961).

5. *in Russian:*

   М.А.Завьялов, Ю.Е.Крендель, А.А.Новиков, Л.П.Шантурин, "Плазменные
   процессы в технологических электронных пушках", Энергоатомиздат, Москва,
   1989.

   translation in English:

M.A.Zavialov, U.E.Kreindel, A.A.Novikov, L.P.Shanturin, "Plasma processes in the electron guns for technological applications", Energoatomizdat, Moscow, 1989.

and in transcription:

M.A.Zavialov, U.E.Kreindel, A.A.Novikov, L.P.Shanturin, "Plasmennye processy v technologicheskich electronnych pushkach", Energoatomizdat, Moskwa, 1989.

6. J.T.Scheuer, M.M.Shamim, J,R.Conrad et al, " Measurement of electron emission due to energetic ion bombardment in plasma source ion implantation", Journal of Applied Physics, V.70(9), pp. 4756-4759 (1991).

7. J.F.Ziegler, J.P.Biersack, and U.Littmark, "The stopping and range of ions in solids", Pergamon Press, Inc., New York, 1985.

8. *in Russian:*

Ю.А.Быковский, В.Н.Неволин, В.Ю.Фоминский, "Ионная и лазерная имплантация металлических материалов" , Энергоатомиздат, Москва, 1991.

translation in English:

U.A.Bykovsky, V.N.Nevolin, V.U. Fominsky, " Ions and laser implantation in metal", Energoatomizdat, Moscow, 1991.

and in transcription:

U.A.Bykovsky, V.N.Nevolin, V.U. Fominsky, " Ionnaya i lasernaya implantatsya metalicheskich materialov", Energoatomizdat, Moskwa, 1991.

9. J.K.Hirvonen, ed., "Ion Implantation", Academic Press, Inc., New York, 1980

LIST OF FIGURE CAPTIONS

Fig.1. The scheme of 3DII device and configuration of the discharge volume.

Fig.2. Typical view of the applied voltage curves and discharge current curves under different pressure and voltage conditions.

Fig.3. The current-voltage characteristics of gas discharge. Working pressure range vs. applied voltage.

Fig.4. The distribution of implanted nitrogen atoms in the surface layer of a silicon sample. Applied voltage is 40kV.

Fig.5. The distribution of plasma density, electron temperature, Langmuir probe potentials along vertical axis of discharge. Scheme of the discharge spatial structure.

Fig.6. The distribution of a high energy ions current on cathode surface. Discharge in nitrogen. Applied voltage is 40kV.

VACUUM CHAMBER

CATHODE

CERAMIC INSULATOR

CATHODE COOLING SYSTEM

CABLE CURRENT FEED THROUGH

TURBOMOLECULAR PUMP

⌀ 510

⌀ 70

30

210

600

CONTROL UNITS

DIAGNOSTIC & RESEARCH EQUIPMENT

GAS SUPPLY SYSTEM

HIGH VOLTAGE PULSE POWER SUPPLY

Figure 1

Figure 2

Figure 3

Figure 4

CATHODE FALL REGION d_U

CATHODE

CATHODE LAYER

NEAR-ANODE PLASMA

ANODE

n, 10^{14} m^{-3}

PLASMA DENSITY

8.0

6.0

4.0

2.0

0.0

Discharge in nitrogen
Copper cathode
Applied voltage 40kV

▲ — 50 µs
■ — 125 µs
● — 200 µs

0   10   20   30   40
DISTANCE FROM CATHODE Z, cm

T_e, eV

PLASMA ELECTRONS TEMPERATURE

2.0

1.0

0.0

■   distribution for 125 µs

0   10   20   30   40
DISTANCE FROM CATHODE Z, cm

POTENTIAL, V

5.0

0.0

-5.0

Distribution for 125 µs

+   plasma potential U_{pl}
◆   "floating" potential U_{fl}

0   10   20   30   40
DISTANCE FROM CATHODE Z, cm

Figure 5

Figure 6

High effective implantation method in the range of the energies (0,5 kev-10 kev) *

Volosov V.I., Churkin I.N.

Budker Institute of Nuclear Physics SB RAS, Novosibirsk, Russia.

Abstract

The report presents the way of the increasing of implantation effectivety by the implantation with atomic beams, which have no limitations on the space charge on the beam intensity. The energy reducing of the intermediate range (0,5 kev-10 kev) can lead to the considerable (up to 10-100 times) increase of intensive atomic beam with keeping of the same power.

One of versions of a source of atomic flows is the source of fast heavy atoms (source with crossed fields - ISP). The physical principles of source operation determine the advantages of this source compare to the traditional ion implanters.

Results of experiments on the irradiation of the titanium and niobium targets by flows of carbon atoms ($<W>\sim 2.5$ kev, $j\sim 50$ mA/sm^2) are showing the possibility of the high effective implantation by atomic flows at the intermediate energy.

Keywords: implantation, intermediate energy, heavy atoms, source of atoms, source of fast heavy atoms.

1.Introduction

The possibility to use the ions at the intermediate energy (0.5 kev-10 kev) for updating of surfaces is discussed for a long time. Among many problems retarding work in this area main was the absence of enough effective implanter. The new approach and decision of this problem with use the high efective source of fast heavy atoms is below considered. Data of experiments have shown an possibility of the effective implantation at these energies, having advantages before known methods.

* Corresponding author. e-mail: volosov@inp.nsk.su

2. Problems of the implantation in the range of intermediate energies.

2.1. Now two methods of the implantation of constructional materials are well known. One of them is a traditional ion implantation, in which are flows of accelerated ions with energies 40 kev - 100 kev [1], other method is a plasma-ion implantation, in which ions with energies 200 ev - 500 ev [2] are used. It is evident from comparison of parameters these two techniques, that in the area of the intermediate energy (0.5 kev - 10 kev) can exist favorable conditions for a implantation.

We shall consider in more detail arguments in protection of this statement.

A) First of all, as is marked above, the fact of existence of two energy rangies, in which process of the implantation will be successfully realized, means, that in intermediate range this process should too exist.

B) Projective run of an ion in both methods of the implantation is much less than depth, on which atomic and phase structure of a target can be changed at availability of diffusion processes depended on parameters of implantation (intensity of flow, doze of implantation, temperature of target and etc.) [3].

C) The number of experiments confirms the possibility of the implantation at energy of ions the order of 5 kev-10 kev [4].

D) In the range of the intermediate energies (0.5 kev-10 kev) practically for all materials factor of the sputtering S≤1 [5] (left-hand branch of curve of sputtering), that is one of arguments for use of the intermediate energy range for purposes of a implantation.

The listed above arguments specify necessity of more detailed research of processes of the implantation in the range of intermediate energies.

2.2. One of main problems at study of possibilities of the implantation at the intermediate energies - absence is enough effective means of creation of ion flows in this area of energy. It is connected to some basic defects of traditional methods.

In ion implantation using ion sources with subsequent acceleration of ions in vacuum gap, there is the basic limitation on ion current. It is connected with charge and weight of ions: $I \sim W^{3/2}/M^{1/2}$. The intensity of ion flow decreases at decrease of ion energy , especially it is essential for ions of large weights (Ti, Ni, Mo, W and etc.), that results

in significant growth of time of the irradiation and can change of process of the implantation due to diffusion prosses.

One of disadvantage of the plasma-ion method of the implantation at the increase of ion current density is transition of the discharge to arc discharge causing the destruction of a target. Rise of voltage results to the intensive sputtering of a target and pollution of plasma.

Practically all these problems are solved at the implantation by intensive atomic flows at the intermediate energy. It is possible to receive such flows using special powerful sources of atomic flows.

One of such sources, source of type ISP, the description of which is given below and based on following physical principles:

A) The acceleration of ions occurs in the plasma volume. Thus in plasma there are the enough electrical fields for acceleration of ions across magnetic field up to required of a energy. At fulfilment this condition there are practically no limitations on the current of accelerated ions.

B) Fast heavy ions are magnetized in the plasma volume of source. The flow of accelerated heavy particles is removed from source not in the form of ions, but in the form of neutral atoms. The main channel of leaving of ions from plasma is charge-exchange in plasma volume and leaving as fast heavy atoms. That results in high efficiency of use of working substance and low power losses. Besides the transportation of atomic flows hasn't any limitations due to space charge.

C) The heavy ions are created at ionization of cold neutral atoms (gas of neutral atoms). These atoms, in turn, are created at the sputtering of the cathode material by fast heavy ions of plasma.

Principle of creation of working substance by self-sputtering of the cathode material permits to work for this source practically with any material.

Below we consider a principle of work and design of the source of fast heavy atoms (ISP) in detail. Early the brief reports on this source were published on conferences in Ekaterinburg [6] and Dubna [7].

3. Source of fast heavy atoms.

Source of fast heavy atoms is the system with crossed fields (axial magnetic and radial electrical) - ISP is shown in Fig.1.

Main processes occurring in the source are is shown in Fig.2:

The radial electrical field in plasma volume is supported by the electron conductivity along the lines of a magnetic field and system of end electrodes. The born in plasma ion falls on cathode and sputters substance of cathode. Sputtered heavy atom move in radial direction and is ionized in plasma. In crossed fields of the source the heavy ion is accelerated moving on the cycloidal trajectory.

The part of fast heavy ions falls on cathode and due to the effect of the self-sputtering support the balance of particles in the discharge. The other ions moving on cycloid are in plasma volume up to moment of the charge-exchange on neutral gas consisting mainly of sputtered heavy atoms.

As this process is the main channel of losses of ions, the source is rather economic. The significant part of energy from source go out by fast heavy atoms.

The energy of fast heavy atom is close to energy expended for reception of this atom in the source, that specifies high profitability of the source.

From considered above circuit of work of the source follows, that the source is universal and can work practically with any substance sputtered at ion bombardment.

Feature of work of the source is a stable voltage on plasma at change of discharge current in wide range as seen in Fig.3.

The quantity of discharge voltage depends on material of the cathode and macroscopic parameters (magnetic field, geometrical dimensions and etc.).

In considered variant the source works in pulsing mode, the duration of discharge depends on capacity of power supply systems (t~1-20 msec). There is not enough restriction on discharge currents (up to 600 A and more).

Serviceability of a source with various materials of the cathode (Mo, W, Ti, C, Cu, Ni, BN) is shown.

Experimental results are in agreement with numerical calculations of main parameters of the source [8].

4. Main parameters of atomic flows.

Leaving from the source the fan atomic flow has practically absolute azimuthal uniformity (angle-2π). In longitudinal direction the uniformity is order of 25 % on distance 25 mm from central plane as seen in Fig. 4.

The simultaneously irradiated area by an atomic flow is not less than 1000 sm². The energy spectrum of fast heavy atoms is shown in Fig. 5. The energy spectrum is spreaded because of features of work of the source.

5. Results of experiments.

For check of possibility of the implantation at the intermediate energies by the intensive atomic flows experiments on source of fast heavy atoms (ISP) were fulfilled.

The carbon atoms beam with appropriate parameters were used for this experiments : $<W> \sim 2.5$ kev at wide energy spectrum W <5 kev, j~ 50 mA/sm². Targets are titanium and niobium samples (12 class of processing). Temperature of targets was t$\sim 100°$C at heating by the falling beam in time of the irradiation.

The doze of implantation was in limits - $(1-5)*10^{18}$ sm⁻². As is known, the atomic and ion implantations do not differ significantly because the interaction of implanted flow with target does not depend from of the charge of particles.

Diagnostics of the implanted samples was made by X-ray diffraction on the SR station "Anomalous scaterring ", INP.

The carbide phases (Nb_2C, TiC) are detected in Fig.6, 7.

Measurement by the sliding x-ray beam has allowed to evaluate the thickness of impurity layer TiC. Intensity of the TiC reflex depending on angle of sliding x-ray beam is shown in Fig.8.

Thickness of impurity layers: TiC ~ 3.5 microns, $Nb_2C \sim 0.8$ microns.

It shows the deep penetration of carbon atoms in target with formation of a new phase.

6. Discussion.

6.1. Received results on the implantation at the intermediate energies with use the powerful source of fast heavy atoms:

Depth of penetration of carbon into titanium ~ 3.5 microns at projective run ~45 A testify on the availability of powerful diffusion, first of all radiation-stimulated, in process of the irradiation. The most probably it is connected with high intensity of flow (~50 mA/sm^2).

Similar conclusions underlining influence to process of a implantation besides energy of particles, such parameters as intensity of a falling flow, temperature of a target were made before in theoretical and experimental works [3,9,10,11,12]

It is shown that the intensive flows of implanted particles at the intermediate energy can modify surface layers of enough large thickness.

6.2. An important feature of the implantation at the intermediate energies - possibility of essential increase of productivity of implantation process.

The main limitation on speed of processing of materials and, accordingly, on productivity are connected to thermal regime of implanted details or to limitation on maximum speed of heat transfer.

With equal conditions the decrease of energy of falling nucleuses, for example from 50 kev up to 1.5-2 kev, means an possibility of increase of flows of falling nucleuses (atoms) in 20-30 times at preservation of thermal flow on a target. That means increasing of productivity in the same number of times.

The increase of intensity of flow, which naturally occurs in this case, can essentially increase speed of diffusion processes, that in turn results in improvement of some parameters of implanted materials.

Thus, transition from traditional ion implantation to the implantation at the intermediate energy permits not only essentially to increase the productivity of implantation, but also appreciably to improve its efficiency.

7. Conclusions

7.1. It is shown, that the implantation at the intermediate energies is realized at energy of carbon atoms of 2.5 kev and as result the carbide phase (TiC) in titanium on depth 3.5 microns had formed.

7.2. Implantation at the intermediate energy permits essentially to increase the technological productivity in comparison with traditional methods.

7.3. The high intensity of flows can essentially improve the quality of the implantation due to diffusion processes.

7.4. The problems of the implantation of insulator materials can be solved by using the atomic flows.

7.5. Use of the source of fast heavy atoms (ISP) permits to realize all advantages of the implantation at the intermediate energies.

References

[1]. Didenko A.N., Ligachev A.E., Kuragin I.B. // Interaction of charged particles - M., Energoatomizdat, 1987

[2]. Matosian Jn. // Journal of Vacuum Science and Technology, 1994, B.12 (2), p.850-853

[3]. Makarets Ќ., Fal'ko G.L., Fedorchenko A.M. // Poverkhnoct', N5, 1984, p.29-32

[4]. Gabovich M.D., Budennaja L.D., Poritsky V.Ya., Protsenko I.M. // Interaction of nuclear particles with firm body. P.2, Kiev, 1974, p.136-139.

[5]. Gabovich M.D., Pleshivtsev N.V., Semashko N.N. // Beams of ions and atoms for controlled thermonuclear fusion and technological purposes., M, Energoatomizdat, 1986, p.71-111

[6]. Volosov V.I. // Theses of the reports on II All-Union conference "Updating of properties of constructional materials by beams of charged particles ". - Sverdlovsk. 1991.-p.63.

[7]. Volosov V.I., Churkin I.N., Poljakov ,.Ђ. // "Source of fast heavy atoms", 1 International Symposium " Beam Technologies -95 ", Dubna.

[8]. Volosov V.I., Churkin I.N. // Current-voltage characteristics of the characteristic of the discharge with heavy ions in crossed fields. Preprint INP 94-75.

[9]. Shalaev A.M. //Radiation-stimulated diffusion in metals. - M., "Atomizdat ", 1972, p.147

[10]. Guseva M.I. // Poverkhnoct'. N4,1982, p.32

[11]. Guseva M.I. // Itogi nauki i tekhniki. Ser. Fizicheskie osnovy lazernoj i puchkovoj tekhnologii., v.5, 1989, VINITI, p.13.

[12]. Guseva M.I. // "Depth ion implantation" , 1-st International Symposium "Beam Technologies - 95", Dubna.

Fig. 1 Source of fast heavy atoms (1 - coil of electromagnet, 2 - vacuum chamber, 3a - cathode, 3b - anode, 4 - end electrodes, 5 - insulator, 6 - power supply, 7 - outlet pipe, 8 - vacuum valve, 9 - target)

Fig. 2 Main processes in source of fast heavy atoms (A - fast heavy atom, a - sputtered atom, i - heavy ion).

Fig. 3 Characteristic oscillograms of current and voltage of the source of fast heavy atoms.

Fig. 4 Uniformity of atomic flow in longitudinal direction.

Fig. 5 Characteristic energy spectrum of fast heavy atoms (Wo= 5 kev).

Fig. 6 Reflex X-rayogram of irratiated titanium sample (~5%-TiC on 13.5 micron at D~3*10^{18} sm^{-2}).

Fig. 7 Reflex X-rayogram of irratiated niobium sample (~3 % Nb_2C on 10 micron at $D\sim10^{18}$ sm^{-2}).

Fig. 8 Intensity of the TiC reflex depending on angle of sliding x-ray beam.

DEVELOPMENT OF TECHNOLOGICAL SOURCES OF GAS IONS ON THE BASIS OF HOLLOW-CATHODE GLOW DISCHARGES

N.V. Gavrilov, G.A. Mesyats, G.V. Radkovski and V.V. Bersenev

Institute of Electrophysics, Ural Division of Russian Academy of Sciences,

34 Komsomolskaya Str., 620049 Yekaterinburg, Russia

ABSTRACT

The paper deals with design principles and basic properties of ion sources with large-cross-section beams on the basis of a low-pressure glow discharge. It is shown that properties of the discharge in a coaxial electrode structure with a hollow cathode in a magnetic field favor its use in sources of gas ions. Application of a weak magnetic field facilitates igniting of the discharge in an reverse-magnetron electrode system with a hollow cathode and a rod anode, ensures stable running of the discharge at high currents and low gas pressures, and provides for formation of a homogeneous plasma ion emitter with a large working surface. The discharge realized in a strong magnetic field in the cathode region, which is used in a plasmatron-type electrode system with extraction of ions from the plasma generated in the anodic part of the discharge, gives improved gas and energy efficiency of the ion source. The conditions of discharge igniting, discharge characteristics, ion-emission properties of the plasma, mass-charge composition of the plasma, contamination of the plasma as a result of the cathode sputtering in the glow discharge, features specific to extraction of ions and formation of beams in electrostatic ion-optical systems are compared for the two plasma-emission structures employing a hollow-cathode glow discharge. The paper describes characteristics and possible applications of gas-ion sources generating ion beams having the cross-sectional area of 5-200 cm^2 and the energy of 1-50 keV under pulsed and continuous regimes. The beam current density is from 10 $\mu A/cm^2$ to 10 mA/cm^2.

1. INTRODUCTION

Glow-discharge glow discharge plasma ion emitters show promise as one of the leads in the development of the technique for generation of broad beams of gas ions to be used for technological purposes, specifically for ion implantation and ion-assisted deposition of coatings. Cold-cathode sources are simple and reliable in service. They can continuously operate in a reactive gas atmosphere.

The glow discharge properties determine certain characteristic features of the ion sources. The ion-electron type of emission of the cathode determines a high operating voltage of the discharge and, correspondingly, a high cost of ion. The cathode sputtering may cause contamination of the plasma and the ion beam. A self-contained low-voltage high-current glow discharge is stable at higher gas pressures compared to the hot filament discharge.

The glow discharge in a source generating a broad ion beam (BIB) must not only operate at the lowest possible values of gas pressure p and discharge voltage U but also create a large-size plasma ion emitter with a high homogeneity of ion-emission properties. The gas pressure in the discharge depends on the efficiency of gas ionization by primary electrons. Minimum values of p are achieved in discharges with electrons oscillating in an electric field (hollow-cathode discharge) and crossing electric and magnetic fields (magnetron and Penning discharges) [1] . Magnetic confinement of fast electrons leads however to a creation of plasma density gradient normal to the magnetic field [2]. On the contrary, electrostatic confinement of electrons in a hollow-cathode (HC) discharge provides not only an efficient ionization of the low-pressure gas but also a high spatial homogeneity of the generated plasma [3].

The characteristics of the HC glow discharge ion emitter can be considerably improved by using of electrostatic confinement of fast electrons and magnetic confinement of low-energy plasma electrons. This principle is realized in an inverse-

magnetron electrode system [4], where a weak longitudinal magnetic field provides control over the radial profile of the plasma density. Strong magnetic field in the cathode chamber, which provides a decrease in the values of breakdown and operating voltage of the discharge, can be used in a plasmatron electrode system comprising cathode and anode chambers separated with an open diaphragm. Ions are extracted from the plasma generated in the anodic part of the discharge.

This paper deals with the results of the development and study of BIB sources employing magnetron and plasmatron plasma-emission structures. A comparison analysis of their properties has been performed.

2. EXPERIMENTAL

a. Electrode systems

Diagrams of the magnetron (M-structure) and plasmatron (P-structure) electrode systems are shown in Fig. 1. The discharge runs between the hollow cathode 1 and the rod (Fig. 1a) or hollow (Fig. 1b) anode 2. Ions are extracted from the plasma generated inside chambers with dimensions $l = d = 150$ mm along the magnetic field through 121 holes 8 mm in diameter. The solenoid 4 produces a weak magnetic field (up to several mT), while the permanent magnet 5 generates a strong magnetic field (10-100 mT). Dimensions of the hollow cathode of the plasmatron system were $l = 50$ mm and $d = 30$ mm, while the diaphragm's hole diameter was ~10 mm. Hollow electrodes were made of stainless steel. The rod anode was made of tungsten and had dimensions $l = 100$ mm and $d = 3$ mm. The igniting electrode 3 in the P-structure is the anode of the auxiliary discharge ensuring striking of the main one. The multi-aperture electrostatic optical system (IOS) 6 used to extract ions from the plasma and to form a broad ion beam.

b. Discharge igniting

A study of glow discharge igniting in the coaxial electrode system at low pressures in weak electric and magnetic fields was aimed not only at determination of the static

3

breakdown voltage U_{st} and the possibilities of its lowering but also at examination of the breakdown dynamics, which is necessary for estimation of the frequency properties of the source under the pulsed-periodic regime. We measured the delay time t_d of the breakdown and its statistical spread, and the average time of the high-current discharge transition to a steady state and formation of an extended plasma ion emitter t_s.

A pulse- forming line with 1 μs - rise time < and 20 μs - pulse duration was used in the experiments. The voltage applied to the gap was 2-5 times as high as the static breakdown voltage (Fig. 2a), the discharge current was 5-20 A,.

The experimentally observed static spread in the delay time t_d was ~2-3 μs and was independent of the pulse repetition frequency over the range of 0.01-50 pps. Hence, considering that the probability of the electron return to the cathode is ~0.5 [5], the frequency of occurrence of initiating electrons at the cathode 1000 cm^2 in area equals about 10^6 1/s. The delay time of breakdown decreases with the growing magnetic induction B, gas pressure p and the applied voltage (Fig. 2b) and on the average is equal to several tens of μs. However the possibility of increasing these quantities in a magnetron-type ion source is limited.

The discharge igniting in the low-pressure inverse-magnetron system with oscillating electrons obeys the basic laws of the Taunsend breakdown, though electron avalanches are not spatially formed under these conditions. An avalanche rise of the current is accompanied by an increase in the charged particle density throughout the gap. When the current $I_t > 10$ mA is reached, the glow discharge occurs.

The estimates made using measured t_d and I_t and also the relations of the current multiplication coefficient $\mu = \gamma(\exp l/\lambda - 1)$ and the time dependence of the current in the gap $I \sim \exp[t(\mu - 1)/\tau]$ [6] suggest that the primary electrons perform on the average 3-4 ionizing collisions. Correspondingly, the number of avalanche electrons exp (l/λ) is ~

10-20. The electron path $1 \sim 10$ m, a value which is 2 orders of magnitude larger than the interelectrode spacing. The secondary electron emission coefficient γ was taken to be 0.1 and the avalanche formation time $\tau \sim 2$ μs.

The time of glow discharge transition to a steady state and the formation of the large-size plasma ion emitter t_s was estimated from the time shift of the oscillograms of the discharge I_d and ion beam I_b currents and was about $\sim 5\text{-}10$ μs (Fig. 3).

The discharge igniting in a plasmatron system has been studied elsewhere [7]. Because of a high value of igniting voltage it is more expedient to use an auxiliary discharge producing plasma in a HC. The main discharge is fired when the condition of blowing up of near-electrode layers of the space charge in the cathode diaphragm aperture is fulfilled. Since the layer thickness depends on the plasma potential, the effect of lowering of the decaying plasma potential is used in ref. [7]. To facilitate igniting of the plasmatron discharge, we lower the plasma potential and increase the auxiliary discharge current by auxiliary glow-to-arc transition. The use of a pulsed arc discharge on condition the current is limited in the main discharge circuit provides for reliable and economic igniting of the discharge. Strong magnetic fields and a high pressure of the gas leaked into the chamber ensure sufficiently small time of igniting (several μs).

c. Discharge characteristics and ion-emission properties of the plasma

Current-voltage characteristics of the magnetron discharge represent increasing curves (Fig. 4(1,2)). The discharge voltage U lowers with growing B (Fig. 4(3,4)) and the pressure p. In addition to the decrease in U, the growth of B enhances anisotropy of the discharge. Fig. 5 illustrates redistribution of the current between parts of the hollow cathode as B is varied and no voltage is applied to the IOS. A drop of the current at the end-face emitter electrode (1) leads to a decrease in the ion beam current.

5

Strong magnetic fields in the cathode region of the P- structure ensure a considerable decrease in the operating voltage of the plasmatron discharge. The voltage does not exceed 450 V under the currents >0.2 A, B ~ 0.05-0.1 T and gas (argon) flow rate <10^3 cm³ atm/h and is little sensitive to conditions in the anode chamber [8].

In addition to the value of the magnetic induction, I-U characteristics of the discharge in the P-structure largely depend on the size of the diaphragm aperture, which serves as a small-sized anode for the HC discharge. To minimize U, the cross-sectional area of the current-conducting channel S should be close to the optimal value determined from the ratio $S_c/S \sim (M/m)^{1/2}$, where S_c is the HC surface area [2]. If S exceeds the optimal value, the loss of fast electrons increases and U rises. If S is small, an electrostatic double layer appears in the neck and ionization in the anodic region of the discharge improves [2]. But with small S, the minimum stable current of the discharge rises and glow discharge igniting conditions are impaired. For this reason S is optimized considering a set of requirements to be met by a specific source of ions.

Parameters of the magnetron discharge plasma in under low B were measured using a probe technique and the method of double electron differentiation of the U-I probe curve. The measured temperature of the plasma electrons is several eV. The plasma potential lowers relative the anode potential to ~50 eV with growing B to 5 mT, a fact which testifies a positive anodic potential drop formation. As soon as the threshold induction B ~ 0.8-0.9 mT is reached, the plasma instability develops that modulating the plasma potential and density. Amplitude of the beam current modulation can be as high as ~25 % and the frequency of modulation >$2 \cdot 10^4$ 1/s.

The ion emission current exhibits an almost linear dependence on the discharge current I_d at small B. As B is increased, the current density in the central part of the ion emitter drops. At small B this adds to homogeneity of the emission properties of the discharge plasma [4]. The current density attains 1 mA/cm² under the continuous regime

6

with the discharge current up to 2 A and is as high as 10 mA/cm^2 under the pulsed regime (1 ms) with the I_d up to 15 A. Efficiency of extraction of ions from the plasma, which is determined as the ratio I_b / I_d, amounts to 6-8 %. The energy efficiency of the ion source with the beam 150 cm^2 in cross-section is about 0.1 A/kW.

Emission properties of the plasmatron discharge plasma are close to the above values and are described elsewhere [8,9]. One of the principal problems is a high density of the plasma near the system axis. For a more uniform distribution of the ion emission current one has to use redistributing electrodes, which are installed in the plasma region, or ion optics with radius-variable transmittance.

d. Mass-charge composition of the plasma

Contamination of a gas ion beam of a glow discharge based source is caused mainly by sputtering of the cathode. If the discharge runs in reactive gases, the chemical composition of near-surface layers of the cathode is determined by the prehistory of the discharge. It was shown [4] that the glow discharge plasma and, correspondingly, the nonseparated ion beam contain both ions of the cathode material and ions of the previously used gas, which dissolved in the cathode material or formed chemical compounds with it. After nitrogen was replaced by argon the content of impurity nitrogen ions in the discharge with a noncooled (~400 °C) cathode was as high as ~20 % and decreased to ~1 % in several dozens of minutes.

The aim of the experiments was to study the influence of the cathode temperature on contamination of the plasma with gas and metal ions and to determine the composition of the nitrogen plasma under different values of I_d, B, p in M - and P - electrode systems. The experiments were performed in the I_d range of 0.1 to 10 A. A high density of the plasma hinders a direct measurements using a standard mass spectrometer. The method used by us consisted in ion extraction and formation of a divergent beam of 1 keV-ions with a lowering density in a drift space. Diaphragms with

7

small apertures cut part of the ion beam and ensure gas pressure difference. A radio-frequency unipolar mass spectrometer was used for the analysis. The input ionizer of the spectrometer was replaced by an IOS, which decelerated ions to an energy of 100-300 eV. This provided acceptable values of the mass resolution ($\Delta M \sim 1$ amu) and the sensitivity threshold (0.1 at.%) of the analyzer.

As distinct from [4], in our experiments the cathode electrode was water-cooled and ions were extracted from the plasma using a multi-aperture IOS. Thanks to this, gas conditions in the source were maintained identical to those for the normal source operation. To lower the measurement error due to gas atom - ion collisions, the gas pressure in the drift region and the analyzer was kept at a level of $4 \cdot 10^{-5}$ Torr using differential pumping.

Cooling of the cathode to ~ 20 °C almost completely eliminated the gas contamination. After switching from N_2 to Ar the content of impurity nitrogen ions did not exceed ~ 1 % and was not detected even in 1-2 minutes. The content of the cathode material ions (Fe^+ and Cr^+) in the plasma produced using a cooled cathode discharge increases linearly with the discharge current I_d (Fig. 6). The Ar plasma is characterized by the largest amount of metal ions.

The ratio of atomic to molecular ion concentration in the nitrogen plasma versus the discharge current is shown in Fig. 7. As the I_d is increased, the fraction of atomic ions rises and exceeds 40 % at $I_d > 2$ A. Measurements of the mass-charge composition of the nitrogen plasma in the anode chamber of the plasmatron discharge showed that the plasma contains predominantly (~ 90 %) molecular ions. Content of metal ions was below the detection limit.

e. Formation of a broad ion beams

The beam was formed using electrostatic multi-aperture three-electrode systems. IOS with large-diameter (8 mm) apertures, which are the same for all the electrodes, was

employed. The ion optics is easy to manufacture and maintain. Performance of the optics is optimized by changing the electrode thickness and the accelerating gap length under both high-current pulsed and continuous modes of the beam generation. The aim of the optimization is to form divergent beams with half-angle of ~5° in separate apertures without the loss of the ions at the IOS electrodes. For the smaller angles a local beam inhomogeneities appear in the plane of the sample holder. If the angle is larger, homogeneity of the broad ion beam may be impaired owing to a redistribution of the beam current density along the drift length (150-200 mm) [10].

The IOS is simulated using the BEAMCAD software developed by Dr. Yu. A. Kovalenko (All-Russian Electrotechnical Institute, Moscow). The simulation and experimental results are indicative of a radical difference in the formation of the beam by the electrostatic IOS in M- and P-structures. An extended near-electrode layer of space charge with a potential drop of hundreds of volts, which exists in the M-structure, screens the field of the accelerating gap. For this reason, as distinct from the P-structure, where focusing is due to the formation of a concave plasma boundary (Fig. 8 a.c), in the M-structure the decisive role is played by the lens effect in the apertures of the emitter electrode and focusing can be realized even if the plasma boundary is convex (Fig. 8 d). Screening of the accelerating field hampers most the formation of the beam at low accelerating voltages (~1 kV) and high current densities (~20 mA/cm^2) [10].

f. Characteristics and application of the sources

An ion sources have been designed for modification of materials by ion implantation and for ion-assisted deposition of coatings. The ion source [11] based on the M-structure generates beams of argon, nitrogen and oxygen ions and ions of carbon-containing gases with the ion energy up to 50 keV and an average current up to 100 mA. The source of this type permits producing broad homogeneous beams (~200 cm^2) with the current density from 10 μA/cm^2 to 10 mA/cm^2 and the pulse duration

9

from ~10 μs to the continuous mode. By present the source has run for ~1000 hours and emission properties of the cathode has not changed. A P-structure continuous-mode ion source has been developed, providing the large-cross-section beam with the beam current of up to 70 mA and offering a higher energy efficiency (0.35 A/kW) [8].

Advantages of the plasmatron structure have been realized most in a small-size source of low-energy beams of gas ions for ion-beam sputtering and deposition of coatings [10]. At a low gas flow rate (200 cm^3 atm/h) and a small discharge voltage (400 V) this source generates 1-keV ion beam with the current up to 40 mA, and the cross sectional area of ~5 cm^2. A magnetron-discharge ion source has been designed for preliminary ion beam cleaning of surfaces before coating deposition using vacuum arc. The cross section of the ion beam is of 200 cm^2, the current is up to 150 mA, and the ion energy is 2-3 keV [11].

The sources were used to study the influence of ion treatment on the structure and properties of various materials. The effect of 30-keV beams of nitrogen and carbon ions on the X18H10T stainless steel has been analyzed over a broad range of doses (10^{16}-10^{18} 1/cm^2) and temperatures (100-600 °C) [12]. Profiles of implanted particles were measured, XRD-analysis of the surface layer structure was performed, nano- and microhardness of samples was determined, and wear tests were carried out. Various structures, including a martensitic structure, formed in near-surface layers subject to treatment with carbon ions provide a 3- to 4-fold increase in microhardness. The wear rate decreases by ~100 times under optimal temperature-dose conditions of nitrogen ion implantation (10^{18} cm^{-2}, 380 °C) ensuring the required combination of the impurity concentration and depth of the modified layer.

Polyethylene and fluoroplastic underwent a low-dose (10^{13}-10^{15} 1/cm^2) treatment with beams of nitrogen, oxygen and carbon ions [13,14]. Samples were analyzed using IR and UV spectroscopy and IR ATR spectroscopy. The wetting angle was measured

and adhesion tests were performed. Adhesion of the polymer surface improves considerably on exposure to small doses (10^{13}-10^{14} 1/cm^2 for polyethylene and up to 10^{15} 1/cm^2 for fluoroplastic). A strong joint between the polymers and reactive adhesives like epoxy resin has been achieved.

The influence of ion-beam treatment on adhesion of a copper coating to polyethylene and fluoroplastic has been analyzed. XRD-method was used to examine the polymer and coating structures. The interface was analyzed by the RBS-method. Spectroscopic techniques were employed to examine the molecular structure of the polymers. Tear tests were performed. It is shown that ion beam treatment has a great effect on the joint strength. The result depends both on the ion energy and on the ratio between the accelerated ion flow and the flow of atoms of the sputtered material at the initial stage of the coating formation.

The influence of preliminary implantation of nitrogen and carbon ions in stainless and tool steels on abrasive wear resistance of diamond-like coatings (DLC's) has been studied [15-17]. We measured implantation profiles, substrate microhardness and durability of DLC's in a stream of abrasive particles. The film durability increased by 3-5 times when the P6M5 tool steel was treated with an optimal dose (10^{18} 1/cm^2) of nitrogen ions irrespective of other implantation parameters.

3. DISCUSSION

The principal difference between magnetron and plasmatron plasma-emission systems is that in the P-system the cathodic and anodic parts of the discharge are spatially separated according to their functions in the ion source. The processes in the cathodic part are responsible mainly for the cold-cathode emission, whereas those in the anodic part determine ion-emission properties of the plasma. This makes it possible to independently optimize, to a certain extent, the conditions of discharge running and

extraction of ions from the plasma and also depress the effect of the ion extraction on the glow discharge characteristics. In turn, the M-structure also has some merits associated with improved conditions of discharge igniting owing to an optimal distribution of electric and magnetic fields, a lower probability of the glow-to-arc transition due to a larger area of the cathode, and the possibility of creating and scaling a homogeneous large-size plasma emitter with a high density of the ion emission current.

Use of a weak magnetic field improves confinement of primary electrons in the magnetron system, because their trajectories do not pass through the central region of the discharge where the anode is installed. As a result, the discharge develops faster, the igniting and operating discharge voltages lower, and/or the minimum working pressure of the gas decreases. Here plasma electrons are magnetized and therefore a flat profile of the emitting plasma density can be formed by changing B.

Our examination of the conditions of the glow discharge igniting under a pulsed-periodic regime confirms the existence of an effective mechanism by which initiating electrons are generated. The mechanism is due to the exoelectron emission of the cathode [18] arising from disturbance of the cathode surface structure under an intensive ion bombardment. The possibility of accelerating the discharge development by using higher B, p and applied voltage in the magnetron-type broad beam ion source is limited since in this case the emission current density j lowers, the homogeneity of j distribution is impaired, and the electric strength of the accelerating gap deteriorates. After the glow discharge appears during the characteristic time <100 µs, a high-current discharge is established and a uniform large-size plasma ion emitter is formed in 5-10 µs. So, the M-system in question provides generation of broad ion beams with duration >10 µs and pulse repetition rate ~10^4 pps. Use of a strong magnetic fields in

the magnetic shielded cathodic region of the P- structure makes it possible to generate broad ion beams and improves the energy and gas efficiency of the ion source.

The plasma of the low-pressure glow discharge in the cathode chamber is characterized by the presence of impurity metal and gas ions. They are due to an intensive ion sputtering of the cathode, the sputtering rate at the sputtering coefficient ~ 0.5 being $\sim 2\text{-}4 \cdot 10^{-4}$ g/C. A relatively low content of metal ions in the plasma is explained by a high kinetic energy (1-10 eV) of the sputtered atoms [19] and, as a consequence, low probability of their ionization in the volume and predominant condensation of the metal ions on the cathode chamber walls. Formation of the chemical compounds on the surface layer of the noncooled cathode leads to appearance of a gas impurity in the plasma when the working gas is replaced. This effect can be reduced if the cathode is cooled efficiently. A lower content of metal ions in the discharge plasma produced using a noncooled cathode can be attributed to a smaller selective sputtering rate of metal entering the chemical compounds [20].

The mass-charge composition of the plasma in molecular gases, specifically, nitrogen, is determined by the plasma concentration and temperature of electrons, i.e. depends on the type and parameters of the discharge [21,22]. A high energy of primary electrons in the cathode chamber ensures a high (up to 50 %) content of atomic ions in a high-current nitrogen plasma. The plasmatron-discharge anode plasma contains mainly molecular atoms of nitrogen. This may be due to the fact that the mean energy of ionizing electrons in the anodic part of the discharge is much lower. Contamination of the anode plasma with metal ions is insignificant (<0.1 %), because sputtering products are deposited mostly on the walls of the screened cathode chamber.

So, by a proper selection of the parameters, conditions of discharge running and type of the electrode structure of a hollow-cathode glow discharge it is possible to decrease the content of both gas and metal impurities in the ion beam to 0.1-1 at.%.

13

A near-cathode layer of space charge with a potential drop of hundreds of volts does not permit the use of plasma focusing for formation of beams in an electrostatic IOS. But the focusing effect of the electrostatic field in the aperture of the emitter electrode proves to be sufficient for formation of convergent laminar beams crossing over outside the IOS at a high density of the emission current. Moreover, the layer of space charge makes it easier to match properties of the plasma emitter and the ion optics over a broad range of current densities j and ion energies , except the case of a high j and a low ion energy, where the use of the P-structure is preferable [10].

4. CONCLUSIONS

The use of glow discharge for generation of large-cross-section ion beams provides for a considerable improvement of reliability and durability of technological gas-ion sources and simplifies their design and maintenance. We looked into the properties of a hollow-cathode discharge in a magnetic field at low pressures. We also analyzed the conditions under which a dense quiescent homogeneous plasma is generated in the discharge and properties of the plasma ion emitter and the electrostatic beam formation system match. The comparison analysis of the properties of the plasmatron and magnetron plasma-emission structures can serve as a basis for purposeful selection of electrode systems, discharge running modes and conditions of beam formation, which would provide such characteristics of the source and parameters of the beam as required in particular applications. The results of the research were used for development of ion sources operating under continuous and pulsed regimes and generating large-cross-section beams over a broad range of ion energies and beam current densities.

REFERENCES

[1]. V.V. Bersenev, N.V. Gavrilov, S.P. Nikulin. Proc. of Conf. on Low-Temperature Plasma Physics, (2) (1995) 251-253 (In Russian).

[2]. E.M. Oks, A.A. Chagin, P.M. Schanin, Zhur. Tekhn. Fiz., 65 (8) (1995) 151-155 (In Russian).

[3]. A. S. Metel, Zhur. Tech. Fiz., 54 (2) (1984) 241- 247 (In Russian).

[4]. N. V. Gavrilov, G. A. Mesyats, S. P. Nikulin and G. V. Radkovskii, J. Vac. Sci. Technol. A 14(3) (1996) (to be published).

[5]. J. A. Thornton, J. Vac. Sci. Techol. 15 (2) (1978) 171-177.

[6]. Yu. D. Korolev, G. A. Mesyats, "Physics of pulse breakdown in gases", Moscow: Nauka (1991) (In Russian).

[7]. Electron sources with a plasma emitters. Edited by Yu.E. Kreindel. Novosibirsk: Nauka (1983) 5-14 (In Russian).

[8]. N.V. Gavrilov, A.V. Ponomarev , Proc. of II Conf. "Modification of properties of materials for constructions by charged particle beams" (In Russian), Sverdlovsk, Russia (1) (1991) 30-32.

[9]. Charged-particle beam sources with a plasma emitter. Edited by P.M. Schanin. Ekaterinburg: Nauka (1993) 98-107 (In Russian).

[10]. V.V. Bersenev, N.V. Gavrilov, G.V. Radkovskii, Proc. of IV Conf. "Modification of properties of materials for constructions by charged particle beams" (In Russian), Tomsk, Russia (1996) 66-68.

[11]. N.V. Gavrilov, S.P. Nikulin, G.V. Radkovskii, Prib. i Tekhn. Experimenta (In Russian), (1) (1996) 93-98.

[12]. D.J.Rej, N.V.Gavrilov, D.Emlin, I.Henins, K.Kern, T.Kurennykh, V.N.Mizgulin, C.P.Munson, M.Unson, M.Nastasi, J.T.Scheur, V.Vykhodets, K.C.Walter, 1995 Materials Research Society Fall Meeting Proceedings, vol. 396.

[13]. G. A. Mesyats, Yu. S. Klyachkin, N. V. Gavrilov, V.N. Mizgulin, R.M. Yakushev, A.V. Kondyurin, Proc. of III Conf. "Modification of properties of materials for constructions by charged particle beams" (In Russian), Tomsk, Russia (2) (1994) 19-21.

[14]. N. V. Gavrilov, A.V. Kondyurin, V.N. Mizgulin, F.Z. Gilmutdinov, O.M.Kanunnikova, E.D. Yakusheva, V.V. Nasonov, Proc. of IV Conf. "Modification of properties of materials for constructions by charged particle beams" (In Russian), Tomsk, Russia (1996) 308-310.

[15]. O.M.Bakunin, A.B.Vladimirov, N.V.Gavrilov, V.N.Mizgulin, I.Sh.Trakhtenberg, Proc. of IV Conf. "Modification of properties of materials for constructions by charged particle beams" (In Russian), Tomsk, Russia (1996) 305-307.

[16]. I.Sh.Trakhtenberg, S.A.Plotnikov, O.M.Bakunin, S.G.Yakovleva, A.A.Nichaev, S.D.Gorpinchenko, A.B.Vladimirov, L.G.Korshunov, N.V.Gavrilov, V.N.Mizgulin, Diamond and Related Materials (4) (1995) 1020-1024.

[17]. S.D. Gorpinchenko, I.Sh. Trakhtenberg, O.M. Bakunin, S.A. Plotnikov, A.A. Nechaev, V.N. Mizgulin, N.V. Gavrilov, Diamond and Related Materials (3) (1994) 779-782.

[18] H. Paetow, Z. Physik (111) (1939) 770.

[19]. M.W. Thompson, Nucl. Instrum. and Methods in Phys. Research, B18 (1987) 411.

[20]. Sputtering by Particle Bombardment II. Edited by R. Berish. Springer-Verlag (1983) 161.

[21]. T. Ludwig, K. Volk, H. Klein, and A. Schempp, Rev. Sci. Intrum. 63 (4) (1992) 2616-2618.

[22] D. Van Vechten, G.K. Hubler, E.P. Donovan, Vacuum, 36 (11/12) (1986) 841-845.

FIGURE CAPTIONS

Fig. 1. Schematic diagram of the magnetron (a) and plasmatron (b) electrode structures:
1 - cold hollow cathode, 2 - anode, 3 - igniting electrode, 4 - solenoid, 5- permanent
magnet, 6 - ion optical system.

Fig. 2. Time of glow discharge formation (1-3) and static breakdown voltage (4)
vs magnetic induction.

Gas (nitrogen) pressure p = 0.06 Pa (1,3), 0.04 Pa (2,4).

Applied voltage U_a = 3 kV (1), 5 kV (2,3), magnetic induction B = 1 mT (4).

Fig. 3. Waveforms of beam current (1-3) and discharge current (4).

Gas (nitrogen) pressure p = 0.04 Pa, magnetic induction B = 1,3 (1); 0,8 (2); 0,4 (3) мТ.

Fig. 4. Glow discharge voltage vs discharge current (1,2) and magnetic induction (3,4).

Magnetic induction B = 1 mT (1,2), discharge current I_d = 0.4 A (3) and 0.1 A (4).

Gas (nitrogen) pressure p = 0.01 Pa (1), 0.02 Pa (3,4) and 0.03 Pa (2).

Fig. 5. Distribution of the discharge current among the flat (1,2) and cylindrical (3)
parts of the hollow cathode of the M-structure as a function of magnetic induction.

Discharge current I = 0.1 A, gas (nitrogen) pressure p = 0.06 Pa.

Fig. 6. Metal ion concentration in plasma vs discharge current.

Gas pressure p = 0.06 Pa, magnetic induction B = 1 mT.

Fig. 7. Atomic to molecular nitrogen ion concentrations ratio vs discharge current.

Gas pressure p = 0.01 - 0.06 Pa, magnetic induction B = 0.5 - 3 mT.

Fig. 8. Computer simulation of ion extraction and beam formation in M (b, d) и P (a, c)
electrode structures.

Emission current density of argon ions 0,6 мА/см^2 (a, b) and 6 мА/см^2 (c, d).

Accelerating voltage 40 kV, cut-off voltage 1 kV(a,b) и 3 kV (c, d).

Accelerating gap length - 15 mm, diameter of holes - 8 mm.

A positive plasma potential relative to emitter electrode - 1 kV (b, d), 50 V (a) и 0 V (c).

Fig. 1

Fig. 2.

Fig. 3

Fig. 4.

Fig. 5.

Fig. 6.

Fig. 7.

Fig. 8

GASEOUS ION BEAMS SOURCES WITH THE CURRENT UP TO 60 A FOR TECHNOLOGICAL APPLICATIONS

N.N. Semashko, V.M. Kulygin, A.A. Panasenkov, N.V. Pleshivtsev

Institute of Nuclear Fushion, Russian Research Centre "Kurchatov Institute", Sq.I.V. Kurchatov, Moscow 123182, Russia, e-mail: nfi@wowa.net.kiae.su, FAX:+7095 9430073

Abstract

Ion beam sources of hydrogen, nitrogen, and other gases as well as of their mixtures witch the energy 10-60 keV, at pulse duration from 1 ms to 1.5 s, were developed and produced in small batches, an average hydrogen ion current density in the beam is equal 150-250 mA/cm^2. The beam cross-section is varied from 7x15 cm^2 to 12x35 cm^2 at the distance of 1 m from the source, its inhomogeneity is 95% of the maximal density. The ion beams are used for heating the plasma in fusion facilities, Tokamak-11 and OGRA-4, as well as for strengthening and enhancing the life time of cutting plates for lathes, rolls, knifes for woodworking machines, cutting elements for soil cultivators.

Keywords: Ion current/density: Nitrogen ion beams

1. Introduction

The first hydrogen ion sources with the currents 10-20 A, cusp-geometry and "MIR"-Types, using a magnetic cusped field and a radial discharge with a rising plasma density along the radius and a ring-like configuration of emitters were designed and developed at INF in 1967-74 [1,2]. However, the magnetic field strength in the zone of ion extraction was insufficient for production of magnetic isolation, and it assisted in the emergence of electric breakdowns. Therefore, in the production of the second ion source generation with the currents 4-100 A; IBM-3,-4,-5,-6-Type, the magnetic fields were not used for enhancement of the plasma density in the zone of ion emission. However, these sources, at relative simplicity in their design, had a rather high energy consumption in the arc discharges with hot cathodes for production of an ion beam of 1 A, namely, about 2 kW/A and relatively low proton fraction in the flux of H_1^+, H_2^+, H_3^+ -ions entering, the emission plasma border, is about 65%.

2. Experimental

In the ion source, IPM-type, peripheral magnetic fields in the vicinity to the discharge chamber surface (Fig.1) were used. The balance of particles and energies in the discherge, IBM-type, is considered in [3] in detail. The main energy losses in that discharge are related with the bad confinement of charged particles in the discharge chamber volume and with their fast escape to the walls. The parameters of importance are: ratio of plasma volume to the wall area in the discharge chamber, on which the ion losses take place, $\eta = V_{pl}/S_n$, and the relative cathode area, $\kappa = S_c/S$. An increase in η from $\eta = 4.5$ to $\eta = 10$ cm results in that an increase the proton component fraction in the extracted ion beam up to 80-90% and in a reduction in the required hydrogen density within the gas dischargechamber from 3.10^{14} to 2.10^{14} cm^{-3}.

The energy efficiency of a discharge, in the process of ion production, $F_+ = I_+/W_p$, where I_+ is the total ion current produced in the discharge, W_p is the discharge power, can attain the maximal value of about 8 A/kW, at optimal of $\kappa = 0.03\text{-}0.04$.

The ion cost in the discharge, $C_+ = 1/F_+$, is about 125 V. However, the discharge efficiency respective to the total ion beam extracted from the source and equal $F_i = I_H^+/W_p$, where I_H^+ is the ion current in the beam, will be considerably lower, since the ratio $F_i : F_+ = S_{em} : S_n$ in true, for a homogeneous plasma, where S_{em} is the slit area in the emissive electrode of the source ion optics. For example, in the source, IBM-5-type (30 A, 30kV), $S_{em} : S_n = 1.14$, $F_i = 0.55$ A/W, $C_i = 1.8$ kV. Implementation of a peripheral magnetic field preventing the escape of charged particles from the plasma volume-rapidly decaying towards the discharge chamber centre-allowed one to enhance the ion source characteristics. In the IPM-1, at conservation of the IBM-5 discharge power, the hydrogen ion current was increased was increased to 60 A. This allowed one to double the power of the fast atomic beams injected into the plasma without any changes in the low voltage power supply sources in the injectors for T-11 tokamak. The initial ion beam cross-section equal 15x25 cm² was chosen, proceeding from the geometry of on inlet window into T-11.

The discharge chamber of that source is the SS-frame cooled with water, 20x30 cm² in its cross-section, 12 cm deep. Upon the rear lid along the long sides of the discharge chamber two rows of the cathodes mode of W-wire, 1 mm in diameter, are located. The number of the cathodes can attain 18, the area is up to 50 cm².

The magnetic system of the source is produced with permanent magnets in the form of the parallelepipeds made of solid barium ferrite cores. The total length of the magnets was 600 cm.

The ion current density distribution across the emissive surface along the long side of the discharge chamber is rather uniform at the length of 20 cm (Fig.2).

The study of hydrogen ion emission current density dependence on the discharge power under various pressures in the chamber (Fig.3) has shown that the optimal pressure for the IPM is $P_0 = 6.10^{-3}$ Torr.

In this source the cathod area (with holders) is about 120 cm², the internal discharge chamber surface area is 2000 cm², $\eta = 5.5$, $\kappa = 0.06$, $F_+ = 6$ A/kW, $F_{+n} = 2.5$ A/kW is a net efficiency corresponding to he uniform ion current density distribution across the emissive surface. The last number about twice exceeds the value obtained for the sources without external magnetic field.

The ion-optics system (IOS) in the IPM-1 includes the emissive, accelerating and grounding electrodes made of Mo-alloy as five lattices having 12 slots each. The slit geometry within the emissive electrode is 0.2x12 cm², they are located upon the surface 12x25 cm², and their total emissive surface is 14.4 cm². At the length of an accelerating gap, $d_1 = 3.3$ mm, emissive electrode thickness 1 mm, slit width in the accelerating electrode 2.4 mm, and at the optimal ion emission current density, the minimal divergence angle, perpendicular to the slits, is $\theta_\perp = \pm 1.2°$ (Fig.4). The beam divergence angle along the emissive slits is about $\theta_{11} = \pm 0.5°$. The geometric ion beam focussing along the slits is realized due to the lattice bend at the curvature radius equal 2 m. The electric focussing perpendicular to the emissive slits $\theta_\perp$, is done by a shift of the accelerating electrode lattices respective to the emissive electrode ones. The lattices nearby to the middle ones are shifted from them by 150 μm, those at the edge, by 300 μm. The focal distance at this shift is determined by the known relationship: $F = 1.5 y_0 d_{eff}/\Delta y$, where y_0 is the distance from the shiffed lattice to the average one; Δy is the lattice shift; $d_{eff} = t_1 + d_1 + \delta_2$ is the effective length of an accelerating gap, where δ_2 is a halfwidth of the slit in accelerating electrode. The minimal divergence angle, $\theta_\perp$, depends on the voltage over the source, U_o, and on the ion emission current density, j_+,

which is determined by the discharge current, I_p (Fig.5). The hydrogen ion beam with the current up to 70 A is produced in IPM-1.

The focussed beam dimensions, 6x22 cm² (at the 1/e-level from the maximal j_+-value), at the distance 1.4 m from the IOS, are smaller than the initial ones. It allowed one to inject a fast atomic beam with the energy 25 keV, with the average power density, 5 kW/cm², and with the maximal one 10 kW/cm², into T-11 from the charge exchange chamber.

The gaseous efficiency of the source under the pressure 6.10^{-3} Torr in the discharge chamber at the beam current 70 A, was 60%. The current pulse duration was usually equal 20 msec.

For heating the plasma in T-15 the ion beams with the power 5-6 MW from one source, IVIS-70/80, at the pulse duration up to 1.5 sec (Fig.6), are needed. The gas discharge chamber (1), made of SS, serves as an anode for dissipating a high discharge current in hydrigen with the 26 hot (emissive) cathodes (2) made of tungsten alloy. The filament current introduction into the discharge chamber is realized through the bushing insulators (3) fastened to the holders made of molybdenum. A few rows of permanent magnets (4) are located so that they produce a "magnetic well" in the vicinity to the anode (1) and used for enhancing the plasma uniformaly upon the emissive surface and for increasing the gaseous and energy discharge efficiencies (at the necessary plasma density of about 5.10^{12} cm^{-3}). The high voltage insulator design includes the ceramic insulators (5) vacuum-sealed with resin, the flangers (6) to which the electrode holders (7) are fastened. The plasma (emissive) electrode (8) is a discharge chamber continuation. Then, the gradient (9), negative (10) and grounded (11) electrodes follow each other. Each multislit electrode includes an SS-holder and the profiled molybdenum rods brazed to the holder with one end, and its another end is freely moving in the opposite direction to prevent the rod deformation under its heating by particles and by radiations..

The emissive electrode has the transversal cross-section equal 120x360 mm, its transparency is 50%, the distance between the slit orifice centers is 7 mm. The electrode holders and their flanges are cooled with water. The negative IOS-electrode serves as a reflector of electrons from the secondary plasma in the beam neutralizer, it prevents the electron incidence upon the emissive electrode and the electron entry into the discharge chamber. The gradient electrode is used for extraction of a high ion current density (0.35 A/cm²) under high (higher than 50kV) accelerating voltages. The distances among IOS-electrodes is equal a few millimeters.

The potential distribution between them is determined by the operating conditions and can be equal for the mentioned sequence of electrodes to +80 kV, +55 kV, -8 kV, 0 kV, respectively. If the ion beams with the energies no greater than 50 keV are needed, one can use a three-electrode system, without the gradient electrode (9).

In 8-10 seconds before the ion current pulse start-up the cathodes are heated up to about 3000 K by the direct current of about 3000 A. The discharge current is about 2000 A. It is raised for 0.25 seconds, 2 seconds before the ion current pulse start-up.

The discharge starts before applying high voltages to the IOS-electrodes and terminates after switching the mentioned voltages "off" [5].

3. Results

Sources of beams of ions and atoms of hydrogen, helium, nitrogen and other gases and their mixtures have been developed. Their main parameters are given in the Table 1 and 2.

The sources of beams of ions and atoms of hydrogen were used in injectors intended for plasma heating up to temperature 20-150 mln.K in Tokamak-11,-15, Ogra-3,-4 thermonuclear systems.

The nitrogen ion beams...

The nitrogen ion beams with current 5-8 A and with the energies 15-25 keV were used for 2-5 times enhancement of the wear and corrosion resistance for a number of structural steels, solid alloys and other materials [6-9]. In cooperation with a number of Institutes and Plants the following main results were obtained:

1. Depth of a subsurfase layer with enhanced microhardness by 24-28 % for the steel, SHH-15-Type, is 50-75 μm, that is thousand times longer than the range of the 15-keV nitrogen ions.

2. The strengthened layer thickness can be two-four-times greater, when mixed ion beams including N+H, N+He and/or the successive thermal treatment of nitrogen ion-implanted specimens made of steel, H12M-Type are used.

3. The wear resistance of hardened steels, 40H and HVG-Types, is 2-4-times increased after nitrogen ion beam implantation; the pressure limit, at which the scuffing of friction surfaces takes place, is up to 4-times and higher increased in comparision with the hardened (only) specimens.

4. The wear resistance of the steel, ST.3-Type, after nitrogen ion-beam implantation is 2.5-times increased with the increase in the micohardess by 25% and the with reduction in friction coefficient by 19%.

5. The 4-times enhancemrnt in the wear resistance of a counterbody in the friction pair made of non-

implanted steel, USA-Type, is observed after implantation of a mixed beam, including N-and He-ions, into the steel, HVG-Type.

6. The durability of the cutting blades made of the steel, R6M5-Type, under turning of the high strength steel, 38HS-Type, without cooling, at the cutting rate 20-63 m/minute, 1 mm deep, rises 3-5-times up and higher after nitrogen ion implantation.

7. The durability of the cutting blades, made of hard alloys, T15K6, T5K10-Types, under mechanical treatment, see above, but at the cutting rate 260 m/min rises by 30-370% after nitrigen implantation.

8. The service life of the rolls made of R6M5-stell, 42 in diameter, 210 mm long, rises 2-times under rolling the foil made of W-Re and Mo-Re alloys, 20-50 mu thick, after nitrogen implantation.

9. Durability of drills, 11.7 in diameter, rises 1.5-2-times in the treatment of gray cast iron.

10. Durability of the reamers 6.9 mm in diameter, made of the steel, P5M5-Type, under treatment of the steel, 40X-Type, rises 1.33-1.54-times.

11. Elasticity limit for the foils made of the alloy, 36HXTЮ-Type, after nitrogen ion implantation increases by 13%.

12. The samples of cutting elements for cultivators after hardening in oil and tempering underwent irradiation at the "ISTRA"-facility in the dose range $(1-3,8)10^{17}$ ion/cm^2, at the maximal current density 80 mA/cm^2, by 40 pulses, 20 ms long each. The abrasive wear tests were performed at the "Circular Soil Stand" which consists of the circular duct, about 2 m in diameter, filled with a soil including 67% of sand and 33% of clay. The rate of ripping was equal 2 m/s, the length was up to 144 km. Under optimal irradiation doses the resistance increased by 200-300% in comparision with the non-irradiated samles which were tested simultaneously with those treated by the ion bombardment.

13. Service life of the bolts, M6-Type, made of the alloy BT-16- Type, under cyclic loading rises 5-7-times after nitrogen ion implantation.

14. Corrosion resistance of the stainless steel, X18H10T-Type, and thet of the titanium alloy, BT-1-Type, in the 40%-solution of sulphuric acid rises 4-6-times after nitrogen ion implantation.

8

4. Conclusions

The high energy beams of hydrogen were used in the injectors intended for plasma heating up to the temperature 20-150 mln.K in fusion facilities Tokamak-11, Ogra-4.

The beams of nitrogen ions with the current 5-8 A and with the energy of particles 15-25 keV were used for a 2-5-times increase in the wear and corrosion resistances for a number of structural steels, solid alloys, metal-, kapron-, soil treating cutting tools, as well as for the rolls to produce the foil of molybdenum-renium alloys.

Advantages of pulsed high current and densities ion beams:

- thickness of a layer with enhanced microhardnes is increased to 100 μm,

- irradiation time is reduced to a few tens of seconds,

- detail or a tool are not heated to high temperatures,

- current density, at the distance of 1 m from the ion source, in the transversal beam cross-section, 12x35 cm^2, is equal 136 mA/cm^2; at the distance of 5 m, 20x60 cm^2, is equal 33 mA/cm^2 that allows one to treat the large size items,

- at the energy 60 keV, the power and energy densities are 8.2 kW/cm^2 and 8.2-12.3 kJ/cm^2, respectively, which allow one to melt and evaporate high melting materials,

- mixed ion beams of noble and chemically-active gases allow one to realize the ion cleaning processes of surfaces, radiation damge, phase conversion and structure changes, simultaneously,

- processes of ion treatment and coating environmentally pure.

References

[1]. Pleshivtsev N.V., Semashko N.N., Chuhin I.A. Plazmennyi istochnik ionov-
"Antiprobkotron". Avtorskoe svidetelstvo SSSR N 294545, prioritet ot 7.05.1968.
Opubl. v Biull. izobretenii, 1973, N6, pp.1-18; Pat, France N71.28566, 1973, N12; U.S.
Pat. 3, 798,488, Mar. 19, 1976; Pat. U.K. Great Britain N1348562, 1974, Mar.20,1974.

[2]. Semashko N.N., Pleshivtsev N.V., Kuznetzov V.V., Maximenko B.P., Malakhov
N.P. The Ion Source with Radial Discharge in the Cusp Magnetic Field. Proc. of the
Symposium on Ion Source and Formation of Ion Beams. Berkeley, California, 22-25
Oct. 1974.-Supplement LBL-3399. P.VI-11; Materialy II Vsesoiuznoi konferentsii po
plazmennym unskoriteliam. Minsk. Izd-vo MPTI, 1973, S.187.

[3]. Kulygin V.M., Panasenkov A.A. Balans chastits i energii v razriade ionnogo
istochnika, Preprint IAE-3322.M.: IAE, 1980.

[4]. Panasenkov A.A., Ravichev S.A., Rogov A.V. Istochnik ionov vodoroda s
periferiinym magnitnym polem. Voprosy atomnoi nauki i tehniki.
Naucchnotehnicheskii sbornik. Seriia Termoiadernyi sintez. 1984. Vyp.2(15).S.55-63

[5]. Tilinin G.N., Barsukov A.G., Vodo A.H., Kulygin V.M., Makarov Yu.V., Nikulin
V.A., Panasenkov A.A., Semasko N.N. Neutral beam heating system (NBHS). Plasma
Devices and Operations, 1992, Vol.1, pp.277-288.

[6]. Pleshivtsev N.V., Semashko N.N., Panasenkov A.A., Sidorov P.P. Multiampere
pulsed sources of ionic. In Proceedings International Conference "New Leading-Edge
Technologies in Machine Building". Rybachie, Ukraine, September 18-20, 1992.
Kharkov, 1992. Kharkov Aviation Institute, pp.21-25.

[7]. Krukov V.K., Kozma A.A., Sobol O.V., Pleshivtsev N.V., Sidorov P.P.
Wear resistance of parting-off tool made from R6M5 steel after impulse nitrogen ions
implantation with high density of ion current. Ibid.pp.156-8.

[8]. Pleshivtsev N.V. Implantatsiia metallicheskih materialov vysokointensivnymi puchkami ionov azota. Metally. 1994, N6. s.53-63

[9]. Pleshivtsev N.V., Sidorov P.P., Sidorov S.A., Novinskii A.V.

IV Vserossiiskaia Konferentsiia po modifikatsii svoistv konstrktsionnyh materialov puchkami zariajennyh chastits. Tezisy dokladov Tomsk, 13-17 Maia 1996, N11 Iadernoi fiziki, 1996, S.280-282

Beam parameters	Ion sources			
	IPM-2	IPM-1	AIST-20/50	IVIS-70/80
Max. energy, keV	25	30	50	60
Max. ion current: H/He/N/Ar, A	25/12/7/4	60/30/16/9	20/10/5/3	60/30/16/9
Average current density: H/He/N/Ar, mA/cm^2	200/100/54/32	250/125/67/40	200/100/54/32	150/75/41/24
Pulse duration, ms	5-150	5-150	5-100	100-1500
Transversal beam cross section at the distance 1 m from the source with the homogenity of 95%	7x15	10x20	∅10	12x35

Table 1. Parameters IPM.

Beam parameters	Ion sources	
	IBM-5	IBM-6
Max. energy ion, keV	25	25
Max. ion $H^+_{1,2,3}$ current	35	110
Emission current density, mA/cm^2	500	350
Pulse duration, ms	5-150	5-100
Beam cross section, cm^2	8x18	22x42
Yield H^o_1, %	65	60

Table 2. Parameters IBM.

List of figure captions

Fig.1 Diagram of source with peripheral magnetic field.

Fig.2 Ion current density under hydrogen pressure 6.10^{-3} Torr within IPM-1.

Fig.3 Hydrogen ion current density vs. discharge power at various pressures of a gas in the IPM-1 chamber.

Fig.4 a) Slit cell geometry in the system of ion optics; b) beam divergence angle dependence, $\theta_\perp$, on the reduce ion current dencity, at $t_1=1$ mm, $d_1=3.3$ mm, $\delta_2=1.2$ mm.

Fig.5 Optimal hydrogen ion current (I_H^+), ion current density (j_+) and discharge current (I_p) vs. accelerating voltage (U_o)

Fig.6 Circuit-diagram of the ion source, IVIS-70/80.

Fig. 1

Fig. 2

Fig. 4

Fig. 3

Fig. 5

Fig. 6.

EQUIPMENT AND METHODS OF SURFACE MODIFICATION OF THE MICROSTRUCTURE AND PROPERTIES OF METALS BY ADSORPTION ASSISTED ION IMPLANTATION

A.D. Korotaev, A.N. Tyumentsev, Yu.P. Pinzhin, O.V. Panin, A.F. Safarov

Siberian Physical Technical Institute, 1 Revolution Sq., 634050, Tomsk, Russia

S.P. Bugaev, P.M. Shchanin, G.Yu. Yushkov

High Current Electronics Institute, Siberian Division, Russian Academy of Sciences,

4 Akademichesky Ave., Tomsk 634055, Russia

Abstract

Data on phase and structural transformations in the surface layers of metallic alloys as a function of the conditions of ion implantation are reviewed. It is noted that the ion mixing of the surface-absorbed active elements from the implantational gas medium plays an important role in the formation of the element and phase composition of the ion-doped layers. New possibilities for microstructural modification during high-dose implantation are identified with the formation of high-energy defect (including nanocrystalline) structures, heterophase and other phase-structural states and their combinations in ion-doped layers of metallic alloys. Taking advantage of these possibilities makes it possible to reduce by an order of magnitude the implanted dose necessary to upgrade the performance of the surface, to raise the productivity and lower the cost of the ion-beam technological treatment.

1. Introduction

Up to now the basic regularities of the structure-phase transformations in the alloyed surface layers have been studied intensively for a wide class of targets irradiated and ions implanted. The possibilities and limits of changing the element composition of these layers were established. The theoretical analysis of interacting accelerated ions with a solid combined with the experimental study of the metallic material structure state made it possible to draw a rather complete picture of such an interaction.

However, all the above said may be attributed to ion implantation with the use of the implanters of the type under investigation with high vacuum and mass separation of ions being implanted. As a rule, the effects of adsorption and doping of the surface layer with the elements of the implanter gas media, which were found experimentally under the high dose ion implantation (HDII) in the vacuum $10^{-2} \div 10^{-5}$ Pa, are not properly taken into account at that.

Meanwhile, on the basis of a great number of studies [1-6] we came to the conclusion that saturation of surface layers with oxygen, carbon or nitrogen may radically change the physico-chemical state of a surface layer under the HDII.

This effect become principal when ion sources with rather a high (up to 20 μA/cm^2) density of ion current are used to increase the output of equipment and to decrease to cost of the technological process. Here the requirements to the ion-beam purity are lowered; the target temperature may by considerably increased. The ion implantation is carried out under conditions of high partial pressure of such gas components as oxygen, carbon, nitrogen.

Adsorption of these components gives rise to ion mixing, radiation-enhanced diffusion and, therefore, saturation of the alloyed target surface layer with the above interstitials.

The article presents the results of an investigation into the peculiarities of the variation in element composition, of the structural phase transformations and properties in the ion-alloyed layer of molybdenum in the process of the HDII under specified variation of the implantation conditions and the composition of the implanter gas medium.

2. Experimental technique

Used as targets were commercial-type molybdenum specimens of size 20×20×0.2 mm recrystallized at 1773 K. The ion-beam treatment was performed on the Diana pulsed-arc implanter in a vacuum of $(1-2) \cdot 10^{-4}$ Torr created by an oil-vapor diffusion pump. The Titan ion source [7] was also used that was initially evacuated by the same procedure as the Diana and then gradually filled with Ar or N to increase the pressure in the chamber to $(3-4)*10^{-4}$ Torr. Ion implantation was performed at a pulse duration of $t_p = 250$ μs for the Diana implanter and at a pulse duration of $t_p = 400$ μs for the Titan implanter. Specific HDII modes and conditions are given in the table.

An analysis of the element composition of thin surface layers was performed by the method of secondary ion mass spectroscopy (SIMS) on a type MS-7201 device. The microstructure and phase composition were examined by the transmission electron microscopy and electron diffraction methods.

3. Results

3.1. Influence of the implantational gas medium and ion mass on the elementary and phase composition of ion-doped layers

It has been established that the common feature of the electron diffraction patterns obtained for the ion-doped layers produced by implantation for 1.1-1.5 irradiation modes is the presence of additional diffraction maxima. An analysis has shown (Fig. 1a) that these maxima can be identified with an accuracy of $\pm$ 0.002 nm as the result of the electron diffraction on the hcp lattice of Mo_2C with a = 0.297, c = 0.485 nm, and c/a = 1.63. Dark-field electron microscopy has shown thin solid surface layers of this phase with a varied thickness (10-100 nm, see below) in the Mo_2C reflexes at the foil edges. SIMS examination has revealed that the ion-doped layer was enriched with carbon for 1.1-1.5 irradiation modes (Fig. 2). This enrichment seems to be due to the adsorption of carbon from the vacuum medium of the implanter followed by its ion mixing.

After treatment in conditions of type 2.2, 2.3 in a medium with nitrogen at $\leq$ 500 K (see the table), the basic phase liberated in HDII is the fcc nitride Mo_2N with a =0.418 $\pm$ 0.002 nm (Fig. 1b). The presence of Mo_2C is recorded by very weak diffuse reflexes, indicating the presence of thin ($\leq$ 1 nm) plates of this phase. Mass-spectroscopic data reveal a considerable amount of nitrogen in the surface layer (Fig. 2, curve 4), which is not seen after HDII in conditions of types 1.1-1.5; also, the carbon concentration is lower than in conditions of types 1.1-1.5. The nitrogen concentration is so high that continuous films of the fcc nitride Mo_2N of thickness ~ 10 nm and more are formed [3, 4].

The principal mechanisms for the ion mixing of carbon and nitrogen are most likely, first, ballistic ion mixing and, second, ion-stimulated diffusion of the carbon or nitrogen adsorbed on

the target surface. Ballistic ion mixing is an athermic phenomenon, while the efficiency of the ion-stimulated diffusion enrichment of the surface layer with carbon or nitrogen depends on temperature. Therefore varying this parameter should affect substantially the proportional contribution of the above mechanisms for carbidization or nitridization of the ion-doped layers under ion implantation.

According to Ref. 8, in the process of ion implantation at $T = 370$ K, the coefficient of carbon diffusion in molybdenum is $D_{Mo}^{C} \approx 10^{-30}$ m²/s. So for the ion implantation time ($t \leq 1$ h) the average diffusion length should be $\sqrt{Dt} \leq 6 \cdot 10^{-5}$ nm. This precludes the diffusion saturation of the surface layer with carbon since, for the actual thickness of this layer (several tens of angstroms), this would require to increase D_{Mo}^{C} by no less than 9–10 orders of magnitude which is impossible even with the radiation-stimulated diffusion occurring under ion implantation.

Thus, for the Me⁺ ion implantation at 370 K, ballistic ion mixing should be considered to be the principal mechanism for ion mixing. This is supported quantitatively by the experimental data as follows: First, the depth of the layer with a high carbon or nitrogen content after this treatments (curves *1 - 4* in Fig. 2) is not in excess of the projective range R_{p}^{Y} for Y ions. For an accelerating voltage of 60 kV and an average charge number of these ions of ~ 2.3, their energy is $E = 138$ keV and $R_{p}^{Y} \approx 35$ nm. Second, the efficiency of ballistic ion mixing is determined in the main by the mass of the implanted ions. The latter is confirmed by the fact that when Y ions (curve *1* in Fig. 2) are replaced by heavier Pb ions (curve *2* in Fig. 2), the carbon concentration more than doubles.

3.2. Role of target temperature in the phase transformation in the implanted layers

The above twofold increase in the thickness of the carbon-enriched surface layer observed under Y ion implantation (curves *1* and *3* in Fig. 2) on increasing the target temperature from 370 to 670 K seems to be due to the involvement of the ion-stimulated diffusion mechanism in the enrichment process. This is revealed electron-microscopically by a substantial increase in the intensity of the diffraction maxima produced by the Mo_2C phase in diffraction patterns on increasing the Y ion implantation temperature, which testifies to a severalfold increase of the volume fraction of this phase or of the thickness of its solid layer.

A more substantial increase in the carbide content in the surface layer of molybdenum is observed for copper ion implantation. In this case, in the presence of a solid Mo_2C layer on the molybdenum target surface, the intensity of the diffraction maxima from this phase is higher than that of the diffraction maxima from the bcc lattice of molybdenum (Fig. 3*a*). So the thickness of the Mo_2C layer can be estimated to be about half the limited translucent thickness of the foil in the electron microscope, i.e., $\Delta h \approx 100$ nm, which is several times greater than for Y and Pb ion implantation.

The average diffraction length $\sqrt{D_{Mo}^{C} t}$ required for such a layer to form should be no less than 100 nm. For this to take place within $t = 1$ h., the coefficient of carbon diffusion in molybdenum should be $D_{Mo}^{C} \approx 10^{-18}$ m²/s. According to Ref. 8, this value of D_{Mo}^{C} is achieved at $T \approx 800$ K close to the target temperature under copper ion implantation. This is in good agreement with the supposition about an important role played by the ion-stimulated diffusion

mechanisms for the carbidization of the surface layer of molybdenum in the process of ion mixing.

Increase in target temperature may also modify the adsorbing properties of the target surface. The variation in these properties must depend on the element being absorbed, as observed on increasing the temperature of an Mo target from T ≤ 500 (conditions of types 2.2 and 2.3 in the table) to 800 K (conditions of type 2.4) in Zr implantation with a nitrogen containing medium. It is known that, below 500 K (Fig. 1b), the surface layer is enriched predominantly with nitrogen; deposits and continuous layers of Mo_2N are formed, with a small volume fraction of Mo_2C particles. Increasing the target temperature sharply increases the molybdenum-carbide content in the ion-doped layer. Sections with different ratios of the volume content of Mo_2C, Mo_2N, MoC, and molybdenum phases are observed electron-microscopically. A section of continuous layer is shown in Fig. 3 b,c. These results indicate that the adsorptional activity of the molybdenum surface with respect to carbon increases significantly with increase in temperature. This plays the determining role in forming the phase content of the ion-doped molybdenum layer, even in a medium with a higher partial pressure of nitrogen.

Electron-microscopic phase analysis has revealed no secondary phases based on the implanted elements (Y, Pb, Cu, Zr) in the ion-doped layer. This seems to be due to the low diffusion mobility of these elements in molybdenum at $T ≤ 770$ K. Despite their low equilibrium solubility in molybdenum, they are in a solid solution. We have substantiated this experimentally having detected Y_2O_3 and ZrO_2 particles in layers doped by yttrium and zirconium ions and then subjected to thermal treatment at $T = 1273$ K. The oxygen needed for

this to occur is provided both from the surface layer saturated with oxygen in the process of

ion implantation and through the thermal treatment of specimens in a vacuum of ~ $2 \cdot 10^{-5}$ Torr.

There are strong grounds for believing that the formation of solid solutions on implantation of

substition impurities in the absence of second phases of the implanted element is an inherent

feature of HDII at temperatures T $\leq$ 0.3T$_m$. We have confirmed this general statement by

implanting substitutional impurities into Ti-base and Fe-base alloys.

3.3. Features of the defect substructure of an ion-doped layer

The considerable mismatch of the lattice parameters of the matrix and the coherent or

semicoherent Mo$_2$N and M$_2$C particles deposited at high particle densities results in the

formation of very high inhomogeneous internal stress. Partial relaxation of this stress leads to

the formation of high-energy defect structures with unusually high (up to 1 rad/μm) crystal-

lattice curvature, corresponding to the high (up to $5*10^{11}$ cm^{-2}) density of excess dislocations

of the same sign,. for more details, see [4, 9]. The formation of such substructures is indicated

by the azimuthal smearing of the diffractional maximum due to the secondary-phase particles

(Figs. 1a and 3a).

We have revealed similar effects for HDII of Si, Zr, Ti, and other elements into molybdenum,

austenitic stainless steel and Ti-base alloys. This suggests that the formation of high-energy

substructures with a high curvature of the lattice, strong internal stresses, and high stress

gradients in the ion-doped layer should be considered an inherent characteristic of the surface

layers doped with ions under the conditions of saturation with interstitials.

In the process of HDII, a partial relaxation of the above structures is possible. However, in the presence of extremely small particles ($r \leq 10nm$), the possible rearrangement of this substructure is limited to dislocational motion over paths of the order of the interparticle distance, which leads to fragmentation of the crystal lattice into nanometric grains and only partial relaxation of the internal stress. The formation of high-defect nanocrystalline structure is observed both in heterophase ion-implanted layers and in continuous films of interstitial phases: TiN on Ti, Mo_2N on Mo [4]; Mo_2C on Mo (Fig. 1a,c). There is an additional dispersion mechanism associated with the deposition of particles of several orientations on account of the crystal-lattice symmetry, even within the limits of a single orientational relation (Figs. 1a, and 3b,); these particles grow and combine, to form nanocrystals of dimensions no greater than the interparticle distances. Electron-microscopically, this is indicated from the appearance of contrast spotting on dark-field micrographs, one of which is presented in Fig. 1c where in the reflex $\bar{g} = [\bar{1}\bar{1}2]$ (see Fig. 1a) only Mo_2C crystallites are indicated in which the $\bar{c}$-axes are parallel to the $[\bar{1}01]$ or $[101]$ faces of molybdenum. As can be inferred from Fig. 1c, these crystallites are from 5 to 20 nm in size.

3.4. Feature of the amorphization of molybdenum under HDII in various gas media

A study of the features of the structure-phase transformations in molybdenum under implantation of Si ions (modes 3.1 to 3.3) has shown that a change of the implanter gas medium, with the HDII mode being the same, affects the feature of the amorphization in the ion-doped layer.

After HDII in conditions of type 3.1, at doses of $D = 2 \cdot 10^{16}$ cm^{-2} we observe highly dispersed Mo_3Si particles. With an increase in the implantation dose up to $5 \cdot 10^{16}$ cm^{-2}, on the electron

diffraction patterns in addition we observe diffuse effects and significant smearing of the reflections form the molybdenum matrix. Analysis of the misorientations by the method in [10] suggests the presence of continuous misorientations of the crystal lattice, reaching values of (15-25) degrees/μm. With an increase in the dose up to $(1-2)*10^{17}$ cm^{-2}, amorphization of the surface layer occurs (Fig. 4). In this case, the positions of the maxima of the intensity of the diffuse rings from the amorphous phase correlate well with the characteristic interplanar distances $d_{110} \approx 0.345$ nm and $d_{112} \approx 0.198$ nm for the cubic silicide Mo_3Si.

After HDII in vacuum (mode 3.2), amorphization is preceded by heterophase state with highly dispersed Mo_2C particles, formed at $D \leq 2*10^{16}$ cm^{-2}, and thin (some tens of nanometers) solid nanocrystalline layers with the crystalline structure of MoC, formed at $D \approx 5*10^{16}$ cm^{-2}. With an increase in the implantation dose up to $(2-5)*10^{17}$ cm^{-2}, we observed complete amorphization of the surface layer. In this case, within 0.002 nm the maxima of the radial scattering function for electrons correspond to the characteristic interplanar distances for the hcp carbide Mo_2C.

Replacing argon by nitrogen, with the mode of treatment on the Titan implanter being the same, prevents amorphization of molybdenum with silicon and results, at doses below 10^{17} cm^{-2}, in the formation of second phases of Mo_3Si and Mo_2N, with a predominance of the latter. At doses about $(2 \div 5) *10^{17}$ cm^{-2} a nanocrystalline solid layer of nitride phase is formed.

Thus, a change of the implanter gas medium for the same HDII mode may change both the phase composition of the ion-doped layer preceding amorphization and the radial scattering

function for electrons and, hence, the microstructure and element composition of the amorphous phase.

The above the qualitative changes in the features of the formation of structure-phase states under the influence of the effects of interaction of targets with elements of implanter gas media have been observed in a vacuum of $\sim (1 \div 4) * 10^{-4}$ Torr. From the data available in the literature [12, 13] it is known that similar effects of the saturation of metals with carbon and oxygen, for metals actively interacting with these elements, may occur in a vacuum of 10^{-6}-10^{-7} Torr. Since the use of a higher vacuum in technological -purpose implanters is inefficient, the effects observed in these implanters, similar to those discussed here, are most likely the general feature of the phase-structure transformations in surface layers. Moreover, we anticipate that the control of the partial pressures of active elements in implanter gas media within a range of 10^{-4} to 10^{-5} Torr offers much promise in HDII-based technologies. As we have demonstrated for a number of alloys (various types of steels, Mo, Ti-base alloys), this allows an optimal upgrading of the material performance with implanted doses being an order of magnitude lower than those used in the experiments reported in the literature. Thus, specifically increasing the partial pressures of active elements of the implanter gas media (N, O, or C, depending on the material under treatment) may substantially raise the productivity of technological processes based on ion modification of constructional , tool, and operational metallic materials.

References

[1]   A.N. Tyumentsev, A.D. Korotaev, and S.P. Bugaev, Izv. Vyssh. Uchebn. Zaved. Fizika, **37** (1994) 452 (Rus. Phys. J).

[2]   A.D. Korotaev and A.N. Tyumentsev, Ibid., **37** (1994) 703.

[3]   A.N. Tyumentsev, A.D. Korotaev, Yu.P. Pinzhin et al., Nucl. Instr. & Meth. in Phys. Res., **B80/81** (1993) 491.

[4]   A.N. Tyumentsev, Yu.P. Pinzhin, A.D. Korotaev et al., Fiz. Met. Metalloved., No. 9 (1992) 123.

[5]   A.N. Tyumentsev, Yu.P. Pinzhin, A.E. Bekhert et al., Fiz. Met. Metalloved., No. 9 (1992) 131.

[6]   V.G. Abdrashitov, A.E. Bekhert, S.A. Gashenko et al., Poverkhnost., No. 5 (1993) 141.

[7]   S.P. Bugaev, E.M. Oks, P.M. Schanin, and G.Yu. Yushkov, Prib. Tekh. Eksper., No. 6 (1990) 125.

[8]   E. Fromm and E. Gebhardt, Gases and Carbon in Metals [Russian translation], Metallurgiya, Moscow (1980).

[9]   A.D. Korotaev, A.N. Tyumentsev, and V.F. Sukhovaᵣov, Disperse Strengthening of Refractory Metals [in Russian], Nauka, Novosibirsk (1989).

[10]   V.Ch. Gonchikov, A.N. Vergazov, A.D. Korotaev et al., Fiz. Met. Metalloved., **64**, No. 1 (1987) 170.

[11]   A.D. Korotaev, A.E. Bekhert, and A.N. Tyumentsev, Izv. Vyssh. Uchebn. Zaved. Fizika, **37** (1994) 3 (Rus. Phys. J).

[12]   D.M. Follstaedt, Nucl. Instr. & Meth. in Phys. Res., **B7/B8** (1985) 11.

[13]   M. Iwaki, K. Yabe, M. Suzuki, and O. Nishimura, Instr. & Meth. in Phys. Res., **B19/B20** (1987) 150.

TABLE Conditions of Ion Implantation. Radiation Dose D = $(2*10^{16} \div 2*10^{17})$ cm^{-2}

Conditions	Medium	Ions	Accelerating voltage, kV	Pulse frequency, Hz	Current density, mA/cm^2	T at end of HDII K
1.1	Vacuum	Y	60	50	1	≤ 370
1.2	Vacuum	Mo	60	50	1	≤ 370
1.3	Vacuum	Pb	60	50	1	≤ 370
1.4	Vacuum	Cu	85	50	1	≈ 800
1.5	Ar	Y	60	50	2	≈ 670
2.1	N	Y	60	50	2	≈ 660
2.2	N	Zr	60	5	2	≈ 520
2.3	N	Zr	30	50	2	≈ 480
2.4	N	Zr	60	60	2	≈ 800
3.1	Ar	Si	60	5	2	≈ 460
3.2	Vacuum	Si	60	10	1	≈ 470
3.3	N	Si	60	5	2	≈ 460

Figure captions

.Fig. 1. A schemes for microdiffraction patterns interpretation (*a*, *b*), and a dark-field image of

Mo_2C (*c*) after treatments in type-1.1 (*a*, *c*) and type-2.2 (*b*) conditions.

Fig. 2. Relative-intensity distribution of secondary ions as a function of the time of sputtering

of the surface layer for the HDII of molybdenum in conditions of type 1.1 (curve *1*), 1.3 (*2*),

1.5 (*3*, *3'*), 2.1 (*4*).

Fig. 3. Electron diffraction pattern (*a*), a scheme for microdiffraction pattern interpretation

(*b*), and a dark-field image of Mo_2C (*c*) after treatments in type-1.4 (*a*) and type-2.4 (*b,c*)

conditions. a - the numbers on the diffraction pattern denote the reflexes: [00.2] of Mo_2C (*1*),

[11.0] of Mo_2C (*2*), and [200] of Mo (*3*).

Fig. 4. Electron diffraction pattern for surface layer of molybdenum after amorphization by

silicon (HDII in type-3.1 conditions).

a

- Mo[001]
- Mo$_2$C[1$\bar{1}$.1]
- Mo$_2$C[11.0]

1$\bar{1}$.2 10.1 11.0
1$\bar{1}$.1
110 00.2
020

b

- Mo[001]
- Mo$_2$N[001]
- Mo$_2$C
- [11.0]
- [$\bar{1}$1.1]

1$\bar{1}$.2 10.1 11.0
11.1
200
110 00.2
020
200

c

0.4 μm

I_{rel}

C
N
Y

0,30
0,15

3'
2
1
3
4

0   10   20   30   40   t, min

Neutron-capture-induced radiation treatment of polymeric materials

Donald J. Rej,[a] Mark M. Pickrell, and Debra A. Wrobleski
Los Alamos National Laboratory, MS-D434, Los Alamos, New Mexico 87545

A method for the bulk treatment of polymeric materials is proposed. Energetic ions created after capture of a neutron beam by constituent atoms located within the polymer can be used to cause radiation-induced modifications such as cross linking in the polymer. In contrast to traditional ion implantation, the proposed method enables bulk treatment because of the relatively deep penetration of neutrons. Analytical estimates and Monte Carlo computations are performed for the $^{10}B(n,\alpha)^7Li$ reaction for the cross linking and hydrogen depletion of boron-doped polystyrene. Requirements for the polymer composition and microstructure, as well as potential synthesis methods are discussed. © *1996 American Institute of Physics.* [S0003-6951(96)01518-5]

Polymers are useful materials because of their ease of fabrication, moldability, light weight, chemical inertness, and low cost. Additional structural applications are limited since polymers are inherently soft materials with relatively low mechanical strength and abrasion resistance. To alter these properties, cross-linking methods utilizing chemical reactions (e.g., thermoset or vulcanized rubber), x-rays, or electron beams, have been employed for some time. Recently, superior improvements in surface mechanical properties have been achieved by implantation of energetic light ions into polymers.[1-4] In ion implantation, ions are accelerated and extracted from an external source and injected into the surface of a target polymer [Fig. 1(a)]. Implantation results in modified molecular structures (e.g., three-dimensional cross linking) and compositional changes (e.g., hydrogen depletion). Dramatic increases in hardness, electrical conductivity, and gas permeation resistance have been achieved with light ions with energies of order 0.1–1 MeV, and implanted doses of order 10^{15} ions/cm^2. In contrast to electrons or photons, energetic ions are desirable since they produce sufficient linear energy transfer (LET) into electronic stopping $(dE/dx)_{el}$ which is large enough to result in significant cross linking within the polymer. During implantation, adjacent hydrogen–carbon bonds in polymer chains are broken by the ion LET. The hydrogen recombines into a gas, eventually diffusing out of the polymer. Free carbon radicals located on adjacent polymer chains subsequently combine to form new C–C bonds, resulting in carbon rich, highly cross-linked polymer chains.[2,3] To break adjacent C–H bonds, one requires an electronic LET

$$\frac{dE}{dx}\bigg|_{el} \gtrsim \frac{a\,e}{\delta}\left(\frac{\epsilon}{\delta}\right) \tag{1}$$

where ϵ is the binding energy (≈ 4 eV), δ is the interatomic spacing, which for many polymers is of order 1 Å, and a is a numerical factor, greater than unity, which accounts for other reactions with polymer electrons which lead to ion slowdown, but do not result in the breaking of C–H bonds. Assuming $a \approx 3$, one needs $(dE/dx)_{el}$ of 12 eV/Å or more.

A fundamental limitation with ion implantation is that since the ions are injected from an external source, only an outer surface of the polymer, corresponding to the projected ion range R_p (typically $\leqslant 10$ μm for most ions with energies below 1 MeV) can be treated. In many applications, deeper modified layers are desirable, especially for wear applications where plastic deformation of the soft substrate severely restricts the effectiveness of the much harder ion-implanted surface.

In order to extend the known benefits of energetic ion implantation to bulk material properties rather than only surfaces, we introduce the concept of neutron-capture-induced polymer treatment illustrated in Fig. 1(b). Neutrons from an external source are injected into a polymer material. Neutrons readily penetrate the polymer and interact with "target atoms" that reside inside the polymer. Target atoms may be the constituent atoms that make up the polymer, or they may be dopants, such as boron, which are introduced into the polymer prior to the neutron treatment. Modification of the chemical and physical properties of the polymer occur from radiation damage caused by the slowdown and stopping of energetic light ions that are produced by the disintegration of target atoms after they capture a neutron. A particularly appealing reaction is

$$n + {}^{10}B \rightarrow {}^4He + {}^7Li, \tag{2}$$

which results in an energy release of 2.79 MeV. In 93% of the reactions, the ^7Li nucleus is created in an excited state which relaxes through the emission of a 0.48 MeV γ ray. The remaining 2.31 MeV is in the form of kinetic energy
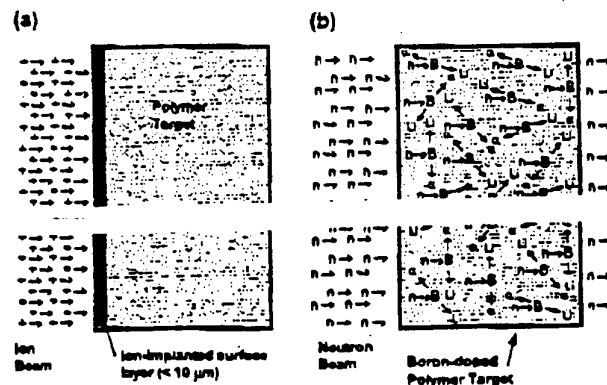

FIG. 1. The (a) ion implantation and (b) neutron capture induced radiation treatment methods.
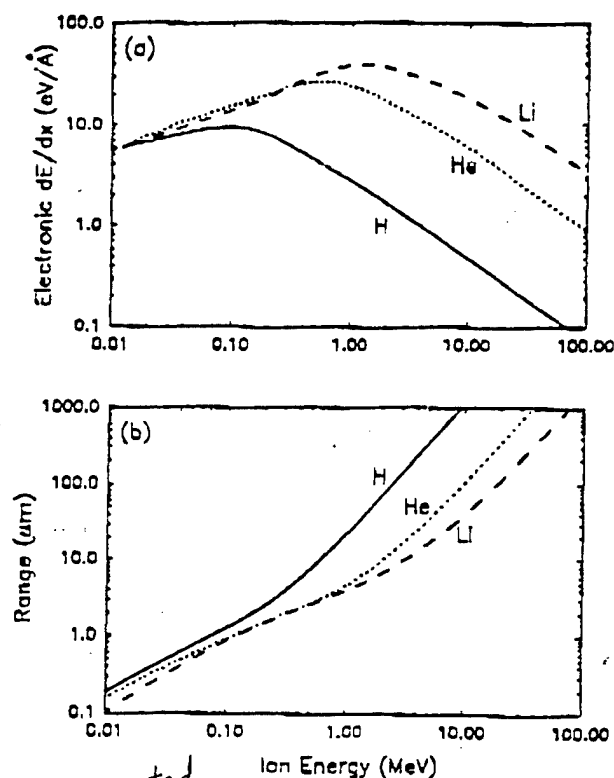
computed

FIG. 2. The (a) electronic linear energy transfer and the (b) projected range of energetic protons, helium, and lithium ions in polystyrene, computed with the TRIM code (Ref. 6).

shared between a 1.46 MeV alpha particle and a 0.85 MeV ^{7}Li recoil nucleus. The remaining 7% of reactions result in ground state ^{7}Li, with all 2.79 MeV being transferred into a 1.78 MeV alpha particle and a 1.01 MeV ^{7}Li kinetic energy. Reaction (2) is attractive because of the high naturally occurring concentration (20%) of the ^{10}B isotope and the reaction's high probability with a cross-section $\sigma = 3.8 \times 10^{-25}$ m^2 for thermal neutrons.[5] The energetic ^{4}He and ^{7}Li particles are ionized as they move through the polymer and are rapidly slowed down and stopped, primarily by electronic and nuclear stopping inside the polymer. The maximum electronic LET, which has been computed with the TRIM code,[6] is between 20 and 30 eV/Å which appears well suited to this application, with projected ranges of about 3–8 μm (Fig. 2).

The neutron-capture method results in the injection of the requisite MeV ions from *inside* the target. In contrast to the ion implantation process, the neutron process results in the treatment of bulk materials rather than just surfaces, since neutrons readily penetrate thick samples, allowing the formation of energetic disintegration products throughout the polymer.

To estimate the requisite neutron dose, $\phi_n = \int \Gamma_n dt$ (where Γ_n is the neutron flux), and ^{10}B atomic density n_B, we extrapolate the ion implantation parameters of Lee *et al.*[2] The total number of neutron capture reactions per unit volume $\mathcal{N}$ is given by

$$\mathcal{N} = \int n_B(t) <\Gamma_n \sigma> dt. \quad (3)$$

An ion fluence of 10^{19} m^{-2} implanted into a 5 μm depth is

equivalent to $\mathcal{N} = 10^{24}$ m^{-3}, where both ^{4}He and ^{7}Li nuclei are assumed to cause cross linking. For $n_B = 5 \times 10^{26}$ m^{-3} (1% ^{10}B concentration) doped into polystyrene (50% C, 50% H, specific gravity=1.06), and thermal neutrons, ϕ_n is 5×10^{21} m^{-2}, while the thin-target exposure time is about 1.5 h in a $\Gamma_n = 10^{18}$/m^2/s reactor beam.

In addition to the intended n, α reaction, we consider radiation damage from other sources and reactions. Gamma and neutron radiation effects on polymers are well known.[7,8] Polymers with a tendency to cross link harden slightly with gamma radiation before degradation and destruction at doses of up 0.1–4 Grad. For thick targets, the 0.48 MeV γ from the ^{7}Li product will result in a dose D of ~8 Grad for $\mathcal{N} = 10^{24}$ m^{-3}. D will be considerably smaller for thin targets with thicknesses less than the γ absorption range (about 0.1 m for polymers) since a significant portion of the γ's can escape from the target. While thermal neutrons tend not to deposit significant energy into a polymer, accompanying epithermal and fast neutrons and gamma rays can. For example in a reactor, ~1 rad of radiation from gammas and fast neutrons is deposited into a polymer per 10^{13} m^{-2} of thermal neutron fluence.[7] Thus, for $\phi_n = 5 \times 10^{21}$ m^{-2}, this dose is about 0.5 Grad, which is well below the damage threshold for polystyrene.

The details of neutron transport and absorption have been modeled using the Monte Carlo Neutron Photon (MCNP) code.[9] MCNP simulates neutron transport, one particle history at a time in sequence, into three-dimensional targets using a fully probabilistic, Monte Carlo method with self-consistent reaction cross sections. The uncertainty of the simulation is limited primarily by the accuracy of the cross-section data, the statistics of the particle histories, and the details of the target material composition and geometry. For a well-known target geometry and a sufficient number of particles, the uncertainty is typically better than 1%.

Simulations have been performed for a neutron flux at normal incidence onto a surface of a $100 \times 100 \times 100$ mm polystyrene cube. ^{10}B concentrations relative to hydrogen n_B/n_H of 0, 0.01%, and 1% are modeled. The target is irradiated with a "beam" [Fig. 1(b)] of 10^5 neutrons having a Maxwellian energy distribution with a 0.025 eV temperature. In addition to the desired ^{10}B$(n, \alpha)^7$Li reaction, other principal reactions are elastic scattering (mostly from the protons in the polymer) and the H(n, γ)D reaction which releases a 2.2 MeV γ ray and has a cross section of ~0.3 barn for thermal neutrons,[5] a value 10^4-times smaller than the ^{10}B reaction. MCNP tallies of the ^{10}B$(n, \alpha)^7$Li and H(n, γ)D reaction rates are computed in 10 volumes, evenly spaced into the target beginning from the front surface and averaged over the 100×100 mm lateral area. In addition, surface flux tallies are performed over the sides of the target to estimate lateral loss from elastic scattering.

MCNP tallies of the relative neutron population and the absorption reaction rates are plotted in Fig. 3. For the undoped target [Fig. 3(a)] elastic scattering is an important effect since the mean-free path for elastic scattering (the dominant reaction), $\lambda_{el} = 1/n_H \sigma_{el} \approx 8$ mm, is significantly smaller than the 100 mm target thickness. Consequently, neutrons diffuse through the cube and also out the sides, leading to an attenuation of the neutron population. For undoped targets,
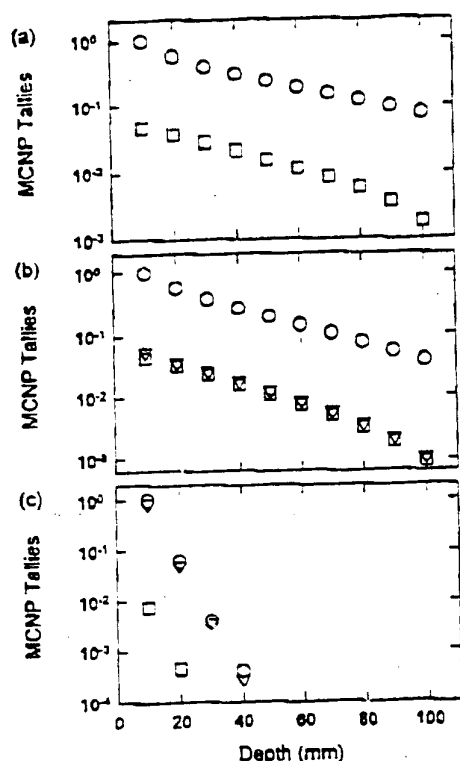
FIG. 3. Monte Carlo simulations of thermal neutron transport and absorption with the MCNP code (Ref. 9) for thermal neutrons injected into a .00×100×100 cm thick polystyrene cube with (Ref. 10) ^{10}B concentrations of (a) 0, (b) 0.01%, and (c) 1% molar. (O): relative neutron flux; (□): average H(n,γ)D reaction rate per 10 mm; (∇): average ^{10}B(n,α)^{7}Li reaction rate per 10 mm.

the flux lost through the lateral surfaces accounts for most of the 93% attenuation in flux, with the H(n,γ)D reaction being responsible for only about 4%. For 0.01% n_B/n_H concentration, increased attenuation is observed due to the ^{10}B(n,α)^{7}Li reaction, which has become comparable to the H(n,γ)D reaction, and results in an increased neutron attenuation of ~4%. At 1% concentrations, ^{10}B(n,α)^{7}Li dominates, capturing most of the neutrons with a reaction mean free path $1/n_B\sigma \approx 5$ mm.

For doped polymers, dopant atoms must be evenly dispersed within the 3–8 μm ranges of the ^{7}Li and ^{4}He ions, respectively. For effective ion energy transfer into the polymer, dopant domain sizes need to be significantly smaller than the ion range in the dopant phase. B-doped polyethylene is routinely used for neutron shielding. However, for these materials, B is often concentrated in, or agglomerates into, relatively large domains with sizes easily exceeding R_p.[10] Ideally, atomic dispersion is desirable. Assuming the 20% natural concentration of ^{10}B, between 1% and 10% (molar) total B concentrations (relative to the polymer repeat unit) should be adequate.

To incorporate boron into a polymer in a well-dispersed fashion, a number of approaches may be explored. For ex-

ample, we have found that dissolving polystyrene and a boron compound together followed by casting gives a boron doped polymer film. In particular, this physical mixing method is useful for polymers containing atoms which can form good Lewis acid-base pairs with B. Polymers containing Lewis bases such as amines, ether, amide or phosphine groups (e.g., polyester, polyacrylamide, amide) can be evaluated. A related method is to chemically treat a polymer containing groups such as hydroxyl groups (such as polyvinylalcohol) with a boron precursor compound to give a polymer containing boron covalently bonded to the polymer backbone. Another approach is to incorporate boron in the polymer through copolymerization of a boron compound (e.g., boron allyloxide) with a monomer such as styrene. Depending on the physical properties, these materials could be formed into a given shape using standard polymer processing techniques. These methods of processing include techniques such as compression molding or injection molding of the copolymer or mixture into a shaped part.

Activation of impurity atoms residing within the polymer poses a potential safety issue. As an example, we consider ^{197}Au present at an atomic density $n_{Au}=5 \times 10^{19}$ m^{-3} (1 ppb). The ^{197}Au(n,γ)^{198}Au reaction has a cross section of 98 barn for thermal neutrons, with ^{198}Au decaying over a 2.7-day half-life. For $\phi_n=5\times10^{21}$ m^{-2}, the target activation level immediately after irradiation is estimated to be ~300 nc/g.

In conclusion, we have proposed a treatment technique for the modification of polymeric materials. The technique builds on the known benefits of ion implantation, but it enables the treatment of bulk materials rather than just surfaces. While this letter deals with only one example, the ^{10}B(n,α)^{7}Li reaction, the basic idea of neutron capture, and also, neutron-induced recoil of other heavy atoms residing within polymers may result in similar radiation damage that may alter the materials' compositional, mechanical, electrical, optical, and gas diffusion properties.

[1] E. H. Lee, M. B. Lewis, P. J. Blau, and L. K. Mansur, J. Mater. Res. 6, 610 (1991).
[2] E. H. Lee, G. R. Rao, M. B. Lewis, and L. K. Mansur, Nucl. Instrum. Methods B 74, 326 (1993).
[3] L. Calcagno, G. Compagnini, and G. Foti, Nucl. Instrum. Methods B 65, 413 (1992).
[4] G. Dearnaley (private communication).
[5] S. F. Mughabghab, M. Divadeenam, N. E. Holden, V. McLane, C. L. Dunford, and P. F. Rose, Neutron Cross Sections (Academic, New York, 1981).
[6] J. F. Ziegler, J. P. Biersack, and U. Littmark, The Stopping and Range of Ions in Solids (Pergamon, New York, 1985).
[7] A. Charlesby, Atomic Radiation and Polymers (Pergamon, New York, 1960).
[8] A. Holmes-Siedle and L. Adams, Handbook of Radiation Effects (Oxford University Press, Oxford, 1993).
[9] MCNP—A General Monte Carlo N-Particle Transport Code, Ver. 4A, edited by J. F. Briesmeister. Los Alamos National Laboratory Report LA-12625, 1993, available from the National Technical Information Center, 5285 Port Royal Rd., Springfield, VA 22161).
[10] S. A. Thiebault, E. R. Long, M. B. Glasgow, R. A. Orwoll, and R. L. Kiefer, Poly. Preprints 35, 954 (1994).

DEFECT STRUCTURES IN METALS EXPOSED TO IRRADIATION OF DIFFERENT NATURE

Yu. P. Sharkeev*[1], E. V. Kozlov**, A. N. Didenko***

* Institute of Strength Physics and Materials Science of RAS, Tomsk, Russia

** Tomsk State Academy of Architecture and Building, Tomsk, Russia

*** Russian Academy of Sciences, Moscow, Russia

Abstract

The regularities of the defect substructures formation in the near surface layers of metals under irradiations (high dose ion implantation, high power ion beam, high power pulsed microwave) are presented. The defect substructures formed under irradiations are similar to the defect substructures formed in metals and alloys during plastic deformation by one axis tension or compression. The main reason of the defect substructures formation in metals exposed to irradiations is the high level of stresses originated in the target near surface layer. The mechanisms of origination of stresses, the value and nature of stresses are determined by the type of irradiation.

1. Introduction

At ordinary loading of metals and alloys (for example, one axis compression or tension) the performed mechanical work is used to increase the internal energy and, first of all, the defect subsystem energy of the deformed sample. With the increase of plastic deformation of metals the scalar dislocation density is also increased. The dislocation substructure is

---

[1] Corresponding author: fax: (382.2) 259576, e.mail: ispms@ispms.tomsk.su
   Present address: ISPMS of RAS, pr.Akademicheskii 2/1, Tomsk, 634021, Russia

changed according to the proper law passing over the certain evolution stages. Classification of the dislocation substructures formed at plastic deformation of metals and alloys was developed by E. Kozlov and his colleagues and was reported in papers [1, 2]. In the papers one can find the electron micrographs of types of dislocation substructures. At increase of deformation the dislocation substructures are originated in a certain sequence following on another. Two main sequences of transformations can be seen (fig. 1). The first is typical for metals with low energy of the packing fault, the second is typical for high energy of the packing fault. At high dislocation densities both sets are merged together. The scalar dislocation density turned to be the main parameter influencing the transformation of a dislocation substructures into another one.

Under exposure of a target to irradiation the absorption of energy of the near surface layer of metallic target takes place. In this case a part of absorbed energy will be transformed into the energy of the defect subsystem of the near surface layer of the target. Specifically, one can see the increase of dislocation substructures of different types. The main peculiarities of the dislocation substructures formed in metals and alloys at high dose ion implantation (HDII), under exposure to high power pulsed microwaves (HPPM) and high power ion beams (HPIB) are presented in the paper.

2. Experimental results

The main parameters of irradiations are given in the Table 1. It is necessary to point out that the HPPM treatment was carried out in the air. The defect structure investigation of the samples initial state was the obligatory regirement. As a rule, before irradiation the samples were subjected to recrystallization annealing and had the low density of dislocations. The dislocation structure of the investigated samples in the initial state was presented by a chaotic dislocation distribution and the tangled dislocations. In the case of HDII the copper samples

deformed by compression up to 6 and 30 % were also chosen. For deformed copper the dislocation structures of the initial states were presented by cell-net and cell dislocation substructures for $\varepsilon=6$ % and $\varepsilon=30$ % correspondingly.

2.1. Dislocation substructures formed at HDII

When investigating the defect structure of ion implanted samples it was established that the ion beam influence were not limited by the thin surface layer alloyed at ion treatment. The thickness of this layer at ion implantation does not exceed one micrometer. It is necessary to point out that in the above said surface layer a series of processes (alloying; formation of point defects, dislocation loops, dislocations, pores, precipitates; amorphization; radiation-induced segregation; radiation-enhanced diffusion and etc.) take place. It turns out that beyond the surface layer in the sublayer (subsurface layer) at ion implantation the strong dislocation structure is formed. The thickness of the subsurface layer with the dislocation structure induced by ion implantation can reach tens microns. The examples of the dislocation substructures are given in the Figure 2. As a rule, it is a net-work, cell-net or cell dislocation substructures without misorientations.

This phenomenon was called the long range effect [3,4]. The following definition can be considered as the most correctly reflecting the essence of this phenomenon. The long range effect consists in formation of a defect structure and/or in change of the structural-phased state of the subsurface layer of irradiated target which thickness exceeds greatly the thickness of the surface alloyed layer. At present four reviews of the long range effect were published in periodicals [5-8].

In the Figure 3a the dependence of the scalar dislocation density on the distance to the surface of α-Fe samples implanted by Hf ions is represented as an example. The dislocation density for the initial state is marked by the dotted line. One can see that all the curves

have a maximum at the distance of several micrometers from the surface. The maximum dislocation density as regards to the initial state is increased in an order and more.

Figure 3b shows the similar dependency for copper implanted by Hf, Zr and Ti ions. In the case of Hf and Zr ion implantation with the increase of distance from the irradiated surface the dislocation density value increases reaching its maximum at a distance of 10 μm from the surface and then decreases. At a distance of 50 μm the dislocation density corresponds to that in the initial state. At ion treatment of the deformed copper (ε=6%) the dependence is the same. Ion treatment of greatly deformed copper (ε=30%) does not lead to a change in dislocation density. The dislocation density dependence on the distance for copper samples implanted with Ti ions is not the same. A maximum of the dislocation density value lies much closer to the irradiated surface than in the samples implanted with Hf and Zr ions. The dislocation density value decreases rapidly with increasing distance from the surface. At the depth of 15 μm the dislocation density value corresponds to that of the initial state. Transmission electron microscopy analysis of the phase state of the alloyed copper layers showed the following. Implantation of Zr ions is accompanied by the formation of ZrO_2 fine-dispersed particles whereas implantation of Ti ions leads to amorphization in the alloyed layer. Undoubtedly, the fine-dispersed particles of the ZrO_2 second phase are the origination of higher stresses in comparison with the armorphous state.

On the basis of the analysis of the character of the dislocation substructures and the quantitative dependencies the following important conclusions were made. 1) The thickness of the subsurface layer with the changed dislocation structure is varied from several to tens microns that exceeds greatly the thickness of the surface alloyed layer. 2) The dislocation density dependence on the distance from irradiated surface has a maximum. 3) The maximum change of the dislocation structure is observed in well annealed metal with low dislocation density in the initial state. In greatly deformed metals with high dislocation density a

change in the dislocation structure at ion implantation is not observed. 4) Thickness of the subsurface layer with the dislocation structure induced by ion implantation and the value of dislocation density in this layer depend on the character of the structural-phased state formed in the alloyed surface layer. 5) The dislocation substructures formed in the ion implanted target are similar to the dislocation substructures of metals deformed up to 10-15 %. Undoubtedly that at ion implantation the dislocation substructures are formed at the expense of dislocation movement under the action of mechanical stresses originated in the surface alloyed layer.

At present several mechanisms explaining the long range effect in the ion implanted metals and alloys are suggested [5-8]. The main essence of the mechanisms is the presence of static and dynamic stresses, acoustic or elastic waves. Unfortunately, none of the considered mechanisms does not allow us to explain the formation of dislocation structures at high dose ion implantation of metals and alloys. Particularly, it is not quite clear why the maximum of dislocation density lies at some distance from the irradiated target surface. The model furnishing an explanation of the dislocation structure formation in a sublayer at ion implantation was suggested by the authors with their colleagues [9]. The main points of the mathematical model can be formulated as follows. 1) By ion implantation the stresses arising in the alloyed surface layer whose values essentially exceed the dislocation motion resistance value. 2) Under these stresses the dislocations moving within the alloyed surface layer reach high velocities and, consequently, the high kinetic energies and then are ejected in the sublayer where the stress value are less than the yield strength. 3) In the sublayer the dislocations moving by inertia up to full stop overpass the distances whose values exceed essentially the thickness of the surface alloyed layer.

The quantitative calculations made are in a good agreement with the experimental data [9,10]. Particularly, we can explain the existence of a maximum on the curves "the dislocation density-the distance to the surface".

2.2. Dislocation substructures formed at HPIB

In figure 4 one can see the typical electron microscopy images of the dislocation structures formed in α-Fe exposed to HPIB. The dislocation structure varies from complex dislocation configurations to uniform dislocation distribution. The dislocation structure turned to be more uniform when the density of ion current is equal to 60 A cm^{-2} and the number of pulses is equal to 1. The increase in the ion current density to 200 A cm^{-2} and in the number of pulses to 5 is accompanied by a significant reconstruction in the dislocation structure. The dislocation structure becomes non-uniform. When comparing the dislocation structure formed under high power ion beam and during plastic deformation it was established that these dislocation structures are similar. We investigated the dislocation structures formed at different distances from the irradiated surface (see fig. 4c, d). It was established that starting from 50 μm thickness, regions with the fragmented dislocation substructure are observed. This dislocation substructure corresponds to a high value of high velocity plastic deformation.

Figure 5 shows the dependence of the mean dislocation density on the distance to the irradiated α-Fe surface. The dependence obtained shows two maximums. The first maximum is near the irradiated surface. This maximum is related to the thermomechanical stresses arising in a near surface layer at melting, evaporation and sublimation. The second maximum, more stretched, is at the distance about of 100 μm from the irradiated surface. This maximum corresponds to the sample region where the shock wave is formed by the recoil momentum under vapor and plasma deposition on the surface. We calculated the depth of the shock wave formation using the following formula [11]

$$Z = \frac{C_1^2}{\xi(\Gamma+2)}\left[\frac{2\tau\Delta m}{(\gamma-1)\chi\overline{q}}\right], \tag{1}$$

where C_1 is the longitudinal sound velocity in solids in the non-excited state; Δm is the mass of evaporated matter; τ is the pulse duration; Γ is Gruneisen parameter; $\overline{q}$ is the effective density of the observed energy flow; γ is an adiabatic indicator; $\xi = \chi = 1$. For α-Fe $Z \approx 120$ - 130 μm that agreed with the experimental results.

2.3. Dislocation substructures formed at HPPM

The exposure to HPPM on the metal samples leads to the generation of dislocations and to increase of the dislocation density. As a result, the different dislocation substructures are formed: net and cell net dislocation substructures without misorientations, tangled dislocations as well as chaotically distributed dislocations. Some types of the dislocation structures formed at HPPM are presented in the Figure 6 . It necessary to point out that these dislocation substructures are similar to the dislocation substructures formed in the deformed metals and alloys as well as at exposure to other type irradiations. The maximum changes in the dislocation structure occurred in the near surface layer the thickness of which, as a rule, was equal to several micrometers, i. e. to one-three values of the skin layer thickness.

The characteristic dependencies of the average dislocation density on the distance from the irradiated surface are given in Figure 7. The calculated boundaries of the skin layers are shown by vertical dotted lines. With the increase of the distance from the surface the dislocation density is increased reaching a maximum and then it is decreased. A maximum of the dislocation density lies near the skin layer or immediately beyond the skin layer.

The carried out evaluations of the incident electromagnetic wave pressure showed that the HPPM pressure value is by many orders of magnitude smaller than the target yield

strength value. Consequently, the reflected wave cannot be the reason of the dislocation structure formation.

Let us evaluate the quantity of the HPPM energy absorbed by the target. For the flux density of the absorbed HPPM there exists the following expression:

$$P_{absb.} = P_{inc.} \cdot \sqrt{\frac{f}{\sigma}} , \qquad (2)$$

where σ is the static conductivity (for pure copper $\sigma = 5 \cdot 10^{17}$ s^{-1} for the HPPM of 3–5 GHz. ε_e is the electric constant, f is the frequency of the HPPM field and $P_{inc.}$ is the flux density of ir-radiated power on the sample surface. The energy absorbed by a square unit of the sample surface during exposure to HPPM is equal to

$$W = P_{absb.} \tau N , \qquad (3)$$

where τ is the pulse duration. N is the pulses number. For N=100, τ=30 ns and P_{inc}=1x10^5 Wt cm^{-2}. From (2) and (3) one can receive W≅5x10^{-4} J cm^{-2}.

The quantity of energy which is necessary for the dislocation structure formation in the material volume unit can be evaluated as follows [12]:

$$W_u = \rho E_c , \qquad (4)$$

where ρ is an average dislocations density, E_c is the dislocation energy of a unit length [13]:

$$E_c = Gb/4\pi k \; \ln(R/r) , \qquad (5)$$

where G is the shear module, b is the dislocation Burger vector value, k = 1 for the screw dislocation and k=1−v for the edge dislocation (v is the Poisson coefficient; usually k=1), r is the dislocation nucleus parameter (usually r≅b), $R=1/\sqrt{\rho}$ is the characteristic size of the dislo-cation area. For copper G=42 GPa, b=0.25 nm. In the near surface layer with the changed dislocation structure the maximum dislocation density value does not exceed 1.2x10^{10} cm^{-2}. Let us assume ρ=1x10^{10} cm^{-2}. The energy necessary for the dislocation structure formation of

the above said density in a unit of the material volume turned to be 0.125 J cm^{-3}. Consequently, one should assume $W_\Sigma = W_0 d$ is the energy of the dislocation structure formation in the thin surface layer the thickness of which is equal to d. Let d=4 μm, than $W_\Sigma = 0.5 \times 10^{-4}$ J cm^{-2}. The value received is smaller than the HPPM energy absorbed by a square unit of the metal surface. It should be noted that under the exposure to HPPM the metal reflectiveness can be significantly changed and the quantity of the absorbed energy will be appreciably higher [14]. Thus, the given evaluations showed that the quantity of the HPPM energy absorbed by the metal is enough for the dislocation structure formation in the target near surface layer.

As it was pointed out above the dislocation structures formed under exposure to HPPM are similar to the metal dislocation structures deformed up to 10–15%. Naturally, the dislocation generation in the near surface copper layer under exposure to HPPM is initiated by the thermostresses induced by the absorption of a part of the HPPM energy [15]. However, the evaluations done showed that the temperature in the subsurface copper layer is changed in fractions of a degree. The stress resulted from the crystal lattice distortion under the electrical component of the HPPM field appeared to be one of the possible reasons of the dislocations generation. Mechanisms of the dislocation structure formation under exposure to the HPPM field are called for further theoretical consideration.

4. Discussion

The dislocation density dependencies on the distance to the irradiated surface for HDII, HPIB and HPPM (Fig. 3, 5, 7) take on the same form. All the curves have a maximum lying at some distance from the surface. The character of irradiation exposure determines the position of the maximum relative to the irradiated surface as well as the thickness of the near surface layer where the defect structure modification takes place. For example, the thickness

of the near surface layer for HPPM is equal to the several micrometers, the same value for HPPM is equal to tens micrometers, whereas the layer thickness for HPIB exceeds considerably greater than 100 µm. It is necessary to point out that in target near surface layers under exposure to all types of irradiation used the identical dislocation substructures are formed. The pointed peculiarities testify to the fact that nature of the defect substructure formation in the metals under exposure to irradiations is the same. Deviation is seen only for HPIB. Two maxima were revealed on the curve "the dislocation density-the distance to the irradiated target surface".

Analysis of the character of the dislocation substructures formed in the metal near surface layers under exposure to ion beams (HDII and HPIB) and HPPM irradiation showed that they are similar not only between themselves but also to the dislocation substructures of metals and alloys deformed up to 10-15 %. Undoubtedly, the dislocation substructures in the irradiated metals are resulted from the plastic flow of the target near surface layer under exposure to irradiation. Actually, the irradiation exposure on the target is similarly to the mechanical loading. In this case in the near surface target layer the high level of mechanical stresses are formed (static and/or dynamic), that lead to the dislocation generation, the dislocation density increase and to the formation of the dislocation substructures. The nature of the stresses arising in the target near surface layers under irradiations is different and depends on the character of the irradiation and calls for further investigation. Some mechanisms of the formation of stresses and the defect structures under exposure to ion beams are considered in [5-9].

5. Conclusions

The exposure to irradiation of HDII, HPIB and HPPM types leads to generation of dislocations in the near surface layer of metallic target. The formed dislocation substructures

are similar to the dislocation substructures formed in the deformed metals and alloys. The thickness of the near surface layer of the irradiated target with the induced dislocation substructures depends on the type of irradiation. It is equal to some micrometers for HPPM, tens micrometers for HDII and hundreds micrometers for HPIB. The main reason of dislocation generation is the high level of stresses originated in the near surface layer of the target in the process of irradiation or/and after it. The mechanisms of the stresses origination, the value and character of stresses in the near surface layer depend on the type of irradiation that are used for treatment of the metallic target.

Acknowledgments

12

REFERENCES

[1]   N. A. Koneva and E. V. Kozlov, *Izv. Vuzov. Fiz.* 2 (1990) 89.

[2]   N. A. Koneva and E. V. Kozlov, *Izv. Vuzov. Fiz.* 3 (1991) 56.

[3]   A. N. Didenko, E. V. Kozlov, Yu. P. Sharkeev, A. S. Tailashev, A. I. Ryabchikov,
L. Pranjavichus and L. Augulis, *Surf. Coat. Technol., 56 (1993) 97*.

[4]   A. J. Perry, J. R. Treglio, J. P. Schaffer, J. Brunner, V. Valvoda and D. Rafaja, *Surf.
Coat. Technol., 66 (1994) 377*.

[5]   Yu. V. Martynenko, in *Itogi nauki i tekhniki. Puchki zaryazhenykh chastits i tverdoe
telo.* Moscow, VINITI. no. 7, 1993, pp. 82-112.

[6]   Yu. P. Sharkeev, A. N. Didenko and E. V. Kozlov, *Russ. Phys. J., 7 (1994) 478*.

[7]   Yu. P. Sharkeev, A. N. Didenko and E. V. Kozlov, *Surf. Coat. Technol. 65 (1994) 112*.

[8]   A. Z. Pivovarov, *Metalofizika i Noveishie Technologii. 16 (1994) 3*.

[9]   A. N. Didenko, E. V. Kozlov, Yu. P. Sharkeev, S. N. Kolupaeva and N. V. Vihor, *Surf.
Coat. Technol., 1994,* to be published.

[10] S. N. Kolupaeva, Yu. P. Sharkeev, N. A. Vihor, L. E. Popov, The absracts of the fourth
Russian Conference on the modification of properties of construction materials with
beams of charged particles. May 13-17, 1996, Tomsk, Russia, pp.139-140.

[11] V. A. Yanushkevich. *Fizika i himiya obrabotki materialov. 5 (1975) 9*.

[12] J. Hirt. Dislocations, in *Fizicheskoe Metallovedenie.* Vol. 3.Moscow. Metallurgiya.
1987.

[13] G. Fridel, *Dislocations.* Moscow. Mir. 1967. 664p. [13]

[14] A. N. Didenko, *Dokladi Akademii Nauk,. 340 (1995) 37*

[15] 19. N. A. Rubtsov, *The Thermal Change of Continues Medias by Irradiation.* Editor
Academician S. S. Kutalidze. Novosibirsk. Nauka. Sibirskoe otdelenie. 1984. 277p.

Table 1

THE PARAMETERS OF IRRADIATIONS

I. HIGH DOSE ION IMPLANTATION		
1.	Sort of ions	C, Fe, W, Hf, Ar, Dy, Pb Cu, Mo, Ni, B, La, Zr
2.	Mean energy of ions	40-200 keV
3.	Incident dose	$1 \times 10^{16} - 1 \times 10^{18}$ ion cm^{-2}
4.	Regime of ion implantation	continuos, repetitively-pulsed
5.	Temperature of target	$< 100°C$
6.	Target	α-Fe, Cu, Mo, Cu-Co-Al, VT18U, Ni$_3$Fe
7.	Type of ion source	Raduga, Diana, Vita, Vezuvii-1, MEVVA
II. HIGH POWER ION BEAM		
1.	Mean value of ion energy	300, 450 keV
2.	Ion current density	60, 100, 200 A cm^{-2}
3.	Duration of pulse	80-100 ns
4.	Number of pulses	1-11
5.	Ion composition	50% C-50% H
6.	Target	α-Fe
7.	Type of accelerators	Tonus, Vera
III. HIGH POWER PULSED MICROWAVE		
1.	Wave length	2.85, 10 cm
2.	Power flux density	2-400 kWt cm^{-2}
3.	Pulse number	2, 50 ,100
4.	Pulse duration	50-300 ns
5.	Target	Cu, α-Fe, Mo, Ni

Figure Captions

Fig. 1. Scheme of dislocations substructures transformations in metals and alloys at plastic

deformations.

Fig. 2. Electron micrographs of dislocation substructures formed in metals at HDII.

(a) Tangled dislocations (Mo⁻→Mo); (b) net dislocation substructure (W⁻→α-Fe); (c)

cell-net dislocation substructure (Ni⁻→Cu); (d) cell dislocation substructure

(Hf⁻→Cu).

Fig. 3. Dependence of the dislocation density on the distance to α-Fe (a) and Cu (b) im-

planted surface. (a) 1) the initial state; the retained doses (ion cm^{-2}) are 2) 0.22×10^{16};

3) 1.18×10^{16}; 4) 2.6×10^{16}; 5) 5.5×10^{16}; 6) 9.3×10^{16}; (b) 1,5) the initial states after an-

nealing and deformation to 6% correspondingly; 2, 3, 4) after implantation with Ti, Hf

and Zr ions correspondingly of annealed Cu; 6) after implantation with Hf ions of Cu

deformed to 6%.

Fig. 4. Electron micrographs of dislocation substructures formed in α-Fe at exposure to

HPIB. (a) Chaotic dislocation substructure; (b) cell-net dislocation substructure; (c, d)

fragmented dislocation substructures.

Fig. 5. Dependence of the dislocation density on the distance to α-Fe irradiated surface after

exposure to HPIB; the ion current density is 100 A cm^{-2}, the number of treated pulses

is 1.

Fig. 6. Electron micrographs of dislocation substructures formed in Cu at exposure to HPPM.

(a) Chaotically distributed dislocations; (b) dislocation tangles; (c) cell-net dislocation

substructure without misorientations; (d) cell-net dislocation substructure with misori-

entations.

Fig.7. Dependence of the scalar dislocation density on the distance to the irradiated copper

surface after HPPM treatment.

(2) $\lambda = 2.85$ cm, $P_{inc} = 200$ kWt cm^{-2}, n = 50 pulses;

(3) $\lambda = 10$ cm, $P_{inc} = 2$ kWt cm^{-2}, n = 100 pulses;
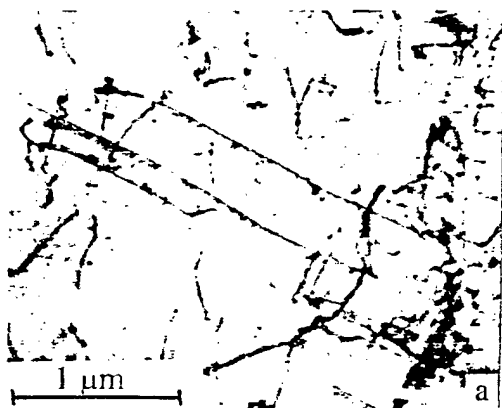
(4) $\lambda = 10$ cm, $P_{inc} = 100$ kWt cm^{-2}, n = 100 pulses;

(5) $\lambda = 10$ cm, $P_{inc} = 10$ kWt cm^{-2}, n = 100 pulses;

the dotted line (1) shows the dislocation density in the initial state of copper; the verti-

cal lines mark the skin layer boundaries in copper at the wavelength of 2.85 and

10 cm.

Value of deformation

Scale of dislocation density, cm^{-2}

1×10^{9} 2×10^{9} 5×10^{9} 1×10^{10} 2×10^{10} $< 4\times10^{10}$

Dislocation substructures

Dislocation-disclination substructures

Chaotic dislocation structure

Dislocation pile-ups

Dislocation tangles

Dislocation nets

Non-misoriented dislocation cells

Cell-net DSS

Misoriented dislocation cells

Fragmented DSS

Microband DSS

DSS with non-stop and discrete misorientations

Amorphous microstructure

Non-misoriented substructures

Misoriented substructures

ρ, 10⁹ cm⁻²

λ=10 cm

λ=2.85 cm

d, μm

HIGH POWER ION BEAM SOURCES FOR INDUSTRIAL APPLICATION

G. E. Remnev, I. F. Isakov, M. S. Opekunov ,V. L. Kutuzov*,

V. S. Lopatin, V. M. Matvienko,M.Yu. Ovsyannikov*,

A. V. Potyomkin, V. A. Tarbokov

Nuclear Physics Institute, Lenin Street 2a, Tomsk 634050, Russia

«Linetron» Scientific Industrial Enterprise, N.Novgorod, Russia

ABSTRACT

Two sources of high power ion beams of nanosecond duration are described, MAC and TEMP units. They generate ions with the energy of up to 125 and 300 keV respectively, and the pulse duration of 20-200 and 50 ns respectively. The sources are powered by magnetically insulated strip diode systems.

The accelerators are used both for applied research on modification of structural material properties, and for practical application of ion beam technologies for industry.

1. MAC SUPERCURRENT SHORT-PULSED IMPLANTER

The short-pulsed ion implantation allows to combine implantation of doping additions and annealing of defects emerging in the surface layer structure, with one operation [1, 4]. The following requirements are imposed on such short-puled high current implanter machines: high pulsed repetition frequency, long life, a possibility of changing of ion kind and power flux density.

The machine comprises an initial energy storing unit, a step-up peaking transformer, a vacuum chamber equipped with magnetic ion diode (MID). It allows to form a single pulse or two voltage pulses of the opposite polarity [6] with a possibility of the

varying of the pulse interval between two pulses. The amplitude of the high voltage pulse at the ion diode can reach up to 150 keV; pulse duration and pulse interval are strongly depending on the length of the forming line. A Marx generator, which was used for preliminary study of the short-pulsed implantation for the charging the pulse forming line [3, 4], was replaced by the pulse transformer with 300 keV output voltage and 24 transfer coefficient.

To set up a pulsed insulation magnetic field in the ion diode, the current source circuit of a generator with a step-down peak transformer having k=1/10 was used. The amplitude of the insulation current was up to 60 kA and the current pulse duration was 20 μs.

The machine is demonstrated to operate in bipolar pulse mode, where the first negative voltage pulse serves for the plasma formation on the potential electrode surface and the second positive one serves for the acceleration of ions formed by this plasma.

The cathode serves for magnetic insulation of the electron flux in the anode-cathode gap as a whole, as well as for the effective control of the electron flux on the anode. It allows to vary the efficiency of plasma formation on the anode surface and attain emission homogeneity. The MID anode is made of aluminum; however, the coating of the MID active parts can be replaced by different kinds of material. The MID has the following dimensions: 45 mm width, 200 mm length, 80 cm^2 active part area. The cathode beam output side is a system of 4x40 mm slits, with 60 per cent total cathode transparency.

For the generation of heavy ion beams, the MID anode was made of the same material with the regular spaced protrusions on the surface. The total current of output beam was up to 1.5 kA. Fig. 1 presents characteristics in the case of diode with aluminum anode. When Al^{n+} ions are generated, their portion constitutes 70% of the beam composition, the remaining 30 % beam part is presented by H^+ and C^{n+} ions. Fig. 2 presents Al distribution profile depending on depth in Si target (MID with aluminum anode with regular spaced protrusions on the surface and irradiation dose of $5 \cdot 10^{15}$ cm^{-2}). The results were obtained by two different procedures, i.e. instantaneous gamma-resonance spectroscopy with 27Al(p,g)28Si (bar chart) nuclear reaction and secondary emission spectroscopy (dashed line) [7].

2. TEMP SOURCE OF HIGH POWER ION BEAMS

On metal treatment by the HPIB action of nanosecond duration, these undergo structural changes (mainly in the near-surface layers) and carbides of target components are formed, the carbon diffused in and than absorbed on the metal surface taking part in the reaction [8].

The functional capabilities of practical implementation of HPIB are extended to the possibility of the film deposition on the surface treated by specific chemical composition before HPIB irradiation; it provides the layer mixing. Besides, HPIB treatment allows to obtain metastable compounds, which can not be obtained by other techniques. A similar approach is used in the laser implantation technique.

Fig. 3 shows a vacuum chamber. The unit has a semi-automatic remote control panel, a carrousel specimen handling system installed in the vacuum chamber. Specimen treatment can be performed in both a manual an automatic control mode. The time required for opening the chamber, replacing the chargeable carrousel unit with specimens, chamber pressurisation and pumping to 10^{-4} mm Hg operation pressure is 10 min.

Beams are produced by the magnetically insulated diodes (MID) without external magnetic field. The 500 mm section vacuum chamber is made of stainless steel tube of 500 mm diameter. On it's lateral section, there are 3 windows and some high voltage power and signal bushings for physical and optical diagnostics. To provide mixing of multilayer targets, a device intended for thin metal film deposition on treated surfaces was installed in the vacuum chamber. It allows to use magnetron technique for target sputtering and to obtain the films of various materials. The two 300x100x30 mm magnetrons were installed on the back flange of the vacuum chamber opposite to MID (Fig. 3). The unit operation depends on the power supply system, which consists of two 3 kW d.c. sources with voltage up to 1,000 V, as well as gas-feeding and water-cooling system. HPIB treatment and film deposition can be performed in any desired sequence without causing any de-pressurization of the

3

vacuum space. Current density at the target is controlled by the gap between the target unit and the focusing diode.

Thus, the functional capabilities of the machine have been extended to the following operations in one cycle:

- deposition of metal film and their mixing with substrate by HPIB treatment;
- target pre-treatment and metal film deposition;
- target pre-treatment, film deposition and mixing of materials by HPIB treatment;
- target pre-treatment, deposition of two metal films in one or N cycles and their mixing by HPIB treatment.

3. HARDENING OF CUTTING TOOLS

The treatment of steel tools irradiated by HPIB with more than 100 A/cm^2 current density, with more than 2 pulses, leads to the formation of fine-grained structure in the near-surface layer. Polished specimens, which are subjected to the HPIB treatment, have a high level of the surface roughness compare to the original ones, while a similar treatment of the specimens with more rough surface leads to the smoothing of the surface and improvement of the surface characteristics. As a result of HPIB treatment, the density of dislocations in the near-surface layer and depth of ion rate in the specimen have been found to increase by an order or two orders of magnitude with resultant three-fold or better increase of the wear resistance of the treated surface.

The SIE «Linetron» and the «Temp» Engineer Physical Center are developed the industrial technology for the cutting tool hardening on the base of TEMP accelerator for the wagon wheels' treatment. The annual production has reached 100,000 plates per year. The accelerator resource is more than 10^6 times to the moment. The tool hardening is varying from 2 to 6 times depending on the sort of tool and material.

CONCLUSION

The TEMP and MAC accelerators have a different applications. In the first case, it is an ion energy influence; in the second case, it is a ion implantation method. The accelerators are based on the same approach of the ion formation in diode systems.

The industrial application of TEMP accelerator for the tool hardening promises the wide perspectives of the use of the high power ion beam source for industry. In the near future, the next TEMP-4 accelerator with increased productivity and 1 Hz repetition rate will be put into the operation.

REFERENCES

1. R.T.Hodgson, J,E.Baglin, R.Pal, I.M.Neri and D.A.Hammer, *Appl. Phys. Letters*, 37, 187 (1980);

2. M. Nastusi, R. Fastow, J.Gyulai, J.W.Mayer, S.J.Plimton, E.D.Plimpton, E.D.Wolf, B.M.Ullrich, *Nuclear Instruments and Methods in Physics Research*, B7/8, 1985, p. 585-590;

3. I. Krafcsik, L. Kiralyhidi, P.Riedl, M.Fried, J.Gyilai, E.Panlijak, *Nucl. Instrum. and Methods in Physics Research*, B21, 1987, p. 604-607;

4. F.F.Komarov, A.P.Novikov, *Itogi nauki i tekhniki*, Ser. Fizicheskie osnovy lasernoi i puchkovoi thkhnologii. V. 5 - M.: VINITI, 1989, p. 135;

5. I.F.Isakov, E.I.Logachev, S.A.Pechyonkin, G.E.Remnev, Yo.P.Usov, *Proceedings of the 4-th Workshop on Charged Particle Accelerator Application for Industry*, Leningrad, 1982, v.1, p. 191-193;

6. I.F.Isakov, V.N.Kolodii, M.S.Opekunov, Vacuum, v.42, No.1/2, 1991,pp.159-162.

7. Ryzhkov V.A., Opekunov M.S., Remnev G.E. et al. *Abstr. 10-th Confer. on the Chemistry of Big-Purity Substances.* Nizhnii Novgorod, Russia, June 1995.: 1995, p.151-152.

8. G.E.Remnev, V.A.Shulov, *Laser and Particle Beams*, 1993, v.14, No. 4, pp.707-731.
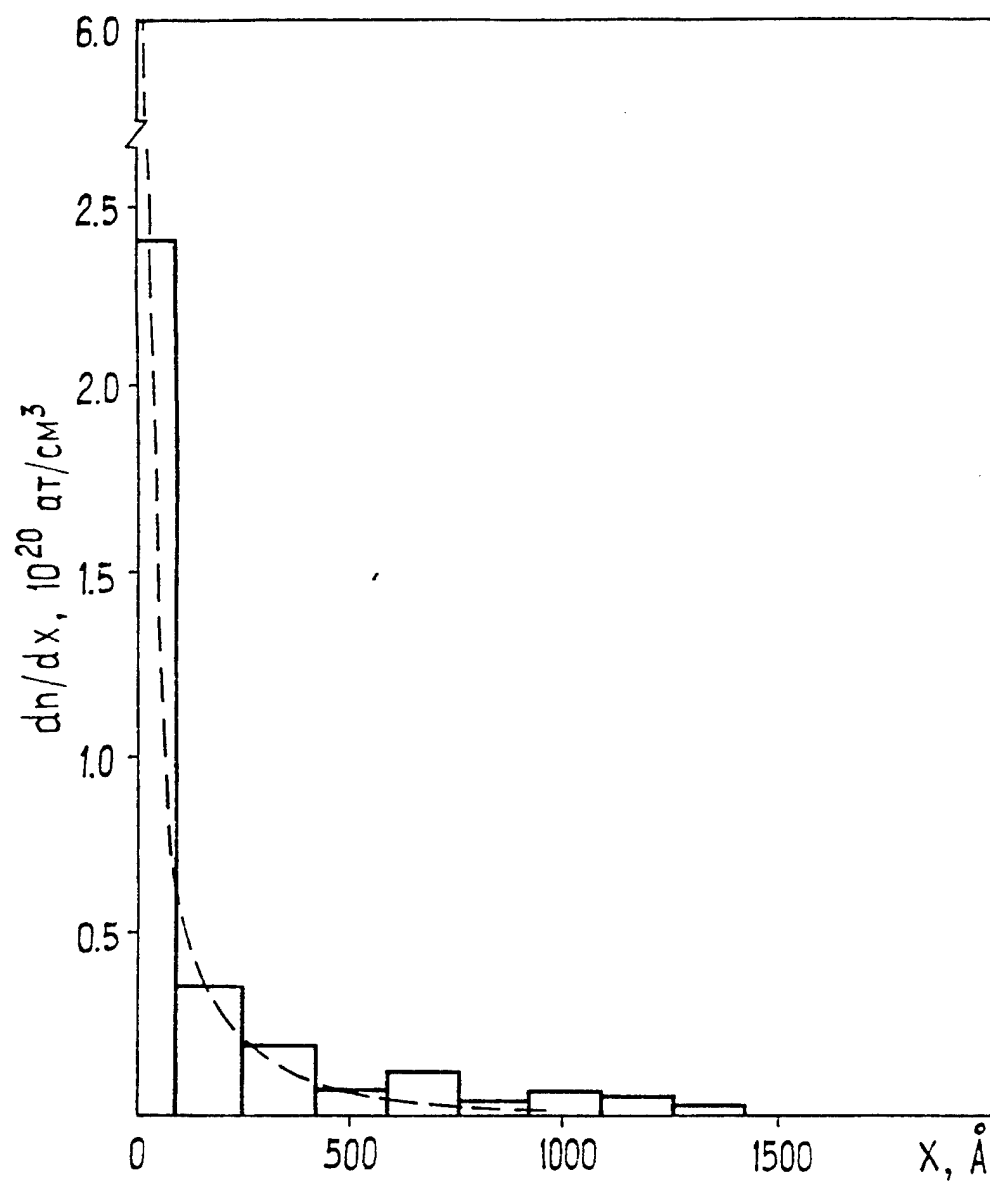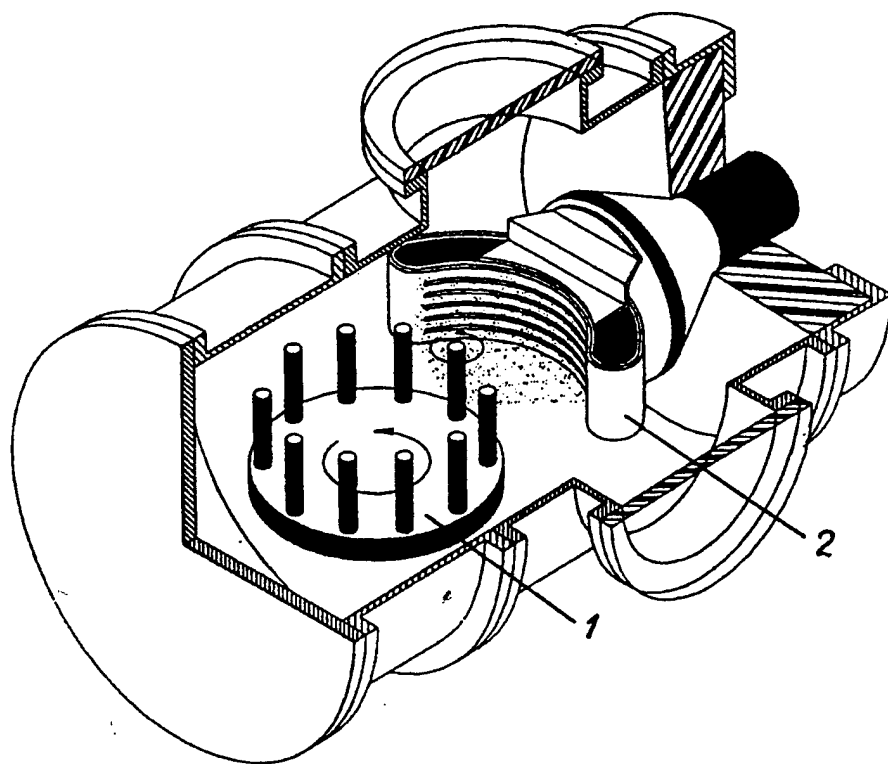
LIST OF FIGURES
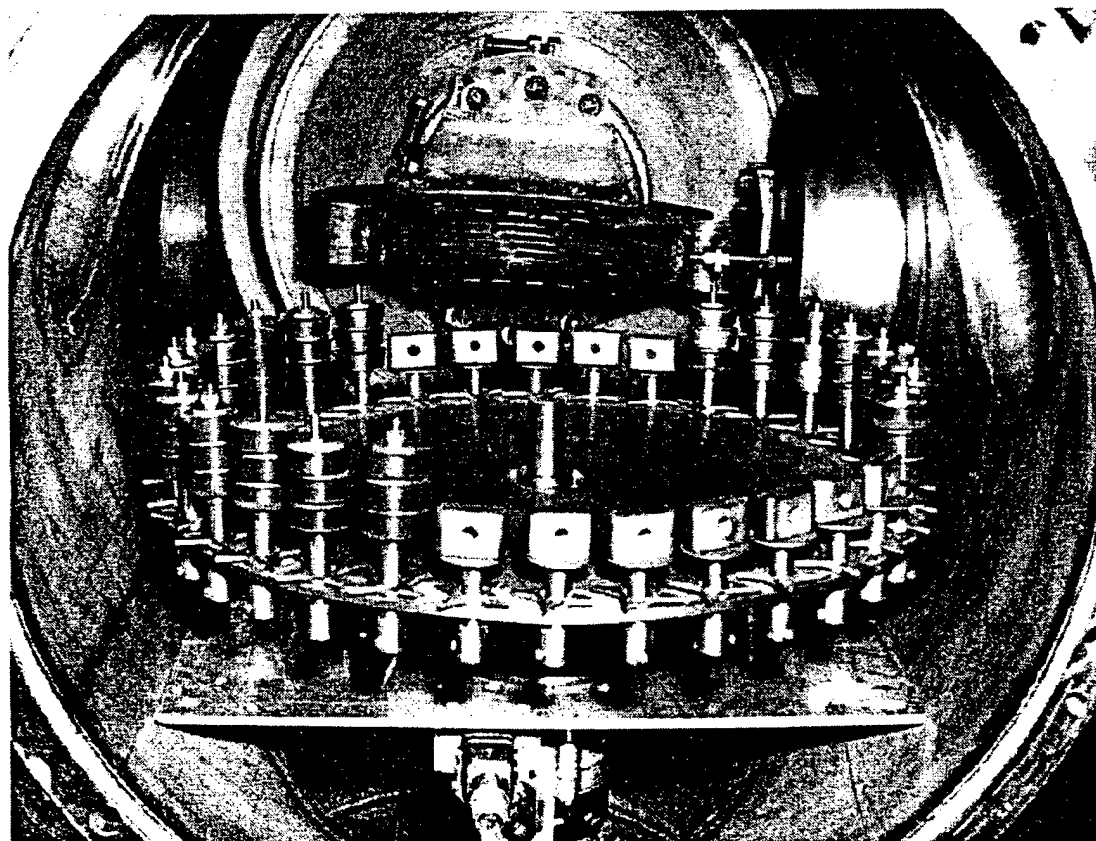
fig.1.

fig.2.

fig.3a.

fig.3b.

USE OF HIGH TEMPERATURE PULSED PLASMA FLUXES
IN MODIFICATION OF METAL MATERIALS [*]

B.A. Kalin[a], V.L. Yakushin[a], B.I. Vasiliev[b], S.S. Tserevitinov[b]

[a] Moscow State Engineering Physics Institute (Technical University):
Kashirskoe sh. 31, Moscow, 115409, Russian Federation
[b] Troitsk Institute for Innovation and Fusion Research:
Troitsk, 142092, Moscow Region, Russian Federation

Abstract
The results of the modification of metal materials treated by high temperature pulsed plasma fluxes (HTPPF) with a specific power of incident flux changing in the $(3...100) \cdot 10^9$ W/m^2 range and a pulse duration lying from 15 to 50 µs have been presented. The microstructure and properties of modified materials (mechanical, tribological, erosion, and other properties) and surface alloying of metals exposed to HTPPF action have been investigated.

Keywords: Pulsed plasma: Metal modification: Microstructure: Properties

1. Introduction

At present, non-traditional technologies based on the use of laser radiation, electron and ion beams, ion-plasma action, and other types of treatment have found a wide utility in modification of the material structure and properties. The interaction of the named types of radiations with the solid results in the formation of the near-surface layers with modified structure and phase composition being non-equilibrium and having, as a rule, high physical, mechanical, and chemical properties: microhardness, wear resistance, strength characteristics, erosion and corrosion resistance, and others.

The investigations [1-3] carried out in recent years have shown that the use of high temperature pulsed plasma fluxes (HTPPF) is promising among non-traditional methods of material treatment. They have a number of advantages in comparison with not only conventional processes of heat and chemical treatment, but also with other types of intensive energy fluxes and continuous ion beams as follow:

- a finished unit with total surface of up to 0.5 m^2 could be treated for a short period of time;
- the surface treated has a sufficiently high microhomogeneity of the composition and structure;
- the possibility of using the working substance (gas) simultaneously both for heating the near-surface layers and for material alloying.

It should be pointed out that the main disadvantages of the HTPPF action are the necessity of evacuation of the samples and units, and that these processes have not been adequately studied in comparison with other methods.

[*] Corresponding author. Fax: (095) 324-3165,
e-mail: kalin@phm.mepi.msk.su

This work presents the results of investigations of the microstructure and properties of metal materials (mechanical, tribological, erosion, and other properties) treated by HTPPF with a specific power of incident flux changing in the $(3...100) \cdot 10^9$ W/m^2 range and a pulse duration lying from 15 to 50 μs.

2. Experimental

The material modification by HTPPF action was performed on the pulse electrodynamic plasma accelerators of MK-200 type and plasma installations of "Desna" type. The main parameters of HTPPF are : 1. The maximum energy of ions $E_i = 2...6$ keV; 2. The incident flux specific power $Q = (3...100) \cdot 10^9$ W/m^2; 3. The pulse duration $\tau = 2...50$ μs ; 4. The number of impact pulses $N = 1...100$.

Different gases were used as working substance, including hydrogen (deuterium), helium, and nitrogen. The operation of the plasma accelerators and the irradiation conditions are presented more fully in [4].

Material treatment by its degree of action can be divided into three types:

1. hard action ($Q \geq 5 \cdot 10^{10}$ W/m^2, $N > 10$);   2. moderate action ($1 \cdot 10^{10} \leq Q < 5 \cdot 10^{10}$ W/m^2, $1 \leq N \leq 10$);   3. weak action ($Q < 1 \cdot 10^{10}$ W/m^2, $1 \leq N < 10$). This division was made on the basis of different degree of heating the irradiated materials and of topography changes of the surface after treatment. The materials exposed to hard action undergo intensive melting and boiling; moderate action results in melting the near-surface layers; weak action heats the near-surface layers, and in some cases when the incident flux specific power is in the vicinity of its upper limit, local melting is observed.

Results of HTPPF action were studied on the stainless steels of 18Cr-10Ni, 16Cr- 15Ni, 13Cr-2Mo types; on the structural steels of 13Cr, St. 3, St. 45 types; on the tool steels of U8, 65G types, and others; on nickel and high nickel alloy of 20Cr-45Ni type; on zirconium-base alloys and other metals.

The samples treated by HTPPF were studied by means of optical, scanning. and transmission electron microscopy. Investigation of microstructure along the depth of layer modified by plasma treatment was performed on cross and angle ($\theta = 7^\circ$) metallographic specimens and with the help of layer-by-layer transmission electron microscopy.

The friction tests were carried out in accordance with the method of reciprocating slip of the investigated samples in combination with a counterbody, made of solid alloy BK-5, under a load of 25 N and a velocity of the sample movement of 3.6 mm/s.

Surface alloying of metals has been investigated. This method is based on the use of significant temperature increasing and melting of the near-surface layers of materials under HTPPF action and thus on the use of the possibility of alloying through liquid phase. Armco-iron and steel of St. 3 type were used as a sample base for alloying. Layers of different alloying elements (Ni, Cr, Ti), used for corrosion resistant steels of complex composition, were coated on the surfaces of substrates prepared by means of electroplating (EP) and vacuum evaporation (VE). The substrates coated with alloying elements on their surfaces were exposed to diffusion annealing in argon at 1273 K for 3 h., then they were irradiated by helium pulsed plasma fluxes ($Q = (1...6) \cdot 10^{10}$ W/m^2, $t = 15...20$ μs). The used values of Q significantly exceeded the values of critical specific powers q_c^1 which are necessary for melting-down the layer of allowing elements and

substrate on which this layer is coated. The values of $q_c{}^1$, according their estimations, lie in the $(6.5...12)\cdot10^9$ W/m^2 range and depend on the kind of alloying element.

3. Results

The investigation of microstructure of face metallographic specimens by optical and scanning microscopy shows [5] that HTPPF action results in the changes of the near-surface layers, in this thin layers with a decreased tendency to grain etching are formed. The quantity and thickness of these layers depend on the parameters of HTPPF action, in particular on the incident flux specific power Q, and on the thermal and physical properties of the material which determine the degree of heating the surface exposed to HTPPF action. It has been found experimentally that with an increase of the incident flux specific power Q and when attaining the conditions of melting the near-surface layers, i.e. at $Q\geq(1...2)\cdot10^{10}$ W/m^2, several layers of different modified structures are formed practically in a leap manner. In the case that $Q<(1...2)\cdot10^{10}$ W/m^2, most of the experiments show that only one layer of changed microstructure is formed. This layer has a decreased tendency to grain etching and is in the form of a white strip, its thickness being equal to 15...20 µm. It has been revealed that when the materials are exposed to relatively weak regimes of HTPPF action, a modified layer of columnar structure is observed. Its axis is oriented to the surface and to the modified layer - initial material interface, and changes along the treated zone.

Investigation of the fine structure of samples under HTPPF action by transmission electron microscopy demonstrates [3, 5, 6] that the cellurar structure is formed as a result of such HTPPF action (Fig. 1). As it is seen from the figure, the cells can be of different forms in the section parallel to the surface of the foil (target), from almost right hexagonal till cylindrical. In some cases they can be formed side by side, and it may be seen that hexagonal cells are within one grain, while cylindrical cells are within another neighbouring grain.
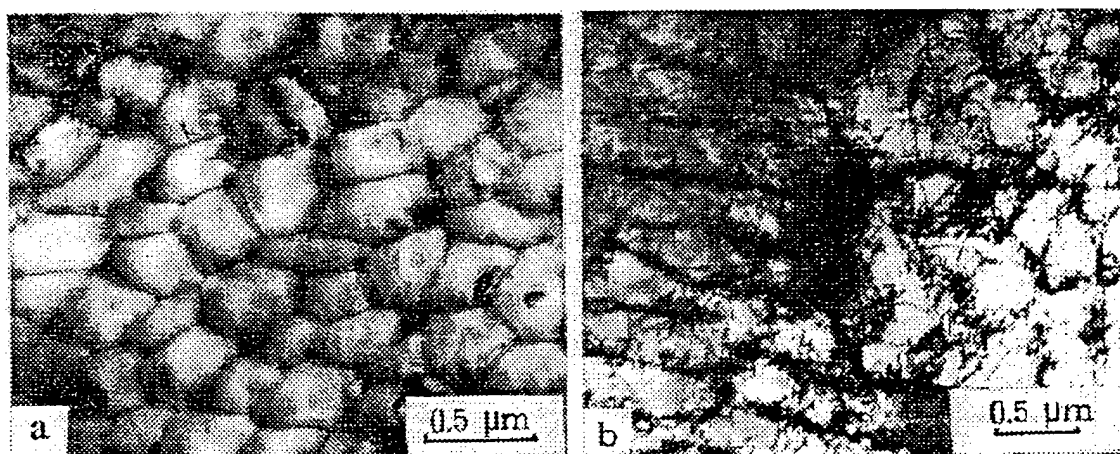

Fig. 1. Electron microscopy images of the cellular microstructure of steel 16Cr-15Ni-3Mo-Nb (a) and purity nickel (b) after HTPPF irradiation :
a, hard impact;   b, weak impact

An analysis of the results obtained by electron microscopy shows that the walls of these cells have, as a rule, a dislocation structure. As for the materials with complex composition are concerned, they are decorated with small bubbles of 20...30 mm in size and with fine-dispersed depositions of particles of refractory primary phases, supposedly of NbC and Nb(C,N) in steel 16Cr-15Ni-3Mo-Nb, and (Nb,Mo)(C,N) in alloy 20Cr-45Ni-4Mo-Nb. In a number of cases when these materials are exposed to hard HTPPF action, an interlayer of a phase, having a different contrast as compared to that of the matrix, is observed along the cell boundaries (Fig. 1,a). Austenitic γ-phase in pseudoamorphous state is formed at the boundaries of the cells in steel 16Cr-15Ni-3Mo-Nb [7].

A statistical analysis of the electron microscopy photographs obtained has demonstrated that characteristic dimensions of the hexagonal cells vary from 0.1 to 1.5 μm and depend on the conditions of irradiation (Q), on the kind of material and the character of its preliminary treatment (Fig. 2). It can be seen from this figure that the dimensions of the cells (l_h) decreases monotonically, something like a $Q^{2/3}$- function, with an increase of Q. As this takes place, the dimensions of the cells for fixed values of Q are smaller in the materials having more quantity of fine-dispersed particles resistant to high temperature action, they are carbides or carbonitrides, and in the materials preliminary exposed to cold strain.

Layer-by-layer electron microscopy of the fine structure of modified layer has shown [5] that mean dimensions of the cells practically do not change with distance from the surface within the experimental error. For instance, the range of mean dimension changes equals to 0.3...0.4 μm for steel 18Cr-10Ni-Ti irradiated under the following conditions: $Q=1.3\cdot10^{10}$ W/m^2 and N=3. The formation of the cell structure did not take place at a depth about 20 μm and more.

The results of electron microscopy have shown that annealing the steel 18Cr-10Ni-Ti at 893 K during 1 h. does not change the fine cell structure. Increasing the annealing temperature up to 1173 K during 1 h. does not result in full disappearance of the given structure. The experimental results obtained demonstrate that this austenitic steel exposed to HTPPF treatment has a high heat resistance.

An analysis of the given results shows that the mechanism of the cell structure formation depends on the parameters of HTPPF action. In particular, the microcrystalline columnar structure is formed as a result of HTPPF action which causes the near-surface layers to melt. This takes place through the mechanism of concentration overcooling owing to the microsegregation of alloying elements and impurities when cellular crystallisation of the melt material occurs. Plastic deformation of high velocity is a result of thermal and mechanical stresses, it is responsible for the formation of the cellular structure with dislocations when materials are exposed to HTPPF action with undercritical parameters ($Q\leq10^{10}$ W/m^2).

Modification of metal materials treated by HTPPF results in the changes of their mechanical properties, including microhardness, strength and tribological characteristics [2,3]. The changes of microhardness on the surface of various materials in their initial state and after HTPPF treatment under hard and moderate regimes are presented in Table 1. As it is seen from the table, the surface of all the materials treated undergoes hardening. But its degree depends on many factors: on irradiation regimes, on the kind of material and its initial

Table 1.
Microhardness of different materials in their initial state and after HTPPF treatment under hard (1, 3) and moderate (2, 4) regimes

N/N	Material	Microhardness, MPa		The extent of hardening, %
		Initial state	After HTPPF treatment	
1	Structural steels:			
	16Cr-15Ni-3Mo-Nb (annealed)	1450 ±150	2000 ±200	40
	16Cr-15Ni-3Mo-Nb (powder)	1700±170	2550±250	50
	18Cr-10Ni-Ti (annealed)	1800±180	2100±200	20
	13Cr-2Mo+ 1.5 mass. % TiO_2	1900±190	2750±250	45
	13Cr-2Mo-Nb	2050±200	4350±350	120
	Steel St. 3 (cold strained)	1590±50	2150...3480[*]	35...120
2	Tool steel:			
	65 G (annealed)	4800±400	9000±800	90
	65 G (quenched and tempered)	7300±700	8500±800	15
3	Nickel and its alloys:			
	Nickel (of high purity)	900±90	1100±100	20
	20Cr-45Ni-4Mo-Nb (annealed)	1750±170	2200±200	25
4	Zirconium and its alloys:			
	Zirconium (of high purity)	340±30	900...1100[*]	160...220
	E-110	760±70	1350±130	80
	E-635	870±80	1300...1700[*]	50...95
5	Vanadium	1160±110	2070±200	80
6	Vanadium alloys	1570...1980	2340...3160[*]	40...90

[*] - microhardness range for different regimes of treatment and for different alloy composition.

treatment. The most considerable extent of hardening more than by 2 times, under equal conditions of treatment, is observed for two-phase materials with allotropic modifications and for monophase low-alloyed steels with small content of carbon.

The extent of the surface hardening under HTPPF action depends heavily on the incident flux specific power Q. As this takes place, the dependence of hardening from Q is not a monotone function. The degree of hardening increases with the incident flux specific power Q of up to $2 \cdot 10^{10}$ W/m^2. Topography investigation has shown that a porous layer of solidified melt is formed on the surface of materials at higher values of Q. Its microhardness is significantly less than that of the layer lying under it. In consequence of this, the surface microhardness for relatively weak regimes of HTPPF treatment (for example, $Q \sim 5 \cdot 10^9$ W/m^2) is more than that for hard regimes.

The revealed decrease of the surface microhardness for hard conditions of irradiation in comparison with moderate ones strikingly shows up when the changes of H_μ through the target depth are studied. In Fig. 3 are shown the changes of microhardness through the target depth for steel 18Cr-10Ni-Ti treated by HTPPF under different conditions.
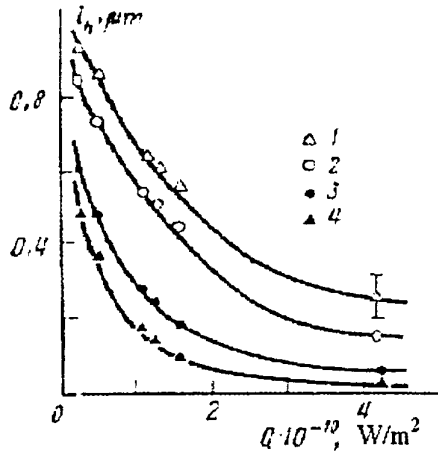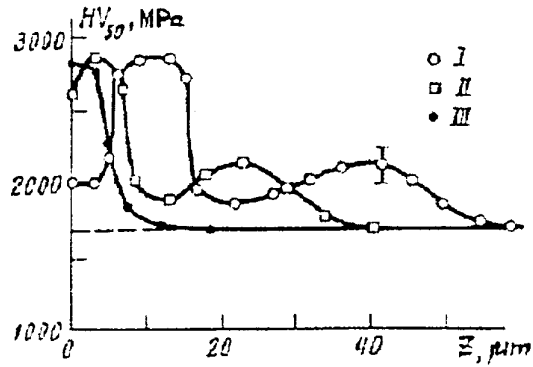
Fig. 2.

Fig. 3.

Fig. 2. Cell mean size to flux specific power dependence : 1, steel 18Cr-10Ni-Ti; 2, purity nickel; 3, steel 16Cr-15Ni-3Mo-Nb; 4, nickel alloy 20Cr-45Ni type

Fig. 3. Microhardness to depth dependence of steel 18Cr-10Ni-Ti irradiated by HTPPF : I, II, III - hard, moderate and weak impact respectively

As it is seen from the figure, the peak of microhardness displaces to the surface with decreasing the extent of hard action. This results in hardening of the surface thin layer by a factor of 1.5.As for hard action is concerned, the thickness of the layer exposed to hardening is significantly more (of up to 60 μm) and another peak (the second peak) H_μ is observed at a considerable distance from the surface.

The first peak is conditioned by the structure and phase changes in the modified layer and determined by its thickness. The second peak was observed at a significantly more depth than the modified layer thickness and was in the area with a high dislocation density. It seems likely that its formation can be explained by the modification of microstructure at a great distance from the surface as a result of deformation caused by structure and thermal stresses. Estimations of the thermal and mechanical stresses, resulted from HTPPF action, demonstrate that this mechanism can occurs.

Tribological characteristics (dry friction coefficient, wear resistance) were studied of modified steel 18Cr-10Ni-Ti [3]. The friction coefficient (f_{fr}) dependence of the friction path for the steel in its initial state (~20% cold strained) and after HTPPF action under hard conditions is shown in Fig. 4. The treatment by HTPPF causes a substantial change of the friction coefficient and the character of its dependence of the friction path (L_{fr}). In particular, the coefficient f_{fr} for this steel in run-in state, treated by HTPPF, is two times smaller than that of the same steel in cold strained state. In this, the process of running-in for the steel in modified state occurs for a short period of time for the friction path of 6...8 m. An analysis of the wear tracks obtained has shown that modified steel has more high wear resistance at less roughness of the surface of the tracks. This testifies that the process of running-in and wear for plasma treated steel happens under more weak conditions.

Plasma treatment results in not only surface hardening but the change of the strength properties of materials [2, 3]. In Fig. 5 are presented the diagrams of tension for standard flat samples of modified materials exposed to tensile tests. These results show that the modification of materials by HTPPF results in increasing the elastic characteristic σ_y and rupture strength σ_r. It must be emphasised that the enhancement of the mechanical properties occurs even for relatively thick samples (t=1.5 mm), when $t/t_m>50$, where t_m is the thickness of modified layer having the cellular structure.

Fig. 4.   Fig. 5.

Fig. 4. Influence of HTPPF impact on dry friction coefficient of steel 18Cr-10Ni

Fig. 5. Load - extension diagrams of nickel in initial condition (1,4) and after HTPPF impact (2,3,5): exposed to irradiation on one side (2) and two sides (3,5)

The quantitative changes of mechanical properties depend on the parameters of HTPPF, the kind of material and its preliminary treatment, in this case hardening peaks for the preliminary annealed samples when their two sides are exposed to plasma treatment. In this case the most significant changes of elastic characteristics were observed, the maximum in the increase of σ_y was up to 4 times for definite conditions of treatment. That the initial plasticity (δ) of the materials studied does not change after their treatment is a characteristic feature.

These results showed that hardening the materials treated by HTPPF could be caused by the joint action of the following factors:

- by the formation of the near-surface layers having the cellular structure;
- by the formation of high dislocation density resulted from the structure and thermal stresses at depths far exceeding the thickness of modified layer;
- by great residual stresses;
- by additional wear hardening of the main (massive) material when the material is exposed to static tensile stresses and is blocked by the modified layer.

The influence of preliminary HTPPF treatment of metal materials on their erosion followed by ion irradiation was studied [2, 3, 6]. The main experimental results on the erosion coefficient changes for materials, preliminary exposed to HTPPF action, owing to radiation blistering and physical sputtering are

presented in Table 2. The table shows that HTPPF action causes a decrease of erosion coefficients because of blistering and physical sputtering by up to 25 and 2...7 times, respectively. The most effect is attained when Q changes in the $(1...2) \cdot 10^{10}$ W/m^2 range and N=1...3. Analogous results were obtained in [8].

Table 2.
Changes of erosion coefficients of materials, preliminary treated by plasma fluxes, owing to radiation blistering (1-4) and physical sputtering (5-7)

№	Material	Ion type	Erosion coefficient, x10^{-2} atom/ion		K = S_o/S_l
			Initial, S_o	After HTPPF, S_l	
1	18Cr-10Ni-Ti	He$^+$, 20 keV	1.2	0.6	2.0
2	16Cr-15Ni-3Mo-Nb	He$^+$, 20 keV	17.5	5.0	3.5
3	13Cr-2Mo	He$^+$, 20 keV	4.2	2.1	2.0
4	Ni	He$^+$, 40 keV	68.5	2.8...13.5*	5.0...25.0
5	18Cr-10Ni-Ti	Ar$^+$, 1 keV	14.0	2...5*	2.8...7.0
6	16Cr-15Ni-3Mo-Nb	Ar$^+$, 1 keV	40.0	8...16*	2.5...5.0
7	Ni	Ar$^+$, 1 keV	135.0	25...60*	2.2...5.0

* - the scatter of the erosion coefficients is due to different conditions of the preliminary plasma treatment.

Formation of uniform cones on the entire ion irradiated surface is a characteristic feature of sputtering for all the modified materials [3,6]. The cones are not of circular shape in their base, as it is usually seen for high dose ion irradiation [9], and they have a section close to hexagonal one with a characteristic cross size less than 1 μm. It can be concluded that the formation of the cellular structure in the near-surface layers is of paramount importance and, may be, the main factor resulting in the formation of such cones and the decrease of HTPPF treated material sputtering.

The main quantitative characteristics of the surface alloyed layers, according to X-ray spectrum microanalysis, are listed in Table 3. [10]. An analysis of the results obtained has shown that the penetration depths of the alloying elements are significantly greater than the thicknesses of the preliminary coated layers and the layers with modified by plasma treatment structure. Auger spectrum analysis has shown that HTPPF action results in mixing the elements in the near-surface layers. This makes itself evident in the appearance of iron on the surface of the irradiated samples , as well as the tracks of carbon, nitrogen, and other elements that present in the substrate. These results point to the possibility of purposeful surface alloying of metals, exposed to HTPPF action, over a depth of up to 20...45 μm and at a concentration of alloying element of up to 20 wt.%. In doing so, there occurs great hardening of the surface and near-surface layers. In particular, the microhardness of steel St. 3 can be increased to 1700...2500 MPa, that depends on the kind of alloying elements and the conditions of alloying. Its microhardness is 2.4...3.4 and 1.5...2.0 times greater, under analogous to alloying conditions, than that of the same steel in its initial state and after plasma modification, respectively.

Table 3.
Main characteristics of surface alloyed layers

N/N	Alloying element	Method of coating	Thickness of coating, mm	Thickness of modified layer, mm	Maximum concentration of alloying element, %	Penetration depth of alloying element, mm
1	Nickel	EP	1.7	4.3	10...12	47.5
2	Nickel	EP	4.3	4.2	18...20	28.0
3	Chromium	VE	0.2	3.2	1...2	18.2
4	Chromium	EP	0.65	4.5	5...6	34.1
5	Titanium	VE	0.2	2.5	2	8.5
6	Titanium	VE	0.3	0.9	0.5...0.7	24.3
7	Vanadium	VE	0.85	2.2	3...4	34.0
8	Vanadium	VE	0.9	2.9	2	28.1

4. Conclusion

An analysis of the results obtained for metal materials exposed to HTPPF action allows to conclude the following - this treatment is a complex method of purposeful changes of the structure and phase state and, owing to this, of different operational properties of materials, including surface hardening, the enhancement of mechanical and tribological characteristics, corrosion and erosion resistance, and others. The determining factor of the changes observed is the formation of the fine cellular structure in the near-surface layers at a depth of 20 μm with dimensions of the cells changing in the range from 0.1 to 1.5 μm depending on the kind of material, its preliminary treatment, and the parameters of plasma fluxes.

An important factor of the material modification by HTPPF is an simultaneous increase of several properties of the units treated: microhardness of the surface and layers of 40...60 μm in depth, tribological characteristics (friction coefficient, wear resistance), mechanical properties (σ_y, $\sigma_{0.2}$, σ_r) on retention of the initial plasticity, corrosion resistance, radiation erosion under ion irradiation, and others. As a summary it should be stated that taking into consideration the advantages of the material modification by HTPPF action, mentioned above, in comparison with other sources of intensive energy fluxes and with ion implantation, as well as the positive results on the improvement of a number of operational characteristics under plasma treatment, high temperature plasma fluxes can be considered as a promising source for developing new kind of non-traditional technology.

References

[1] Interaction of radiation, plasma and electron fluxes with material: Abstracts (Russia), Moscow, (1990) 164p.

[2] B.A. Kalin, V.I. Polsky, V.L. Yakushin et al., Phisika i khimiya obrabotki materialov 2 (1991) 20.

[3] B.A. Kalin, V.L. Yakushin and V.I. Polsky, Izvestiya vysshikh uchebnykh zavedeniy. Phisika 5 (1994) 109.

[4] V.I. Polsky, B.A. Kalin et al., At. Ener. 56 (1984) 83.

[5] B.A. Kalin, V.I. Polsky and V.L. Yakushin, Problemy phisicheskogo materialovedeniya, Moscow, MEPhI, (1991) 15.

[6] B.A. Kalin, V.I. Polsky, V.L. Yakushin et al., J. Nucl. Mater. 220-222 (1995) 934.

[7] V.F. Zelenskiy et al., Report 89-64, Kharkov, KhPhTI (Ukraine), (1989) 12p.

[8] G.V. Gordeeva, M.I. Guseva, E.S. Ionova et al., Poverkhnost. Phisika , khimiya, mekhanika 8 (1989) 154.

[9] G.K. Wehner, Whiskers, Cones and Pyramids Created in Sputtering by Ion Bombardment, NASA, CR-159549 (1979) 45p.

[10] V.L. Yakushin, B.A. Kalin, V.I. Polsky, Izvestiya RAN. Metally 6 (1994) 74.

Use of Low-Energy, High-Current Electron Beams for Surface Treatment of Materials

D.I. Proskurovsky, V.P. Rotshtein, and G.E. Ozur

Institute of High Current Electronics, Siberian Division, Russian Academy of Sciences. 634055 Tomsk, Russia

Abstract

The article describes the characteristics of original sources of low-energy (10–45 keV), high-current (up to 50 kA) electron beams of microsecond duration, designed for surface thermal treatment of materials.

Under the action of this type of beam, graded structures are formed that may impart improved physicochemical properties and strength to the surface layers. This permits the use of these beams for improving the strength and electrochemical properties of pieces and tools and for increasing the electric strength of vacuum insulation. Some technological operations, such as deposition and removal of coatings and surface alloying can be realized in the intense evaporation mode.

Key words: pulsed electron beams; surface treatment of materials.

1 Introduction

Under the action of concentrated energy flows (intense pulsed laser, electron, and ion beams and pulsed plasma flows) on a material, there occur superfast heating, melting, evaporation, and superfast solidification of the material and dynamic temperature and stress fields are formed. These processes produce new structure-phase states in the surface layers that are able to provide improved physicochemical and strength properties of the material, unattainable with ordinary surface treatment techniques.

In recent years, low-energy high-current electron beams (LEHCEBs) have extensively be used as concentrated energy flows. Below we describe the principles of generation of LEHCEBs, the characteristics of the LEHCEB sources, the main regularities of the formation

1

of the beam-affected zone. and some examples of using these beams for surface treatment of metallic materials and articles.

2   LEHCEB sources

Conventionally. LEHCEBs. like high-energy beams. have been produced using direct-action vacuum diodes with explosive-emission cathodes [1–3]. The beam duration in these diodes is generally $\sim 10^{-7}$ s. The electron beams generated in these diodes are characterized by the presence of substantial local nonuniformities in the current density distribution [4]. LEHCEBs of duration $\sim 10^{-6}$ s allow one to improve substantially the uniformity of the beam-cross-section energy density distribution and reduce abruptly the mechanical stresses generated in the material on irradiation. The beam duration can be increased and the beam homogeneity can be improved by using plasma-filled diodes [5-7].

The principle of generation of LEHCEBs in plasma-filled systems is illustrated in Fig. 1. The explosive-emission cathode is made of graphite. The anode is made of stainless steel and has a hole in its center to pass the beam. Graphite-cathode spark plasma sources are placed evenly in a circle behind the anode. The electron beam is transported in the anode plasma to the collector. To prevent the beam from pinching, an external magnetic field is used.

The electron source operates as follow: As the magnetic field reaches its maximum, the spark sources are switched on and the anode plasma fills the acceleration gap and the beam drift space. After 2–3 μs an accelerating voltage produced by a voltage pulse generator is applied to the cathode. The anode plasma, owing to its good conductivity, acquires the potential of the anode, and the effective gap spacing in the diode shortens abruptly. This results in the initiation of explosive electron emission at the cathode. The voltage applied to the diode is localized across the double layer between the cathode and anode plasmas where the electron beam is generated. Since the acceleration gap spacing is a few centimeters, the beam duration is a few microseconds.

The experiments have shown that up to 90% of the diode current passes through the anode hole. The beam transportation in plasma prevents the beam from degeneration into an tubular beam and from filamentation (which is typical of vacuum diodes) and permits the distance from the anode to the surface under treatment to be increased to 15–20 cm.

Table 1 gives the characteristics of the electron sources we have developed. The compar-

2

atively low accelerating voltage ensure the X-ray safety of the technology and the simplicity, reliability, and economy of the electron source. The sources have been in use from two to six years.

3 Formation of the beam-affected zone

The principal factors that determine the state and properties of the beam-affected zone are the nonstationary temperature fields that appear in the surface layers as a result of the absorption of the beam energy and the stress fields caused by the nonuniform heating of the material.

Figures 2 and 3 present the results of calculations for iron irradiated in the characteristic melting and evaporation modes. From the calculations it follows that the velocity of the crystallization front sharply increases near the very surface reaching 8 m/s in the melting mode. The cooling rate reaches its maximum ($\sim 3 \times 10^9$ K/s) at the surface immediately after the passage of the crystallization front. The thickness of the heat-affected zone (HAZ) where the maximum temperature exceeds the recrystallization temperature increases from ~ 7 to ~ 20 μm, in going from the melting to evaporation mode.

An analysis of the data available in the literature [8] suggests that in iron irradiated by an LEHCEB in the initial melting mode a bipolar stress wave is formed whose amplitude is far below the dynamic yield limit of the material, $\sigma_{0.2}^{dyn}$. In addition, quasi-static compressive stresses act in the HAZ, whose magnitude, according to estimates [9], may be over $\sigma_{0.2}^{dyn}$. After the termination of the pulse in the near-surface layer residual tensile stresses are formed whose magnitude is 40–80 MPa, which is about an order of magnitude lower than that of the compressive stresses acting on irradiation. In the intense evaporation mode, the stress wave amplitude, according to estimates [8], is close to the yield limit of the material and it should be taken into account in analyzing the conditions under which the HAZ is formed.

Investigations of the structure and properties of metals and alloys irradiated by LEHCEBs have made it possible to reveal the regularities as follows:

1. The action of an LEHCEB results in the formation of an extended ($\sim 10^{-2}$ cm) graded structure showing a nonmonotonic depth variation of the stress-strain state and the degree of hardening (Fig. 4) [10]. This effect is related to the fragmentation of martensite and the formation of the particles of cementite under the action of low-amplitude bipolar stress

3

waves.

2. The melt-quenched layers ($\leq 10^{-3}$ cm) show reduced etchability in acids which is related to the fact that the structure formed is more homogeneous than the initial one. The most pronounced structure-phase changes occur in the near-surface layers (Fig. 5) [10], which correlates with the fact that the cooling rate and the velocity of motion of the crystallization front reach their maxima at the surface. In these layers secondary phases (carbides and intermetallides) are partially or completely dissolved.

4 Use of LEHCEBs for surface treatment

4.1 Improvement of tribotechnical characteristics

Tests with a friction pair consisting of a rotor (steel, HRC 55) and a plate (ball bearing steel, HRC 60) in the presence of lubricant have shown that on irradiation the wear rate of the plates decreased by a factor of 1.5 and the friction moment decreased by a factor of 1.7 [8]. Under the conditions of dry friction, the wear rate of irradiated plates almost halved. With that, the depth of the friction trace was $\sim$25 μm, which corresponds to the position of the first maximum of microhardness (Fig. 4). This points to the fact that there is a correlation between wear resistance and microhardness.

4.2 Increasing the life of steel tools

For optimal modes of hardening of tool steels the thickness of the molten layer is not over $\sim$1 μm. Therefore, the irradiation might be the finishing technological operation. Tests have demonstrated that the irradiation allows a 2–3-fold increase in the life of drills, cutters, punches, mandrels, and other tools.

4.3 Treatment of hard-alloy cutting tools

It has been established [11] that the irradiation of cutting plates made of hard alloys of type BK8 (WC–8%Co) and type T5K10 (WC–5%TiC–10%Co) increases the tool life by a factor of two to five (Fig. 6). The increase in tool life correlates with the increase (by 15–20%) in microhardness at the surface, which is related to the additional dissolution of the carbides in the cobalt binder.

4.4 Treatment of titanium alloys

The irradiation of titanium alloys in the initial melting mode not only makes the surface much smoother but also cleans it from oxygen and carbon impurities and improves the uniformity of the element distribution in thickness in the surface layer. Subsequent annealing recovers the phase composition, increases the microhardness, and raises the fatigue strength of the parts by about an order of magnitude. The latter, as is evidenced by fractography. is due to the fact that the surface destruction mechanism changes to the subsurface one [12].

4.5 Smoothing of heat-resistant protective coatings

Heat-resistant protective coatings based on Ni (e.g., Ni–Cr–Al–Y) have a rather rough surface. Experiments have shown [13] that melting of a thin surface layer of such a coating allows an increase in heat resistance (by 25% at 1050 °C) due to the sharp reduction of the surface roughness.

4.6 Removal of heat-resistant protective coatings

The existing technology for removing worked-out coatings is characterized by a high laboriousness and harmful working conditions. To eliminate these disadvantages, LEHCEBs can be used. Experiments have shown that a beam of energy density ≥ 20 J/cm^2 can efficiently (1–2 μm per pulse) remove this type of coating, changing the substrate structure only slightly [13].

4.7 Production of highly concentrated surface alloys

With beam energy densities of over 10 J/cm^2, there is an opportunity of the production of surface alloys by pulsed deposition of coatings and remelting of the surface layer. The results of this "micrometallurgical" process are presented in Fig. 7.

Similar results have been obtained for the systems Al–Fe, Ti–Fe, W–Fe, Ti–Cu, Al–Ti, and the like. The thickness of the layers produced is an order of magnitude greater than that attained by ion implantation.

4.8 Enhancement of the corrosion resistance of stainless steel

Cyclic treatment of type 12X18H10T steel (steel 302 being US analog) in the mode of weak evaporation of the surface layer efficiently cleans the surface from undesirable impurities and results in the formation of a fast-quenched structure with a smoothed microrelief. The increased degree of chemical homogeneity of the surface leads to a shift of the stationary potential to the positive region and to a significant decrease in dissolving current [14].

4.9 Enhancement of the electric strength of vacuum insulation

It has been established [15] that the irradiation of electrodes efficiently smoothes the working surface due to its melting and cleans the near-surface layers from impurities and dissolved gases. This treatment followed by conditioning of the vacuum gap with low-current pulsed discharges reduces substantially the prebreakdown currents and enhances the electric strength of the vacuum insulation (Fig. 8). The best effect has been achieved for stainless-steel electrodes.

5 Summary

The principle of operation and characteristics of the sources of wide LEHCEBs based on an electron gun with an explosive-emission cathode and a plasma anode are described. It has been shown that the use of these sources makes it possible to develop new efficient techniques for surface treatment of materials.

Acknowledgments

References

1 A.C. Greenwald, A.R. Kirkpatrick, R.G. Little, and J.A. Minnucci, J. Applied Physics, 50 (1979) 783.

2 B.A. Koval', G.A. Mesyats, G.E. Ozur, D.I. Proskurovsky, and E.B. Yankelevich, Pisma v Zh. Tekhn. Fiz., 7 (1981) 1227.

3 G. Leggieri, A. Luches, V. Nassisi, A. Perrone, and M.R. Perrone, Vacuum, 32 (1982) 9.

4 G.A. Mesyats and D.I. Proskurovsky, Pulsed Electrical Discharge in Vacuum, Springer-Verlag, Berlin, 1989.

5 G.E. Ozur and D.I. Proskurovsky, Pisma v Zh. Tekhn. Fiz., 14 (1988) 413.

6 G.E. Ozur and D.I. Proskurovsky, Proc. XIVth Intern. Symp. on Discharges and Electrical Insulation in Vacuum, Santa Fe, USA, September, 1990, p. 665.

7 D.S. Nazarov, G.E. Ozur, and D.I. Proskurovsky, Izv. Vyssh. Uchebn. Zaved. Fizika, No. 3 (1994) 100.

8 V.P. Rotshtein, Modification of structure and properties of metallic materials by intensive pulsed electron beams, D. Sc. thesis, Institute of High-Current Electronics, Tomsk, 1995.

9 E.F. Dudarev, G.P. Pochivalova, D.I. Proskurovsky, V.P. Rotshtein, and A.B. Markov, Izv. Vyssh. Uchebn. Zaved. Fizika, No. 3 (1996) 126.

10 Yu.F. Ivanov, V.I. Itin, S.V. Lykov, A.B. Markov, G.A. Mesyats, G.E. Ozur, D.I. Proskurovsky, V.P. Rotshtein, and A.A. Tukhfatullin, Metally, No. 3 (1993) 130.

11 I.M. Goncharenko, D.V. Lychagin, D.S. Nazarov, G.E. Ozur, P.V. Orlov, K.N. Poleshchenko, D.I. Proskurovsky, V.P. Rotshtein, and A.A. Tukhfatullin, Proc. 4th Intern. Conf. "Computer-aided Design of Advanced Materials and Technologies", Tomsk, 1995, p. 120.

12 N.A. Nochovnaya, V.A. Shulov, D.I. Proskurovsky, V.P. Rotshtein, D.S. Nazarov, and G.A. Ozur, submitted for publication in Proc. 11th Intern. Conf. on High Power Perticle Beams, Prague, June 1996.

13 Yu.D. Yagodkin, K.M. Pastukhov, S.I. Kuznetsov, N.F. Ivanova, and E.Yu. Aristova, Fizika i Himija Obrabotki Materialov, No. 5 (1995) 111.

14 I.M. Goncharenko, V.I. Itin, S.V. Isichenko, S.V. Lykov, A.B. Markov, O.I. Nalesnik, G.E. Ozur, D.I. Proskurovsky, and V.P. Rotshtein, Zashchita Metallov, 29 (1993) 932.

15 A.V. Batrakov, A.B. Markov, G.E. Ozur, D.I. Proskurovsky, V.P. Rotshtein, IEEE Trans. on Dielectrics and Electr. Insul., 2 (1995) 237.

Table 1. Parameters of LEHCEB sources.

Figure 1. Production of low-energy intense electron beams in a plasma-filled diode: *1* – explosive-emission cathode; *2* – anode unit with spark plasma sources; *3* – collector; *4* – vacuum chamber; *5* – solenoid; *6* –cathode plasma; *7* –anode plasma.

Figure 2. Time dependence of the surface temperature for iron irradiated in the mode of melting ($\tau = 0.8\mu s$, E_s =3.2 J/cm^2) (*1*) and evaporation ($\tau = 2.5\mu s$, E_s =25 J/cm^2) (*2*).

Figure 3. Variation of the position of the melt-solid boundary for iron irradiated in the melting mode ($\tau = 0.8\mu s$, E_s =3.2 J/cm^2) (*1*); the same (*2*) and the variation of the surface coordinate (*3*) for iron irradiated in the evaporation mode ($\tau = 2.5\mu s$, E_s =25 J/cm^2).

Figure 4. In-depth distribution of microhardness for a pre-quenched steel 45 (0.45% C) specimen irradiated by an LEHCEB with $\tau = 0.7$ μs, $E_s = 2.5$ J/cm^2; number of pulses $N = 1$ (*1*), $N = 300$ (*2*).

Figure 5. Structure of the heat-affected zone in pre-quenched steel 45 treated with an LEHCEB ($\tau = 0.7$ μs, $E_s = 2.5$ J/cm^2).

Figure 6. Width of wear area on the rear surface of a cutter made of T5K10 alloy as a function of cutting length before (*1*) and after (*2-4*) irradiation with different values of E_s. The material under treatment was a steel 40X (0.4% C, 1% Cr). Conditions of cutting: $S = 0.14$ mm/rev, $d = 1.5$ mm; $V = 300$ m/min.

Figure 7. Concentration profiles of the elements in the surface Cu–Fe alloy formed with the use of an LEHCEB on a Fe substrate.

Figure 8. Conditioning curves (250 kV, 40 ns) for vacuum gaps with stainless-steel unirradiated (*1*) and preliminary LEHCEB-irradiated (*2*) electrodes.

Table 1:

Source parameters	Type 1	Type 2	Type 3
Electron energy, keV	10–30	10–30	20–45
Beam current, kA	up to 2	up to 15	up to 50
Pulse duration τ, μs	1.5–1.2	1–5	2–4
Beam energy density E_s, J/cm^2	0.5–6	1–10	2–40
Beam cross-section area, cm^2	up to 3	up to 30	up to 50
Pulse repetition rate, Hz	up to 0.2	up to 0.2	up to 0.2
Operating vacuum, Torr	10^{-4}–10^{-5}	10^{-4}–10^{-5}	10^{-4}–10^{-5}
Input power, kW	1	3	5

Fig. 1

Fig. 2

Fig. 3

Fig. 5

Fig. 4

E_{br}, MV/cm

N, breakdowns

a-C:H Films Deposited in the Plasma of Barrier and Surface Discharges at Atmospheric Pressure

S.P. Bugaev, A.D. Korotaev*, K.V. Oskomov, and N.S. Sochugov

Institute of High Current Electronics

Siberian Division of Russian Academy of Sciences

4 Akademichesky Ave., 634055 Tomsk, Russia

*Siberian Physical-technical Institute

1 Revolution Sq., 634050 Tomsk, Russia

The aim of the work is the synthesis of the diamond-like coatings in a barrier and surface discharges at the atmospheric pressure and the investigation of their properties. The best characteristics had the coatings obtained from methane (the ratio of hydrogen atoms to carbon ones is H/C=1.04, the share of the diamond-like and graphite-like C-C bonds sp^3:sp^2 = 100%: 0%) and from the acetylene and hydrogen mixture (1:19) (H/C = 0.73, sp^3:sp^2 = 68%: 32%) in barrier discharge, as well as the from methane in surface discharge (H/C=0.98, sp^3:sp^2 = 86%: 14%). By their chemical and phase composition these coatings are close to the diamond-like hydrigenated (a-C:H) films obtained by traditional methods of plasma assisted chemical vapor deposition at low pressure (<10 Torr). At the same time proposed methods for fast deposition of a-C:H films make this process less expensive compared to the conventional techniques, which gives promise that the field of application of these films can be widen substantially.

INTRODUCTION.

A rather rich variety of techniques for vacuum plasma deposition of diamond-like amorphous hydrogenated carbon (a-C:H) films are now available. However, these techniques are limited in use because of their low productivity and high cost. In view of this, the attempts to produce a-C:H films with the use of electric discharges at atmospheric pressure, in particular, with the use of barrier [1] and surface discharges, seem to be worth-while. Besides, the simplicity of these types of discharges those can be realized without complicated vacuum equipment, they are attractive because they allow fast deposition of a-C:H films on large-area low-melting-point substrates. However, no data are now available on the structure and properties of carbon coatings deposited with the use of the plasma of such atmospheric-pressure discharges . This was just the goal of the work under discussion to obtain this information.

EXPERIMENTAL.

Barrier-discharge carbon film deposition was performed in a reaction chamber (Fig. 1) that consisted of two plane-parallel electrodes (*1* and *2*), with a dielectric barrier (a 1.5-mm thick glass plate) (*3*) placed between them, and a vacuum-tight gas gap (*4*) of thickness about 1 mm through which the reactive gas (CH_4, C_2H_2, $C_2H_2 + H_2$, $C_2H_2 + Ar$) was pumped with the use of an input-output system (*5*). The pressure in the chamber was atmospheric. When unipolar voltage pulses of duration 100–200 μs and amplitude of 17 kV were applied to the high-voltage electrode with a pulse repetition rate of 1 kHz, a barrier discharge was initiated in the gas gap. With that, the reactive gas whose flow rate was 3–4 l/h was dissociated and carbon films from the radicals formed were deposited on the dielectric barrier and on the grounded electrode. The reaction chamber designed for the deposition of a-C:H films in a surface discharge is shown schematically in Fig. 2. The discharge was initiated with the use of the same high-voltage pulse generator operating in the bipolar-pulse mode. Films were deposited on glass and mylar substrates. Methane was used as a reactive gas.

A quantitative analysis of the chemical and phase composition of the coatings produced was carried out with the use of absorption IR spectroscopy by a method similar to that described in [2]. To examine the structure of the coatings, transmission electron microscopy and electron diffraction analysis were used.

RESULTS AND DISCUSSION.

With methane used as a reactive gas. the growth rate of the film in barrier discharge was about 2 μm/h. The coating density measured by the immersion method after detachment of the coating from the substrate was 1.3 g/cm^3. Transmission electron microscopy examination of the films has shown that they are amorphous in structure. The diffraction pattern taken from a section of such a coating consists of two diffuse rings whose centers correspond to interplane distances of 2.08 Å and 1.18 Å. It has been shown theoretically and experimentally [3] that such a pattern is typical of diamond-like films where the regions of coherent electron scattering are no more than 5–10 Å in size. An examination of the IR spectrogram (Fig. 3) shows that this coating contains a significant content of hydrogen (H/C = 1.04), with diamond-like C–C bounds consisting 100%. The microhardness of the film is about 2000 kg/mm^2 , that confirms diamond-like nature of this a-C:H coating.

The dependence of the absorption coefficient for a coating produced from acetylene on the wave number (Fig. 4) differs from the corresponding dependence for the coating produced from methane (see Fig. 3) by the presence of graphite with the absorption bands near 3020 and 3070 cm^{-1}) and carbine (3300 cm^{-1}) phases (H/C = 0.66, $sp^3 : sp^2 : sp$ = 34% : 55% : 11%). Even high dilution of acetylene with argon (7% C_2H_2 + 93% Ar) caused no favorable change in the film structure (H/C = 1.30, $sp^3 : sp^2 : sp$ = 39% : 54% : 7%) (see Fig. 4). Dilution of acetylene with hydrogen also did not result in any change until 5% C_2H_2 + 95% H_2. Figure 5 gives the absorption coefficient as a function of the wave number for a coating produced from this mixture in a barrier discharge. As distinct from the two above specimens, the carbine phase was not indicated and the content of graphite-like carbon decreased substantially (H/C = 0.73, $sp^3 : sp^2 : sp$ = 68% : 42% : 0%). On further dilution of acetylene with hydrogen (2.5% C_2H_2 – 97.5% H_2), hand in hand with an increase in the fraction of diamond-like bonds ($sp^3 : sp^2 : sp$ = 89% : 11% : 0%) is an increase in the atomic ratio H/C in the film to 1.45 (see Fig. 5), and thus the coating becomes polymer-like.

At the same time, it has appeared that the a-C:H films grown in a barrier discharge have a significant quantity of defects which is related to the physical nature of the barrier discharge consisting of a number of microdischarges. Therefore, it was of interest to find a type of discharge free from the disadvantages inherent in the barrier discharge. In our opinion, the surface discharge over a dielectric holds promise. Having the same, attractive from the viewpoint of technological use, properties as the barrier discharge. the surface discharge also has some advantages over the latter, namely:

- the more efficient spatial distribution of the energy delivered to the discharge;
- the absence of microdischarges and, hence, an almost total absence of microdefects in the coating;
- the more efficient transport of film-forming particles toward the substrate, and
- the wider selection of means for controling the discharge parameters and, hence, the properties of the coating produced.

The growth rate of the films deposited from methane in surface discharge was 60–120 μm/h and their density was 1.2–1.3 g/cm^3. Examination of a typical IR spectrogram (Fig. 6) shows that H/C = 0.98 and the percentage of the diamond bonds is 86%. The microhardness of the given coating measured at a load of 20 g is 2000 kg/mm^2. Owing to the small content of defects and the amorphous nature of the film produced in a surface discharge, this film shows high transmittance in the IR (up to 98%) and visible ranges. The adhesion of the a-C:H film to mylar and other polymers was satisfactory.

The profitableness of the use of diamond-like films is determined to a large measure by the cost, productivity, and consumed power of the technological equipment.

To estimate the power demand for the production of a-C:H films, we can use the quantity P that characterizes the power demand (kW·h) for the production of a a-C:H film of thickness 1 μm over an area of 1 m^2. Calculations have shown that for the films deposited in a surface discharge we have $P = 0.5$–1 kW·h/(m^2·μm). For the films deposited in the plasma of a low-pressure microwave discharge [4], $P = 0.5$–1 kW·h/(m^2·μm) was obtained taking into account only the microwave power. However, with the efficiency of the microwave generator and the power consumed by the vacuum pumps taken into account, the value of P will be increased 3–5 times. The efficiency of the system with a surface discharge may reach 70–80%, that is the total consumed power will be severalfold lower than for the microwave system.

5

CONCLUSIONS.

Thus, the coatings produced from methane (H/C=1.04, sp^3 =100%)and from an acetylene–hydrogen mixture (1 : 19) in barrier discharge (H/C=0.73, sp3: sp2= 68%o: 32%o) as well as from the methane in surface discharge (H/C=0.98, sp3:sp2 = 86%o:14%o) had the best characteristics. These coatings are similar in chemical and phase composition to amorphous diamond-like hydrogenized (a – C: H) films (H/C < 1, sp^3 : sp^2 > 2) produced at low pressure by the conventional plasma-assisted chemical gas-phase deposition techniques. Investigation of the structure of the coatings produced with the use of electron diffraction has confirmed this observation.

The equipment for a-C:H film deposition in the barrier and surface discharges is much simpler and cheaper than the vacuum systems with various types of plasma generator conventionally used for this purpose. The specific nature of these discharges makes it possible to deposit a-C:H films on plane dielectric substrates of any area, roll polymer materials (mylar, polyethylene) included. Thus, the proposed methods for fast deposition of a-C:H films make the process of film production less expensive compared to the conventional techniques, which gives promise that the field of application of these films can be widen substantially.

REFERENCES.

1. R. Schwarz, I. Salge // ISPC-11, 1993, p. 1071.

2. J.Zou, K. Schmidt// J. Appl. Phys. 1989. V. 67. N1. p.484.

3. E. Tchaikovsky// Arch. Nauki o Materialach. 1986. V.7. N.2. p.187.

4. R. Hytry, W. Moller // Appl. Phys. Lett. 1994. V.64. N. 25. p.3401.

FIGURE CAPTIONS.

Fig. 1. Schematic of the reaction chamber for a film deposition in barrier discharge: 1,2- electrodes, 3- dielectric barrier (substrate), 4- gas gap, 5- gas inlet and outlet.
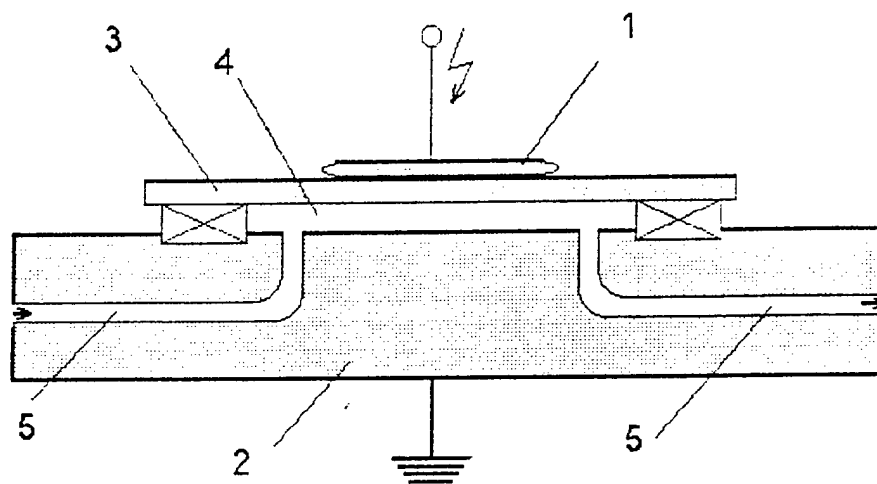
Fig. 2. Schematic of the reaction chamber for a film deposition in surface discharge: 1,2- electrodes, 3- dielectric plate, 4- gas inlet and outlet.

Fig. 3. IR absorption from CH stretch vibration for the coating deposited in barrier discharge from CH_4 and its decomposition into subbands.

Fig. 4. IR absorption from CH stretch vibration for the coatings deposited in barrier discharge from: 1- C_2H_2 , 2- 7% C_2H_2 + 93% Ar.

Fig. 5. IR absorption from CH stretch vibration for the coatings deposited in barrier discharge from: 1- 5% C_2H_2 + 95% H_2 , 2- 2.5% C_2H_2 + 97.5 % H_2 .

Fig. 6. IR absorption from CH stretch vibration for the coating deposited from CH_4 in surface discharge and its decomposition into subbands.
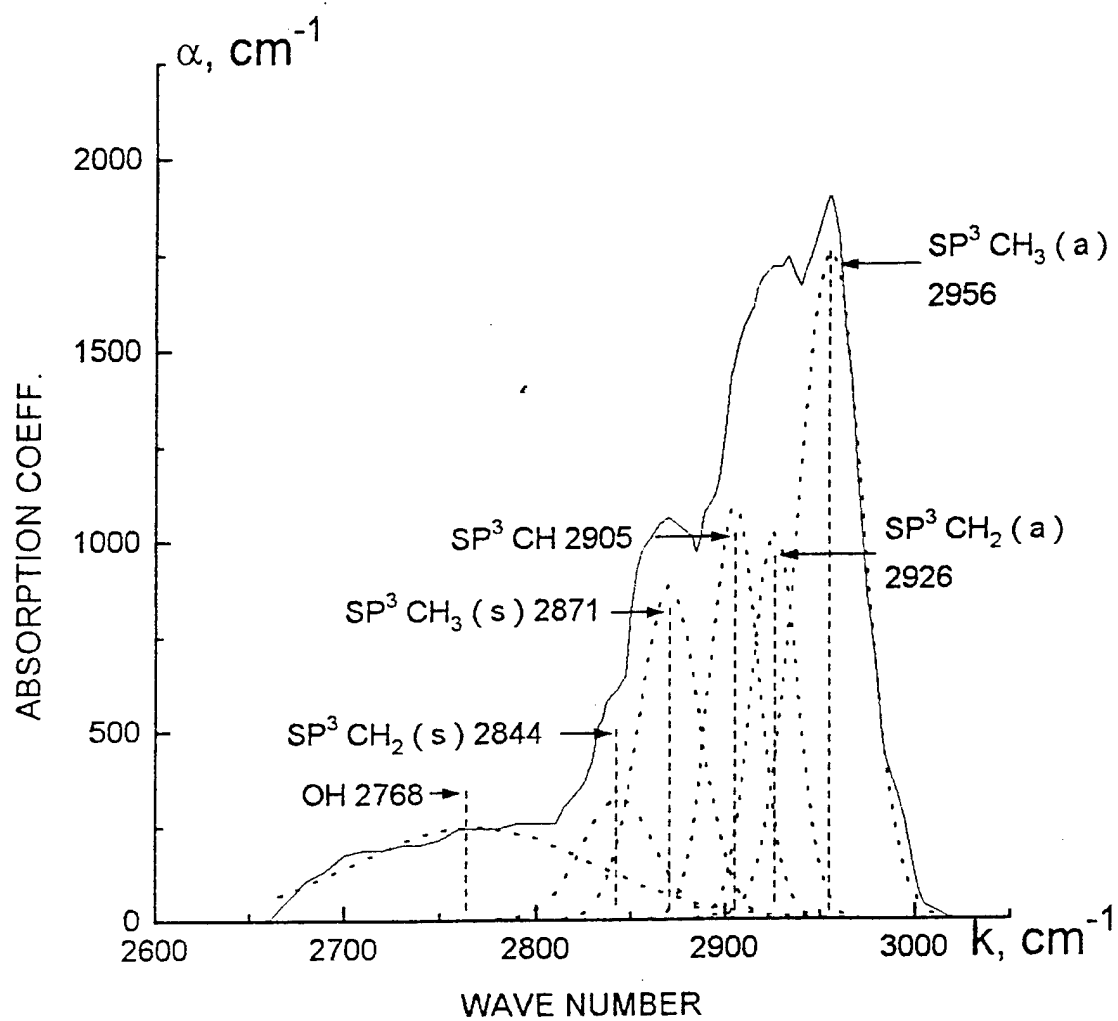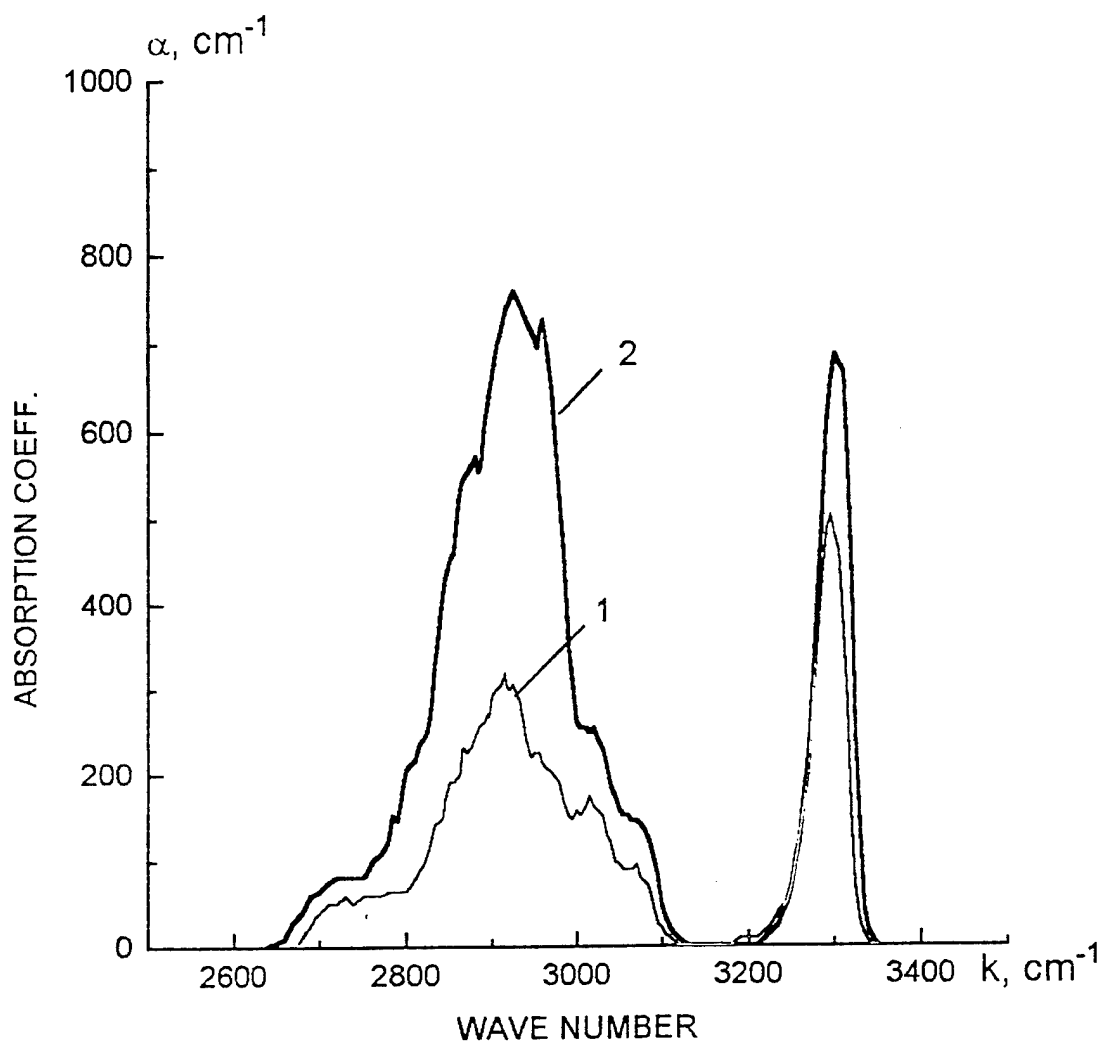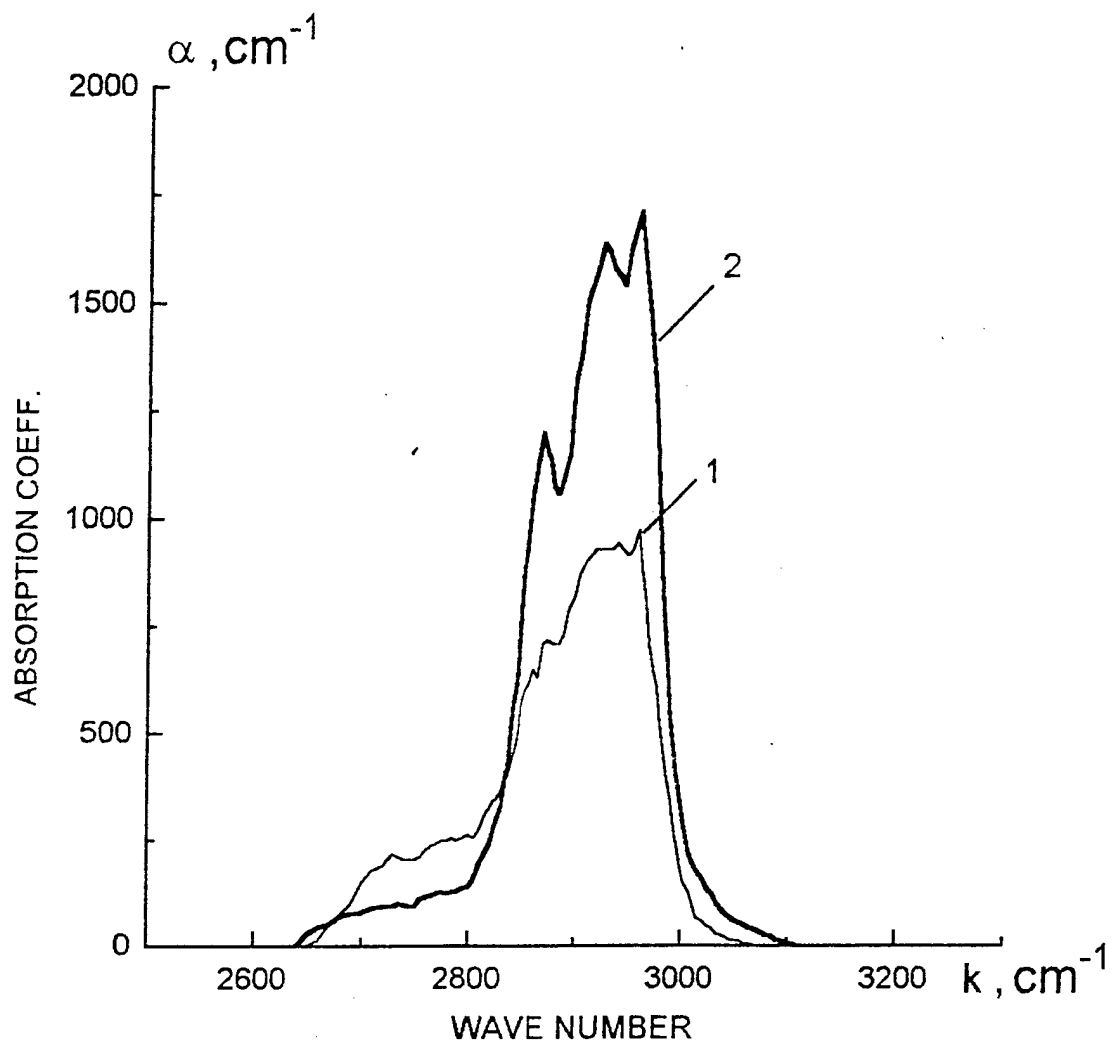
Fig 3

Fig. 14

Fig. 5

1600 α , cm^{-1}

ABSORPTION COEFF.

1400

1200

1000

800

600

400

200

0

SP^{3}CH$_3$ (a)
2961

SP^3 CH 2924

SP^3 CH$_3$ (s)
2880

SP^{2}CH 3009

SP^2 CH$_2$ 3045

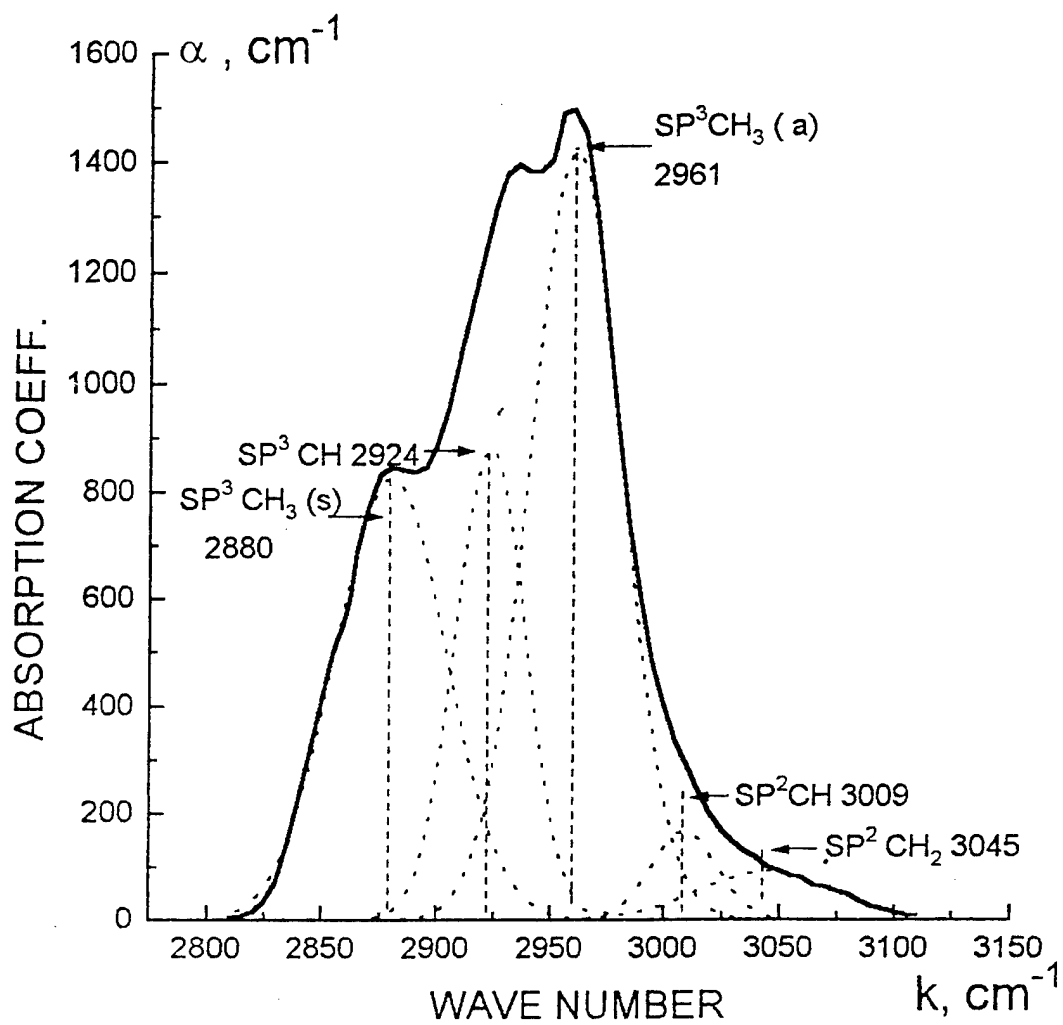2800 2850 2900 2950 3000 3050 3100 3150

WAVE NUMBER

k, cm^{-1}

DEPOSITION AND MIXING OF COBALT, TITANIUM AND TUNGSTEN ON THE PULSE MELTED SURFACES OF SUBSTRATES

J.Langner, J.Piekoszewski, J.Stanislawski, Z.Werner

Soltan Institute for Nuclear Studies,
05-400 Otwock/Swierk, Poland

Summary

A new method of the formation of thin metallic coatings on steel substrates is demonstrated. The method is based on the use of high intensity plasma pulses. Depending on the choice of the operation conditions of the plasma pulse generator, it is possible to form the pulses containing either both, nitrogen and metal plasma or pure metallic plasma. In the present experiments plasma pulses of Ti, Co, and W, are used. The feasibility of a two-step process is shown. In the first step there is a mixing of deposit-substrate components induced by melting and mutual diffusion process occurs. In the second one, there is a deposition of the metal coating of practically unlimited thickness on the intermediate mixed layer.

1. Introduction

One of the approaches to modification of the surface properties of materials relies on the use of the high intensity pulsed ion or plasma beams. The first experiments on the application of such beams were performed by Cornell University group [1] . They successfully used 280 keV proton beams with current density of order of 100A/cm^2 for post implantation annealing of silicon wafers. The proton beams were generated in magnetically insulated high voltage diodes. This kind of generators was also used for modification of metallic materials in series of experiments reported by Tomsk group [2] and recently by Wurzburg group [3] in mixing experiments of the overlayer-substrate systems. In the experiments cited above, the modification was achieved mainly via thermal effects since the dose of ions delivered to the substrate in a single pulse was too small to alter its macroscopic properties by doping effects, or by formation of new compounds.

An alternative approach to the surface modification is to make use of the thermal effects combined with mass deposition. The first experiments of this kind were successfully demonstrated by Swierk-Warsaw group [4] using the rod plasma injector (IONOTRON) type facility. The high intensity pulsed plasma streams, generated in these machines can melt the near-surface layers (of the order of 1μm) of practically any kind of solid and then dope it with plasma brought atoms . The doping occurs mainly via fast diffusion of these atoms in the melted near-surface layer. Such technique can be used for doping semiconductors (p-n, n-p silicon junctions formation), introducing the high doses of nitrogen into steels etc. [5,6]. In majority of our experiments carried out thus far, the plasma pulses were formed mainly from the working gas injected into the interelectrode space. The present work was aimed at the

extension of the possibilities of this technique by providing the IONOTRON generator with a separate metallic pulsed plasma source based on the metal vapour vacuum arc. The appropriate synchronisation between the discharge ignition and the metallic source action makes it possible to accomplish the process in which the stream of metallic plasma impinges on the melted surface of the processed material. Cobalt, titanium and tungsten plasma pulses were used for mixing and formation of metallic coatings on the AISI321 stainless steel substrates. The coatings were characterised by: Glow Discharge Spectroscopy (GDS), Auger Electron Spectroscopy (AES), roughness measurements and Scanning Electron Microscopy (SEM) observations.

2. Experimental

2.1. Apparatus

Details of the IONOTRON operation appeared elsewhere [5] and will not be repeated here. Briefly, the ions are produced by a low pressure, high current electric discharge initiated between two concentric cylindrical sets of rods allowing a free passage of particles through them. A fast valve injects the working gas (nitrogen) into the interelectrode space and after a delay time Δt required for the gas cloud to achieve the appropriate density, the energy from the capacitive storage bank is applied. Depending on the delay time Δt various operating modes are possible.[7].

In the period between 1970 and 1980, a number of experimental devices devoted for thermonuclear study purposes were constructed and examined at the Soltan Institute of Nuclear Studies. Next, some of these facilities have been adapted for materials research.

The key concept of the present work was to equip the IONOTRON with the additional, metallic plasma source making it possible to form metal-nitrogen plasma pulses. For this purposes we designed the high current pulsed metallic plasma source based on the metal vapour vacuum arc. It is well known that in this kind of source the erosion factor amounts to about 10-7 kg per coulomb. Our estimates have shown that to form metallic films of several tens nanometer thickness during the pulse of 100 microseconds length at the distance of 50 cm from the source, the magnitude of arc current must reach the level of several kA. This imposes special requirements on the mechanical construction of the source and current supply system. In this work, cylindrically symmetric configuration of the metallic plasma source with 20mm and 36mm diameter electrodes was used. The main ceramic insulator of the electrode set was shielded to prevent the condensation of metallic vapours on its surface. The arc was initiated by the 15kV trigger pulse applied between a tubular trigger electrode, and the cathode. The arc current was supplied from trigatron switched high current generator (25kV/48μF) via 50kV separating transformer. The arc current reached 120kA and the pulse width was 100μs. The scheme of the electrical circuit and plasma source is shown in Fig.1. This source was installed inside the ring type fast valve injecting the working gas placed in the central part of the electrode system of IONOTRON type device. The discharge in the working gas, i.e. nitrogen was initiated after some electronically controlled delay time Δτ elapsing from the moment of the ignition of the metallic source. The device was operating under the following conditions:

- diameters of outer and inner electrodes were 350 and 310 mm respectively,

- supply energy - 100 kJ

- discharge current on the level of 1 MA,

- energy density in the plasma stream at the distance of 60 cm from the end of electrodes was

in the range 2-10J/cm^2,

- delay time was in the range from 0 to 150 μs.

The schematic view of the whole system is shown in Fig. 2.

2.2 . Coatings deposition

In our previous experiments on the titanium coatings [8] it was found that as regards the delay time Δτ, three typical situations can be distinguish. When Δτ < 50 μs, the nitrogen ions reach the substrate first and melt its surface. Since the time of flight of metallic ions is about 50-70μs, they reach the surface when it is already solidified. In other extreme, i.e. when Δτ > 100 μs, the metallic ions reach the surface before the nitrogen ions. However, the oncoming N ions can not melt the surface since it is shielded by a cloud of the metallic ions. The intermediate case, 50-70 μs appeared to be the most effective in melting and mixing the deposit- substrate components. Assuming that the same is true for Co and W, the majority of experiments were carried out at Δτ = 75μm. The substrates were cut of AISI 321 stainless steel in the form of discs of 50 mm in diameter and 1mm thick, and with the surface roughness of Ra= 0.2 μm. They were positioned at the distance of 50 cm from the end of the electrodes in the holder equipped with four miniature calorimeters, measuring the total energy density E in the single pulse. E was kept at a level of 3.5 to 5 J/cm^2. Inhomogenity of E over the area of 25 cm^2 did not exceed 30%. As a rule, each sample was irradiated with 5 pulses in optimum mixing conditions. Some of them were additionally subjected to the deposition of pure metallic plasma pulses (10) without heating by nitrogen ions.

3. Results and discussion.

The surfaces of all samples exhibit the granular morphology, characteristic for arc - based deposition techniques. This is illustrated by SEM micrograph shown in Fig.3 presenting the cobalt coating in which mixing with 5 pulses was followed by the additional deposition of pure cobalt plasma pulses. The mean roughness, expressed by Ra was ranging from about 0.2 μm to 0.6 μm depending on the energy density in the pulse, i.e. higher E causes greater roughening the surface.

Figs 4a - 4c show the in-depth profiles of Ti, Co, and W in AISI 321 s/s, obtained using GDS method. Inspection of these profiles reveals the following facts: First, it is clear that mixing of the metallic deposit with substrate occurs. Secondly, the mixing efficiency is different for different elements. Taking the in-depth location of the triple backgroud value of a given element as a measure of its penetration efficiency, we estimate that for Ti, Co, and W, these values are 6, 0.8, and 0.35 μm, respectively. This is obviously associated with different diffusion constants for various elements in liquid steel. Thirdly, one observes a deep nitrogen penetration, extending to 3 - 4 μm. The profiles shown in Fig.5, refer to the structure in which after mixing the additional cobalt layer was formed. This results demonstates a feasibility of forming the substrate/mixed layer/deposit structure and building up a metallic layer of practically unlimited thickness. It is interesting to note that nitrogen present initially in the mixed layer (see Fig. 4b) is apparently extracted from the bulk towards the surface.

Another interesting conclusions can be drawn from the results of AES analysis presented in Fig.6. They show the spectrum of Co-plasma treated sample after removal of about 5nm thick surface layer using 5 keV argon ions. Apart from the expected presence of Co lines at 654 , 718, and 775 eV, the spectrum reveals the presence of strong C (273 eV), O (514 eV), N (384 eV), Cr (489 and 530 eV), and Fe (598, 651 (merged with 654eV Co line), and

705 eV) lines, weak Al^{ox} line (57 eV), and traces of S (150 eV), Cl (183 eV) and Ar (220 eV). Among these elements, carbon, oxygen, aluminium and chlorine are detected on the sample surface prior to ion etching and the intensity of their signals decreases with depth. Hence they can be treated as surface contamination. However the carbon and oxygen signals maintain a significant value even at a greater depth, suggesting that they constitute also the components of the formed layer. On the other hand, the aluminium signal markedly decreases with depth and its behaviour is consistent with the assumption that its presence originates from plasma-induced erosion of alumina insulator of the plasma source. The nitrogen signal seems to be stable as a function of depth and hence nitrogen should also be treated as the layer component.

Of special interest is the behaviour of Cr and Fe signals. The are both absent at the unetched sample surface and their intensity grows with depth, in marked contrast to all other elements present in the surface layer. Such behaviour is fully consistent with the assumption that their presence results from melting the substrate material (nickel-chromium stainless steel) and rapid diffusion in the molten Co deposit It is also of interest that nickel, being another substrate component, is apparently absent in the surface layer, thus suggesting that different substrate components diffuse at different rates in Co layer.

Similar results, demonstrating the presence of substrate components in the near-surface region of plasma-deposited layer have been obtained (although to smaller extend) for Cr deposits but not for W ones, suggesting that the diffusion rate of substrate constituents depends also on the deposit material. Concluding, the results of AES analysis provide strong evidence of the mechanism of mutual mixing in the substrate-deposit system using pulsed metallic plasma beams.

Acknowledgements

References

1. J.E.E.Baglin, R.T.Hodgson et al: *Nucl. Instr. and Meth.* 191 (1981) 169.

2. A.D.Pogrebniak, G.E.Remnev et al.: *Nucl. Instr. and Meth.* B36 (1989) 286.

3. D.Popp, A.Mehling, R.Wilzbach, H.Langhoff: *Appl. Phys.* A55 (1992) 561.

4., J.Piekoszewski M.Gryziński, J.Langner, Z.Werner: *phys. status solidi* (a) 67 (1981) K163

5. J.Piekoszewski, J.Langner: *Nucl. Instr. and Meth.* B53 (1991) 148

6. J.Piekoszewski, J.Langner et al.: *Matrials Letters* 14 (1992) 131

7. J.Langner, J.Piekoszewski, C.Pochrybniak, F.Rosatelli, S.Rizzo, A.Miotello, L.Guzman, P.Lazzeri: *Surface and Coatings Technology* 59 (1993) 281

8. J.Langner, J.Stanisławski, J.Piekoszeski: *Surface and Coating Technology* (in print)

List of figure captions

P - power supply   C - crowbar   S - spark gap
T - trigger   Tr -transformer   V - voltage divider
R - Rogowski coil   I - ignition electrode   A - anode, K -cathode

SAMPLES

4 CALORIMETERS

ION BEAM

TO VACUUM PUMP

ELECTRODES

TO CONDENSER BANK

METALLIC
PLASMA
SOURCE

TO PULSE
CURRENT
GENERATOR

GAS

FAST VALVE

50 μm

Fig3

Signal

ISA   JOBIN-YVON FRANCE   SURFACE ANALYSIS

Ele Hv S
Fe2 876
N1 660
T1 848
Cr2 804
N1 848

a

4500

3500

2500

N1

1500

500.

T1

30.0   90.0   150.   210.   270.   Sec

File   :
  L23-1
Sample :

Comments:
  IBJ
  700V30m
Date:
  08/23/9

ISA JOBIN-YVON FRANCE   SURFACE ANALYSIS

Ele	Hv	Sca
Fe2	948	
Co	800	
N1	972	

b

File :
  L45-1
Sample :
  SS321
Comments:
  IBJ
  700/60/9
Date:
  01/04/96

Signal

ISA   JOBIN-YVON FRANCE   SURFACE ANALYSIS

Ele Hv Sc
Fe2 948
W   996
N1   996

c

4500

3500

2500

1500

500.

Fe2.

N1 .

W

2.50   7.50   12.5   17.5   22.5   Sec

File :
  L43-2
Sample :
  SS321
Comments:
  IBJ
  700/60/9
Date:
  01/05/9E

Signal

ISA   JOBIN-YVON FRANCE   SURFACE ANALYSIS

Ele	Hv	Sca
Fe2	948	
Co	748	
N1	972	

4500

3500

2500

1500

500.

Fe2   Co

N1

5.00   15.0   25.0   35.0   45.0   Sec

File   :
  L47-4
Sample :
  SS321
Comments:
  IBJ
  700/60/9
Date:
  01/04/96

Sample # IPJ44
(Co deposition)
After 45 min
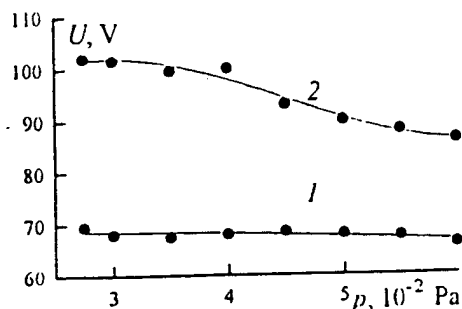ion etching

Technical Literature

Fig. 5. Discharge operating voltage V_d and floating probe potential V_f versus pressure.

absence of discharge at a pressure of 10^{-3} Pa, bear witness to the pulsed character of this emission. The most intense emission from the cathode was observed at the filament current zeros.

When the filament was powered by a dc current, no modulation of the discharge current was observed. For this case, at a pressure of 10^{-2} Pa when the operation of a non-self-sustained arc discharge was hindered, an excess of the floating probe potential magnitude over the discharge operating voltage and a reduction of the probe potential measured with respect to the cathode potential by the same value were indicated.

The plasma parameters were measured with a Langmuir probe biased with respect to both the cathode and the anode. With a pressure of 7×10^{-2} Pa and a discharge current of 50 A the plasma density in the center of the working chamber was $\sim 10^{10}$ cm^{-3} and the plasma potential with respect to the cathode was +63 V. The plasma contained two groups of maxwellized electrons with the temperature $kT_e \approx 4$ and 10 eV, respectively. The measured plasma density distribution over the central section of the working chamber at a diameter of 500 mm was uniform to ±20% of the average plasma density.

4. DISCUSSION

The pulsed character of the current of a low-pressure arc discharge at a dc supply voltage can be attributed to the magnetization of the electrons emitted by a hot cathode by the magnetic field created by the ac filament current. The magnitude of this field at the filament current maxima estimated for currents of 150–200 A is 0.03–0.04 T. The same magnetic field under similar conditions [3] exerted a pronounced effect of the distribution of the primary electron density in a discharge system with a hot cathode. Since a

hot-cathode arc discharge is non-self-sustained, a modulation of the thermal electron emission results in a modulation of the discharge current to the point of its extinguishing at the filament current maxima. With that, the electron emission from the hot cathode becomes much less intense. Additional supporting evidence for the above mechanism is the burst of the discharge current that is observed once the filament current has been switched off, when the cathode temperature still remains high enough to sustain the thermal emission and there is no magnetic field. When the discharge current is cut off, the potential distribution in the gap is disturbed and bursts of the floating probe potential are detected. This can be caused by the fact that the probe is charged by the flows of high-energy unrelaxed electrons having appeared at the instants the discharge rearranged. Since abnormally high potentials of the floating probe at low pressures were observed as well with a dc filament current (steady-state case), it can be stated that the high-energy electron flows generated in this type of discharge is its characteristic property exhibited when the discharge operation is hindered. The abrupt decrease in the negative potential of the probe as it is turned by $\geq 30°$ from the diode axis testifies to the fact that the electron flows are accelerated in the working chamber from the cathode region toward the anode plasma region.

5. CONCLUSION

The study we have carried out has revealed that a low-pressure non-self-sustained arc discharge may operate in modes with a deeply modulated discharge current, such that high-energy electron flows are generated in the discharge. It has been shown that the modulation of the arc discharge current is related to the bursts in filament current. The modes discovered offer promise for the development of high-current gas-discharge devices with a completely controllable discharge current and of efficient repetitive plasma generators for technological purposes.
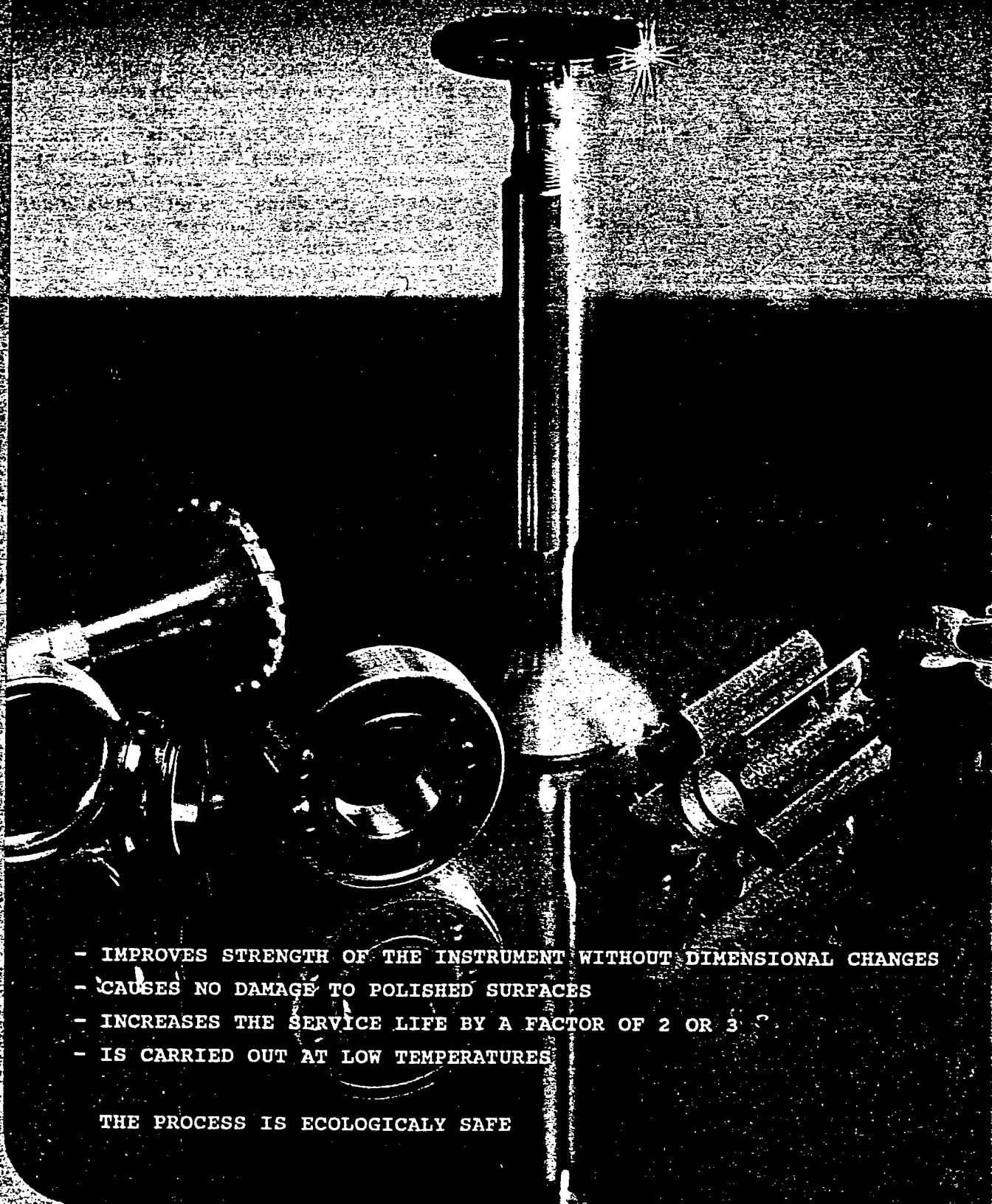
6. REFERENCES

[1]   B.S. Danilin and V.Yu. Kireev, Use of Low-Tem-perature Plasmas for Etching and Cleaning. Energoatomizdat, Moscow 1987.

[2]   D.P. Borisov, N.N. Koval, and P.M. Schanin, Izv. Vyssh. Uchebn. Zaved.: Fizika, No 3, 115 (1994).

[3]   Y. Ueda, M. Doi, M. Nishikawa, and S. Goto, Rev. Sci. Instrum., 62, 105 (1991).
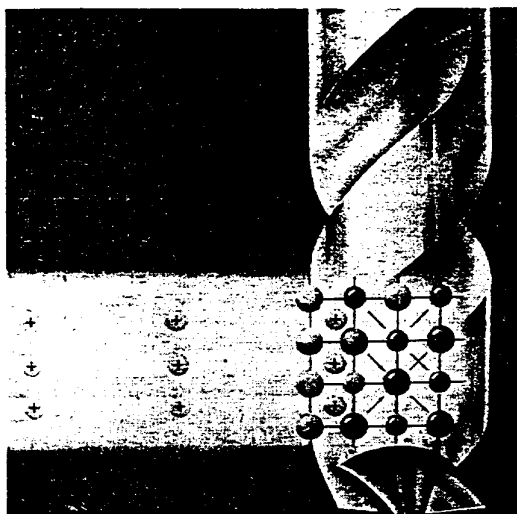
REPUBLIC ENGINEERING CENTER

on reactivition and hardening of machine parst and details

ION IMPLANTATION

- IMPROVES STRENGTH OF THE INSTRUMENT WITHOUT DIMENSIONAL CHANGES
- CAUSES NO DAMAGE TO POLISHED SURFACES
- INCREASES THE SERVICE LIFE BY A FACTOR OF 2 OR 3
- IS CARRIED OUT AT LOW TEMPERATURES
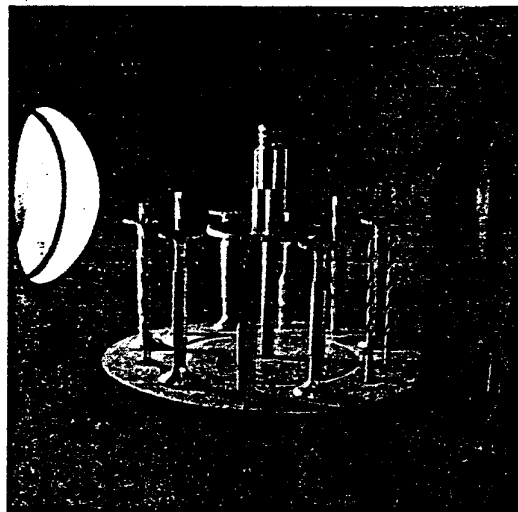
THE PROCESS IS ECOLOGICALY SAFE

ION IMPLANTATION

ION IMPLANTATION is a process of irradiation of material surface by accelerated ions.

ION IMPLANTATION process is used to improve the exploitation properties of instruments operating under conditions of high sliding, rolling, corrosive or cavitation wear.

ION IMPLANTATION modifies metals and ceramics structure to the depth of 100 microns.
- imparts durability, wear resistance or surface hardness
- increase fatigue life
- reduces coefficient of friction

ION IMPLANTER "DIANA"

- generates multielement ion beams (from boron to uranium in any composition)
- provides the depth of implantation up to 0,1 micron, under the accelerating voltage 20...100 Kv
- has removable compositional cathodes

SPECIFICATION

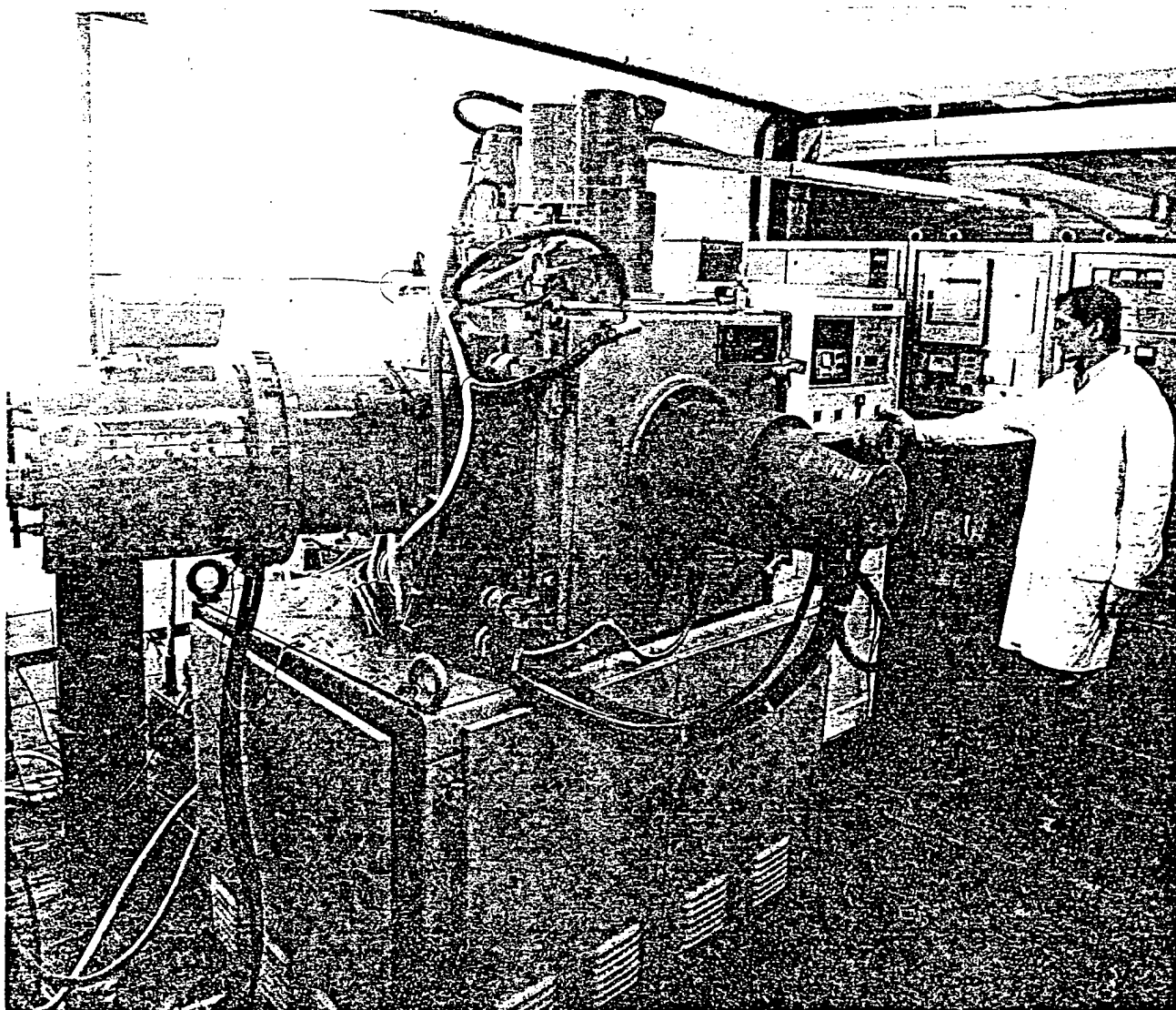|	
- impulse duration	300 ms
- impulse frequency	2,5-50 Hz
- ion beam cross-section area	300 sq.cm
- rate of dosage accumulation of 10^{17} cm^{-2} over 300 sq.cm	10-20 min

ION SOURCE 'DIANA' has attached accelerating voltage unit. High - voltage protected.
Compositional cathodes allow to vary in broad range the surface properties.

ION SOURCE 'DIANA' IS SIMPLE AND RELIABLE IN OPERATION.

INDUSTRIAL SITE EQUIPMENT

- **ION IMPLANTER "DIANA"** (includes ion source - diametre 350 x 570 mm, control and electrofeeding rack - 500 x 500 x 1700 mm)

- vacuum chamber with limiting vacuum of 1×10^{-5} torr

- ultrasound bath with generator

- table, shelving, drying cabinet

- the premises are equiped with forced ventilation and supplied with hot and cold water.

Our address: Akademichesky, 8/2, RITS,
                634050, Tomsk, USSR
Telex: 133179 RITS
Teletype: 128243 Plazma
Telefax: (382-2) 25-88-63
Phone: 25-84-81, 25-85-91, 25-87-01

ION SOURCE OF "DIANA" SERIES

- Universal high-intensive implanter for surface modification of materials by ion beam;
  - Unlimited ability of modifying surface micro-structure of materials;
- Allowing to supply with single- or multi-charged ions of metals and composite materials;
  - Energy of the single-charged ions is in the range of 20-100 KeV, energy of the multi-charged ions is up to 200 KeV;
    - There are up to 70% of multi-charged ions in the ion beam;
    - The density of the currant in the ion beam up to 2 mA/cm^2;
      - Ion beam diameter is 200 mm;
      - Uniform density of the ions across the beam;
      - Automatic control of implantation dose;
      - The implanter is simple and comfortable in use;
      - The implanter is interference protected and reliable in use;
- The implanter may be used with any vacuum equipment convenient for implanting.

INTRODUCTION

Multi-element ion beam modification gives new wide advantages to improve surface parameters of materials. Implanting by these beams allows to alloy surface layers properly that increases tribological and mechanical properties as well as corrosion and erosion parameters of the part as a whole. It also allows to obtain solid phase reactions which are impossible to realize within surface layers of 100 mcm by conventional methods.

The ION SOURCE OF "DIANA" SERIES is designed for solving engineering problems of increase of working parameters of metallic and ceramic parts by ion beam modification. Change of energy, intensity and components of ion beam is possible without time spending for special re-adjustment of the implanter. Construction of ion sources is original and simple. It is developed up to quantity-produced equipment and may be used in any technological processes requiring ion implantation.

The ION SOURCE OF "DIANA" SERIES is designed for investigation of materials modification by ion beam of two-, three- and more components.

DESIGN

The implanter is constructed to be simple and comfortable in use. It consists of two units: ion source and high voltage power supply unit. The units are mounted in the same case and separated by high voltage isolator. This construction has no outside high voltage connections and ensures safety of an operator.

The ion source is hinged with a vacuum camera by special module. It allows easy access to electrode system while servicing as well as cathode replacement without disconnection of ion source and vacuum camera.
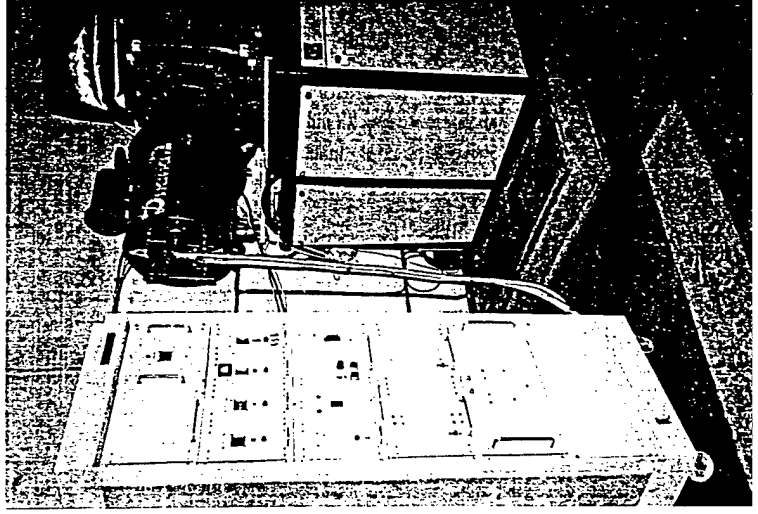
Ion beam control is designed to be easy with control&power panel.

The ion source unit consists of ion generator and ion accelerator. The ion generator consists of cathode module and ion extractor. The ion accelerator is designed for accelerating the ions up to set up energy. It also forms the beam with uniform ion density on the modified surface. The accelerator consists of anode and two nets. The nets serve two purposes. They form uniform ion density over the beam diameter and reflect secondary electrons which spoil the work of the ion source. The accelerator forms the beam of 200 mm in diameter.

The cathode module includes replaceable cathode of 15 mm in diameter and 5 mm in length. The time necessary to replace the cathode is not more than 20 min. The cathodes (both single- and multi-component) are made of powder materials. .

The size of ion source is 350 mm in diameter and 570 mm in length. The control&power panel is of 500 mm in width, 500 mm in length and 1700 in height. The total weight of the implanter is 350 kg.

OPERATION PRINCIPLES

The ION SOURCE OF "DIANA" SERIES operate in frequency-pulse regime. The plasma of metal ions is formed from vapor phase generated by arc discharge in cathode module. The pulse arc regime is synchronized with extracting and accelerating voltages supplying by high voltage unit to the corresponding electrodes. The ion source is powered by low voltage supply line through the control&power panel. Power generators of the panel produce the rectangular pulse voltage of 300 mcsec long with the frequency from 25 to 50 Hz. The accelerating voltage may be varied in the range of 20 - 100 kv. The other feeding voltages remain constant in all working regimes of the ion source.

The ion sources allow to obtain the ion currant on the samples from 100 to 600 mA depending on cathode materials. They ensure the rate of gaining the dose from 0.5×10^6 to 1.0×10^6 ion/cm^2/min. correspondingly. The control panel checks automatically the gaining of the dose by counting the number of ion currant pulses come to the irradiated specimen.

The ION SOURCE OF "DIANA" SERIES requires maximum power of 2 kW and one-phase alternative voltage of 220 v. The isolator between the high-voltage unit and the ion source module is cooled by running water. It takes 0.12 m3/hour.

VACUUM SYSTEM

The ION SOURCE OF "DIANA" SERIES uses vacuum cameras with the pressure limit up to 1×10^{-5} torr. The system has to have fore-vacuum and high-vacuum stages of pumping with the rate of not less than 2000 l/sec at the pressure of $10^{-5} : 10^{-3}$ torr. It also has to have the by-pass fore-vacuum pumping of 10 l/sec at the camera size of 600x600x600 mm^3.

Vacuum systems HHB-6,6П produced by "Sielectroterm" (Novosibirsk, Russia) are used as the basic vacuum system for the ION SOURCE OF "DIANA" SERIES. They have a vacuum camera of 600x600x600 mm^3 in size and satisfy to all necessary parameters of the ION SOURCE OF "DIANA" SERIES.

2

The vacuum camera has a rotating table for specimens. It allows to rotate the specimens around and on their own axis.

CHARACTERISTICS

TYPE OF ION SOURCE AND THE WORKING REGIME:	Arc and frequency-pulse type regime. High frequency, low pressure arc. Pulse duration is 300 mcsec. Pulse frequency is changeable in the range of 25 - 50 Hz. All supplying voltages of the electrode system are synchronized on pulse frequency and duration.
ION ENERGY:	From 20 to 100 KeV for single charged ions. Upto 200 KeV for multi-charged ions.
BEAM INTENSITY:	From 100 to 600 mA depending on cathode material. Currant density of the beam is upto 2 mA/cm^2, the density is uniformly distributed over the beam diameter of upto 200 mm. The rate of picking up the dose is from 0.5×10^{16} to 1.0×10^{16} ion/cm^2/min. (in the case of flat non-moving surface under irradiation). In the case of rotating cylindrical surface the rate is 3 times lower.
CATHODE:	Expendable of a tablet form with the diameter of 15 mm and the length from 3 to 5 mm. Material: pure materials, or multi-component metallic alloys, or composite ones made of powder mixture. There is no limitation on used metals or its compounds. The cathode tablets have to be electrical conductive. The permanent work time of cathode is 8 hours. The time necessary to replace the cathode is not more than 20 min.
POWER:	2 kW, one phase alternative voltage of 220 v.
DIMENSIONS:	Diameter is of 350 mm, length is of 570 mm. The pipe connection to vacuum camera is of 240 mm in diameter. The case of high voltage module of ion source is filled up with transformer oil of electric strength equal to 20 MV/m. The oil amount is 28 l. The size of control&power panel is 500x500x1700 mm^3. The total weight is 350 kg.
RELIABILITY:	The mean time between failures is 700 working hours; the mean repairing time is 8 hours; the mean time for usual service is 3 hours.

3

APPLICATION

The ION SOURCE OF "DIANA" SERIES is desired for ion implantation on special vacuum equipment used for industrial ion beam treatment of tools and parts.

Possible application of the ION SOURCE OF "DIANA" SERIES:

* single element cathode in the ion source, stationary specimen;
* composite powder cathode in the ion source, stationary specimen;
* multi-component metallic cathode in the ion source, stationary specimen;
* the specimen rotating on its own axis; three types of cathode (see above);
* the specimen rotating around and on its own axis; three types of cathode(see above);
* all the cathode types listed above; pulse frequency and ion energy are different.

Selection of composite cathode and the working regime opens unlimited scope for modification of surface micro-structure.

SERVICE AND DELIVERY SET

* The ION SOURCE OF "DIANA" SERIES and control&power panel.
* Engineering specifications on the ion source.
* Spare parts: set of radio parts having no Europe analogues.
* Production of composite cathodes.
* Service
* Personnel training in Russia or in customer place while potting in operation.

ENTERPRISE	TREATED PART	MATERIAL UNDER TREATMENT	INCREASE OF RESISTANCE (times)
"POLYMER" Novopolotsk	Cutting tools for chemical fibers	Lavsan, kapron, nitron	4-6
Oil plant Grozny	Sealing inserts for oil pumps	Pig iron, АС35Г2, Ст 10КП	5-6
"AvtoVAZ" Tollyatti	Drills of 2.2 mm, Screw tap M5, Punching press tool	Pig iron, АС35Г2, Ст 10КП	2.5 2.5 - 3.8 3
"Auto-mobile Transport" Tomsk	Cam shafts, valves, pistons, engine rings,	Pig iron, АС35Г2, Ст 10КП	2-3
"START" Pavlovo-na-Oke	Milling cutter	Ст 45, У7	2 - 2.5
"SibCable" Tomsk	Spinneret	Cu wire	2.8
Milk-preserving Plant Tyazhin	Seaming rollers	Plate	4
Regional Photographic Association Tomsk	Hair cut scissors		3
Radio Plant Tomsk	Punching press tool, Drills of 0.9 mm	Stainless steel Glass-textolite	4 3.8
Town Milk Plant Tomsk	Carving press tool	Al foil	31

*Combined technology (ion-plasma and ion-beam)

VACUUM ARC TECHNIQUE *TAMEK*:
BROAD METAL ION, PLASMA AND ELECTRON BEAMS GENERATION

Alexander M. Tolopa

Applied Physics Institute, Ukraine Academy of Sciences, FAX +38(0542) 333-436.
TAMEK, P.O.Box 561, Sumy, 244024 Ukraine.

1. ABSTRACT

This paper presents a review of vacuum arc facilities to be as injectors for metal ion accelerators. A vacuum arc in different modes: 1). Arc current I_{arc}=2-50 A, pulse duration t_p=10 µs to 20 ms; 2). I_{arc}=20-100 A, t_p=50-1000 µs; 3). I_{arc}=100-2000 A, t_p=100-2000 µs; 4). I_{arc}=10-100 kA, t_p=1-10 µs were investigated as metal ion injectors. The metal flows generated by cathode spots are expanded for diameters of 10-50 cm, and then, or deposited on the grounded target, or post accelerated between grids at U_{accel}=10-120 kV. On the basis of such injectors the series of TAMEK sources were investigated with metal ion current from $I_i>$ 0.01 A, pulse duration up to 20 ms, to $I_i<$5 kA, t_p=1-5 µs. Any from following surface (of metals, ceramics, glass, ect.) treatment modes: metal ion deposition, high intensive metal ion implantation, ion mixing, ion beam assisted deposition, high power metal ion beam irradiation, or electron beam irradiation are implemented by TAMEK sources. These results are also presented.

1. INTRODUCTION

Ion beam modification of metals, composite materials, ceramics, glass, polymers is used to improve surface properties such as wear, corrosion and friction resistance, hardness, electrical conductivity, wettability, etc., [1].

In 1984 the authors of Refs.[2-8] started to develop vacuum arc metal ion sources for surface modification technologies. Such implanters generated high-energy ($E_i<$150 keV) ions of a variety of metals and alloys with the ion beam spot diameter of 20 cm and the rate of dose accumulation on the grounded target $D_i/dt<10^{16}$ ion/cm^2 per minute. The next step in the development was made by designing Technological Accelerator of Metal Ion and Electron Kit (TAMEK source) which was capable of generating both high-energy metal ion beams and low-energy plasma from the same cathode material, thus providing high-dose (intensive) metal ion implantation (HDI), ion deposition, ion mixing and ion beam assisted deposition (IBAD). Unlike other IBAD systems we used only the TAMEK source for IBAD. The vacuum arc injectors were also used in TAMEK-M

source for generation of high power metal ion beams (HPIB) with ion current of $I_i<$5 kA, t_p=1-5 µs.

2. BROAD METAL BEAMS GENERATION

2.1. Versatile TAMEK source

TAMEK is a vapour vacuum arc source of multiply charged ions (from Me^{+2} up to Ta^{+6}, W^{+6}) emitted from any hard cold electroconductive cathodes (fig. 1).
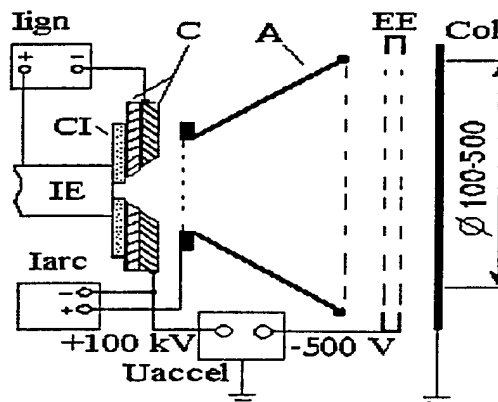

Fig. 1. Scheme of the TAMEK source. A-anode, C-replaceable disk cathodes, IE-igniting electrode, CI- ceramic insulator, EE-grid extracting electrode, Col-grounded collector, I_{ign} (10 kV, 20 µs), I_{arc} (60 V, 50 A at 300 µs and 2000 A at 1000 µs), and U_{accel} (100 kV, 300 µs, 2 A)- pulse transformers, power supply of which is shown on fig. 4.

A low current vacuum arc stability is one from the main problems to be decided to construct vacuum arc accelerators. A low arc current mode is desired for better adjusting of anode plasma density with Child-Langmuir ion current density limit in an accelerating gap. For TAMEK source in HDI mode (with ion accelerating) this problem was decided by means of determination the optimal time duration (t_p=300 µs for $I_{arc}<$50 A), and also by using arc discharge configuration with better cathode sports moving by the using radial arc current feedthrought for outer cathodes (Fig. 1), or ferromagnetic insertion inside central axial cathodes. But at

I_{arc}<50 A a vacuum arc became unstable for t_p>500 µs due to an electron thermalization in the arc discharge plasma.

The alternation of HDI and low-energy ion deposition (fig. 2a) was proposed [5]. In the pulsed mode (f<100 Hz) both ion implantation at E_i<200 keV, U_{accel}<100 kV, the dose accumulation rate on the grounded target dD_i/dt<10^{16} ion/cm^2/min, and deposition of the same ions at E_i<100 eV, coating growth rate dH/dt=50-200 nm/min, are implemented during each pulse.

As the accelerating voltage polarity is reversed, the source generates an electron beam with E_e<100 keV, I_e<5 A.
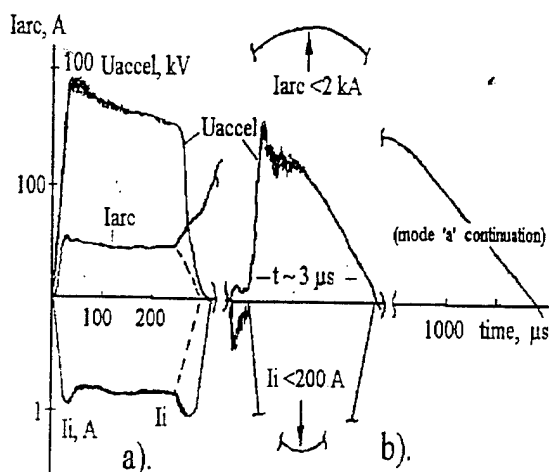

Fig. 2. Signals of TAMEK source operational modes. a), IBAD mode with HDI; b), IBAD mode with HPIB. U_{accel}, accelerating voltage; I_{arc}, vacuum arc discharge current; I_i, ion current. Dashed lines indicate I_i and I_{arc} in the HDI mode without ion deposition.
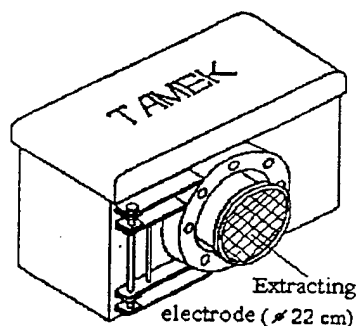

Fig. 3. TAMEK source picture. High-voltage power supplies and an ion gun are located in the space of 70x40x25 cm^3.

Modular design of the TAMEK source (fig. 3) permits us to install it on a vacuum chamber. The TAMEK source discussed was intended to be installed on the industrial units which were operated in the vacuum arc PVD mode and had inlet flanges of 25 cm in diameter. Normally, one or two of each three PVD sources were taken off from the PVD vacuum unit, and TAMEK sources were installed on the free flanges. So, the ion spot size was 300 cm^2 in this case. But, it is easier and quicker to adapt the TAMEK sources for generation of ion beams with the spot size of 2000 cm^2. For this purpose it is only necessary to replace the conical anode and the extracting grids by new ones of corresponding diameter, as the plasma and ion flows from the vacuum arc cathode spots are expanded forward at angles of 60-120 degrees for different cathode materials. In our case, we have lengthened the electrodes to obtain the diameter of 50 cm.

The TAMEK sources can efficiently generate high-melting metal (e.g., W, Ta) ions which are hardly available with other types of sources. To obtain mixed ion beams we used replaceable cathodes made from alloys and composites such as TiB_2, TiC, TiSiC, TiMoSi, SiC, MoS, CuMoSi, CuSiC, AlBW, NiCrAlY.

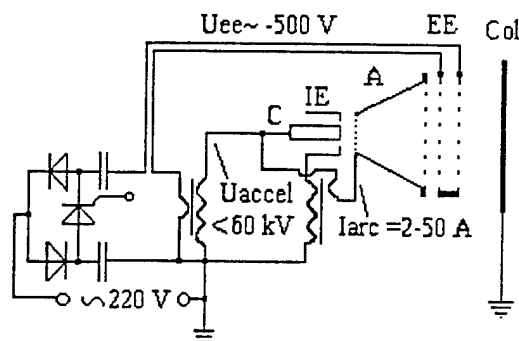## 2.2. Low current millisecond duration vacuum arc source

Fig. 4. Scheme of the source with low current vacuum arc.

Special scheme (fig. 4) was proposed [6] for realization of both an extra low current and long pulse duration vacuum arcs. This scheme automatically reignites the arc for all accelerating voltage. A low current vacuum arc can be produced with the single emitting center in the cathode spot, e.g., a sequence (up to 20 ms) of single short pulses was generated at a current I_{arc}=2-4 A for copper cathode, and I_{arc}=8-10 A for tungsten cathode. At higher arc current the source operates more stable and generates low intensity metal ion beams of time duration determined only by the power supply transformers. Such low current vacuum arc mode generates more highly stripped metal ions due to more less de-ionization of metal ions in the low density near surface cathode plasma.

Fig. 4 also shows additional to the electrostatic (-500 V is applied to EE on fig. 1) magnetic method for reflecting the collector

secondary electrons. Without such reflection the additional (electron) source current is increased up to 6-16 times for light and heavier ions accordingly.

2.3. TAMEK-M sources of microsecond duration high power metal ion beams

At a high current vacuum arc it is possible to use only one discharge gap without triggering for microsecond duration metal HPIB generation [7]. The direct capacitance discharge (fig. 5) is used for metal plasma generation after ignition of Marx generator.
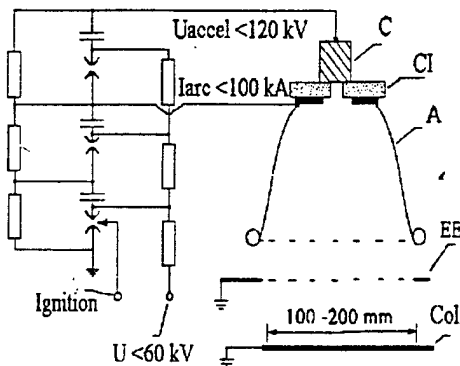

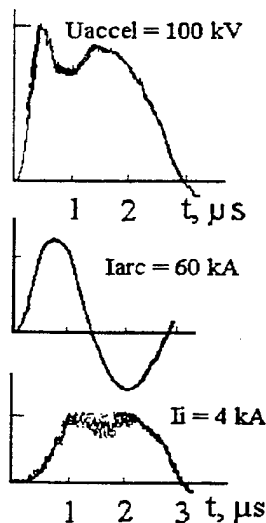Fig. 5. Scheme of TAMEK-M source.

Fig. 6. Typical pulses for TAMEK-M source (fig. 5).

Source on fig. 7 uses Archimedes spiral type path of the anode -AM for creation of a magnetic field for electron insulating. At the beginning of a pulse the electrode -AM has a floating potential, that lead to the surface flashover on the insulator -CI and cathode sports formation on the road part of the anode. Simultaneously, the magnetic field from this electrode increases the anode plasma ionization.

At I_{arc}<100 kA (fig. 6) such sources generate metal ion current I_i<5 kA, t_p=0.5-10 μs. For a shorter pulse duration it is difficult to achieve a low inductance of a vacuum arc discharge circuit, to take

also into account the rather big capacitance which is necessary to generate a high arc current. Upper limit for pulse duration is restricted by necessity to adjust the accelerating gap with Child-Langmuir limit for the ion current density and closing the accelerating gap by an explosive cathode plasma. Due to high speed of vacuum arc anode plasma motion and its erosion during a pulse for vacuum arc ion sources it is possible to use accelerating gaps up to 10 cm. Nevertheless, parameters received: U_{accel}<120 kV, I_i<5 kA, t_p=1-5 μs are enough for successful metal surface modification with the surface energy input of dW=0.5-5 J/cm^2 [4,9,10].

In the reversed mode such sources generate electron beams with current of I_e<50 kA.

Fig. 7. Scheme of the HPIB source with self-generation of an anode plasma and insulated magnetic field.

2.4 Plasma immersion metal ion implantation

A combination of conventional metal vacuum arc PVD method and plasma immersion metal ion implantation (PIII) are proposed [8]. Fig. 8 presents the scheme of the combination of PVD and PIII.
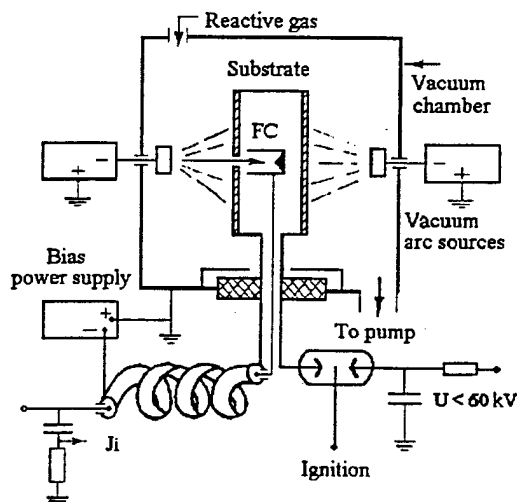

Fig. 8. Scheme of the source for combination of PVD and metal PIII by a high power metal ion beam.

Unlike the other authors [11], we have come to the conclusion that PVD and surface modification by HPIB is a promising combination. We make use of metal plasma density of $D_p = 10^{12} - 10^{13}$ cm^{-3} generated by a vacuum arc at $I_{arc} = 100-2000$ A, and a low induction power source with $U_{accel} < 60$ kV which is periodically (one pulse in 0.5-3 min) switched on between the target and the plasma source. HPIB generation with $I_i < 200$ A, $t = 1-3$ µs takes place through alternation of HPIB and PVD, and vice versa without a time break (fig. 2b). Short pulse mode makes it easier to control the ion current density on the targets located on the potential electrode by using inductive insulated circuits.

3. APPLICATION OF *TAMEK* SOURCES TO SURFACE MODIFICATION

TAMEK source provides HDI, as other well known vacuum arc metal ion sources [12-14], but has a wider range of applications [4,9,10,15,16]. Many element depth profiles and structure modifications obtained are shown in the reviews [4,9].

Samples to be treated can be placed into the vacuum chamber without special preliminary preparation, e.i., they may be only purified from dust and other surface pollution by benzene.

TAMEK source is effective for IBAD treatments. Gradual coating with new metal layers decreases the loss of compounds formed, causing the increased ion concentration and depth of mixed layers at low T<200 °C surface temperature, including elements insoluble under equilibrium conditions. Carbon presence on the surface increases the depth of mixed coatings up to 3 µm due to decreased surface sputtering by HDI.

Coatings with a mixed content of TiN, TiC, TiO (Fig. 9) are formed by IBAD of Ti ions in oil pumping vacuum with additional nitrogen pressure. In these coatings the nitrides TiN and Ti_xN_{1-x} (where x>0.5) and the phases $Fe_{16}N_2$ formed by the interaction of nitrogen with the substrate, and carbonitride $Fe_2Ti(N,C)$ are discovered. Such mixed TiO, TiC, TiN coatings play an important role in the improvement of mechanical, tribological, electrical, electrochemical and other properties, especially as antifriction coatings for mild oxidative wear mechanism.

We have estimated that coatings from mixed TiN+TiC+TiO phases may be useful in the majority of applications for improving wear (fig. 10), friction, corrosion resistance. Such mixed coatings include as hard phases such as TiC, TiN as more mild substratum. In the case of hard, and, as a rule, brittle, coatings such as pure TiN or TiC the hard particles amerged on the surface during wearing play a role as abrasive that increases the wear of the parts. In the mixed coatings the small, 10-300 nm,
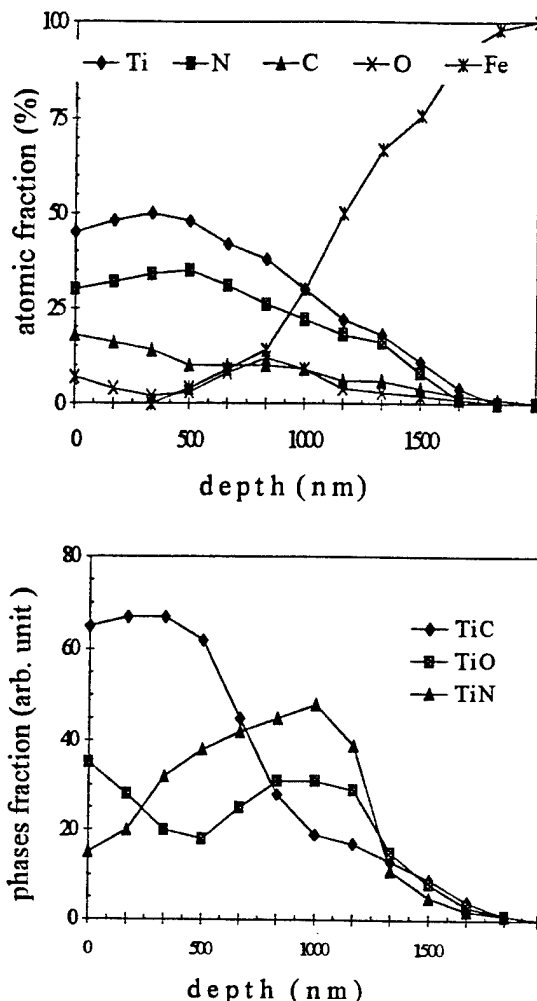

Fig. 9. a), elements (AES), and b), phases (SIMS) profiles of Fe target after IBAD of Ti ions in 15 min at $U_{accel} = 60$ kV under additional nitrogen atmosphere $P = 3*10^{-4}$ Torr.
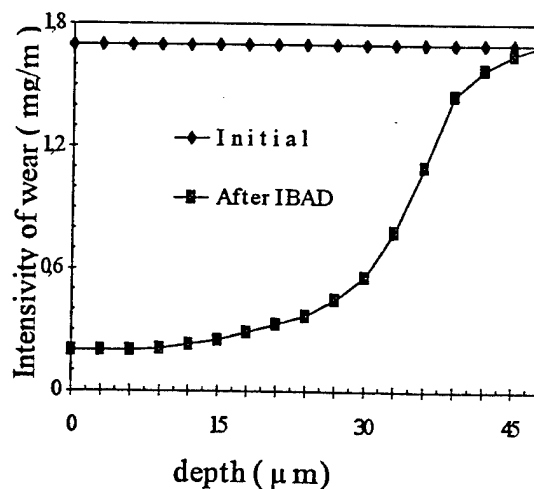

Fig. 10. Intensity of wear of Steel 45 treated as for fig. 9, versus depth of wear.

hard phases are located in the more mild substratum. Hardness of such mixed coatings may be more lower, but wear resistance is higher.

After the same treatment as mentioned on fig .9, the total thickness of the modified Ti-glass layer is found to be 400 nm [15,16]. The coating loses contact rather with certain parts of the glass substrate than along the glass-coating interface. Such coatings can be used for decoration purposes, and Al coatings are also used as mirrors for powerful lasers with high (up to 5 J/cm^2) energy input.

For ceramics like BN, AlN, surface resistivity-σ_s is reduced from the initial $\sigma_s=10^{17}$ OhM by 2...15 orders as the dose of C$^+$ ions with $E_i=60$ keV is increased from 10^{13} to 10^{17} ion/cm^2. The surface coatings are thermostable up to T=1700 ^{o}C. Such thermostable coatings are used in high voltage technology for the distribution of electric field over the insulator surface, in high temperature plasma devices, and can be used in production of resistors with low temperature resistance coefficient.

The erosion resistance of electric contacts including relay contacts, switch converters, contactors and switchboards, and also electrodes of high-voltage switches is increased by IBAD treatment.

TAMEK-M sources are employed to increase the microhardness (2-4 times) of subsurface layers up to 100 μm in depth, including high-strength materials such as WC. The desired effect achieved with energy input into the surface equal to dW=1-5 J/cm^2 (compared with dW=1 kJ/cm^2 for HDI and IBAD) permits HPIB to be used for treatment of precision and small size items, e.g., drills with diameter smaller than 1-3 mm [4,9,10]. The same result can be achieved by combining PVD and HPIB irradiation. In this case, HPIB without adding a large amount of new atoms into the surface, intensifies the plasma-chemical synthesis at low substrate temperature and coating-substrate atoms interdiffusion, simultaneously increasing the subsurface layer microhardness. In such a way it is possible to form coatings with a good adhesive, and with the total thickness up to several millimeters.

Besides the above applications TAMEK sources can be used successfully in conventional application fields of ion implantation and physical vapour deposition, e.g., in textile, paper, plastics, food, aeronautics and space industries, medical sector, etc. As a rule, service time of treated parts is increased by 2-15 times, but it is much longer for parts whose service time depends on corrosion and wear resistance, such as notching dies, disk milling cutters, trimming knives, blades of aviamotors, valves from a cryogenic and other compressors, relay and other contacts. The most attractive examples here are tools used for shaping, cutting, and piercing of plastics, papers, synthetic fibers, soft tissues and similar materials [1,4,9,10].

4. CONCLUSIONS

This short review has demonstrated that using unique properties of vacuum arc to generate metal ions it is possible to construct metal ion accelerators with broad range of parameters. Improved coating adhesion with easy sample preparation and modular design of the TAMEK sources make they convenient for industry applications. Vacuum units can thus become versatile and capable to implement surface modifications by HDI, IBAD, HPIB and metal PIII, or electron irradiation. So, it seems that vacuum arc sources such as TAMEK can occupy an important position on the technological market of devices for surface modifications by ion, plasma and electron beams.

At present, we determine a lower level for accelerating voltage which will be suitable for receiving effects described in this review. Sources with a lower voltage will be more suitable for industry applications.

5. REFERENCES:

[1]. Proc. Intern. Conf. on Surface Modification of Metals by Ion Beams, Japan, Kanazawa, 1993. Surface and Coating Technology, volms 65 and 66 (1994)

[2]. A.I.Aksenov, N.G.Pankovetz, and A.M.Tolopa, Prib. Tekn. Eksp. 3(1987)139.

[3]. A.M.Tolopa, Rev.Sci.Instrum., 65(4)(1994) 1322.

[4]. A.M.Tolopa, Rev.Sci.Instrum., 65(10)(1994) 3134.

[5]. A.I.Aksenov, S.A.Lukovnikova and A.M.Tolopa, Patent USSR (Author Certificate) # 1457446 from 2.12.1986.

[6]. A.I.Aksenov, D.A.Noskov and A.M.Tolopa, Patent USSR (Author Certificate) # 1419495 from 2.12.1986.

[7]. G.S.Kazmin, L.N.Orlikov and A.M.Tolopa, Patent USSR (Author Certificate) # 1494835 from 27.02.1987.

[8]. D.A.Noskov and A.M.Tolopa, Patent USSR (Author Certificate), # 1517376 from 10.04.1987

[9]. A.D.Pogrebnjak and A.M.Tolopa, Nucl.Instrum. and Methods. B52 (1990) 25.

[10]. A.M.Tolopa, Mat.Res.Soc.Symp.Proc., 316 (1993)1059.

[11]. Abstract of Intern. Workshop on Plasma Immersion ion implantation, Australia, 12-15 February, 1995.

[12]. I.G.Brown, Rev.Sci.Instrum., 65(10)(1994) 3061.

[13]. A.I.Ryabchikov, S.V.Dektjarev and I.B.Stepanov, Rev.Sci.Instrum., 65(10)(1994) 3126.

[14]. S.P.Bugaev, A.G.Nikolaev, E.M.Oks, P.M.Shanin and G.Yu.Yushkov, Rev.Sci. Instrum., 65(10)(1994)3119.

[15]. S.M.Duvanov, A.P.Kobzev and A.M.Tolopa, Nucl.Instrum. and Methods., B85 (1994) 264.

[16]. S.M.Duvanov, A.P.Kobzev and A.M.Tolopa, in Ion Implantation Technology-94, S.Coffa et.al., (eds.), Elserier Science B.V. (1995)741.

PULSED-PERIODIC ELECTRON -
- ION SOURCE "DRAKON"

The source is based on the use of a grid plasma emither with a low-pressure constricted arc. The source is mounted on a vacuum system providing pressure of 10^{-2} Pa and includes a self electron-ion source of 500 mm dm and 500 mm length and the unit of isolation transformers with $500 \times 500 \times 400$ mm³ dimensions. Voltage can be applied to the accelerating gap from standard high-voltage rectifiers of the required power.

BASIC TECHNICAL CHARACTERISTICS OF THE SOURCE "DRAKON"

	Electron operation	ion one
beam diameter	200 mm	200 mm
Energy of accelerated particles	2-20 keV	2-20 keV
Beam current in a pulse	10-100 A	0,1-1 A
Pulse duration	50 s	50 s
Pulse repetition	1-1000 s⁻¹	1-1000 s⁻¹
Average beam power	(up to)20 kW	500 W
Inhomogereity of beam density distribution	15%	15%

The main characteristic features of the source are:

- The use of three plasma generatirs with cold cathodes operating to a common hollow anode.
- Habbilization of plasma emission boundary by a fine-mesh metal grid.
- Possibility of opertion in conditions of a considerable gas separation from the details treated.
- Possibility of a wide rearrangement of basic paramerters.

All the features pointed out allow the source application in such technological processes as low-inertir heating and degasing of details, ion cleaning and activation of details, surfaces, as well as under cyclical action of electron or ion beams.

Using the source in cocperation with the Republic Engineering Center on Stregthening Details of Mashines and Mechanisms, the technoligy was developed for covering 3H/3mm adherence film polyamid with ~ 50 μm thick copper layers. The tecnoligy can be utilized when constructing flexible multi-layer printed circuit boards, for transported electronic units etc.

Akademichesky Ave. 4, Tomsk, 634055 USSR
Electronic mail: Root@hcei.tomsk.su
Phone (o) (3822) 258-544
Telex: 128114 TAKT SU
Fax (3822) 259-410

Nuclear Physics Institute
Engeneering Physical Center

Change of Mechanical-and-Physical Properties of Metals at the High-Power Ion Beam Effect

1. Brief Description of the Scientific Achievement

The phenomenon of changing the physicochemical and stress-strain properties of the surface layers in metals and alloys under the influence of high-power ion beams with nanosecond duration, power density of 107-108 W/cm², power of 105-106 eV has been found.

The mechanism of this interaction are being studied theoretically and experimentally. It is found that various processes accompanying the beam effect allow to change metal characteristics at the depth exceeding the length of the free ion path in metals considerably.

This effect has been discovered experimentally in 1980, and later it has been confirmed on the number of metals. Research method of interaction between the high-power ion beam and metals have been worked out, approved, and now they are used.

4 high-power ion beam sources have been made for research purposes.

2. Application of the Achievement in the Solution of Scientific and Applied Problems

Using the described effect, the following problems can be solved:
•the controlled change of the physical, structural characteristics of the surface layer of metals, semiconductors, ceramics under the power-producing effect of high-power density;
•the hardening of tools and different machine parts;
•high rate deposition of thin metal films, components, etc.;
•the beam erosion staining;
•the cleaning of the surface layer for various purposes, solving the number of other applied problems.

The available experimental base includes:
- "Luch", "Vera", "Temp", ÝÑÃ-2,5 accelerators;
- analytic equipment for surface studying;
- mathematical program of the calculating the beam energy with various parameters.

Investigation are supposed to extend to the following problems:
- short pulse implantation;
- production of new accelerators with 1-50 kW energy;
- fundamental and applied research on obtaining and application of non-equilibrium plasma;
- obtaining of the quantum-sized multilayer coverings, diamond-like films; making-up the set with more perfect equipment.

It is possible to obtain new materials with improved operating characteristics, as well as scientific information on the surface layer of materials.

Nucl.Phys.Institute, 634050 Tomsk, Russia
Tel (382-2) 440097   Fax (382-2) 440812
E-mail: REMNEV@tsinph.tomsk.SU
Dr. Remnev G.E., director EPC

Nuclear Physics Institute
Engeneering Physical Center

Technological accelerator "Temp"

The accelerator can be used in machine-building for increasing of wear resistance of tools and other parts, for improving of adhesion of different coatings, increasing of material resistance to corrosion. Also it can be applied in other branches of industry for deposition of films and conducting layers in ceramics, for cleaning from impurities, etc.

Pulsed high-current ion accelerator has a chamber, which provides automatic changing of the patterns under hermetic conditions. Under the action of high-power ion beam, physical and chemical properties of materials' surface layers are changing.

1. Technical characteristics:

Ion energy	300 keW;
Pulse duration	$5 \cdot 10^{-8}$ s;
Current density on the pattern	40-150 A/sm^2;
Pulse frequency	0.3 Hz;
Surface area treated by 1 pulse	40-100 sm^2;
Productivity	1 m^2 per hour;
Maximum dimensions	2500 x 1650 x 1000 mm;
Input power	5 kW;

2. Distinctive features

Comparable to the pulse lasers, which are applied for the some purposes, the accelerator has efficiency some dozen large than pulse laser afficiency, increased beam size and ecological cleaness.

3. Consumers

The consumers are enterprises of machine-building industry and tool production, developing new technologies in machine-building industry research institutes.

4. Realization

The pilot acceleration is developed and tested in laboratory conditions. The industrial realization of the accelerator includes:
- accelerator shipment;
- treatment of different products;
- technological license;
- development of new technologies.

In dependence on transfering on "know-how", the price varies from 100 000 to 300 000 USD.

Nucl.Phys.Institute, 634050 Tomsk, Russia
Tel (382-2) 440097   Fax (382-2) 440812
E-mail: REMNEV@tsinph.tomsk.SU
Dr. Remnev G.E., director EPC

NUCLEAR PHYSICS INSTITUTE
ENGINEERING PHYSICAL CENTER
CHARGED PARTICLES ANALYTICAL LAB

The accelerated ion beams from Cyclotron U-120 and electrostatic generator EG-2.5 are used for:

- a certification of solid probes by destructive CPAA trace determination of C, N and O in wide various of high-purity materials with the detection limits of 1, 3 and 10 ppb, respectively;

- a certification of solid probes by nondestructive CPAA and HIAA trace determination of light elements and isotopes with a detection limit of 0.1 ppm for ^2H, Li, Be, B, F, Na, P, S. and 1 ppm for K and Ca, and 10 ppm for C, N, O;

- a nondestructive CPAA , HIAA /HIIGE determination of stoichiometric ratio of the chemical compounds and of isotopic ratio of elements with the relative standard deviation of 0.001-0.005;

- a nondestructive concentration depth profiling of Be, B, C, N, F, Na and Al by PIGE, the depth resolution is about n(10-100)A;

- a certification of mineral raw materials by CPAA-technique for directly isotopic analysis of ^{187}Os in 0.5 gram-probes: a determination limit of ^{187}Os in MoS_2 is 0.1 ppm and relative standard deviation is 0.05-0,1 for n(1-0,1) ppm ^{187}Os contents;

- a study of mass transfer processes in solids by radio-labelling with radionuclides of ^{11}C, ^{15}O, ^{13}N, ^{18}F and ^{24}Na implanted in testing probe via nuclear recoil without irradiation of probe from incident heavy ion beam. Yields of implanted radionuclides are being reached n(1-100) microCu;

- a directly HIAA/ERDA-determination of D /H ratio are used for study of hydrogen isotopic ratio in biological and environmental microprobes: the detection limits are about 1 at.ppm D and n100 at. ppm H relative standard deviation is less than 0.02.

Nucl.Phys.Institute, 634050, Tomsk, Russia
Tel: (3822) 440097
Fax: (3822) 440812
E-mail: remnev@ifc.tiasur.tomsk.su

Dr. Remnev G.E., EPC director
Dr. Ryzhkov V.A., chief of CPA Lab

The new type of electrical discharge in vacuum

The new type of pulsing electrical discharge is experimentally established, which has not been described earlier.

With its origin it is the volume discharge in constant electrical field in evaporation of material of electrodes, arising in initial vacuum $P<10^{-5}$ with help of auxiliary spark.

The main parameters of discharge:

i - discharge current.. 1 - 300 A

U_z - voltage on electrodes .... 200 - 2000V

$P_z = i \cdot U_z$ - power of discharge .... 2 10^2 - 6 10^5 W

i - current pulse duration .... 10^{-4} - 10^{-2} s

$$\eta = \frac{(Pz \; \hat{\imath}) \; 100 \%}{\dfrac{CU^2}{2}}$$ - efficiency... 20% - 50%

The possible applications of discharge:

1. Drawing of metal covers in conditions of high vacuum. The speed of filling at use of volume discharge in vacuum is 200 times higher in comparison with magnetron method and is 0,1 *mkm/s* at average capacity of rectifier of 1 *KW*. The distance between substrate and filling element is 15 *cm*.

2. Producing of pulsing ion beams of metals in conditions of high vacuum. The concentration of ions in vacuum discharge can reach 10^{16} *cm^{-3}* and higher in volume about 1 *cubic cm*, that allows to receive ion beams of maximal intensities, limited only to own volumecharge.

Persons interested in additional information with the purpose of use of volume vacuum discharge, can apply to the author, phone# (095)-948-81-82 or e-mail: *penates@glas.apc.org*

The author - Boris N. Mashkovtsev

Comparative characteristics
of various electric discharges

type of discharge	voltage on electrodes	discharge current	power evolved on discharge	primary pressure
	V	A	W	torr
normal glow discharge	100	$10^{-4} - 10^{-2}$	0,01 - 1	$10^{-3} - 10^{1}$
abnormal glow discharge	500	1	500	$10^{-3} - 10^{1}$
arc discharge	30	100	3000	любое
glow discharge in magnetic field	500	1 - 5	500 - 2500	$10^{-3} - 10^{1}$
discharge in magnetic field: in plasma, created by superhigh frequency source $P_{shf}=800$ W	continuous operation			$10^{-1} - 10^{1}$
	2000	0,25	500	
	pulsed operation		$\tau_p = 10^{-6}$ c	
	6000	5	$3 \cdot 10^{4}$	
volume discharge in vacuum	pulsed operation		$\tau_p = 10^{-4} - 10^{-2}$ c	10^{-6}
	500 - 2000	1 - 300	$5 \cdot 10^{2} - 6 \cdot 10^{5}$	

The Raduga multipurpose ion/plasma source for surface modification of construction materials

A.I. Ryabchikov, N.M. Arsubov, N.A. Vasilyiev and S.V. Dektyarev

Nuclear Physics Institute, PO Box 25, 634050 Tomsk, USSR

In this article a repetitively pulsed vacuum arc ion/plasma source for property modification of near-surface layers in construction materials is described. The Raduga ion source provides both high concentration implantation and optimum two-element implantation. These advantages can be achieved by using not only pure single-element or mixed fluxes, but also pulsed beam sequences with controllable composition and energy of each ion species. Another unique feature of the source is its ability to generate a sequence consisting of ion beam and plasma stream pulses. Switching between ion irradiation and plasma deposition can be done from pulse to pulse, within each pulse, or after accumulation of a required dose. Two-element operating conditions provide the possibility of compensating for sputtering during implantation by neutral atom and plasma deposition. The technological capabilities of the source are: (a) single-element ion implantation; (b) multi-element implantation using compositional cathodes; (c) multi-element implantation with beam composition and ion energy controlled during irradiation and even from pulse to pulse; (d) high-concentration implantation; (e) thin-film deposition; and (f) thin-film deposition under ion irradiation conditions.

1. Introduction

In recent years, sources of accelerated ion beams as tools for modifying the physical and chemical surface properties of different materials have become a great interest. Numerous fields of applications of ion implantation for improving the surface properties of metals and alloys as well as other construction materials have required a substantial increase in irradiation dose, up to 10^{17}–10^{18} ions/cm^2, hence the development of high intensity ion sources [1]. Among the ion sources in existence and under development, the repetitively pulsed vacuum arc sources rank highly [2–4]. These sources can produce high intensity ion fluxes of metals as well as metals and gases together. The Raduga ion source can provide beams of composition and energy-controlled ion fluxes for multi-element implantation. The operation of the repetitively pulsed vacuum arc sources under ion/plasma conditions allow thin film deposition to be performed, as well as ion bombardment. The high-concentration implantation operation, with surface ion sputtering compensation using the deposition of low energy ions and neutral atoms, is of special interest. Within this regime any implanted species concentration in different materials can be obtained with a simultaneous substantial reduction of irradiation dose [5].

This report presents results of the development and investigation of the multipurpose ion plasma source Raduga IV, suited for the realization of all regimes of ion material treatment mentioned above.

2. Source design and operation

The Raduga IV ion plasma source is composed of a metal vapor vacuum arc plasma source, a plasma shaping region and a set of grids for ion extraction. The source is placed in a vacuum chamber with a base pressure of less than 10^{-4} Torr. Plasma generation in the source is due to cathode material evaporation and ionization by the cathode spot of the vacuum arc. Plasma formation occurs during the existence of the cathode spot. Generally, at pulse arc discharge durations of some hundreds of microseconds and discharge currents of 100 A, the cathode spots persist for the duration of the discharge pulse on cathodes which are made of fusible materials. However, for low discharge currents of about 10 A and, in particular on refractory cathodes such as Ta, W, Mo and others, the lifetime of the cathode spot is limited to some tens of microseconds. This problem is resolved in the Raduga IV.

The cathode of the source is designed to be compound. Each of the cathode elements has a system of independent trigger electrodes. The ceramic insulators are installed between cathode and trigger electrodes. The initiation of arc discharge is caused by breakdown on the insulator surface between the cathode and trigger electrode.

The anode of the source is a cone with a 20 cm diameter base situated on the same axis as the cathode. The faced anode (i.e., base of the cone) is covered by a grid. The grid is fabricated from a stainless steel disk in

which 8 mm diameter holes are drilled. The distance between the grid and the cathode is adjusted for the cathode material and the angular divergence of the generated plasma plume. After initiation of the discharge between the cathode and the trigger electrode the plasma plume expands towards the anode. The pulse duration of the trigger is chosen so that during the trigger discharge, the plasma puff approaches the anode region. As a result, the discharge between the cathode and anode is initiated. The polarity of the trigger pulse is such that the cathode spot is initiated on the cathode only. The trigger pulse can be applied to either of two trigger electrode systems and the plasma is generated from the corresponding cathode material. Thus we see how to control the ion species during multi-element implantation. The ion extraction system consists of a set of three grids. Each grid has 250 holes. The hole patterns of the grids are well aligned. The middle grid is the electron suppressor and is held at approximately -1 to -2 kV. The electron suppressor prevents the flow of secondary electrons back across the accelerating gap. The third grid is connected to ground. The bias voltage for the grid is formed using an additional winding of the pulse transformer.

3. Power supply of the source

Fig. 1 shows a schematic diagram of the source. The formation of pulse voltages for the arc discharge supply and ion acceleration is accomplished using the pulse transformers T1, T2 and T3. The primary windings of the transformer arc are fed from the corresponding pulse-forming LC-lines.

Since the principles of generation of both the accelerating voltage pulse and the arc discharge voltage pulse are similar, let us consider just one of the systems in detail. The filter capacitor C_f is charged from the ac mains of 380 V through a three-phase autotransformer and rectification system. When triggered by the clock pulse generator, thyristor D-10 is closed and the pulse line LC is charged up to a voltage of 1.7 to 1.9 V through a charging inductance. While the D-10 thyristor is suppressed (at the current feedback of secondary carriers), the IT-2 pulse transformer signal will be delayed for the duration of the vent property regeneration using the D-10 circuit C_3D_9. After switching thyristor D-11, the pulse-forming line is connected to the primary winding of pulse transformer T1. The primary winding utilizes a variable number of turns to generate the pulse accelerating voltage. By feeding a control signal to a suitable thyristor, D-11 or D-12, the pulse-forming line is switched a certain number of primary windings of the transformer. By varying the number of primary turns, it is possible to control the magnitude of the accelerating voltage. The supply system can provide a variable accelerating voltage from pulse to pulse. Thus the voltage can be varied in steps of 10 kV from 20 up to 100 kV. As has been noted above, the supply system of T2 and T3 pulse transformers operates analogously. The maximum output voltage of the transformers is 10 kV. The two terminals of the secondary windings of transformers T2 and T3 are connected to the anode and the corresponding elements of the cathode, respectively.

By switching thyristors D-11, D-12 and D-13, D-14, we can connect in series the transformers to the circuit of the pulse-forming line supply and thus form ion or plasma fluxes of one or another cathode material. Thus the switching of thyristors T_1, T_2 and T_3 provides control of both the species and energy of the ions. Pulse transformers T2 and T3 provide both the initiation of the discharge between the cathode and the trigger electrode and the arc current supply. While the pulse voltage originates at the secondary winding of one of the

Fig. 1. Schematic diagram of the Raduga ion/plasma source.

transformers, the C_1 and C_2 capacitors are charged. The ratio of capacitances chosen, $C_1 \ll C_2$, provides a regime of preferable release of the C_1 capacitor voltage. When the C_1 capacitor voltage is adjusted to the breakdown potential, breakdown occurs between the cathode and trigger electrode across the surface of the ceramic insulator. As a result, a low-voltage arc discharge with a cathode spot is generated. The U_{C1} voltage drops to a value corresponding to the voltage drop of the arc discharge. The capacitor C_2 is charged through a plasma channel. Plasma formed by the cathode spot expands from the cathode towards the anode. The basic arc discharge is ignited between the cathode and anode, and is of a duration determined by the pulse-forming line. Note that the burning voltage of the vacuum arc discharge depends on the cathode and anode material as well as their geometric sizes, and varies in the range of 20–150 V. Arcing between the cathode and trigger electrode ceases when the voltage drop across capacitor C_2 exceeds that of the arc discharge between the cathode and anode. The elements of the capacitor charging circuit are chosen so that when the plasma approaches the anode, U_{C2} exceeds the arc voltage drop between cathode and anode. At the same time, diode D-7 prevents the reduction of the discharge voltage of C_2. The current of capacitor C_2 is stopped from flowing through the trigger electrode. Thus there is a possibility of the cathode spot forming a pure ion beam from the cathode material only.

It is important to note some more features of the arc discharge triggering and supply system. An accidental extinction of the arc between the cathode and anode leads to a sharp voltage increase. The capacitors C_1 and C_2 start charging again with subsequent breakdown across the insulator surface and re-initiation of the arc discharge between the cathode and anode. Multiple re-initiation of the arc discharge will occur while the difference in the transformer and C_2 capacitor voltages is high enough for breakdown of the ceramic insulator surface. C_2 capacitor discharge occurs through an additional electric circuit between the pulses. The pulse durations of the accelerating voltage and the arc discharge are adjusted by discrete changes in the number of sections in the pulse-forming lines. The bias voltage for the suppressor grid is formed using an additional winding of the pulse transformer T_1.

4. Operational conditions of the Raduga IV ion/plasma source

4.1. Repetitive pulsing

Under conventional repetitively pulsed conditions, the source forms a flux of accelerated ions of the conducting material. Pure metals and alloys as well as gas-containing compounds may be used as cathodes.

The mean energy of the accelerated ions is determined by the accelerating voltage and the mean ion charge state. The latter depends, in turn, on the cathode material and varies from 1 to 3 [6]. The pulse duration of the accelerated beam in the Raduga IV can be varied over the range 50 to 200 μs. The maximum pulse repetition rate is determined by the charging time, which in our case amounts to 1.2 ms. The supply system developed for the source has been tested with a repetition rate of up to 500 s^{-1} into a dummy load. Reliable source operation with an ion beam current of 0.5 A has been achieved with a frequency up to 100 s^{-1}; with further increase of the repetition rate, one can observe overheating of the cooled elements of the source construction. The problem of modification of the cooling system is currently under consideration.

4.2. The formation regime of the species and energy-controllable ions for two-element implantation

In accordance with the expected mean ranges of the two ion species in the target material and the mean ion charge state, the required accelerating voltages are selected. Control of the accelerating voltage and the cathode material is done in synchronism.

The D-11, D-12 and D-13, D-14 thyristor triggering in pairs is performed by the control system. The durations of the pulse-forming lines approximately coincide. The source control system allows the irradiation dose ratio to be adjusted for different ion species. Using this method, both the ion implantation of metals and metal and gas implantation may be carried out. In the second case one of the cathodes is manufactured from a compound, gas-containing, conducting material. Subsequently, by combining the different distribution profiles of the different species, or from other conditions, the required source operation regime is defined.

4.3. High-concentration implantation conditions

High-concentration implantation is accomplished using ion sputtering compensation of a target by ion plasma and neutral atom deposition [6]. This can be done by a combination of ion implantation and plasma deposition, i.e. ion/plasma operation conditions of the source. Plasma deposition occurs when the accelerating field is not switched on, and the free-expanding plasma is deposited onto the target. According to the specific task or the need to form an implantation distribution profile with high concentration below the surface (at the ion range depth) or near the surface for sputtering compensation of the surface layer, plasma deposition is used with the composition coinciding with the target material or the implanted ion species. In the latter case, the additional dopant introduction from the surface is done by recoil implantation. In this case the source

operating conditions of high-concentration repetitively pulsed implantation can be varied from ionic to plasma after a given irradiation dose, from pulse to pulse or within a pulse. In the latter, the pulse duration of the arc discharge exceeds that of the accelerating voltage. Thus this excess is defined by the geometric parameters of the source, such as the distance to the target, the degree of ionization of the cathode material, and the coefficient of target sputtering. The arc discharge duration in the source is adjusted from 50 μs up to 1000 μs, while the pulse duration of the accelerating voltage is controlled in the range of 50–200 μs.

4.4. Conditions of thin film deposition

This can be accomplished by single and multi-element operation conditions of the source, without an accelerating voltage.

4.5. Conditions of thin film deposition with ion bombardment

This can be accomplished when the repetitively pulsed deposition rate for coating exceeds that of surface ion sputtering under implantation.

5. Conclusions

The Raduga IV repetitively pulsed vacuum arc ion source described here provides a means for the genera-tion of both accelerated ion fluxes and neutral plasma streams, with control over ion species and energy. Moreover, the Raduga apparatus may be used for conventional repetitively pulsed implantation conditions and for high-concentrations, as well as for two-element implantation. The multipurpose Raduga IV ion source opens up a wide range of possibilities for the investigation of the technological processes of ion/plasma modification of material properties.

References

[1] I.G. Brown (ed.), Proc. Int. Conf. on Ion Sources, Berkeley, CA, USA, 1989, Rev. Sci. Instr. 61 (1) (1990) part 2.
[2] I.G. Brown, Nucl. Instr. and Meth. B37/38 (1989) 68.
[3] N.M. Arzubov, G.P. Isaev and A.I. Ryabchikov, Izvest. Vuzov Fizika 8 (1989) 68.
[4] N.M. Arzubov, G.P. Isaev and A.I. Ryabchikov, Prib. Tech. Exp. 5 (1988) 28.
[5] A.I. Ryabchikov, V.M. Zavodchikov, R.A. Nasyrov, V.V. Sohoreva and A.A. Yatis, Materialy Vsesoyuzn. Konf. po Ionno-luchevoi Modifik. Mater., Kaunas, 1989, p. 122.
[6] I.G. Brown, The Physics and Technology of Ion Sources (Wiley, New York, 1989).
[7] A.I. Ryabchikov, R.A. Nasyrov, Yu.P. Sharkeev, G.V. Puchkareva and G.I. Shahtmeister, Materialy Vsesoyuzn. Konf. po Cilnotochnoy Electronic, Sverdlovsk, 1990, no. 2, p. 149.

Repetitively pulsed, high-concentration implantation

A.I. Ryabchikov and R.A. Nasyrov

Nuclear Physics Institute, 634050, P.O. Box 25, Tomsk, USSR

We report our work on high dose ion implantation, emphasising the limiting concentration of implanted species that occurs because of surface sputtering. We present experimental results showing that during repetitively pulsed implantation, sputtering of the surface layer can be compensated for by simultaneous neutral atom or low energy ion deposition, thereby arbitrarily high alloying levels can be reached. Experimental data on pulsed implantation of Hf, Tb and Ni into Al, Ti and Fe demonstrate that alloy layers with implanted species concentration of up to 100% can be formed. With implantation of 100 keV Ni into Al and with sputtering compensation and radiation stimulated thermal diffusion conditions, an alloy layer of thickness 0.5 μm and with a Ni concentration of approximately 77 at.% has been obtained. In this paper we review our data on concentration profiles, relating these to the alloy layers and also showing that the layer depth considerably exceeds the ion range. We discuss and generalize our results for high concentration implantation, and consider potential applications of the technique for the modification of surface properties of different materials.

1. Introduction

The properties of the alloyed surfaces of different materials are determined by both the alloying dopant content and its concentration. The use of conventional alloying technology (volumetric metal alloying) can be disadvantageous because of the cost of alloying dopants, especially when the total operation lifetime is determined by the surface-and near-surface layer properties.

There is also a limitation in that some compounds cannot be obtained using ordinary metallurgical techniques. Nevertheless, the fact that chemical, mechanical and other material properties are determined by the impurity concentration and its compounds has stimulated a search for methods for increasing the concentration.

Ion implantation is an effective method for alloyed surface layer generation with an impurity concentration of several tens of atomic percent [1–3]. The saturation level of the dopant concentration in the metal surface has been exceeded by more than an order of magnitude [4] over that obtained by using, for example, borating, cementation and nitriding. At the same time, with normal ion implantation there is a limiting level of the obtainable concentration that is determined by ion sputtering of the surface material layer. Methods for increasing the dopant concentration include the use of surface coatings with low sputtering factor (carbon, oxides), implantation through a layer of material de-

posited onto the target and the achievement of composition due to atomic mixing during ion bombardment [5].

The concentration of the alloying species in a sample can be increased by a judicious combination of implantation processes and coating deposition in both continuous and repetitively pulsed irradiation conditions [6–10].

The present work investigates a method of high-concentration implantation into metals using repetitively pulsed ion implantation and sputtering compensation of the sample surface by low-energy ion and atom deposition.

2. Experimental procedure

These investigations were performed with the Raduga repetitively pulsed ion source [11–13]. The source operating concept is based on plasma generation from a cathode material by a repetitively pulsed arc discharge in vacuum followed by ion extraction and acceleration.

Regeneration of the sputtered layer was accomplished by operating the source without the accelerating voltage. The optimum version of high-concentration ion implantation was attained using a combination of accelerated ion irradiation and plasma deposition in each pulse. In this case, the duration of the plasma forming vacuum-arc discharge exceeded the pulse duration of the accelerated ion beam. Surface regeneration due to deposition occurred immediately after surface sputtering by the ion beam during implantation.
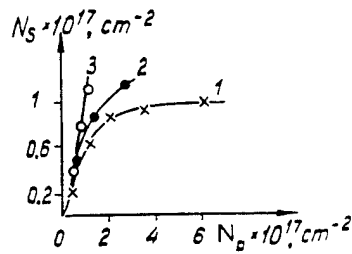
Fig. 1. Implanted dose dependence on iradiation dose by Tb-ions under different conditions: 1 – conventional implantation; 2 – combined with deposition; 3 – optimum conditions of the implantation and deposition.

By varying the relationship between the pulse durations of the arc discharge and the accelerating voltage, we could control the effective sputtering factor.

Multielement operation of the source [14,15] provides the possibility of varying the composition of the ion beam and of the film deposited during the repetitively pulsed combination of implantation and surface regeneration. In our experiments, two operating regimes of the source were investigated. In the first case, the same cathode material was used for implantation and coating deposition. In the second case, during implantation of a particular ion species, surface layer regeneration was accomplished using a cathode material corresponding to the element of the initial sample material.

3. Results

Fig. 1 shows data on Tb accumulation in iron during implantation under different conditions. As mentioned above, under conventional conditions when the implantation is accompanied by surface layer sputtering (fig. 1, curve 1) a saturation is reached at an irradiation dose of $(1-3) \times 10^{17}$ cm^{-2}. Increasing the ion irradiation dose does not lead to a surface concentration increase.

Implantation under partial compensation of sputtering is accompanied by an increase in both the surface concentration accumulation rate (curve 2) and its absolute value. Under optimum irradiation conditions,

Fig. 3. Conceentration profile distributions of Hf-implanted α-Fe at different implanted doses of $N_\square$, cm^{-2}: 1 – 2.3×10^{15}; 2 – 2.4×10^{16}; 3 – 2.4×10^{16}; 4 – 9.3×10^{16}; 5 – 2.4×10^{17}; 6 – 9.3×10^{16} (a) and dependence of the distance up to concentration maximum of the corresponding profiles on implanted ion dose under conventional implantation (b).

when sputtering is completely compensated by Fe-deposition, the implanted terbium dose is practically equal to the irradiation dose (curve 3).

This version conforms to the full ion capture conditions. It is important to note that during high-concentration implantation the dopant accumulation rate at large irradiation dose rises by S-times, as can be seen from fig. 1. When the sputtering factor is large, the required material ion beam treatment time will be decreased.

An investigation of Ti-alloy target for implantation and deposition using Tb-cathodes has been used. Fig. 2 illustrates the concentration depth distributions for different elements under two different conditions. Tb, Ti and preliminarily implanted Mo were measured by Auger-electron spectroscopy.

These distributions show an increase in the Tb-film in the treatment process by preferential deposition (fig. 2). The Tb-film growth can be seen from the position of

Fig. 2. Depth distribution of the Tb, Ti and Mo concentrations during irradiation under preferential Tb-deposition (a) and under optimum conditions of implantation and deposition (b).

the previously introduced Mo. The Mo-position indicates that the irradiation conditions were close to optimum, when the deposition rate of the Tb-layer compensated its sputtering rate. The maximum concentration obtained in this case amounted to 67.6 at.%.

The results of Hf-ion implantation into α-iron are also shown in fig. 3. The implanted species depth distribution profiles, obtained by RBS, reveal a number of specific features of high-concentration repetitively-pulsed implantation. By increasing the irradiation dose we observe the maximum displacement of impurity concentration to the surface (fig. 3). During conventional repetitively pulsed implantation, this result is explained by the influence of two factors. Firstly, with a large dose of heavy Hf the target density increases and, consequently the ion range decreases. Secondly, due to ion sputtering the substance carry over and surface boundary translation occur [1]. After an irradiation time the profile will be saturated with its concentration maximum on the surface with $N_{max} \approx N/S$, where N_{max} is the maximum impurity concentration, N is the target material atomic concentration and S is the sputtering factor.

It should be noted that the ion beam of the repetitively-pulsed vacuum arc source contains a considerable fraction of multicharged ions [16]. Thus, with low irradiation doses the concentration maximum is found to be at a depth corresponding to the ion range of the mean charge. During surface sputtering, the concentration maximum is moved into an ion distribution region with lower energy, i.e. lower charge state. The experimental dependence of distance from the surface to the profile maximum, for Hf-implantation into iron on the ion dose is shown in fig. 3. The point numerations in the figure coincide with those of the corresponding concentration profiles. This dependence was extrapolated up to intersection with the distance axis ($N_{\square} = 0$). Extrapolation to "zero dose" [17] revealed a value of ion range of 200 Å, which is in good agreement with the mean charge of the introduced ions, $\overline{Z} \approx 2.5$.

During implantation under full sputtering compensation conditions the concentration maximum displacement is influenced by the surface layer content variation only. Partial sputtering compensation must be accompanied by moderated translation of the concentration maximum to the surface (fig. 3, curve 6). When for sputtering compensation film deposition is used with content close to the corresponding ion species, so the additional maximum displacement and its output to the surface will depend on the amount of implanted dopant as recoil atoms (curve 2).

A study of α-Fe sample microstructure by means of electron transmission microscopy after Hf-irradiation at depths substantially exceeding the ion range has shown the developed dislocation material structure that is formed in a near-surface layer with thickness of some

tens of microns under conventional implantation conditions [18]. It was found that since under high-concentration implantation conditions the same dose of implanted ions may be obtained at different irradiation doses, the maximum dislocation density is correlated with the introduced impurity dose and its maximum concentration. A correlation is observed in the dependence of dislocation density and microhardness on the maximum concentration of introduced dopant. These results are evidence of the important role of static stresses arising after ion introduction into solid surface for pure metal property modification.

Ti, Ni and Fe accumulation during high-concentration implantation in Al were stidied both under low heating conditions (the sample temperature did not exceed 350 K) and the temperature variation due to pulse repetition frequency increase. Under two-element operating conditions of the ion source and sputtering compensation by aluminium deposition at low diffusion (low temperature ~ 350 K), the obtainable concentration level during implantation both for titanium and iron amounted to 70 at.% [9]. Note that a periodic irradiation temperature increase up to 673 K provides diffusion of the implanted nickel from the surface into the bulk with simultaneous decrease in its concentration in the near-surface region. Our experiments have illustrated that the combination of high-concentration implantation with sample temperature control due to beam intensity variation provides not only deep but also high-concentration alloying. The value obtained of maximum nickel concentration exceeds the limiting level of conventional implantation by more than two times (up to 77 at.%), and the alloying depth is increased by 10 times.
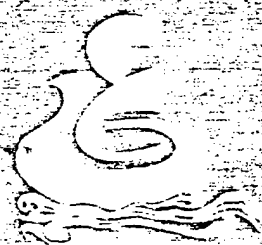
4. Conclusions

(1) Repetitively pulsed high concentration implantation, where target ion sputtering is compensated for by neutral atoms and plasma ion deposition, allows the formation of alloyed layers with arbitrarily high level of impurity concentration.

(2) At the large irradiation doses (10^{16}–10^{18} cm^{-2}) necessary for property modification of surface layers in metals, alloy and other construction materials, the high-concentration implantation technique allows the formation of the chosen impurity concentrations at substantially lower irradiation doses. It will improve the technigue productivity and reduce the specific energy expense.

References

[1] M.I. Guseva, Poverkhnost 4 (1982) 27.
[2] A.N. Didenko, and A.E. Ligachev, I.B. Kurakin Vozdeist-

vie puchkcov zar. chastiz na poverkhnost metallov i spla- vov. (Energoatomizdat, Moscow, 1987) p. 184.

[3] A.A. Nikitin, N.T. Travina, M.I. Guseva et al., Poverkh- nost 3 (1989) 132.

[4] Yu.M. Lachtin and Ja.D. Kogan. Azotirovanie stali. (Mashinostroenie, Moscow, 1976) p. 276.

[5] Z. Lian and I.W. Mayer. Jorn. Vag. Sci. Technol. 15 (1978) 1629.

[6] L. Pranyavichus. Nucl. Instr. and Meth. 182/183 (1981) 251.

[7] A.G. Pusyrevich, A.I. Ryabchikov, A.L. Shipilov and R.A. Nasyrov, Tezisy dokl. I Vsesoyuzn. konf. Modificatiya svoistv konstr. materialov puchkamizar. chast., Tomsk (1988) p. 45.

[8] A.I. Ryabchikov, V.M. Zavodchikov, R.A. Nasyrov, V.V. Sokhoreva and A.A. Yatis, Tezisy dokl. Vsesoyuzn. konf. po Ionno-luchevoi modifik. mater., Kaunas (1989) 122.

[9] A.I. Zhukova, A.I. Ryabchikov and R.A. Nasyrov, Mater. IX Vsesoyuzn. konf. Vsaimod. atomn. chast. s tevrd. telom. (MIFI, Moscow, 1989) p. 149.

[10] A.I. Ryabchikov, R.A. Nasyrov, V.A. Shulov, A.A. Stry- gin, Tezisy dokl. IX Vsesoyuzn. konf. po vsaimod. atomn. chast. s tverd. telom. Moscow (1989) p. 109.

[11] A.I. Ryabchikov, N.M. Arsubov and E.I. Lukonin, Tezisy dokl. I Vsesoyuzn. konf. Modifik. svoistv konstruk. mater. puchkami zar. chast., Tomsk (1988) p. 17.

[12] N.M. Arsubov, G.P. Isaev and A.I. Ryabchikov, Izvest. Vuzov Fizika 8 (1989) 68.

[13] N.M. Arsubov, G.P. Isaev and A.I. Ryabchikov, PTE 5 (1988) 28.

[14] A.I. Ryabchikov, Proc. Int. Conf. on Ion Sources, Berke- ley, California, USA. (July 1989) Rev. Sci. Instrum. (1990) p. 641.

[15] A.I. Ryabchikov, N.M. Arsubov and R.A. Nasyrov, Tezisy dokl. VII Vsesoyuzn. simp. po silnotochnoi elektronike, Tomsk (1988) p. 225.

[16] I.G. Brown, The Physics and Technology of Ion Sources. (Wiley, New York, 1989).

[17] I.G. Brown, Nucl. Instr. and Meth. B37/38 (1989) 68.

[18] A.N. Didenko, A.I. Ryabchikov, G.P. Isaev, N.M. Arsubov, Yu.P. Sharkeev, E.V. Kozlov, G.V. Pushkareva, I.V. Nikonova and A.E. Ligachev, Mater. Sci. and Eng. A115 (1989) 337.

Институт физики прочности
и материаловедения
Сибирского отделения
Российской академии наук

Institute of Strength Physics
and Materials Science
of the Russian Academy of Sciences
Siberian Branch

РОССИЯ, ТОМСК
RUSSIA, TOMSK

1928 — Professor V.D.Kuznetsov established Tomsk school of strength physics on the basis of Siberian Physicotechnical Institute associated with the Tomsk State University.

1979 — Professor V.E.Panin, the leader of the Tomsk school of strength physics and materials science, and his coworkers accepted an offer of academician V.E.Zuev, President of the Tomsk Division of the Siberian Branch of the USSR Academy of Sciences, to establish the department of strength physics and materials science at the Institute of Atmospheric Optics of the Siberian Branch of the USSR Academy of Sciences.

1984 — the department of solid-state physics and materials science was rearranged to the Institute of Strength Physics and Materials Science (ISPMS) of the Siberian Branch of the USSR Academy of Sciences. V.E.Panin, a corresponding member of the USSR Academy of Sciences, took charge of the Institute.

1985 — the Republican Engineering Center associated with ISPMS was formed to provide pilot-scale and series production of new materials and devices developed at ISPMS.

1991 — the Russian Materials Science Center was established on the basis of ISPMS, comprising materials science subdivisions of the Tomsk State University, Tomsk Polytechnical University, Tomsk Cutting Tool Plant and Tomsk State Academy of Architecture and Civil Engineering. The goal of the Russian Materials Science Center is to accelerate scientific and technological progress in the national economy.

1994 — a Pilot Plant associated with ISPMS is being put into operation.

ORGANIZATIONAL STRUCTURE AND SCIENTIFIC POTENTIAL

The State Research Center of Russia INSTITUTE OF STRENGTH PHYSICS AND MATERIALS SCIENCE is composed of
the Institute of Strength Physics and Materials Science of the Russian Academy of Sciences (Siberian Branch),
the Republican Engineering Center associated with ISPMS, and
the Pilot Plant associated with ISPMS.

The total floor area of the production facilities is 15000 sq.m. The available modern process equipment makes it possible to produce prototypes and small quantities of marketable products.

The State Research Center employs 500 workers, including 1 academician, 20 doctors of sciences professors and 130 candidates of sciences (Ph. D.).

The State Research Center of the Russian Federation provides in-service and on-the-job training and retraining of scientific brainpower and skilled personnel in the following fields:
— mechanics of deformable solid;
— solid-state physics;
— strength and plasticity physics;
— physical metallurgy and heat treatment of metals;
— powder metallurgy;
— welding techniques and procedures;
— computer elements and devices.
Target-oriented programs of the State Research Center are implemented in close cooperation with:

V.E. Panin
Academican RAS

В.Е. Панин
Академик РАН

1928 г. – профессор В.Д. Кузнецов создает Томскую школу физики прочности на базе Сибирского физико-технического института при Томском государственном университете.

1979 г. – профессор В.Е. Панин – лидер Томской школы физики прочности и материаловедения – и часть сотрудников СФТ переходят по приглашению Председателя Томского филиала СО АН СССР академика В.Е. Зуева в Институт оптики атмосферы СО АН СССР и создают отдел физики твердого тела и материаловедения.

1984 г. – из Института оптики атмосферы выделяется самостоятельный Институт физики прочности и материаловедения СО АН СССР. Возглавил институт член-корреспондент АН СССР В.Е. Панин.

1985 г. – для доведения разработок Института до промышленных образцов и организации их серийного производства при ИФПМ СО АН СССР создан Республиканский инженерно-технический центр.

1991 г. – в целях содействия ускорению научно-технического прогресса в отраслях хозяйства РФ на базе ИФПМ СО РАН создан Российский материаловедческий центр, в состав которого вошли подразделения материаловедческого профиля Томского государственного университета, Томского политехнического университета, Томского завода режущих инструментов, Томской государственной академии строительства и архитектуры.

1994 г. – завершается строительство опытного завода при ИФПМ СО РАН.

ОРГАНИЗАЦИОННАЯ СТРУКТУРА И КРАТКАЯ ХАРАКТЕРИСТИКА НАУЧНОГО ПОТЕНЦИАЛА ЦЕНТРА

Государственный научный центр Российской Федерации – Институт физики прочности и материаловедения СО РАН – включает в свой состав:
– Институт физики прочности и материаловедения СО РАН;
– Республиканский инженерно-технический центр при ИФПМ СО РАН;
– Опытный завод при ИФПМ СО РАН.

Их производственные площади составляют 15000 кв. м. Современное технологическое оборудование позволяет не только разрабатывать опытные образцы, но и выпускать малые серии товарной продукции. В составе Государственного научного центра работают 500 человек, в том числе: один академик, 20 докторов наук, 130 кандидатов наук.

Государственный научный центр Российской Федерации осуществляет подготовку и переподготовку высококвалифицированных кадров в следующих областях:
– механика деформируемого твердого тела;
– физика твердого тела;
– физика прочности и пластичности;
– металловедение и термическая обработка металлов;
– порошковая металлургия;
– технология сварки;
– элементы и устройства вычислительной техники.
В выполнении программы Государственного научного центра участвуют:
– Институт гидродинамики СО РАН;

— the Institute of Hydrodynamics of the Siberian Branch of the Russian Academy of Sciences;
— the Institute of Theoretical and Applied Mechanics of the Siberian Branch of the Russian Academy of Sciences;
— the Mining Institute of the Siberian Branch of the Russian Academy of Sciences;
— Institute of the Thermal Physics of the Siberian Branch of the Russian Academy of Sciences;
— the Tomsk State University;
— the Tomsk Polytechnical University;
— the Siberian Physicotechnical Institute.

BASIC RESEARCH TRENDS
— Physical mechanics of non-homogeneous media;
— Computer-aided design of advanced materials and technologies;
— New generations of metal-, ceramics-, and polymer-based materials;
— Basic scientific principles of strengthening and surface treatment of materials;
— Nondestructive Methods of Testing.

MAJOR RESULTS
The State Research Center is deeply involved in development of mezomechanics, a new science linking continuum mechanics (macrolevel) with plasticity physics (microlevel). Mezomechanics treats a solid under load as a multilevel self-organizing system where micro-, meso-, and macrolevels are organically interrelated and described by the same equations. A designer can enter the relevant data for the material under development into the computer, simulate its deformation and fracture under any loading conditions and optimize the composition and structure of the material to reach target physicomechanical properties. This provides the feasibility of computer-aided design of novel materials and prediction of the life time of those in current use. Based on mezomechanics, fundamental principles were formulated of design of materials and strengthening coatings with a damping structure capable of uniform redistribution of internal stresses over the bulk of the material, which averts the danger of sudden fractures and ensures high reliability and durability of structural materials. The damping approach was embodied in the development of new materials for tools and constructions. Advanced materials and strengthening coatings are used for producing a wide range of tools, parts of oil field and drilling equipment, bearings, stop valves and fittings, and medical instruments.

INTERNATIONAL COLLABORATION AND OUTLOOK FOR THE FUTURE
The State Research Center has established close scientific contacts with research centers and companies in the USA, Great Britain, Sweden, Italy, Germany, Slovenija, Japan, Korea and China. Joint projects for computer-aided design of advanced materials and non-destructive method of testing are being implemented at international laboratories of ISPMS. Joint-venture companies with Great Britain and Chinese participation are involved in the manufacture and commercialization of high-tech products. ISPMS holds annual international conferences and workshops and provides in-service and on-the-job training of foreign specialists.

— Институт теоретической и прикладной механики СО РАН;
— Институт горного дела СО РАН;
— Институт теплофизики СО РАН;
— Томский государственный университет;
— Томский политехнический университет;
— Сибирский физико-технический институт.

ОСНОВНЫЕ НАПРАВЛЕНИЯ ДЕЯТЕЛЬНОСТИ:
— физическая мезомеханика структурно-неоднородных сред;
— компьютерное конструирование новых материалов и технологий их получения;
— материалы новых поколений на металлической, керамической и полимерной основах;
— научные основы технологий упрочнения и поверхностной обработки материалов;
— неразрушающие методы контроля.

ОСНОВНЫЕ РЕЗУЛЬТАТЫ РАБОТЫ
В Центре развивается мезомеханика — новая наука, позволившая связать механику сплошной среды (макроуровень) с физикой пластичности (микроуровень). Мезомеханика рассматривает нагруженное твердое тело как многоуровневую самоорганизующуюся систему, в которой микро-, мезо- и макроуровни органически взаимосвязаны и описываются одними уравнениями. Конструктор может ввести информацию о разрабатываемом материале в компьютер, осуществить моделирование его деформации и разрушения в любых условиях нагружения и оптимизировать состав и структуру материала для получения заданных физико-механических свойств. Возникает возможность конструировать с помощью компьютера материалы новых поколений и прогнозировать ресурс работы оборудования и конструкций. На основе мезомеханики разработаны новые неразрушающие методы контроля, принципы создания материалов и упрочняющих покрытий с демпфирующими структурами, которые способны перераспределять внутренние напряжения и выравнивать их по объему изделия, что предотвращает опасность внезапного разрушения и обеспечивает высокую надежность и долговечность материалов. Принцип демпфирования реализован при разработке новых материалов инструментального и конструкционного назначения. Новые материалы и упрочняющие покрытия использованы для изготовления инструмента широкой номенклатуры, деталей бурового и нефтепромыслового оборудования, подшипников, запорной арматуры, изделий медицинского назначения.

УЧАСТИЕ В МЕЖДУНАРОДНОМ СОТРУДНИЧЕСТВЕ И ПРЕДЛОЖЕНИЯ ПО РАЗВИТИЮ РАБОТ И ДАЛЬНЕЙШЕМУ СОТРУДНИЧЕСТВУ
Центр имеет широкие научные и деловые (коммерческие) связи с научными центрами и фирмами США, Великобритании, Швеции, Италии, Германии, Словении, Японии, Республики Корея, Китайской Народной Республики. В международных лабораториях Института выполняются совместные проекты по компьютерному конструированию перспективных материалов, новым неразрушающим методам контроля, разработке материалов новых поколений. Совместные предприятия с Великобританией и Китайской Народной Республикой осуществляют производство и коммерческую реализацию наукоемкой продукции. Институт ежегодно проводит международные конференции и семинары, осуществляет стажировку иностранных специалистов.

Physical mesomechanics of plastic deformation and experimental results obtained by optical methods

(塑性変形の物理的メゾ力学および光学的方法による実験結果)

Victor E. Panin

Physical mesomechanics of plastic deformation and experimental results obtained by optical methods

(塑性変形の物理的メゾ力学および光学的方法による実験結果)

Victor　E.　Panin

本解説では著者らが提案している塑性変形のメゾ力学の物理的基礎に関する理論的および実験的研究について述べる．メゾ力学においては，負荷を受ける不均一媒質は変形の自己無撞着な構造レベルにおける階層を持つものとして考えられる．塑性変形はせん断と回転がメゾスケールの構造レベルにおいて自己適応的に固体中を波動として伝播していくというモデルで記述することができる．固体の破壊は塑性変形の進行に伴い，並進と回転が作る局所的な渦構造が，試料の断面サイズとコンパラブルな大きさに成長するときに生じる現象としてとらえることができる．メゾレベルの塑性変形を観察するための2つの新しい実験方法が論じられる．両方法の一般的原理は，負荷を受ける固体において進展する表面のミクロな凹凸像のメゾ力学的解析を基礎としている．第一はスペックル干渉法のデータを用いる方法であり，第二はテレビ光学的表面観察法である．材料および構造物の非破壊検査のための2種類の装置が論じられる．（要約　豊岡　了）

Keywords : plastic deformation, fracture, mesoscale analysis, speckle interferometry, television-optical analysis, nondestructive testing

1.　Introduction

Traditional description of plastic deformation and fracture is being made on two approaches in its basis :

1. mechanics of continuous medium,
2. dislocations theory.

The mechanics of continuous medium describes behavior of a material under an applied load with the help of integral characteristics of medium. Within such approach an inner structure of a material have not been taken into account ; tensors of stress and tensors of deformation are symmetrical ; plastic deformation takes place due to translational movement of defects under loading. To describe the curve of plastic flow one has to calculate the work-hardening over yield point of material. Phenomenological approach used by mechanics of continuous medium is physically and mathematically correct. However, it may be used only for description of integral properties of macro-homogeneous medium.

The dislocation theory describes microscopic behavior of a solid under loading. The main tasks are to reveal the mechanism of origin of plastic shears and cracks, to describe the behavior of dislocations ensembles and make up the physical interpretation of phenomenological regularities of continuous medium mechanics.

Dislocation theory has achieved a big success in the field of microscopic descriptions of various defects behavior in a solid under deformation. However, the numerous attempts to combine dislocation theory and continuous medium

mechanics appeared to be not successful. For a long time, it was explained by mathematical difficulties in macroscopic description of dislocations ensembles behavior. But now it is evident that our understanding of plastic deformation basic act was not quite correct and was described by a mistaken scheme. As a result, descriptions of behavior of deformational defects ensembles were wrong, as well as microscopic interpretation of phenomenological regularities of continuous medium mechanics.

Our misunderstanding was due to the fact that we had considered the basic act of plastic deformation to be purely translational movement of every deformational defect, (e.g. crystallographic shear) and the condition of continuity conservation had been connected only with certain self-accommodation of shears. All of the known schemes of plastic deformation of heterogeneous media (Sachs, Kochendorfer, Bishop-Hill, Ashby, Taylor, etc.) are based on the various combinations of crystallographic shears. In other words, these schemes use only the translational character of deformation. Such approach doesn't correspond to reality and make it impossible to understand the nature of dislocation sources and the regularities of dislocational ensembles self-accommodation. During the last decade, the author with colleagues developed the new approach in the physical mechanics of solid under loading. This approach is based on the conception of structural levels of a solid plastic deformation[1~35].

Quite new basic act of plastic deformation — "translation-rotation vortex" was theoretically and experi-

mentally grounded within this conception. According to ref. 1), shear in local region of crystal must be accompanied (for given boundary conditions) with the rotation of this local region. Therefore, structural elements movement must be considered in physical mechanics. This movement must include the combination of shear and rotation. As the result of structural elements rotation, all hierarchy of structural levels is involved into deformation. Self-accommodation of different structural elements may be described correctly only by combined consideration of translational and rotational deformation modes. Mesomechanics of such behavior gives a notion about appearance of a vortical mechanical field within solids under loading[10]. Evolution of this field during loading considers plastic deformation and fracture as two successive stages of the same process. In this approach fracture is considered as a rotational mode of deformation. On this basis one can understand the mechanisms of fracture under different loading conditions.

This work is the review of theoretical and experimental research[1~35] devoted to the new approach to plastic deformation and fracture of solids on the basis of mesomechanics of heterogeneous media.

2. Scale levels of solid plastic deformation

Besides the structural levels of solid plastic deformation it is necessary to introduce into consideration the notion about scale levels of plastic deformation. It is important for physical interpretation of plastic deformation as relaxation process. The plastic deformation of a solid under loading is related to a loss of its shear stability and is being developed as a multilevel relaxation process.

At first stage the shear stability loss take place at a microscale level in the local regions of a crystal lattice. Microscale stress concentrators (microSC), arising at the places of structural inhomogeneities, cause a local structural transformation of a crystal lattice in the definite crystallographic directions. Such a structural transformations are displayed as dislocations origin. The microSC action is essentially shortrange, therefore the dislocations can be moving only in the vicinity of microSC. It is common used to consider that dislocations are the translational defects and realise only the deformation translational modes. It is evident that at each definite point of shear-stable crystals a structural stress-induced transformation can not be developed in some crystallographic directions simultaneously: the latter is equivalent to usual phase transformation in an entire volume. It means that only single sliding can take place as relaxation process for definite microSC, But for given boundary conditions when the axis of loaded sample is fixed single sliding within any structural element must lead to arising of couple forces on this element from surrounding

Fig. 1   Mesobands formation during tension of high-nitrogen stainless steel sample previously deformed by rolling.

material. The field of couple forces causes the rotation modes of deformation: cross-slip of dislocations and formation of celulral dislocation substructure, involvement of multiple sliding at different points of crystal as a vortex of material rotation, flows defects at grains boundaries which cause the rotation of grains as a whole.

Thus the first stage of plastic deformation at microscale level is accomplished by formation of dislocation mesoscale substructure which is capable to realize the vortical character of plastic flow of heterogeneous medium. This mesosubstructure is distributed within initial internal structure and is named[33] as mesosubstructure I. Corresponding scale level is named as mesolevel I. It characterizes well developed plastic deformation of heterogeneous medium.

During plastic deformation the density of dislocations increases and, under its certain critical value, there arises the shear stabity loss throughout of crystal lattice. The structural transformations become possible at the long-range volumes and can be realized not only in crystallographic but in the arbitrary directions. There arises opportunity to relax more strong stress concentrators by origin defects of mesoscale sizes. At this stage of plastic deformation such new types of defects (mesodefects) as disclinations, micro-bands and mesobands, microtwins, martensitic plates are being originated. Preferentially these mesodefects are propagating along the directions of maximum shear stress across many structural elements regardless of their crystallographic orientation. The example of such deformation mechanisms is shown in Fig. 1. The flat specimen of highnitrogen steel initially cold rolled at room temperature then was loaded by tension. Cold rolled state of specimen turns out to be very non-equilibrious in condition of tensile loading. As a consequence mesoscale bands oriented along the maximum shear stress directions appears from the very beginning of tension. These mesobands cause the displacement of large mesovolumes of a material relatively to each other. At mesoscale level the movement of mesoscale size structural elements as a whole becomes the main mechanism of plastic deformation. For polycrystals at high temperature separate grains or their conglomerates are playing role of mesostructural elements. The intensity of sliding within different
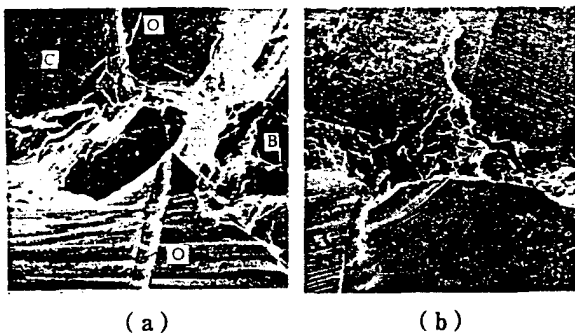
Physical mesomechanics of plastic deformation (V. E. Panin)

(a)   (b)

Fig.2 Creep of polycrystal of allow Pb + 1.9at%Sn, T = 328 K, σ=4 MPa, the third stage[6]: (a)rotation of the grain A under single slip; (O-O)-break of the check mark made as a straight line at the surface of specimen before test. × 1000. (b)vortical structure at the pre-boundary band of the rotating grain. ×300.

mesobands or grains boundaries is non-equal. Therefore each structural element is suffered by action of couple forces. Such movement of structural elements is characterized by scheme "shear + rotation". There arises mesosubstructure II at mesoscale level of sample. For polycrystals the grains boundaries are being such mesosubstructure II. It is capable to realize vortex character of plastic deformation of sample and is correlating with its shape and size, **Fig. 2.**

Thus the second stage of plastic deformation at the mesoscale level of a sample is also accomplished by formation of substructure capable to realize the vortical character of sample plastic deformation. But in contrary to the first stage the mesosubstructure II is the consequence of mesostress concentrators relaxation.

In condition when mesosubstructure II overlap the whole cross section of a specimen and work-hardening of structural elements don't allow them to realize the internal accommodation processes there arise macroscale stress concentrators which cause the plastic deformation localization. As a rule this macrolocalization occurs at the boundaries of mesosubstructure II which have very high extent of shear instability. According to theoretical and experimental investigations[33, 35] big shear localization is accompanied by big value of local material rotation. This causes the appearence of discontinuities in the region of shear localization, material fragmentation and, at last, a material fracture. It is the third stage of plastic deformation which is connected with shear stability loss of a specimen as a whole and is accompanied by sample dividing to parts as the process of macro stress concentrators relaxation.

Thus the third stage of plastic deformation at macroscale level is also vortical process. But rotation of sample parts are accompanied by crack propagation and fracture of loaded solid.

It is followed from above mentioned that any theory of plastic deformation must include into consideration:

1) sources of deformation defects appearing in the places of possible stress concentrators;

2) all the possible relaxational flows of deformation

defects, interconnection of their fields and their interconnections with all interfaces and lateral surface of a solid, formation of vortical mesosubstructure;

3) movement of three-dimensional structural elements according to the scheme "shear + rotation" as translational-rotational vorteces;

4) self-accomodation of translational-rotational vorteces at all structural levels of deformation and evolution of this process during loading.

Such theory was developed[10] on the basis of physical mesomechanics of heterogeneous medium. It predicts the existance of vortical mechanical field in solid under deformation.

3. Vortical mechanical field in solid under deformation

In accordance with ref. 10) in any solid under deformation there arises the mechanical field which is described by the following equations:

$$\text{div } S^a - f^{abc}(A^b \cdot S^c) = I^{a0}/l^{2D_f}, \tag{1}$$

$$(\text{rot } S^a)_\mu - f^{abc}[A^b \times S^c]_\mu = \partial R_\mu^a/\partial t, \tag{2}$$

$$\text{div } R^a - f^{abc}(A^b \cdot R^c) = 0, \tag{3}$$

$$(\text{rot } R^a)^\mu - f^{abc}[A^b \times R^c]^\mu = \frac{1}{c_t^2}\frac{\partial S^{a\mu}}{\partial t} + I^{a\mu}/l^{2D_f}, \tag{4}$$

In (1~4) $I^{a\mu} = -g^{ij}\lambda_i^{ak}\eta_k^a D_\nu \eta_j^\beta C_{a\beta}^{\mu\nu}$, $(\alpha, \beta, \mu, \nu = 1, 2, 3)$; $I^{a0} = -\rho g^{ij}\lambda_i^{ak}\eta_k^\xi \dot{\eta}_j^\beta$, S^a—the change of distorsion tensor component gradient as a function of time, $a=1, 2, \cdots, 9$; A^a—distorsion tensor component gradient, connected with gauge field; c_t—ultimate rate of gauge field propagation in heterogeneous medium; R^a—bend-torsion tensor component gradient; f^{abc}—structural constants; λ^a—group GL(3) generators; I^{a0}-gauge field sources, connected with the change of the local bench mark η as a function of time; $I^{a\mu}$-flows caused by local bench mark η dimension change; $D_\nu = \partial_\nu - \lambda^a A_\nu^a$-covariant derivative; S^a, R^a-gauge field strength tensor components; $C_{a\beta}^{\mu\nu}$-elastic constants; ρ- materials density; l-dimension of structural level, D_f-fractal dimension.

In a common case the values of rotors of a primary slip (2) and of accommodational flows of deformation defects (4) are non-equal at the structural level i. That is why the moment of momentum conservation law is not valid at a single structural level. For its satisfaction in the given boundary conditions several structural levels are to be under self-consistent deformation. In accordance with this the moment of momentum conservation law for defects flows in heterogeneous medium can be written as follows:

$$\sum_{i=1}^{N} \text{rot } I_i = 0. \tag{5}$$

The equation (5) is the law of structural levels of solids deformation. In accordance with this law the sum of rotors

of all
chy N
solid u
conclu
solids[5]
T
It is vi
in the
represe
div
rot
(ro
div
where
at struc
Let
rotor (
hierarcl
The
be obta
Δ I
Δω,
It c
and acc
wave e
shows th
being fa
natural
special
translati
Such
or its str
sample.
bending
necessar
sample.
out signif
from the
tion at
obtained
cases of
localized

4. Exp
pred

Syste
predictior
ture in re
investigat
developed

of all deformation defects flows I_i is equal to zero in hierarchy N of self-consistent structural levels of deformation in a solid under loading. The law (5) leads to very important conclusions about plastic deformation and fracture of solids[33~35].

The equation (1~4) are similar to Maxwell equations. It is visible particularly if one takes sum of equations (1~4) in the group index. In this case the field equations may be represented as follows:

$$\text{div } V_i = g^{ij}\eta_i^a \dot{\eta}_j^a, \tag{6}$$

$$\text{rot } V_i = \partial \omega_i/\partial t, \tag{7}$$

$$(\text{rot } \omega_i)_\mu = (1/c_i^2) \cdot (\partial V_i/\partial t)_\mu + g^{ij}\eta_i^a(D_\mu \eta_{j\alpha})/l_i^{2D\mu}, \tag{8}$$

$$\text{div } \omega_i = 0, \tag{9}$$

where V_i-is velocity of translational flows, ω_i-rotation angle at structural level i.

Let us consider a character of interaction of primary slip rotor (7) and accommodational flows rotor (8) within the hierarchy of structural levels.

The following equations for $V_i = V_i(t)$ and $\omega_i = \omega_i(t)$ can be obtained from (7), (8):

$$\Delta V_i - (1/c_i^2) \cdot (\partial^2 V_i/\partial t^2) = \partial/\partial t(g^{ij}\eta_i^a(D_\mu \eta_j^a)/l_i^{2D\mu}$$
$$- \text{grad } g^{ij}\eta_i^a \dot{\eta}_j^a. \tag{10}$$

$$\Delta \omega_i - (1/c_i^2) \cdot (\partial^2 \omega_i/\partial t^2) = \text{rot}(g^{ij}\eta_i^a(D_\mu \eta_j^a)/l_i^{2D\mu}. \tag{11}$$

It can be seen that interaction of primary slip rotor (7) and accommodational flows rotor (8) are described by wave equations. The right-hand side of wave equations shows that the wave character of this interaction is irregular being fading as a function of coordinate and time. It is quite natural in dissipative heterogeneous medium. However in special cases it is possible to realize the propagation of translation-rotation waves.

Such conditions are existing if the length of defects flow or its stress field are comparable with the cross-section of a sample. Then each defects flow will be accompanied by bending of a sample as a whole what ensures the arising of necessary stress concentrators at the opposite side of a sample. Thus plastic deformation wave can propagate without significant dissipation if it is being multiple reflected only from the lateral sides of loaded sample. With this its dissipation at the interfaces is negligible. Similar results were obtained in[26~35] for anomalous coarse-grained samples, for cases of deformation by shear-bands and for many cases of localized plastic deformation.

4. Experimental investigations of the theory[10] predictions

Systematical experimental research of the theory[10] predictions was undertaken for materials with various structure in ref. 26~31, 33). Two new methods for experimental investigation of plastic deformation on the mesolevel were developed. The general principle of the both methods is based

Fig. 3 Translation-rotation wave along the axis of tension in polycrystal of alloy Fe + 3 at%Si. T = 293 K. grain size 10 mm. deformation 1.8-2.0%[26, 27].

Fig. 4 Translation-rotation wave along the axis of tension in coarse-grained Al. grain size 10 mm. deformation 0.8-1.0%[30].

on mesomechanical analysis of surface microrelief images taken for a solid under loading. The first method uses speckle-interferometry data, the second one is related to television-optical analysis of surface brightness.

Let us consider the investigations of plastic deformation waves by speckle-interferometry method[26~31]. According to the mentioned above, there was undertaken the investigation of samples for which plastic deformation was realized by mechanisms overlaping a whole cross-section (twinning, anomalous coarse-grained specimens).

It is well-known that at sufficiently high plastic deformation there arise so called microbands[36~41], which are propagating at the angle 45° to the direction of tension (or rolling) regardless of material crystallographic orientation. Their stress field overlap the whole cross-section of sample. Similar stress field are formed by microtwins in alloys with low shear stability[42] and also within anomalous coarse-grained specimens[18]. Therefore, first of all there were undertaken the investigations of polycrystals of alloy Fe + 3 at. % Si and Al with anomalous coarse grain size 10 mm. Dimensions of sample were 50 mm × 10 mm × 1 mm and only 1-3 grains were arranged within sample cross-section. For such specimens mesomechanical calculations[33~35] predicted the waves of distortion tensor components ε_{xy} (shear) and ω_{ij} (rotation).

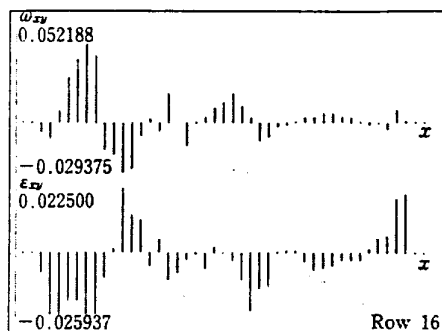For experimental investigation the laser speckle-

Fig. 5 The waves of ε_{xy} and ω_z within Luders band in low carbon steel.

interferometry method was used. It allows to measure the distribution within a whole specimen of shear vectors $|r|$ and their components u_x and u_y. The field of shear vector can be transformed into the field of distortion $\beta_{ij} = \varepsilon_{ij} + \omega = \Delta r$. In case of a flat specimen all components of tensor β_{ij} can be calculated: $\varepsilon_{xx} = \partial u_x/\partial x$, $\varepsilon_{yy} = \partial u_y/\partial y$, $\varepsilon_{xy} = 0.5(\partial u_y/\partial x + \partial u_x/\partial y)$, $\omega_z = 0.5(\partial u_y/\partial x - \partial u_x/\partial y)$.

The results of investigations for polycrystals Fe + 3at. %Si and Al are shown in respectively **Fig. 3** and **Fig. 4**. It can be seen that for both cases wave character of plastic deformation is revealed very clearly. The full phase correlation of ε_{xy} and ω_z is observed for Fe + 3at. %Si, in which an intensive twinning is taken place under tension. The oscillation frequencies of ε_{xy} and ω_z for Al polycrystals, which are being characterized by multiple sliding, are different.

In case of fine grained specimens plastic deformation waves within the whole specimen can't propagate on account of big dispersion. But in cases of localized plastic deformation they are possible [8, 33, 35].

For investigation of localized plastic deformation waves special television-optical method and devices were developed [33, 34]. The general principle of this method is based on computer analysis of television-optical images of the surface microrelief taken for a solid under loading. The characteristics of the surface microrelief are measured by television-optical device "TOMSC" (Television-Optical Meters of Surface Characteristics). It consists of an optical microscope with assorted objective lenses, an illumination unit, a high resolution TV camera, special-purpose interfaces, a power supply, a TV monitor and a personal computer. Magnification of optical images can be varied in wide range that allows to investigate precisely arbitrary specimen regions of any scale.

Numerous investigations of localized plastic deformation showed its wave character. The example of such localized plastic deformation wave for Luders band in low carbon steel is shown in **Fig. 5**.

In any case if the plastic deformation wave of any kind become standing it leads to appearance of localized translation-roration vortex which is accompanied by solid fracture.

5. Criteria and mechanism of fracture

It is accepted in traditional mechanics and physics of fracture that there are initial microcracks in a real solid and fracture is a result of their development. Fracture is calculated as a process of crack propagation under the action of stress concentrator which appears at tip of a crack. Within such approach, the mechanics of a solid under deformation and fracture mechanics had been developed independently from each other. Another approach based on analysis of deformation rotational modes has been developed in mesomechanics. In such approach there is no need to postulate existence of microcracks in initial state of material. Translation-rotation vorteces at lower structural levels cause appearance of microcracks from the very beginning of plastic deformation. In this sense, one can say that the development of fracture takes place from the very beginning of plastic deformation, in a common case. However, two stages of fracture are to be distinguished.

1. The first stage is connected with translation-rotation vorteces evolution at micro- and mesolevels. Translation-rotation vorteces self-accomodation causes continuous movement of localized plastic deformation waves and the formation of mesoscopic interfaces within which microcraks are appearing and developing. These processes don't cause fracture of material.

2. The second stage is connected with appearance of translation-rotation vertex at the upper structural level, when its dimensions become comparable with cross-section of a specimen. Such vortex is localized within the certain volume of specimen and doesn't move in a space. Its evolution is connected with development of a primary slip flows. Rotor of these flows is not compensated by rotational modes of accommodational defects flows. In the given boundary conditions, macrocrack is appearing and developing as rotational mode of deformation which compensates a primary slip rotor. Taking into account the expressions for rotors of primary slip (2) and accommodational rotational flows (4) the criterion of fracture can be written as follows

$$\left[\frac{\partial R_{i\mu}^a}{\partial t}\right]_{i=N} > 0, \tag{12.1}$$

$$(\text{rot } R_{i\mu}^a)_{i=N} = 0. \tag{12.2}$$

Conditions (12) are given for the upper structural level, comparable with dimensions of a specimen. It suggests that translation-rotation vortex of a primary slip is comparable with cross-section of a specimen and it evolves continuously. At the same time, summary vortex of accommodational defect flows equals zero.

Condition (12.2) predicts possibility of both brittle and tough fracture.

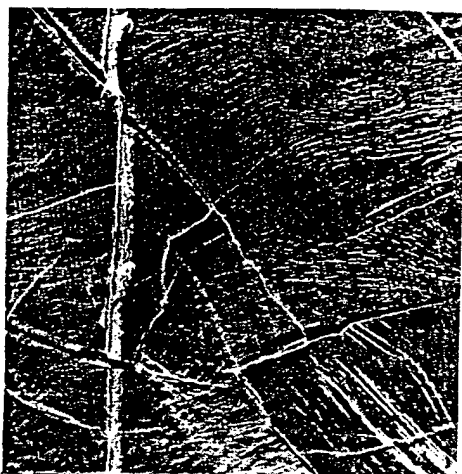1) If all items of $(\text{rot } R_{i\mu}^a)_{i=N}$ in accordance with (4)

Fig. 6 Grain fragmentation of polycrystal of alloy Pb – 1.9 at% Sn during cyclic bending. T = 293 K, N = 10³, ×150[³¹].
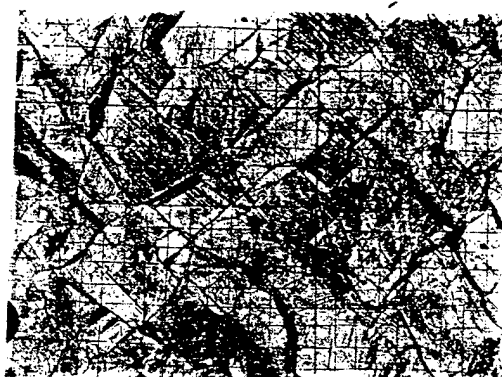

Fig. 7 Mesoscale substructure at the surface of lead specimen during cyclic bending. T = 293 K, N = 10⁵, ×50[²¹].

Fig. 8 Deformed grains self-accomodation into closed loops at the surface of flat specimen of alloy Pb + 0.5 wt. %Sb during cyclic bending. T = 293 K, destroyed, ×50[³³].

equal zero, fracture will be brittle. It can be realized at low temperatures and high velocity of metal loading, in intermetallic compounds, ceramics, chemical compounds. However, even in absolutely brittle fracture there should be signs of a primary slip (12.1). Indeed at "shores" of crack after brittle fracture there are always signs of slip lines.

2) While the summary rotor of accommodational defects flows equal zero its components (of opposite signs) are not zero. It will cause tough fracture of a material. Conditions of fracture (12) allows to formulate an important consequence which can be proved experimentally.

If the summary rotor of all accommodational defects flows equal zero, a primary slip rotor should cause fragmentation within the region of a primary slip in given boundary conditions. In other words, fragmentation of a material within the region of a primary slip must precede to crack appearance. Then, a crack has to propagate as a development of rotational deformation mode along boundaries of fragments which accommodates a primary slip rotor. The example of such fragmentation is shown in **Fig. 6**.

Fracture criteria (12) give the possibility to explain the mechanism of fatigue fracture of various materials and parts of machines[²¹,²²]. The mesoscale substructure developed as a consequence of localized plastic deformation waves self-accommodation during cyclic bending of polycrystals of Pb and alloy Pb + 0.5 wt. %Sb is shown in **Fig. 7** and **Fig. 8** respectively.

For the case of fig. 7 mesosubstructure is being developed as a propagating of localized plastic deformation waves. When this process is accomplished and all a specimen cross-section is overlaped by such mesosubstructure fracture take place: crack is propagating along the interfaces of this mesosubstructure.

In the case of fig. 8 there arise closed mesoscale loops. When the number of bending cycles is small one can observe isolated conglomerates of deformed grains surrounded by non-deformed grains. These are isolated translation-rotation vorteces. As the number of bending cycles has been increased, the number of vorteces is also increased and they

form a closed loop of dimensions comparable with cross-section of a specimen. The successive cyclic bending increases the extent of primary slip in grains forming a loop. This loop is to be rotated as a whole. This process causes crack propagation in the region of loop and then across a specimen as an accommodational rotation relatively to primary slip rotor within grains forming a loop. The kinds of mesosubstructure in different materials can be different. However, the criterion (12) is universal: self-accommodation of translation-rotation vortexes is to occur in a scale of cross section of a specimen. Development of accommodational rotational modes of plastic flow is to be hampered. Then a crack propagates as an only possible accommodational deformation mode.

6. Summary

The new science developed at the last decade physical mesomechanics allowed to connect the mechanics of a continuous medium (macrolevel) with plasticity physics (microlevel). Mesomechanics treats a solid under loading as a multilevel selforganizing system where micro-, meso- and macrolevels are organically interrelated. It leads to arising in a solid under loading vortical mechanical field which is described by wave equations.

Physical mesomechanics characterizes a solid plastic

deformation as self accommodation of translation-rotation vorteces, propagation of localized plastic deformation waves and formation of mesoscale substructure. Evolution of a mesoscale substructure is accomplished by fracture.

Two optical methods based on speckle-interferometry and television-optical investigation of surface microrelief are developed. They allow to investigate the plastic deformation on mesoscale level and can be used for prefracture diagnostics. Experimental results confirm the prediction of mechanical field theory. Two kinds of devices for non-destructive testing of materials are presented.

Acknowledgments

References

1) V. E. Panin, Y. V. Grinyaev, T. F. Elsukova and A. G. Ivanchin: Izv. vuzov. Fizika 6, 5 (1982).

2) V. E. Panin, V. A. Likhachev and Y. V. Grinyaev: *Deformation structural levels of solids. Nauka, Novosibirsk*, p. 229 (1985).

3) V. E. Panin, V. E. Egorushkin, Yu. A. Chon and T. F. Elsukova: Izv. vuzov. Fizika 12, 5 (1989).

4) Y. V. Grinyaev and N. V. Chertova: Izv. vuzov. Fizika 2, 36 (1990).

5) V. E. Panin: Izv. SO AN USSR. Ser. techn. sciences 3, 87 (1987).

6) V. E. Panin, Y. V. Grinyaev, V. I. Danilov and others: *Structural Levels of Plastic Deformation and of Fracture. Nauka, Novosibirsk*, p. 225 (1990).

7) V. E. Panin, T. F. Elsukova, E. N. Novoselova and V. E. Egorushkin: DAN USSR 310, 78 (1990).

8) V. E. Egorushkin: Izv. vuzov. Fizika 4, 19 (1992).

9) V. E. Panin and T. F. Elsukova: *Synergetics and fatigue fracture of metals, Ed. by V. Ivanova, Nauka, Moscow*, p. 248 (1989).

10) V. E. Panin, Y. V. Grinyaev, V. E. Egorushkin and others: Izv. vuzov. Fizika 1, 36 (1987).

11) V. E. Panin, T. F. Elsukova, M. K. Eliseeva and Yu. V. Grinjaev: Surface. Physics, Chemistry, Mechanics 5, 138 (1983).

12) Yu. V. Grinjaev, V. E. Panin: Izv. vuzov. Fizika 12, 95 (1978).

13) V. E. Panin, Yu. V. Grinyaev and others: DAN USSR 309, 356 (1989).

14) V. E. Panin: Izv. vuzov. Fizika 4, 5 (1992).

15) T. F. Elsukova and V. E. Panin: Metals 2, 73 (1992).

16) V. E. Panin: Izv. vuzov. Fizika 2, 4 (1990).

17) V. E. Panin and K. V. Frolov: *The New Physical and Mechanical Methods of Investigation of Materials under Loading, Ed. by V. E. Panin, Tomsk University Press, Tomsk*, p. 332 (1990).

18) P. V. Makarov: *The New Physical and Mechanical Methods of Investigation of Materials under Loading, Ed. by V. E. Panin, Tomsk University Press, Tomsk*, p. 332 (1990).

19) V. E. Panin: *Abstracts of the first European East-West Symp. on Materials and Processes, Helsinki* (1990).

20) V. E. Panin and S. P. Efimenko: *Abstracts of the 2nd European conf. of Advanced Materials and Processes, London*, p. 288 (1991).

21) V. E. Panin, V. E. Egorushkin, T. F. Elsukova and O. V. Veselova: DAN USSR 316, 1130 (1990).

22) V. F. Panin, V. E. Egorushkin, T. F. Elsukova and O. V. Veselova: *The New physical and Mechanical Methods of Investigation of Materials under Loading, Ed. by V. E. Panin, Tomsk University Press, Tomsk*, p. 332 (1990).

23) V. E. Panin, T. F. Elsukova, E. M. Novoselova and V. E. Egorushkin: DAN USSR 276, 630 (1989).

24) K. P. Zhukova, T. F. Elsukova, V. E. Panin and Y. N. Rudenko: Izv. vuzov. Fizika 4, 13 (1988).

25) V. E. Panin, T. F. Elsukova, E. M. Novoselova and V. E. Egorushkin: DAN USSR 310, 78 (1990).

26) V. E. Panin, L. B. Zuev, V. I. Danilov and N. M. Mnikh: FMM 66, 1005 (1988).

27) V. E. Panin, L. B. Zuev, V. I. Danilov and N. M. Mnikh: DAN USSR 308, 1375 (1989).

28) V. E. Panin, L. B. Zuev, V. I. Danilov and N. M. Mnikh: FMM 6, 189 (1990).

29) L. B. Zuev, V. E. Panin, V. I. Danilov, N. M. Mnikh and N. V. Peker: DAN USSR 317, 1386 (1991).

30) V. I. Danilov, L. B. Zuev, N. M. Mnikh, V. E. Panin and L. V. Shershova: FMM 3, 188 (1991).

31) V. E. Panin, L. B. Zuev, V. I. Danilov, P. V. Makarov, V. E. Egorushkin, B. B. Gorbatenko, Y. Hida and S. Yoshida: *Method and Apparatus for Nondestructive Testing of the Mechanical Behavior of Solid State Object under Loading, Patent, N93002731, Ruspatent, Moscow, Russia.*

32) V. E. Panin, Y. I. Meshcheryakov, T. F. Elsukova, A. K. Dyvakov, S. G. Psakhie and N. M. Myshlyaev: Izv. vuzov. Fizika 2, 107 (1990).

33) *Physical Mesomechanics and computer-aided design of materials. Ed. by V. E. Panin, Nauka SO, Novosibirsk*, v. 1, p. 297 (1995) and v. 2, p. 320 (1995).

34) *Physical Mesomechanics of Heterogeneous Media and Computer-Aided Design of Materials, ed, by V. E. Panin, Cambridge Interscience Publishing, Cambridge*, p. 450 (1995).

35) *Design of New Materials and Strengthening Technologies, ed. by V. E. Panin, Cambridge Interscience Publishing, Cambridge*, p. 140 (1995).

36) V. U. Essman: Phys. Stat. Sol. 12, 723 (1975).

37) J. Grewen, T. Noda and D. Sauer: Zs. Metallk 8, 463 (1977).

38) A. S. Malin and M. Hatherley: Met. Sci. 13, 463 (1979).

39) A. S. Malin, J. Huber and M. Hatherley: Zs. Metallk. 72, 310 (1981).

40) Y. Hakayama and K. Morii: Acta Met. 35, 1747 (1987).

41) Ye. E. Zasimchuk and L. I. Markashova: *Microbands in Nickel Monocrystals Deformed by Rolling, Preprint N23. 88. IFM AN UKSSR, Kiev*, p. 36 (1988).

42) V. E. Panin, E. F. Dudarev and L. S. Bushnev: *Structure and mechanical properties of solid solutions. Metallurgija, Moscow*, p. 205 (1971).

MODIFICATION OF THE STRUCTURE-PHASE STATE OF COATINGS BY ION IMPLANTATION TECHNIQUES

A.D. KOROTAEV*, A.N. TYUMENTSEV*, YU.P. PINZHIN, A.F. SAFAROV*, S.P. BUGAEV**, P.M. SHCHANIN**, N.N. KOVAL**, AND A.V. VIZIR**
* Siberian Physical and Technical Institute, 1, Revolution Sq., Tomsk, 634050, Russia
** High-Current Electronics Institute, 4 Akademichesky Ave., Tomsk, 634055, Russia

ABSTRACT

Transmission electron microscopy was used to study the effect of nitrogen-ion irradiation on the microstructure of ion-plasma TiN coating deposited on a substrate of austenitic stainless steel. The principal peculiarities of the changes in the fine structure at the substrate-coating interface and in the bulk of the coatings having a thickness of several micrometers have been revealed for the conditions of ion-beam-assisted deposition and plasma-assisted deposition. Possible mechanisms for the effect of ion irradiation on the microstructure of the substrate-coating composition are discussed.

INTRODUCTION

With the widespread use of the techniques for improving the service and operational properties of articles and tools by depositing type TiN coatings, the tasks concerned with increasing the adhesion of a coating to the substrate and optimizing the coating composition and structural state still remain actual.

Currently a new, highly promising technique for modification of the structure and properties of coatings by irradiating the latter with low-energy (E ≤ 100–1000 eV) and high-energy (E > 1–3 keV) ions has been developed [1–10]. The potentialities of this technique improving specific service properties of coatings, its promise and fields of application have motivated considerable interest in investigating the features of the structural phase states of coatings produced under the conditions of ion-beam-assisted deposition (IBAD) and plasma-assisted deposition (PAD). A major part of this work was carried out with TiN coatings.

It has been revealed unambiguously that the adhesion of these coatings is improved, their porosity decreases [1, 2], the texture changes [1–3] and so does the composition (including a reduced contamination of the coating-substrate interface with oxygen [1, 2, 4]), and so on. There is some evidence [2, 5] on the formation, upon ion irradiation, of nanocrystalline coatings with a grain size $d < 10$ nm. Some studies [2, 3], however, have shown that the texture formation is related to a column-like growth of coatings and to the absence of equiaxial grains in them. The data on the effect of ion irradiation on the level of internal stresses in coatings also remain controversial [2, 6, 7].

In low-energy ion irradiation, because of the absence of cascaded collisions and temperature peaks, the physical possibilities for the ions to affect the coating structure are very limited. Nevertheless, even for the ion energy equal to some hundreds of electron-volts a substantial change in the structural state of ceramic coatings has been found [2, 8, 9], in particular, a decrease in their porosity [2], formation of equiaxial grains instead of a columnar structure, etc. It is supposed [2, 9, 10] that in this case the principal factors affecting the structure of a growing structure are an increased mobility of adatoms and atomic mixing in a thin (2–3 interatomic

distances) surface layer.

In general, however, not only the physical mechanisms of the effect of low-energy and high-energy ion irradiation of the structure-phase state of coatings remain obscure, but even the principal regularities of the structure formation under varied conditions of the coating deposition have not been found.

In view of the preceding, we have performed electron microscopic examination of the structure-phase state of a surface layer ($\Delta h \leq 200$ nm) of the substrate (type X17H14 austenitic stainless steel) after removal of a preliminarily deposited TiN coating, the structure of a thin ($\Delta h < 200$ nm) layer of this coating adjacent to the substrate, and the microstructure of the surface layer of a coating of thickness $\Delta H \approx 3$ μm deposited in standard conditions and in conditions where the growing coating is being irradiated with low-energy (E < 100 eV) nitrogen ions.

EXPERIMENTAL TECHNIQUE

Used as a substrate was austenitic stainless steel of composition Fe–17.2Cr–14.4Ni–2.3Mo–1.1Mn (wt.%). Preliminary investigations have shown that the deposition of TiN coatings under IBAD and PAD conditions results in the formation at the coating-substrate interface of type $(FeCrNiTi)O_xN_y$ oxynitrides that reduce adhesion. Therefore, the substrate was preliminarily cleaned by electropolishing, which followed by deposition of a thin ($\Delta h \leq 30$ nm) TiN layer and mixing of the layer with the substrate by implanting Ti^+ and N^+ (Ti/N = 1) ions of energy E = 30 keV with a dose of 5×10^{16} cm^{-2}. On doing this, a thin TiN layer with a nanocrystalline structure (grain size $d < 50$ nm) and low-intense internal stresses was formed on the substrate surface with no sharp boundary between the layer and the substrate. The dislocation density reached $\rho \approx 10^{11}$ cm^{-2} in the surface layer of the substrate and gradually decreased with depth to its initial value $\rho_0 \approx 2 \times 10^8$ cm^{-2}.

Coatings were deposited by arc sputtering of Ti in the atmosphere of molecular nitrogen at its partial pressure $p_N \approx 10^{-4}$ Torr. The substrate temperature therewith was kept equal to T = 550 °C (mode I).

Ion-plasma-assisted deposition of coatings was performed under the above conditions with simultaneous treatment of the coating by nitrogen plasma with a nitrogen ion energy of E ≈ 100 eV. The substrate temperature therewith was T ≤ 400 °C (mode II).

Transmission electron microscopy (TEM) combined with microdiffraction and a dark-field analysis of disorientations [11, 12] has made it possible to elucidate the features of the fine structure of coatings (in particular, the variation of the fine structure with coating thickness) and to estimate the intensity of internal stresses and the changes in phase composition and texture.

The structure of the coating thin layer adjacent to the substrate was investigated with foils prepared by two methods. First, TiN coatings of thickness $\Delta h < 200$ nm were deposited on the substrate and one-sided jet electropolishing was performed on the substrate side. Second, coatings of thickness $\Delta H = 2$–3 μm were preliminarily thinned by ion etching of the surface to a thickness of 150–200 nm, which was followed by one-sided jet electropolishing on the substrate side.

To prepare a foil, on the side of the external layer of a coating, initially the substrate was removed by electrolytic polishing and then the coating was thinned by ion etching.

RESULTS

Features of the microstructure of coatings produced in mode I

In examination of the microstructure of a thin ($\Delta h \leq 150$ nm) layer of the TiN coating

adjacent to the substrate, an almost annular electron-diffraction pattern is found (Fig. 1*a*), which testifies to a high fineness of the coating structure immediately at the surface and in the neighborhood of the substrate-coating interface. Electron-diffraction analysis has shown that the electron-diffraction pattern corresponds with the TiN phase whose lattice parameter is a = 0.425±0.002 nm. Dark-field electron micrographs (Fig. 1*b*) attest that the average grain size in the layer under examination is $d \approx 25$ nm and the grain is equiaxial in shape. Thus, the structural state of the coating layer adjacent to the substrate is typically a nanocrystalline state with chaotically disoriented equiaxial grains.

At the same time, the layer under consideration shows regions with a substantially dissimilar substructure. This structure is characterized by quasi-annular electron-diffraction patterns (Fig. 1*c*) with pronounced structural maxima that testify to the existence of prevailing orientations. Dark-field analysis (Fig. 1*d*) indicates that in this case TiN grains are thin plates with dimensions of some fractions of a micrometer and large-angle ($\theta \geq 15°$) disorientations.

As the coating is increased to $\Delta H = 2$–3 μm, its microstructure changes. First of all, a clearly pronounced texture with <112> and <111> directions of the normal to the coating surface being dominant has been found in the external surface layer of the coating. Obviously, this is a growth texture, since it is not observed in the coating thin ($\Delta h < 200$ nm) layer adjacent to the substrate. While the texture type depends not only on the anisotropy of the surface energy of TiN crystals but also on the stoichiometry of the growing coating, on the adsorption of impurities, on the growth rate, etc., the accord of the texture we observed with the data available in the literature [1–4] is evidence that the conditions under which we produced our coatings are typical of

Fig. 1. Electron-diffraction patterns (*a, b*) and dark-field images (*c, d*) of a thin (≤ 200 nm) TiN coating deposited in the mode I, taken from areas with equiaxial (*a, b*) and lamellar (*c, d*) nanocrystalline grain structure.

Fig. 2. Electron-diffraction pattern (*a*), a light-field image (*b*), and a dark-field image (in reflexes *1* (*c*) and *2* (*d*) shown in the electron-diffraction pattern) of the microstructure of the surface layer of a 3-μm TiN coating. Arrows I and II in *b*, *c*, *d* show identical areas of the microstructure.

processes like these.

We have been able to observe for the first time the essential features of the coating structure as follows: First, the grain structure of a coating cannot be observed electron-microscopically not invoking a special analysis. The dark lines that resemble in appearance the grain boundaries in light-field images (Fig. 2*b*) are in reality extinction contours. Discrete large-angle disorientations are found only in a dark-field analysis of disorientations. Thus, the neighboring grains I and II in Fig. 2*b* turn out to be in the precisely reflecting positions (Fig. 2*c*,*d*) in those reflexes whose disorientation angle between their vectors is $\theta \geq 20°$ (Fig. 2*a*).

Second, it turned out that the TiN grains revealed in dark-field analysis show a distinctive substructure with a continuous disorientation corresponding with an extremely high curvature of the lattice in individual grains. The continuous disorientation is indicated and measured for the crystallographic planes perpendicular to the incident electron beam by the continuous displacement of extinction contours when the specimen is inclined in the goniometer. The curvature of the planes parallel to the electron beam is estimated [11, 12] by measuring the angular dimensions of the diffraction maxima and the width of the extinction contour. The measurements performed yield the lattice curvature $K \approx 25$–45 deg./μm.

Assuming that the so found curvature values correspond with elastic-plastic deformation of the lattice, the densities of the dislocation charges equivalent to the curvature (same-sign dislocation densities) have been estimated to be $\rho_\pm = (1$–$3) \times 10^{11}$ cm^{-2}. The local internal stresses

4

corresponding to these $\rho_\pm$ values reach $\sigma_s \approx G/30 - G/80$ (with G being the shear modulus for TiN).

There is no doubt that the development of the above peculiarities of the coating thin structure, corresponding with the presence of high nonuniform internal stresses, is related to the nonequilibrium processes involved in the formation of coatings, in particular, to the formation of a columnar structure. This structure seems to prevent the formation of a grainy structure.

<u>Features of the microstructure of coatings produced under the conditions of PAD (mode II)</u>

It has been found that the structure of the thin ($\Delta h < 200$ nm) layer of a TiN coating produced in mode II, adjacent to the substrate, is absolutely identical to that observed for coatings deposited in mode I. The typical structural state for the above thin layers is a nanocrystalline state with equiaxial grains having dimensions ≤ 50 nm.

However, low-energy plasma treatment modifies qualitatively the microstructure of the coating as it grows. First, the formation of a growth texture is suppressed, which is evidenced by the diffraction pattern characteristic of a chaotically disoriented fine-grained structure (Fig. 3a). Second, the formation of a defect substructure with a highly curved lattice and intense internal stresses is prevented. This has been elucidated by dark-field analysis of disorientations. In this case, the electron-microscopic contrast has features of a well-formed grain structure, with the contrast intensity sharply changing at the grain boundaries and being highly uniform within individual grains (Fig. 3b). The latter testifies to an insignificant curvature of the lattice and, hence, to the absence of intense local internal stresses. The grain size found from dark-field images is 0.1–0.2 µm (Fig. 3c).

Thus, under the conditions of exposure to low-energy plasma (E < 100 eV), TiN coatings show changes (formation of an equiaxial grain structure instead of a columnar one, changes in

Fig. 3. Diffraction pattern (a) and light-field (b) and dark-field (c) images of the microstructure of the surface layer of a 3-µm TiN coating deposited in mode II.

crystallographic texture, reduced internal stresses) similar to those found earlier [1–7] for the IBAD conditions. This suggests that the dominant factor in these changes is the increased mobility of adatoms.

REFERENCES

1. W. Ensinger, A. Schroer, G.K. Wolf, Nucl. Instr. and Methods. B80/81, 445 (1993).
2. P. Smidt, G.K. Hubler, Nucl. Instr. and Methods. A80/81, 207 (1993).
3. M. Kiuchi, K. Fujii, T. Tanaka, M. Satou, F. Fujimoto, Nucl. Instr. and Methods. A33, 649 (1988).
4. A. Brieli, H. Kreyrandish, J.S. Colligan, Thin Solid Films. 200, 283 (1991).
5. W. Ensinger, B. Rouschenbach, Nucl. Instr. and Methods. B80/81, 1409 (1993).
6. R.A. Roy, R. Petkie, A. Boulding, J. Mater. Res. 6, 80 (1991).
7. N. Kiratani, O. Imai, A. Ebe, S. Nishiyama, K. Ogata, Surf. Coat. Technol. 66, 310 (1994).
8. D.R. Broghton, G.K. Hubler, Nucl. Instr. and Methods. B28, 517 (1987).
9. K.H. Muller, Phys. Rev. B35, 7906 (1987).
10. C.M. Gilmore, J.A. Spragne, Phys. Rev. B44, 8950 (1991).
11. A.D. Korotaev, A.N. Tyumentsev, V.F. Suchovarov, Disperse Strengthening of Refractory Metals, Nauka, Novosibirsk, 1989, 209 p.
12. A.D. Korotaev, V.Ch. Gonchikov, A.N. Tyumentsev, A.I. Olemskoi, Isv. Vyssh. Uchebn. Zaved. Fizika. 34 (3), 81 (1991).

SOME FEATURES OF VACUUM ARC PLASMAS WITH INCRESING GAS PRESSURE IN THE DISCHARGE GAP

Efim Oks[1,2] and George Yushkov[1]

[1]High Current Electronics Institute, Russian Academy of Sciences, 634055 Tomsk, Russia

[2]State Academy of Control Systems and Radioelectronics, 634050 Tomsk, Russia

ABSTRACT

The application of a magnetic field to the discharge gap of a vacuum arc increases the average charge of the ion flow and, with an elevated gas pressure (10^{-5}–10^{-4} Torr), to the appearance of gas ions in the discharge plasma. The paper presents the results of an experimental investigation into the charge composition of the vacuum arc plasma. A probable physical mechanism for the above changes is discussed.

1. INTRODUCTION

The vacuum arc is a well-known type of discharge. The vacuum arc studies were reviewed in detail by Lafferty [1], Mesyats [2], and Kimblin [3]. During the operation of a vacuum arc, evaporation and ionization of the cathode material occur in cathode spots, small hot regions on the cold cathode surface. The cathode spots of a vacuum arc eject flows of highly ionized cathode-material plasma. All ion species make up about one-tenth of the vacuum arc current. However, there is no generally accepted view on the processes occurring in a vacuum arc cathode spot. This is due to the difficulties encountered in experimentally studying vacuum arc cathode spots being small regions with high-density plasma.

The impossibility of using probe techniques calls for application of "noncontact" techniques to study the vacuum arc, such as spectroscopy and probe measurements of the parameters of the expanding cathode plasma away from the cathode spot, in the regions where it is possible to use probes and to measure charge distributions for the ions emitted by the cathode spot. Brown [4] investigated the charge composition for all cathode materials present in Mendeleyev's table, using the time-of-flight technique. It has been shown [5, 6] that the charge distribution of the ion flow from the cathode is affected by the applied magnetic field. Although a vacuum arc may exist at any low pressure, increasing the pressure in a discharge gap results in a change in the charge-state distribution in the ion flow and even in the appearance of gas ions in the vacuum arc plasma [6, 7]. These effects are interesting from the viewpoint of studying the processes occurring in a vacuum arc cathode spot.

On the other hand, the interest in studying the vacuum arc is related to its application as a plasma generator for vacuum-arc sprayers and for ion sources of the mevva type [8]. The capability of this type of device to produce simultaneously gas and metal ions offers promise for the creation of oxide, nitride, and other compounds of the surfaces of solids.

2. EXPERIMENTAL SETUP

Experiments were carried out on a test bench of Plasma Application group at Lawrence Berkeley National Laboratory with a time-of-flight mass spectrometer and an ion source of the mevva-V type. A detailed description of the mass spectrometer is given in Ref. 9, and the design and principle of operation of the mevva-V ion source are described in Ref. 10. The mevva-V ion source was slightly modified, so that a solenoid creating a pulsed magnetic field of up to 10 kG was placed near the cathode. The magnetic field pulse duration was over 1 ms, which was much longer than the vacuum arc operation time (200 μs). The magnetic field changed within the arc operation time by no more than 20%. To initiate a vacuum arc, we
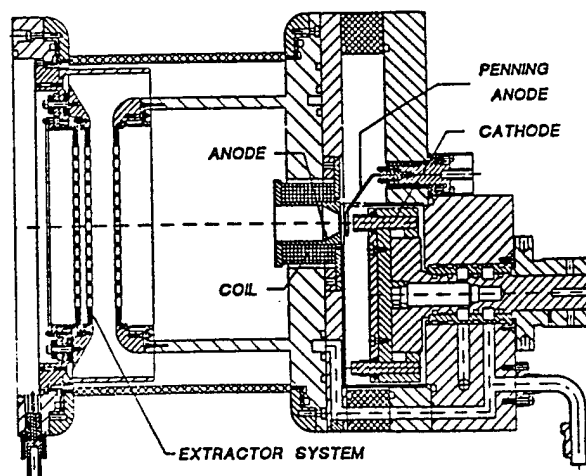

Fig. 1. The vacuum arc ion source with a Penning-discharge trigger.

used pulsed (50 μs) plasma ignition which is, in our opinion, more reliable than the ignition by a surface discharge over ceramics [11]. A schematic diagram of the ion source is given in Fig. 1. Gas was allowed to bleed directly into the cathode region. The data reported here were obtained for an Al cathode and oxygen.

During the operation of the vacuum arc, the anode cavity of the ion source was filled with the plasma flowing out from the cathode spots. The anode plasma served as a medium from which an ion beam was formed. The charge and mass composition of the beam was analyzed on the time-of-flight mass spectrometer placed at a distance of 1.2 m from the extractor system situated on the other end of the chamber. The instant the charge spectra of the ion beam extracted from the anode plasma was lagged by 100 μs behind the instant the vacuum arc was ignited. Therefore, the charge composition of the ion beam was determined by the processes in the discharge gap of the vacuum arc and was not related to the ignition of the arc and to the transient processes that took place during the ignition [12]. The vacuum arc current was 250 A. The pressure measured in the vacuum chamber was varied by varying the flow rate of the gas supplied to the ion source.

Before measuring the charge and mass composition of the ion beam, it is necessary to ensure that the transportation of the beam from the extractor to the time-of-flight spectrometer at an elevated pressure of the residual gas changes the charge spectrum of the beam only slightly. Figure 2 shows the variation in ion beam composition for the accelerating voltage ranging from 10 to 50 kV. With this change in accelerating voltage, the time of flight of an ions changes more

than twice, and the charge-exchange cross section should change substantially. Nevertheless, the ion distributions in charge and type change insignificantly. We have measured these distributions for various magnetic fields and pressures and have found that the beam transportation to a large distance introduces an error over 20% into the measurements.

3. RESULTS

Increasing the pressure in the discharge gap of a vacuum arc varies the ion beam charge composition, as shown in Fig. 3. It can be seen that increasing pressure decreases the fraction of multiply charged ions. With a pressure over 5×10^{-4} Torr, the ion beam consists only of single-charged aluminum ions. Note that with no magnetic field, the vacuum arc plasma is free of gas ions.

Fig. 3. Ion beam current fraction versus gas pressure with no magnetic field.

Gas ions appear in the vacuum arc plasma when a magnetic field is applied to the discharge gap while the latter is being filled with gas. Figure 4 shows the ion beam composition as a function of the magnetic field for a gas pressure of 1.2×10^{-5} Torr. The average charge of aluminum ions increases with magnetic field. It can be seen that the single-charge-ion fraction decreases, the double-charge-ion fraction initially increases and then decreases, while the triple-charge fraction increases continuously. With that, as the magnetic field is further increased, the average charge of aluminum ions continues to increase. The oxygen ion fraction reaches its maximum at a magnetic field of 1.5 kG. With further increasing magnetic field, the molecular ion fraction decreases. Note that
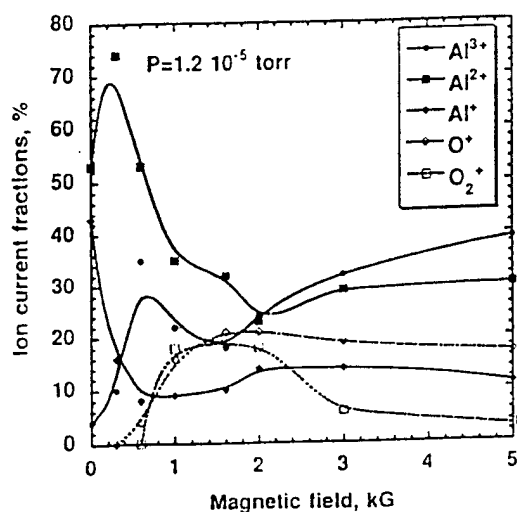

Fig. 2. Ion beam current versus acceleration voltage.

Fig. 4. Ion beam current fraction versus magnetic field. $\bar{p} = 1.2\times10^{-4}$ Torr.

the magnetic field dependencies for all species tend to saturate.

Similar dependencies for a higher pressure are given in Fig. 5. It can be seen that application of a magnetic field causes an increase in the charge of aluminum ions. The magnetic field at which the appearance of oxygen ions becomes noticeable is lower than for the preceding case, while the magnetic field at which the oxygen ion fraction reaches its maximum is higher.

Fig. 5. Ion beam current fraction versus magnetic field. $p = 5\times10^{-4}$ Torr.

Figure 6 presents the dependence of the ion beam composition on gas pressure. It can be seen that increasing pressure decreases the charge of aluminum

Fig. 6. Ion beam current fraction versus gas pressure. $B = 10$ kG.

ions. With that, the oxygen ion fraction increases reaching 70% of the beam current at a pressure of 5×10^{-4} Torr.

We also measured similar dependencies for other gas and metal ions. With the quantitative differencies seen in these dependencies, they show the same trends: (i) increasing magnetic field increases the fraction of multiply charged ions of the metal; (ii) increasing gas pressure decreases this fraction, and (iii) with an applied magnetic field at a gas pressure over 10^{-5} Torr, gas ions appear in the vacuum arc plasma.

4. DISCUSSION

Despite the fact that the effect of the gas type and pressure on the charge composition of the plasma flow generated by a vacuum arc cathode spot has been studied experimentally by a number of investigators that have obtained similar results, it seems that there is no consensus on the mechanism of this process. The effect of the gas is reduced to the following processes occurring in the vacuum arc plasma: charge exchange between the metal ions and the metal vapor neutrals [13], charge exchange between the metal ions and gas molecules and atoms [13, 14], and recombination of the metal ions with the plasma electrons [15]. The appearance of the gas ions is accounted for either by the ionization of the gas by the plasma electrons [15] or by the charge exchange of the metal ions with the gas neutrals [14]. This discrepancy in explanations is due to the difficulties encountered in studying experimentally the vacuum arc plasma in the cathode region which seems to be just the place where charged particles are generated.

In our experiment, increasing pressure with no magnetic field always reduced the charge of the metal ions, and gas ions did not appear in the plasma. The fact of the absence of gas ions as itself, with the gas having a significant effect on the charge composition of the plasma, points in support of the suppositions that the ion charge decreases due to the charge exchange between the metal ions and the metal ions and atoms or due to the recombination in triple collisions with a gas atom being the third particle. However, recombination collisions cannot play a substantial role within the pressure and plasma density ranges under consideration. For metal ions, the most probable mechanism for charge exchange is a stepwise charge exchange of the type

$$M^{+n} + M^{+k} = M^{+n-1} + M^{+k+1}, \qquad (1)$$

where n and k are charge numbers, such that $n > k$.

The cross section for the charge exchange with the native atoms and ions is much greater than that for the charge exchange with the gas atoms, whose electron shells are constructed in another fashion, and equals 10^{-14} cm^2. For single-charge ions, the cross section for the charge exchange with metal neutrals $\sigma^{+1 \to 0}$, depending on the energy, can be expressed as [16].

$$\sigma^{+1 \to 0} = A(1 - B \ln E)^2, \qquad (2)$$

where A and B are constants depending on the material and E is the kinetic energy of the metal ion.

A decrease in ion energy may result in a severalfold increase in charge-exchange cross section. Thus, according to (2), as E for aluminum ions is decreased from 20 to 2 eV, $\sigma^{+1 \to 0}$ increases from 4×10^{-15} to 1.1×10^{-14} cm^2. On the other hand, collisions of metal ions with gas atoms may result in a decrease in E, and the resulting increase in charge-exchange cross section may account for the effect of the gas on the change in charge. Furthermore, collisions resulting in large-angle scattering may also lengthen the ion trajectories which in turn may increase the number of ions participating in charge exchange.

The cross section for the charge exchange of multiply charged ions $\sigma^{+n \to 0}$ is greater than $\sigma^{+1 \to 0}$:

$$\sigma^{+n \to 0} \propto n^a \qquad (a = 2-5) \qquad (3)$$

and the ions with a large n should be the first to enter into the reaction. This accounts for the more rapid fall in the content of Al^{+3} ions with increasing pressure. Since reactions of the type (1) are forbidden for $n < k$, charge exchange reduces the fraction of multiply charged ions and increases the fraction of single-charge ions. As a result of the charge exchange process, the net ion charge does not change but there takes place its redistribution between the particles participating in the reaction. Actually, charge exchange of the type

$$M^{+1} + M^0 = M^0 + M^{+1}, \qquad (4)$$

does not cause any change in the charge composition of the plasma flow. The final product of these processes should be a flow of single-charged metal ions, as this is just observed in experiment. This mechanism is plausible when the average charge of the metal ions and atoms emitted by a cathode spot is lower than or equal to unity. This means that the vapor fraction of the ejected cathode material is greater than the ion fraction. The fact that the total mass lost by a cathode during the operation of a vacuum arc is greater than the mass of the ion flow [17], this mechanism is quite plausible, especially for low-melting-point materials.

A magnetic field applied to a vacuum arc causes an increase in the average charge of the metal ions. This perhaps is a manifestation of the increasing role of ionization processes in the plasma. As the magnetic field is increased, the plasma electrons begin to ionize the gas, and gas ions appear in the vacuum arc plasma. Actually, the gas ion fraction is greater for a gas with a lower ionization potential, the pressure and the magnetic field being the same.

5. CONCLUSION

Thus, the charge state spectrum of the metal ions in the plasma of a vacuum arc at an elevated gas pressure in the presence of a magnetic field is affected by two competing processes: the charge exchange that reduces the fraction of highly charged ions and the electron-impact ionization that increase this fraction. The appearance of gas ions in the vacuum arc plasma is perhaps due to the ionization of the gas by the plasma electrons.

6. ACKNOWLEDGMENTS

7. REFERENCES

[1] Vacuum Arcs. Theory and Application. Ed. by J.M. Lafferty (Wiley,. New York, 1980).

[2] G.A. Mesyats, Ectons (Nauka, Ekaterinburg, 1993).

[3] W. Kimblin, Proc. IEEE 59, 546 (1971).

[4] I.G. Brown, Rev. Sci. Instr., 65(10), 3061 (1994).

[5] I.G. Brown, Nucl. Instr. Methods, B37/38, 68 (1989).

[6] E.M. Oks et al., Appl. Phys. Lett., 67, 200 (1995).

[7] E.M. Oks et al., Rev. Sci. Instr., 65, 3113 (1994).

[8] I.G. Brown et al., Ibid., 57, 1069 (1986).

[9] I.G. Brown et al., Ibid., 58, 1589 (1987).

[10] R.A. MacGill et al., Ibid., 61, 580 (1990).

[11] S.P. Bugaev et al., Ibid., 63, 2224 (1992).

[12] A. Anders et al., IEEE Trans. Plasma Sci., 21, 305 (1993).

[13] I.I. Aksenov et al., Pisma Zh. Tekhn. Fiz., 7, 1164 (1991).

[14] I.I. Aksenov et al., Teplofiz. vysokikh temper., 21, 2:9 (1983).

[15] M. Sakaki and T. Sakakibara, IEEE Trans. Plasma Sci., 22, 1049 (1994).

[16] A. Anders, *A Formulary for Plasma Physics* (Academia Verlag, Berlin, 1990).

[17] V.I. Rakhovsky, *Commutation of Electrical Current in Vacuum: Physical Foundations* (Nauka, Moscow, 1970).

VACUUM ARC TRIGGER SYSTEMS BASED ON E × B DISCHARGES

A.G. Nikolaev[1], G.Yu. Yushkov[1], E.M. Oks[1,2], R.A. MacGill[3], M.R.Dickinson[3]

and I.G. Brown[3]

[1] High Current Electronics Institute, Russian Academy of Sciences, Tomsk 634055, Russia.

[2] State Academy of Control Systems and Radioelectronics, Tomsk 634050, Russia.

[3] Lawrence Berkeley National Laboratory, University of California, Berkeley, CA 94720, USA

ABSTRACT

Triggering systems for vacuum arc plasma sources and ion sources have been developed that make use of a gaseous trigger discharge in a strong magnetic field. Two kinds of trigger discharge configurations have been explored, a Penning discharge and a magnetron discharge. The approach works reliably for low gas pressure in the vacuum arc environment and for long periods of operation between required maintenance: pressures in the mid-10^{-6} Torr range and for $\gtrsim 10^6$ pulses.

1. INTRODUCTION

Vacuum arcs are widely used as plasma generators for metal ion beams and plasma flow sources [1-5]. A major field of application is for surface modification technology [6], and there is also much interest in the application of vacuum arc ion sources as ion injectors for heavy ion accelerators [7]. There is a need for increasing the lifetime between required maintenance of these devices, and an important part of this concern has to do with the triggering system employed.

One kind of commonly-used vacuum arc triggering system is based on cathode spot ignition by the plasma produced by flashover discharge across a dielectric surface [8]. Advantages of this method include its simplicity, relatively stability of operation, and low trigger energy compared to the main arc discharge energy. As a rule the cathode spot is first formed at the metal-dielectric boundary. Because of the dense, high-temperature plasma in the cathode spot, this leads to erosion of the dielectric and/or (in different regions) to metal film deposition on the insulator surface. These factors limit the lifetime of this kind of triggering system to $\sim 10^5$ pulses, or less for high arc current operation.

A gaseous pre-discharge could provide an alternative approach to cathode spot ignition. The glow-to-arc transition has been used for plasma triggering [9,10], but this requires a high background gas pressure of about 0.1 - 1.0 mTorr. Even though the pressure is negligibly small compared to the pressure within the cathode spot, the presence of this small amount of background gas can cause a decrease in the fraction of high charge state ions in the vacuum arc plasma as well as decreasing the total extracted ion current [11,12].

This paper describes an experimental investigation of vacuum arc trigger systems that are based on the low pressure glow discharge. To allow operation at low gas pressure, a special type

of glow with electron oscillation in crossed electric and magnetic fields was used, and a strong magnetic field was also applied to yet further lower the required operational pressure. This work was carried out collaboratively between the Berkeley and Tomsk laboratories.

2. EXPERIMENTAL SET-UP

Two closely-related kinds of gaseous discharges in crossed electric and magnetic fields are the Penning and magnetron discharges. The geometries of these two discharges are different but the physical processes are similar. In both cases the electrons are partially confined by the magnetic field and consequently have a long lifetime within the discharge gap. In general electrons can reach anode after they have lost most of their energy by excitation and ionization. With a low current, high voltage (several kV) discharge the lower pressure limit can be in the 10^{-8} Torr range, although for stable triggering a low voltage (several hundred) mode of operation with higher density plasma is preferred.

We have investigated both Penning and magnetron discharge geometries in the vacuum arc triggering experiments reported here. These kinds of systems are indicated schematically in Figure 1. The Penning system shown Figure 1(a) is formed by two opposing electrodes (cathodes) with a hollow anode located between them. The magnetron system (Figure 1(b)) consists of two cylindrical electrodes – a cathode and trigger, with the latter serving also as the magnetron anode. For both systems the main arc is ignited between the cathode and the hollow anode, and a small solenoidal coil is used in both cases to establish a magnetic field in the plasma region. Because of the pulsed operating mode and the small size of the coil it is possible to produce a magnetic field as strong as 1 to 2 T. A small gas flow is admitted to the trigger discharge gap region; this leads to only a small increase in the pressure both in the discharge region and in the cathode spot region. The triggering concept is the same for both the Penning and magnetron discharges, as can be seen

3

from Figures 1(a) and 1(b). Discharge of capacitor C_1 provides the coil current and the magnetic field in the gap.. Ignition of the Penning or magnetron discharge is supported by the high voltage (several kV), low current (about 0.1 A) power supply II. At the same time capacitor C_2, also charged to the same high voltage by power supply II, is discharged to provide an additional short (~10 μs) current pulse whose value exceeds the minimum current required for the formation of a cathode spot. Subsequently the spot current is supported by the main vacuum arc power supply III, whose voltage is less than 500 V. Note that only one electronic switch (for controlling the magnetic field) is used. The time of trigger discharge ignition as well as the time of cathode spot formation are determined by conditions internal to the discharge system.

To test these ideas, two special designs of vacuum arc ion source were made, utilizing the Penning and magnetron triggers [13]. The LBNL broad beam metal ion source, described in detail elsewhere [14,15], was used as the basic ion source. Schematics of this ion source as modified by Penning or magnetron trigger systems are shown in Figures 2(a) and 2(b), respectively. With the magnetron trigger the source included only a single vacuum arc (in a hollow cathode configuration) and the cathode spot was ignited on the internal surface of the cylindrical cathode. With the Penning trigger, because we used a ring electrode as Penning anode it was possible to use the 'regular' multi-cathode ion source with 18 separate cylindrical cathodes.

3. EXPERIMENTAL RESULTS

The experiments conducted fall into two groups, with Penning and with magnetron trigger systems, and the results were generally similar in both cases. This is indicated for example by the ignition characteristics shown in Figure 3, where similar behavior in the dependence of ignition voltage on background gas pressure is seen for both kinds of trigger systems. There are two regimes of gas pressure, with different effects on the ignition voltage. For relatively high pressure

4

the ignition voltage is approximately constant at about 1 - 2 kV. As the pressure is decreased we find an increase in the voltage required for stable operation of the trigger discharge. Because of the high magnetic field strength, even for pressures near 10^{-6} Torr the voltage necessary is no greater than 10 - 12 kV, which is acceptable for many vacuum arc applications. For pressures less then 10^{-5} Torr the trigger discharge does not fail, but it changes to a high voltage, low current mode (Figure 4). Nevertheless, stable arc ignition was still obtained even for background gas pressure in the 10^{-6} Torr region. More detailed investigations of current-voltage characteristic of the trigger discharge revealed the existence of an unstable discharge zone between the high and low voltage modes. Both the discharge current and voltage fluctuated from one mode to the other, but there was always about 10 microseconds of low voltage, high current discharge. During this time the value of ion flow from the plasma to the negative electrode was enough to form a cathode spot. With further decrease of pressure the unstable mode transferred to a pure high voltage, low current mode. In this mode, because of the negligibly low plasma density and, correspondingly, the low ion current density from the plasma to the cathode, cathode spots were not formed.

As mentioned above, a strong magnetic field moves the vacuum arc ignition process into the low pressure regime. The lower the pressure the stronger the magnetic field necessary for stable operation of the trigger discharge as well as for cathode spot formation (Figure 5). As the pressure is increased, high magnetic field becomes less important, and for some value of pressure (depending on the magnitude of the high voltage trigger) a magnetic field is not required for vacuum arc ignition. Then the trigger discharge with oscillating electrons changes to an ordinary glow.

We have shown previously (see, for example, [11]) that the background gas pressure has a strong influence on the charge state distribution of metal ions in vacuum arc plasmas as well as on the total ion current extracted from the plasma. Both the high charge state fractions and the total ion current fall with increasing gas pressure. As an example, the behavior of the ion charge state

5

distribution with an aluminum cathode as a function of increasing oxygen pressure is shown in Figure 6.

There are no major differences in performance between configurations employing Penning and magnetron trigger discharge systems. There are two different pressure regimes, having weak (on the low pressure side side) and strong (higher pressure) influences. Note that in the vacuum arc trigger systems described here, stable and reliable triggering is accomplished at significantly lower pressures than otherwise possible. This means that the vacuum arc parameters do not experience the presence of the low pressure of background gas, even though this low pressure is adequate for stable vacuum arc triggering. Our experiments have shown that the lifetime of a vacuum arc trigger system based of an oscillating electron trigger discharge in a strong magnetic field can exceed $\sim 10^6$ pulses at a repetition rate of 50 pps.

ACKNOWLEDGMENTS

REFERENCES

1. I.G. Brown, Rev. Sci. Instrum. 65, 3061 (1994).

2. S.P. Bugaev, A.G. Nikolaev, E.M. Oks, P.M. Schanin and G.Yu. Yushkov, Rev. Sci. Instrum. 63, 2422 (1991).

3. H. Zhang, X. Zhang, F. Zhou, S. Zhang, Q. Li and Z. Han, Rev Sci. Instrum. 65, 3088 (1994).

4. A. Anders, S. Anders and I.G. Brown, Plasma Sources Sci. Technol. 4, 1 (1995).

5. I.G. Brown, X. Godechot and K.M. Yu, Appl. Phys. Lett. 58, 1392 (1991).

6. See for instance the proceedings of the biennial International Conference on Ion Beam Modification of Materials, published in Nucl. Instrum. Meth. Phys. Res.

7. B.H. Wolf, H. Emig, D. Rück and P. Spädtke, Rev. Sci. Instrum. 65, 3091 (1994).

8. P.J. Evans, G.C. Watt and J.T. Noorman, Rev. Sci. Instrum. 65, 3082 (1994).

9. S.P. Bugaev, A.G. Nikolaev, E.M. Oks, P.M. Schanin and G.Yu. Yushkov, Rev. Sci. Instrum. 65, 3119 (1994).

10. E.M. Oks, Plasma Sources Sci. Technol. 1, 249 (1992).

11. P. Spädtke, H. Emig, B.H. Wolf and E.M. Oks, Rev. Sci. Instrum. 65, 3113 (1994).

12. E.M. Oks, I.G. Brown, M.R. Dickinson, R.A. MacGill, P. Spädtke, H. Emig and B.H. Wolf, Appl. Phys. Lett. 67, 200 (1995).

13. A.G. Nikolaev, P.M. Schanin, G.Yu. Yushkov and E.M. Oks, Proceedings of the 22nd International Conference on Phenomena in Ionized gases, Stevens Institute of Technology, Hoboken, N.J., July 31 - August 4, 1995, Vol. 1, p. 95.

14. I.G. Brown, IEEE Trans. Plasma Sci. 21, 537 (1993).

15. I.G. Brown, J.E. Galvin, R.A. MacGill and F.J. Paoloni, Rev. Sci. Instrum. 61, 577 (1990).

FIGURE CAPTIONS

Fig. 1   Schematic of the general overall set-up for (a) Penning, and (b) magnetron trigger systems.

Fig. 2   Vacuum arc ion source configurations as developed for the present work;
(a) Penning, and (b) magnetron trigger systems.

Fig. 3   Ignition voltage of Penning and magnetron triggering systems as a function of oxygen gas pressure.

Fig. 4   Voltage and current of Penning trigger discharge as a function of nitrogen gas pressure.

Fig. 5   Magnetic field employed in Penning trigger system as a function of gas pressure.

Fig. 6   Ion beam current fractions as a function of oxygen gas pressure, produced by a vacuum arc ion source with magnetron triggering system.

GAS

CATHODE

C1

T1

I

C3   L1   D1

C13   L10

III

COIL

TRIGGER

C2

D2

II

HOLLOW
ANODE

R1

Nik...   1(a)

TRIGGER GAS

COIL
CATHODE

HOLLOW
ANODE

Ninchi et al. Fig I (6)

PENNING ANODE

CATHODE

ANODE

COIL

EXTRACTOR SYSTEM

NIKOLAEV et al.   Fig 2(a)

CATHODE

TRIGGER

ANODE

GAS

COIL

EXTRACTOR SYSTEM

Nielsen et in   Fig 2 (b)

B = 10 kG
—o— Penning
—•— Magnetron

XBD 9601-00007.ILR

Fig. 3

XBD 9601-00008.ILR

Figure axis labels: Discharge voltage (kV) [left y-axis: 0, 1, 2, 3, 4, 5]; Discharge current (A) [right y-axis: 10^{-3}, 10^{-2}, 10^{-1}]; Gas pressure (Torr) [x-axis: 10^{-6}, 10^{-5}, 10^{-4}, 10^{-3}]

XBD 9601-00009.ILR

Niri... et al   Fig. 5

B = 5 kG

Ion current fraction (%)

Gas pressure (Torr)

- ● — Al^+
- ○ — Al^{++}
- ■ — O^+
- □ — O_2^+

XBD 9601-00010.ILR

NIKOLAEV ET AL   Fig 6.

HIGH POWER ION BEAM TREATMENT OF TITANIUM ALLOYS

SHULOV V.A. [1], DIDENKO A.N. [2], REMNEV G.E. [3], NOCHOVNAYA N.A. [4], ORESHNIKOVA T.M. [4]

1. Moscow Aviation Institute, 4 Volokolamskoye Shosse, Moscow 125871, Russia
2. Russian Academy of Science, 32a Leninsky Prospect, Moscow 117334, Russia
3. The Institute of Nuclear Physics, 2a Lenin Street, Tomsk 634050, Russia
4. All-Russia Institute of Aviation Materials, 17 Radio Street, Moscow 107005, Russia

ABSTRACT.

The influence of high-power ion beam irradiation and final heat treatment regimes on phisical and chemical state of titanium alloy parts surface layers were investigated. It was shown that high-power ion beam treatment allows to improve the following properties; fatigue strength (by 30-200%); heat gas corrosion resistance (in 2-3 times); erosion resistance (in 1.5-2 times); salt gas corrosion resistance (in 6 times and more). The reasons of service properties increasing in result of irradiation were determined. The high-power ion beam technologies are applied into practice in aviation industry of France and Russia.

INTRODUCTION.

The high concentration fluxes irradiation using high-power ion beam (HPIB) is the most progressive treatment

among the methods of surface processing of machine parts. HPIB application allows to increase service properties cardinally [1,2]. The elaboration of technology for titanium refrectory alloys parts [3] (compressor blades of aircraft engines) has been paid much attention. The number of service properties can improved by HPIB-irradiation in this case fatigue strength; heat gas corrosion; erosion and heat salt corrosion resistances, creep, microhardness ets)[3]. The main purposes of present paper are to generalize published data and to discuss new results on the HPIB application for service properties modification of titanium alloys parts which are used in aircraft building industry.

EQUIPMENT AND MATERIALS.

There are several models of accelerators (ТЕМП, ВЕРА, МУК, ТОНУС [3]) for HPIB treatment of metals and alloys. These accelerators are defined by the following parametres:

beam content - caron ions and protons (30-40%);

current density in pulse - $j=40-500$ A$*$cm^{-2} ;

pulse duration - $\tau=50-100$ ns;

pulse frequency - $f=0.2-10$ Hz

beam cross-section area - $s=60-1000$ cm^{-2} .

The BT9, BT8M, BT18Y, BT25Y and BT33 titanium alloys [4,5] samples and blades prepared according to conventional mechanical and thermal treatments have been irradiated. The vacuum annealing of the HPIB-irradiated samples and details was carried out in the ULVAK-furnace at operation temperatures of parts for structure-phase state stabilization of surface layers. Marks, compositions and heat treatment conditions of titanium alloys used in present work are given below:

1) BT8M (Ti, Fe-0.2, Al-5.8, Mo-33.7, Si-0.2, C<0.1, O<0.15, N<0.1, H<0.015), annealing at 920°C, air, 1h, aged at 550°C, air, 4h;

2) BT9 (Ti, Fe-0.25, Al-7.0, Mo-3.8, Zr-2.5, Si-0.3, C<0.1, O<0.15, N<0.05, H<0.015), annealing at 960°C, air, 2h, aged at 550°C, air, 4h;

3) BT18Y (Ti, Fe-0.2, Al-6.3, Mo-3.4, Zr-4.5, Nb-1.5, Si-0.25, Sn-3.0, C<0.1, O<0.14, H<0.015, N<0.05), annealing at 940°C, air, 2h, aged at 600°C, air, 6h;

4) BT25Y (Ti, Fe-0.25, Al-7.2, Mo-2.5, W-1.5, Zr-2.5, C<0.1, O<0.15, N<0.04, H<0.015), annealing at 940°C, air, 2h, aged at 600°C, air, 5h;

5) BT33 (Ti, Fe-0.15, Al-3.7, Mo-4.5, Zr-3.0, Si-0.25, Sn-3.0, C<0.1, O<0.15, N<0.05, H<0.015), annealing at 850°C air, 1h, aged at 550°C, air, 3h.

RESULTS AND DISCUSSION.

Influence of irradiation on state of surface layers.

The surface conditions of initial, irradiated and heat treated samples were studed by the following methods: Auger electron spectroscopy (AES); X-ray analysis; scanning electron microscopy (SEM); exoelectron emission; roughness and microhardness measurement.

It was shown that under the different HPIB irradiation regimes in the near surface layers of titanium refractory alloys the following processes run:

-precipitation (h=0.2-0.3 μm) of fine carbides or oxicarbides;

-melting at j>40A*cm^{-2} (h=1-2 μm);

-sublimation and plasma-formation (h=0.2-0.4 μm per pulse at high values of j>200 A*cm^{-2});

-defects formation (h=10 μm, diffraction lines

broadening and exoelectron emission intensity);

-rapid cristallization accompanied by the elements redistribution at high pulses amount in dependence on the distribution factors (n=100 pulses);

-decomposition and refinement of strengthening phases (TiC; Ti_3Al; β-phase in $(\alpha+\beta)$-titanium alloys and others);

The number of effects having large practical application have been oserved during investigation of the titanium refractory alloys products surface conditions after low temperatures 300-550°C (the vacuum homogenizing of the HPIB irradiated titanium refractory alloy parts should be carried out for the residual tensile stress relief and precipitation strengthening of the recrystallized surface layer):

-recrystallization with forming equiaxed grains of mean size 40-60 μm;

-annealing of defects formed under the HPIB irradiation;

-coagulation of carbides and formation of new carbide precipitates;

-formation of plate structure with high degree of α-plates orientation uniformity within each α-colony (alloy BT18Y, Fig. 1)

-'idealization' of the crystal lattice (this effect is being developed in great decreasing of interplanar spacing and X-ray lines halfwidth, these characteristics being more lower than those observed in the initial state after vibropolishing and even homogenizing at 700°C, (Fig. 2);

-intensive growth of the new phases germs in the craters, (Fig. 3);

-secondary decomposition of β-phase in α-plates with receiving "suplate" microstructure within each primary α-plate, and for this secondary α-plates can be combined in

Fig. 1 Material structure
in surface layers of BT18Y
alloy samples after HPIB ir-
radiation (j=150 A*cm^{-2},n=3)
and annealing (550°C, 2h,
small angle polished section)

Fig. 2 Fragments of diffra-
ction patterns determined
from surface of initial (1)
and HPIB irradiated (j=150
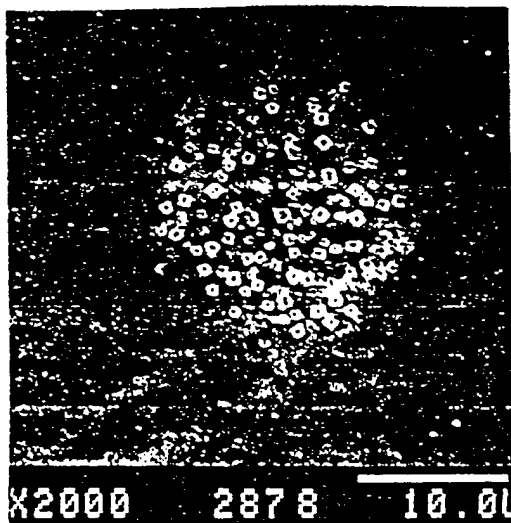A*cm^{-2}, n=3, annealing)BT18Y
alloy samples.

Fig. 3 Annealing crystal
embryoes growth in cra-
ters formed during HPIB
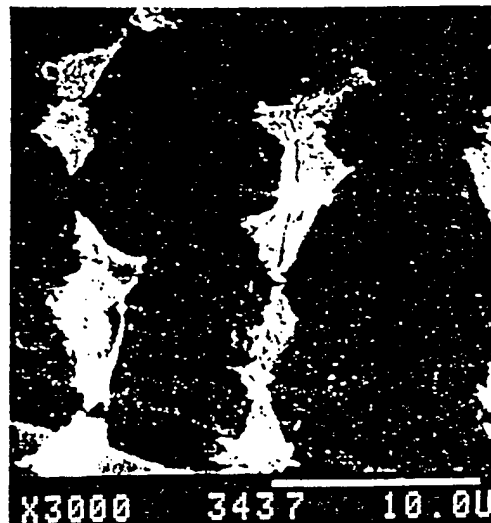irradiation of the BT18Y
alloy samples.

Fig. 4 Secondary decomposition
of β-phase in α-plate during
annealing of the HPIB irradia-
ted samples from the BT25Y al-
loy (j=120 A*cm^{-2} , n=3).

uniformly oriented sub-α-colonies, (Fig. 4).

It is undoubtedly that such considerable changes in phisical-and-chemical state of the titanium refractory alloys surface layers resulted from HPIB irradiation should be led to considerable components properties variations for these alloys.

Influence of HPIB-irradiation on the titanium alloys parts properties.

The influence of HPIB irradiation on titanium alloys parts fatigue strength was investigated in present work.

Table 1.

Fatigue test results for titanium alloy samples after HPIB irradiation and diffusive annealing.*

NN	Alloy	Irradiation regime			Test conductions and results			
		E, keV	J, $A*cm^{-2}$	n, pulses	f, Hz	T, °C	6_{-1}, MPa	N_c, cycles
1	BT8M*	–	–	–	80	550	160±10	$2*10^7$
2	BT8M*	300	60-80	3	80	550	440±20	$\gg 10^8$
3	BT8M*	120	20	15	80	550	280±10	$>10^8$
4	BT8M*	300+120	160+20	3+15	80	550	240±10	$>10^8$
5	BT9	–	–	–	3300	450	420±20	$2*10^7$
6	BT9	300*	60-80	3	3300	450	495±20	$>10^9$
7	BT25Y	–	–	–	3300	500	430±20	$2*10^7$
8	T25Y*	300	60	3	3300	500	520±20	$>10^9$

Some test results are given in Table 1. It was shown that without finishing heat treatment the value of δ_{-1} for HPIB irradiated samples was significantly lower than that for initial state components.

According to fractography investigations increasing of fatique strength for HPIB irradiated titanium alloys samples occurs both through changing of fatique crack nucleation mechanism and decreasing of fatique crack growth rate in comparison with the initial specimens. The latter is explained by decreasing of surface roughness as well as by carbide precipitates formation and structural alterations in surface layers during irradiation and heat treatment.

Table 2.

Effect of HPIB (E=300 keV, τ=50 ns) treatment regimes on gas corrosion resistance of titanium alloys (air, T=550 C, τ=200h).

N	Alloy	Irradiation regime		Annealing regime		Microhardness, $H\mu$, MPa				h_0, μm
		j, A* cm^{-2}	U·P	T· °C	τ, h	0.2 H	0.5 H	1 H	2 H	
1	BT9	–	–	–	–	1100±80	1060±60	900±30	750±60	30±5
2	BT9	80	1	–	–	280±10	600±30	630±20	540±10	12±5
3	BT9	60	7	–	–	350±10	520±10	520±20	430±20	15±4
4	BT9	60	3	550	2	450±30	370±20	360±30	350±30	6±2
5	BT9	60	7	550	2	420±20	400±20	360±20	360±20	6±2
6	BT18Y	–	–	550	2	–	–	–	–	23±3
7	BT18Y	150	3	550	2	–	–	–	–	10±4

Some results of gas corrosion resistance tests are given in Table 2.

Thus it was shown that the usage of HPIB allows to increase gas corrosion resistance of titanium refractory alloy parts in 2-5 times. The main reasons of corrosion properties improvement are following once: surface roughness decrease, formation of fine-dispersed carbide precipitates, "idealization" of crystal lattice and structural stability increase of surface layer material.
Some gas salt test results are shown in Table 3. These data allow to conclude that using HPIB treatment lead to heat gas salt corrosion resistance increasing (in 6 times and more).

Table 3.

Corrosion test results for titanium refractory alloy samples after and befor HPIB treatment (E=300 keV, n=3 pulses, τ=50 ns).

NN	Alloy	Irradiation regime $A*cm^{-2}$	Test conditions		m/Sc, $mg*mm^{-2}$
			T, ^{o}C	n, cycles	
1	BT8M	–	500	150	0.62±0.05
2	BT8M	120-140	500	150	0.10±0.05
3	BT8M	60-80	500	150	0.07±0.01
4	BT9	–	500	150	0:06±0.01
5	BT9	60-80	500	150	0.02±0.01
6	BT9	140-160	500	150	0.18±0.03

Mechanical properties after HPIB and anealing remain without change practically.

CONCLUSION.

Thus, using HPIB irradiation and finishing heat treatment for titanium refractory alloys at optimal regimes it is possible to: decrease the surface roughness up to $0.06-0.1\mu m$; form structure with optimum grains sizes in the surface layer; stabilize material structure by full decomposition of metastable phases; idealize the lattice greatly decreasing the interplanar spacing; form fine carbides or oxicarbides precipitates in the surface layer; provide optimum level of the residual compression stresses in the surface layer; clean surface from dirts; heal surface defects (microcracks, scratches, notches, splits ends); remove oxide or service damaged surface layers or aged protective coatings ($0.2-0.3 \mu m$ per pulse); increase the level of service properties cardinally.

REFERENCES.

1. K. YATSUI:'Industrial Applications of Pulse power and Particle Beams', Laser and Particle Beams, 1989, **7(4)**, 733-741.
2. A.D. POGRENJAK:'Metastale State and Structural Phase Changes in Metals and Alloys Exposed to High Power Ion Beams', Physical State Solid, 1990, **117(1)**, 17-51.
3. G.E. REMNEV, V.A. SHULOV: 'Application of High Power Ion Beams for Technology', Laser and Particle Beams, 1993, **11(4)**, 707-731.
4. S.G. GLASUNOV and V.A. KOLACHOV: Metals Science of titanium Alloys, Metallurgy, Moscow,1980.
5. O.P. SOLONINA, S.G. GLASUNOV: Refractory Titanium aaAlloys, Metallurgy, Moscow, 1974.
6. V.A. SHULOV:'Properties Modification of Refractory Alloys by Uninterruped and Pulse Ion eams', Science, Minsk, 1994.

MODIFICATION OF AIRCRAFT ENGINE COMPRESSOR BLADES PROPERTIES BY UNINTERRUPED AND PULSED ION BEAMS

V. A. SHULOV, N. A. NOCHOVNAYA, G. E. REMNEV,R. I. RAYBCHIKOV

Moscow Aviation Institute, 4, Volokolamskoye shosse, 125871, Moscow, Russia
All- Russian Institute of Aviation Material, 17, Radio Street, 107005, Moscow, Russia
Nuclear Physics Institute, 2a, Lenin Street, 634050, Tomsk, Russia

High Power Ion Beam Treatment
Key Parameters of the Technique

1. 6 types of accelerators (TEMP, TEMP-M, VERA, MUK, TONUS, LUCH)

2. Beam content :   • carbon ions

   • protons (30 – 40 %)

3. Ion energy : E = 100 – 300 Kev

4. Current density in pulse : J = 40 – 500 A/cm^2

5. Pulse duration : τ = 50 – 100 ns

6. Pulse frequency : f = 0,2 – 10 Hz

7. Beam cross section area : S = 60 – 1000 cm^2

High Power Ion Beam Treatment
Effects on surface

→ sublimation (0,6 µm)

→ melting (2 µm)

→ thick modified layer (shock wave) (100 µm)

→ substrate

Depending on process parameters, different mechanisms take place (calculation results)

Surface effect	Beam content	Layer thickness (µm)	Ion current density (A/cm^2)	Alloy
melting	100 % C$^+$	0.5	4.5	VT25Y Titanium alloy
sublimation	100 % C$^+$	0.5	133	
sublimation + melting	70 % C$^+$ + protons	0.5 + 2.1	172	
melting	100 % C$^+$	0.3	15	EP718ID Nickel alloy
decomposition of carbides	100 % C$^+$	0.3	75	
decomposition of γ/γ' phases	100 % C$^+$	0.3	45	

Physical and Chemical Effects (1)

STRUCTURE STABILISATION (VT25U alloy)

25KU X3000 3434 10.0U JEOL

IDEALISATION OF CRISTAL LATTICE

α-Ti (10$\overline{1}$)

α-Ti (00$\overline{2}$)

α-Ti (40$\overline{0}$)

2θ, grad 53, 49, 45,

CARBIDES FORMATION AND COALESCENCE

C 272 Ti 448 O 503 1

C 272 387 Ti 448 O 503 2

C 272 387 Ti 448 O 503 3

Auger-spectra of VT9 surface samples :
1 - initial condition ;
2 - HPIB (J = 150 A/cm^2 ; n = 3 pulses) ;
3 - HPIB and annealing (500°C, 2h)

Diffraction patterns of VT18Y surface
1 initial condition 2 HPIB (J = 150 A/cm^2 ; n = 3 pulses).

High Power Ion Beam Treatment
Physical and Chemical Effects (2)

SURFACE ROUGHNESS
EVOLUTION DURING PROCESS

initial condition;

n=3 pulses;

n=10 pulses;

High Power Ion Beam Treatment
Fatigue Characterization

VT 18 alloy

T = 500°C
F = 3300 Hz

VT 33 alloy

T = 450°C
F = 3300 Hz

☐   initial state (reference)

X   HPIB treatment :   E = 300 Kev, J = 140 - 160 A/cm², n ≥ 3 pulses

■   HPIB treatment + annealing

High Power Ion Beam Treatment
Fatigue Characterization

Legend:
- Initial state (reference)
- HPIB treatment + annealing

Y-axis: Fatigue limit at 2.10⁷ cycles (MPa)

450°C group:
- VT8M: 160, 440
- VT9: 420, 495

500°C group:
- VT25Y: 430, 520

	VT8M	VT9	VT25Y alloys
J (A/cm²)	60 - 80	60 - 80	60
pulse nb	15	3	10

High Power Ion Beam Treatment
Oxidation in air

Mass change ($\times 10^{-3}$ mg/cm^2)

600°C 500 h

650°C 500 h

0,8

0,25

0,45

0,25

EP 866 Ch

EP 718 ID

J(A/cm^2)	60	60
pulse nb	3	5

Initial state
HPIB treatment
HPIB + annealing

550°C 200 h

Oxidized layer thickness (µm)

30

15

6

23

10

VT9

VT18Y Alloys

J(A/cm^2)	60	150
pulse nb	7	3

High Power Ion Beam Treatment
Salt Corrosion

<u>esting conditions</u> : 150 cycles in sea water
(1 cycle = 3 min in temperature + 40 s in sea water)

	VT8M	VT9	EP 866 Ch
J(A/cm²)	120 - 140	60 - 80	60 - 80
pulse nb	3	3	3

Legend: Initial state / HPIB treatment + annealing

Mass change (mg/mm²)

500°C: 0,62 · 0,07 · 0,56 · 0,02

600°C: 0,83 · 0,31

High Power Ion Beam Treatment
Engine Test

esting conditions : VT9 alloy
component : blade from third stage compressor - Russian engine.
860 h engine running

Surface roughness

Roughness, Ra (micron)

	Ref.	HPIB	HPIB	HPIB
value	0,24	0,34	0,3	0,23	0,08

J(A/cm²): - | 150 | 120 | 80 | 60

Oxidation

Oxidized layer thickness (micron)

	Ref.	HPIB	HPIB	HPIB	HPIB
value	45	60	50	35	3

J(A/cm²): - | 150 | 120 | 80 | 60

Fatigue

Fatigue limit at 20°C (MPa)

	Ref.	HPIB	HPIB	HPIB	HPIB
value	480	450	460	480	540

J(A/cm²): - | 150 | 120 | 80 | 60

High Power Ion Beam Treatment

Conclusion

- HPIB Treatment applied on steel, Ti and Ni alloys, allows improvement of following properties :

  - fatigue behaviour

  - oxidation resistance

  - salt corrosion resistance.

- These results have been checked in laboratory and in engine testings.

OPTICAL MIRRORS

Some comparative data

The beaming strength of our aluminium mirrors has been risen to 2 J/cm^2 (for laser radiation wavelength of 308 nm) whereas the damage limit of the most of the existing aluminium mirrors is about 0.7-1.0 J/cm^2.

The beaming strength of our aluminium mirrors has been increased up to 88-90%; known samples of mirrors have 86-87% reflection factor.

The light scattering of our aluminium mirrors is about 0.1 -0.2% whereas the analogous value for the mirrors known to us is more than 0.5%.

The film on the glass endures more than 2300 N/cm^2 normal tearing force which is ultimate tensile strength of glass. The mirrors known to us have films with not so good adhesion which is about 100 N/cm^2.

ADVANTAGES

of the high-adhesion Cu and Al films.

The high films adhesion ensures improvement of strength and thermo-stability.

Films can be:

- washed lightly;
- high temperature soldered;
- heated up to 1000°C in thermo oven or by electrons beam;
- boiled in water;

The aluminium and copper films produced using our technique have a good corrosion stability.

- they don't oxidize in the air and don't need any protective coatings.
- operating life of the aluminium mirrors in fluorinated medium is increased.

OUR TECHNIQUE

makes it possible

- to produce mirrors with abovementioned properties for using them in various areas (optics, medical and office equipment and other);

- to produce complicated optical or other units, which require durable and hermetical joining of heterogeneous materials only by soldering (glass-, quartz-, ceramics-, technical diamond-metal);

- to shade glass and quartz ensuring high durability and needed transparency;

- to apply decorative pictures and inscriptions to glass, ceramic or porcelain goods, assuring good strength.

Please contact us in Tomsk, Russia, phone: (382 2) 25-96-83
25-85-82

RUSSIAN ACADEMY OF SCIENCES. TOMSK SCIENTIFIC CENTER.

ATTENTION *of the firms producing all kinds of lasers and/or using them in research, medicine or technology!*

OPTICAL MIRRORS

GLASS OR QUARTZ BASE LAYER COATED WITH THE ALUMINIUM OR COPPER FILM.

Mirrors have enhanced performance due to the new technique of metallic film high-adhesion application to dielectric materials.

		Al	Cu
Diameter of mirrors		up to 350 mm	up to 350 mm
Beaming strength		1.5–2.0 J/cm' (308 nm)	20–30 J/cm' (10.6 microns)
Reflection factor		88 – 90 %	99 %
Light scattering		0.1 – 0.2 %	
Strength of adhesion		2300 N/cm'	2300 N/cm'
Plasming limit			8 – 10 J/cm'

Our mirrors

don't need any protective coatings!

are thermoduric!

are stable in chemically active Medium!

are washable!

WE ARE READY TO MAKE A CONTRACT ON MIRRORS PRODUCTION WITH THE FIRMS INTERESTED IN BUYING THEM.

The beaming strenght of the aluminium mirrors produced using our technique has risen to 2 J/cm^2 for laser radiation wavelength of 308 nm (analogous value for the most of aluminium mirrors is about 0.7 - 1.0 J/cm^2).

The beaming strenght of the copper-and-glass mirrors for infrared radiation wavelenght of 10.6 microns is 30 J/cm^2.

The aluminium and copper films applicated using our technique have a good corrosion stability:

* they don't become oxidized in the air and don't need any protective coatings:

* aluminium coating keeps its properties very durably in fluorinated medium (the aluminium mirror in the power laser was In operation for more than 2 months whereas the usual aluminium films endure no more than 10 operating circles).

The plasming limit is raised significantly.

Our technique permits to reduce a size of particles forming the film. It means the light scattering decreasing to 0.1 - 0.2 %.

The film adhesion is significantly enhanced due to the new technique but reflective effect hasn't been fallen. (The film on the glass endures 2300 N/cm2 normal tearing force, which is ultimate tensile strength of glass).

It offers some new possibilities and extends sphere of application of this method.

Strength and thermostability of coatings is great because of high films adhesion.

Films can be:

* washed lightly;

* high temperature soldered:

* heated up to 1000°C in thermo-oven or by electrons beam:

* boiled in a water.

Coatings with such properties are obtained on the "K8" glass, quartz, ceramics and glass ceramic.

Please contact us in Tomsk, Russia, phone: (382 2)   25-96-83
25-85-82

Deposition of the high adhesion metallic films on glass, ceramics, semiconductor.

The our techniques of deposition thin metallic films is founded on the combination of processes and regimes of vacuum deposition and ion implantation. It allows adhesion to increase 30-50 times.

The Al and Cu films on the glass were tested at US National Laboratory. The results of the tests are the next:
1. Surface Roughness
Approximately 100-150 Angstroms. This is a high quality film and matches the result we expected.
2. Film-substrate adhesion
As measured by a Sebastian-type pull tester using Sebastian studs under normal loading, is > 45Mpa. This loading value is the limit of the pull tester. Thus we can only say that the adhesion strength is greater than this instrumental limit. The film bonding is very high.

The high adhesion of film offers improvement of the following characteristics of film:

- optical properties;

- mechanical strength;

- thermal strength;

- strength to corrosive media.

At present are resulted and studied the film from Al, Cu, Ti, stainless steel on glass, quarts, ceramics, glass ceramic, Si, technical diamond.

The light scattering of aluminium films is about 0,01-0,02%, whereas it for mirrors know to us is more than 0,5 %. Size of grain is 150 Angstroms.

Our films don't need any protective coatings.

Films can be:

- washed;

- high temperature soldered in a temperature range to 500° C;

- heated to 800° C in thermo-oven or by electrons beam;

- boiled in a water;

- photolithography and so on.

Our technique may be used for:

- to produce mirrors with above mentioned properties for optics, medical and other;

- to produce laser mirrors for high-energy lasers (IR & UV);

- the producing complicated optical units, requiring durable and hermetical joining by soldering;

- **the durable joining ceramics and glass with metals, other ceramics and glass,** metal with diamond by soldering;

- the obtaining small transfer impedance between semiconductor and thin metallic film.

The experiments confirm the possibility of using our technique for solutions of the indicated tasks.

РОССИЙСКАЯ АКАДЕМИЯ НАУК. ТОМСКИЙ НАУЧНЫЙ ЦЕНТР.
RUSSIAN ACADEMY OF SCIENCES. TOMSK SCIENTIFIC CENTER.

СТОМАТОЛОГИЧЕСКОЕ ЗЕРКАЛО.

STOMATOLOGIC SPECULUM.

Метод нанесения высокоадгезионного зеркального покрытия на стекло запатентован!

Преимущества:

- при изготовлении не используются токсичные вещества;
- высокое качество изображения;
- новые возможности стерилизации:
  - кипячение;
  - нагрев в сушильных печах до температуры не менее 200° С;
  - обработка в автоклаве;
  - возможность обработки в любых стерилизующих растворах;

Соответствие международным требованиям профилактики СПИД.

Method of application of high-adhesion specular coating to glass is patented.

Advantages:

- toxic material are not used in production;
- high-qualitative image;
- new sterilization capabilities;
  - boiling;
  - heating in dryer up to the temperature not less than 200° C;
  - autoclave sterilization;
  - sterilization in any sterilizing solutions.

The instrument meets the International Requirements for prophylaxis of AIDS.

Обращайтесь к нам по телефонам в Томске: (382 2) 25-96-83
Please contact us in Tomsk, Russia, phone: 25-85-82
25-88-85
25-99-67
факс (fax): 25-84-70

Institute of High Current Electronics

Siberian Division of the Russian Academy of Sciences
4 Akademichesky Ave., 634055 Tomsk, Russia

Use of Low-Energy, High-Current Electron Beams for Surface Treatment of Materials

LABORATORY OF VACUUM ELECTRONICS
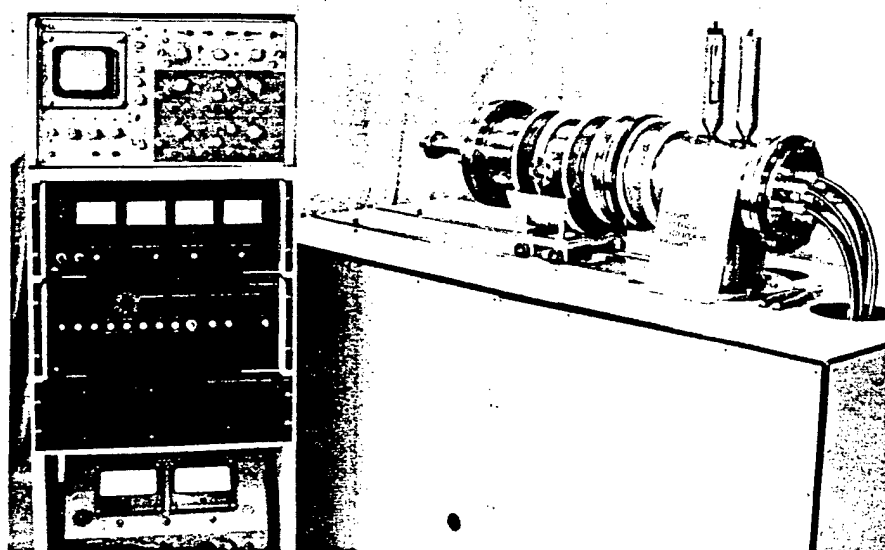
Prof. DMITRY I. PROSKUROVSKY
Head of Laboratory

4, Akademichesky Av., Tomsk 634055, Russia
Phone: (3822) 25-97-09, Fax: (3822) 25-94-10
Telex: 128112 PTB SU, E-mail: PDI@lve.hcei.tomsk.su

Tomsk, May 1996

Use of Low-Energy, High-Current Electron Beams for Surface Treatment of Materials

Beam parameters

- electron energy .... 10 to 40
- beam pulse duration .... 0.5 to 5
- beam energy density .... 0.5 to 40 J/
- beam cross section .... up to 50
- pulse repetition rate .... up to 0.2

Applications

- Increasing the life of tools and articles
- Improvement of tribotechnical characteristics
- Smoothing and cleaning the surface layers
- Deposition of coatings
- Removing the coatings
- Formation of surface alloys
- Enhancement of corrosion resistance
- Improvement of vacuum electrical insulation
- Modification of semiconductor surface layers

Use of Low-Energy, High-Current Electron Beams for Surface Treatment of Materials

D.I. Proskurovsky, V.P. Rotshtein, and G.E. Ozur

Institute of High Current Electronics, Siberian Division,
Russian Academy of Sciences, 634055 Tomsk, Russia

Abstract

The article describes the principle of operation and characteristics of low-energy, high-current electron beam sources having no analog in performance. The electron gun with an explosive emission cathode and a plasma anode, the bipolar pulse of accelerating voltage, and the guide magnetic field used in these systems make it possible to produce wide electron beams with an electron energy of 10 – 45 keV, a duration of 0.5 – 5 μs, and an energy density of 0.5 – 40 J/cm^2, being sufficiently stable and uniform to be used for technological purposes.

It has been shown that the graded structures formed in materials on irradiation may impart improved physicochemical properties and strength to the surface layers. This permits the use of low-energy, high-current electron beams for improving the strength and electrochemical properties of pieces and tools and for increasing the electric strength of vacuum insulation. Some technological operations, such as application and removal of coatings and surface alloying can be realized in the intense evaporation mode.

Key words: pulsed electron beams; surface treatment of materials.

Introduction

In the last few decades, new techniques for surface modification of metallic materials base on the use of concentrated energy flows have been developed extensively. By concentrated energy flows are meant intense pulsed laser, electron, and ion beams as well as pulsed plasma flows [1–4]. As they act on a material, there occur superfast heating, melting, and evaporation followed by superfast solidification of the material where dynamic temperature and stress fields are formed. These processes together produce new structure-phase states in the surface layers that are able to provide improved physicochemical and strength properties of the material, unattainable with ordinary surface treatment techniques.

The intense pulsed electron beams best suited for this purpose are low-energy ($\leq$50 keV), high-current($\geq$1 kA) electron beams (LEHCEBs) since they permit one to develop an X-ray safe technology on the base of a rather simple pulse power equipment.

Below we describe the principles of the generation of LEHCEBs, the characteristics of the LEHCEB sources, the main regularities of the formation of the beam-affected zone, and some examples of using these beams for surface treatment of metallic materials and articles.

1. LEHCEB sources

Conventionally, LEHCEBs, like high-energy beams, have been produced using direct-action vacuum diodes with explosive-emission cathodes [5–8]. The beam duration in these diodes is generally as short as 10^{-7} s since it is limited by the time required to the cathode and anode plasma to bridge the diode gap. Moreover, the electron beams formed in these diodes are characterized by the presence of substantial local nonuniformities in the current density distribution [9]. LEHCEBs of duration $\sim 10^{-6}$ s allow one to handle the same material modification problems; however, an increase in beam duration may improve substantially the uniformity of the beam-cross-section energy density distribution and reduce abruptly the mechanical stresses generated in the material on irradiation. The beam duration can be increased by increasing the diode gap spacing. This way, however, is unacceptable since it requires a proportional increase in accelerating voltage to conserve the high ($\sim 5 \times 10^5$ V/cm) electric field at the cathode necessary for efficient excitation of explosive electron emission [9].

For increasing the electric field at the cathode and the perveance of the electron beam, plasma-filled diodes hold much promise. The authors of Refs. 10 and 11 were first to describe a high-current electron gun where the electron beam was formed in the double layer between the (explosive emission) cathode plasma and the (preliminarily produced) anode plasma, passed through a hole in the anode, and got in a collector. With an accelerating voltage of ~ 100 kV, a beam of duration $\sim 1.6 \times 10^{-6}$ s and current up to 40 kA was generated. The beam was highly nonuniform because it was strongly compressed by the self magnetic field, which is unacceptable for surface treatment of materials. Using the method for production of high-current electron beams proposed in Refs. 10 and 11, we carried out comprehensive studies [12–21] that have permitted us to develop wide-aperture sources of microsecond LEHCEBs with smoothly variable beam parameters suitable for technological applications.

A block diagram of the electron source is given in Fig. 1. The explosive emission cathode is made of graphite. The anode is made of stainless steel and has a hole in its center to pass the beam. Twelve graphite-cathode spark plasma sources are placed evenly in a circle behind the anode. The electron beam was transported in the anode plasma to the collector. To prevent the beam from pinching, an external magnetic field of up to 0.45 T was applied.

The electron source operates as follows: As the magnetic field reaches its maximum, the spark sources are switched on and the anode plasma fills the acceleration gap and the beam drift space. After 2–3 μs an accelerating voltage produced by a voltage pulse generator (VPG) is applied to the cathode. The anode plasma, owing to its good conductance, acquires the potential of the anode, and the effective gap spacing in the diode shortens abruptly. This results in the initiation of explosive electron emission from the cathode. The voltage applied to the diode is localized across the double layer between the cathode and anode plasmas where the electron beam is formed. Since the acceleration gap spacing is a few centimeters, the beam duration is a few microseconds.

With accelerating voltages of 10–25 kV, a VPG producing a double voltage pulse consisting of a short (20–30 ns) positive prepulse and a main accelerating pulse of negative polarity. Within the time of the prepulse, the anode plasma becomes an electron emitter. Under the action of an accelerated electron flow, as a result of the ionization of the desorption products, a dense (10^{14}–10^{15} cm^{-3}) near-cathode plasma appears. This plasma stimulates uniform excitation of explosive emission from the cathode even at an accelerating voltage of 10 kV. When the accelerating voltage is over 25 kV, uniform explosive emission

at the cathode is excited without application of a prepulse, which simplifies substantially the VPG design and reduces its inductance and impedance.

Figure 2 gives typical waveforms of the voltage across the diode, the diode current, and the beam current onto the collector. It can be seen that up to 90% of the diode current passes through the anode hole. The beam transportation in plasma prevents the beam from degeneration into an angular beam and from filamentation (which is typical of vacuum diodes) and permits the distance from the anode to the surface under treatment to be increased to 15–20 cm. The highest efficiency of the conversion of the energy stored in the VPG into the beam energy ($\sim$40%) is achieved with the use of a magnetic field that compresses the beam in the diode region and spreads it in the transportation region. The beam energy density is controlled by varying the VPG capacitance and charge voltage, the magnetic field configuration, and the distance from the collector (Fig. 3).

When using a cathode with a plane emitting surface, the presence of an energy density maximum in the near-axis region of the beam is characteristic (see Figs. 3 and 4). This is related to the fact that in this region ions are accumulated within the pulse, which is due to the falling current-voltage characteristic of the diode [20,21]. The beam uniformity can be improved by using a hollow cathode (see Fig. 4, curve 2).

Table 1 gives the characteristics of the electron sources we have developed. The sources have been in use from two to six years. They turned out sufficiently reliable and simple to operate.

Table 1:

Source parameters	Type 1	Type 2	Type 3
Electron energy, keV	10–30	10–30	20–45
Beam current, kA	up to 2	up to 15	up to 50
Pulse duration τ, μs	1.5–1.2	1–5	2–4
Beam energy density E_s, J/cm^2	0.5–6	1–10	2–40
Beam cross-section area, cm^2	up to 3	up to 30	up to 50
Pulse repetition rate, Hz	up to 0.2	up to 0.2	up to 0.2
Operating vacuum, Torr	10^{-4}–10^{-5}	10^{-4}–10^{-5}	10^{-4}–10^{-5}
Input power, kW	1	3	5

2. Formation of the beam-affected zone

The principal factors that determine the state and properties of the beam-affected zone are the nonstationary temperature fields that appear in the surface layers as a result of the absorption of the beam energy and the stress fields caused by the nonuniform heating of the material. Let us consider the characteristics of these fields for typical LEHCEB parameters.

2.1. Temperature fields and stress fields

The temperature fields were found by solving numerically a one-dimensional heat equation with account for melting and evaporation and in view of actual oscillograms of the current density at the target and the voltage across of the diode [22-24]. Figures from 5 to 8 present the results of the calculations for iron irradiated in the characteristic melting and

evaporation modes. In the first mode, a layer of thickness 1.2 μm is melted; the melting lifetime is ~ 1 μs. In the second mode, a layer of thickness ~ 2 μm is evaporated; the melt thickness is ~ 5.5 μm, the melt lifetime is $\sim 10^{-5}$ s, and the duration of the evaporation process is ~ 1.5 μs. The velocity of the crystallization front sharply increases near the very surface. This velocity in the evaporation mode (~ 4 m/s) is half the velocity in the melting mode, which is related to the increased melt thickness. The cooling rate reaches its maximum ($\sim 3 \times 10^9$ K/s) at the surface immediately after the passage of the crystallization front and depends on the irradiation mode only slightly. In the melting mode, the thickness of the heat-affected zone (HAZ) where the maximum temperature exceeds the recrystallization temperature T_{recr}, so that $T_{recr} \simeq 0.4 T_m$ (T_m being the melting point), is ~ 7 μm, while in the evaporation mode, the thickness of this zone increases to ~ 20 μm.

An analysis of the data available in the literature [24] suggest that in iron irradiated by an LEHCEB in the initial melting mode ($W_s \simeq 10^6$ W/cm^2) a bipolar stress wave is formed whose amplitude is far below the dynamic yield limit of the material, $\sigma_{0.2}^{dyn}$. In addition, quasi-static compressive stresses act in the HAZ, whose magnitude, according to estimates [25], may be over $\sigma_{0.2}^{dyn}$. After the termination of the pulse, the near-surface layer is cooled and compressed at the latest stage of the process. Therefore, residual tensile stresses are formed in this layer, whose magnitude is 40–80 MPa, which is about an order of magnitude lower than that of the compressive stresses acting on irradiation. The tensile stresses have a maximum at a depth of ~ 5 μm and are localized within the HAZ (~ 10 μm).

In the intense evaporation mode ($W_s \simeq 10^7$ W/cm^2), the stress wave amplitude, according to estimates [24], is close to the yield limit of the material and it should be taken into account in analyzing the conditions under which the HAZ is formed.

2.2. Formation of graded structures

Investigations of the structure and properties of iron, carbon and stainless steels, and titanium and aluminum alloys irradiated in the modes of initial melting and intense evaporation have made it possible to reveal the regularities as follows:

1. The action of an LEHCEB results in the formation of an extended ($\sim 10^{-3}$ cm) depth-graded defect and grain structure (Fig. 9) showing a nonmonotonic depth variation of the stress-strain state and the degree of hardening (Fig. 10).

2. The melt-quenched layers have a thickness of 10^{-4}–10^{-5} cm and show reduced etchability in acids ("white" layers, Fig. 11). The latter is related to the fact that the structure formed is more homogeneous than the initial one. The most pronounced structure-phase changes occur in the near-surface layers (0.2–0.5 μm), which correlates with the fact that the cooling rate and the velocity of motion of the crystallization front reach their maxima at the surface. In these layers, depending on the original structure-phase state and the irradiation mode, secondary phases (carbides and intermetallides) are partially or completely dissolved.

3. The dimensions of the hardened zone may be an order of magnitude and even more above the thickness of the HAZ. The most pronounced hardening is attained on irradiation of steels having a martensitic structure (Fig. 10). This is related to the fragmentation of martensite and the formation of disperse particles of cementite under the action of low-amplitude bipolar stress waves.

3. Use of LEHCEBs for surface treatment

The graded structures formed on LEHCEB irradiation may impart improved physico-chemical and strength properties to the surface layers. In the intense evaporation modes,

some important technological operations can also be realized. The principal results obtained on this lines are presented below.

3.1. Improvement of tribotechnical characteristics

Tests with a friction pair consisting of a rotor (steel, HRC 55) and a plate (ball bearing steel, HRC 60) in the presence of lubricant have shown that on irradiation the wear rate of the plates decreased by a factor of 1.5 and the friction moment decreased by a factor of 1.7 compared to unirradiated plates [24]. It has been revealed that this is related to the formation (on irradiation) of a structure consisting of finely divided martensite and a great amount (up to $\sim$60%) of residual austenite that transforms into martensite in the process of working loading [21].

Under the conditions of dry friction, the wear rate of irradiated plates almost halved compared to unirradiated plates. With that, the depth of the friction trace was $\sim$25 μm, which corresponds to the position of the first maximum of microhardness (Fig. 10). This points to the fact that there is a correlation between wear resistance and microhardness.

Tests of metal–polymer friction pairs have shown that the surface melting of disks made of titanium alloys reduces the wear rate of the polymer (based on PTFE) by a factor of $\sim$1.5 [24]. This is related in the main to the smoothing of the surface relief (Fig. 12).

3.2. Increasing the life of steel tools

For optimal modes of hardening of tool steels with a martensitic structure, the thickness of the layer melted by the LEHCEB is not over $\sim$1 μm. Therefore, the irradiation may be the finishing technological operation in the production of vital pieces and tools. Industrial tests have demonstrated that the irradiation in these modes allows a 2–3-fold increase in the life of cutting tools (drills, cutters) and tools used for plastic metal working (punches, mandrels).

3.3. Treatment of hard-alloy cutting tools

Used in the experiment were industrial nonresharpable cutting plates made of hard alloys of type BK8 (WC–8%Co) and type T5K10 (WC–5%TiC–10%Co). It has been established [27] that the LEHCEB irradiation in optimal modes increases the tool life at elevated cutting speeds by a factor of two or three (Fig. 13). An additional effect is attained by annealing the tool after irradiation, owing to the removal of the tensile macrostresses in the carbide phase as a result of irradiation. The increase in tool life correlates with the increase (by 15–20%) of the microhardness at the surface, which is related to the additional diffusion of the carbides in the cobalt binder.

3.4. Treatment of titanium alloys

Experiments have shown that a cyclic LEHCEB action on titanium alloys in the initial melting mode not only makes the surface much smoother (Fig. 12) but also cleans it from oxygen and carbon impurities and improves the uniformity of the element distribution in thickness in the surface layer (Fig. 14). However, melt quenching deteriorates the phase composition, and destructive residual tensile stresses are formed. Subsequent annealing recovers the phase composition, increases the microhardness, and raises the fatigue strength of the workpiece be about an order of magnitude. The latter, as evidenced by fractography, is due to the fact that the surface destruction mechanism changes to the subsurface one.

3.5. Smoothing of heat-resistant protective coatings

Heat-resistant protective coatings based on Ni (e.g., Ni–Cr–Al–Y) have originally a rather rough surface. Smoothing of the surface should improve the performance of vanes made of heat-resistant nickel-based alloys. Experiments have shown [28,29] that melting of a thin surface layer of such a coating allows an increase in heat resistance (by 25% at 1050 °C) due to the sharp reduction of the surface roughness (Fig. 15). With that, the fatigue strength of the vanes is retained.

3.6. Removal of heat-resistant protective coatings

The existing technology for removing a worked-out coating is characterized by a high laboriousness, a low level of automation, and harmful working conditions. To eliminate these disadvantages, LEHCEBs can be used. Experiments have shown that a beam of energy density ≥ 20 J/cm^2 can efficiently (1–2 μm per pulse) remove this type of coating not changing the substrate structure and properties.

3.7. Production of highly concentrated surface alloys

With beam energy densities of over 10 J/cm^2, there is an opportunity of fast deposition of coatings by evaporating the target in the pulsed mode with melting of the surface layer. The results of this "micrometallurgical" process, as applied to a Cu–Fe system on a Fe substrate, are presented in Fig. 16. It can be seen that the total thickness of the alloyed layer is a few micrometers and the copper concentration in a layer of thickness ~ 1 μm is ~ 20 at.%. The alloying is accompanied by cleaning of the surface from carbon and oxygen impurities.

Efficient component mixing was also observed for the system Al–Fe, Ti–Fe, W–Fe, Ti–Cu, Al–Ti, and the like. With that, the alloyed layer thickness was 0.5–3 μm. Thus, the above technique makes it possible to produce highly concentrated surface alloys in layers whose thickness is an order of magnitude greater than that characteristic of high-dose ion implantation and pulsed melting of film–substrate systems [1].

3.8. Enhancement of the corrosion resistance of stainless steel

Cyclic treatment of type 12X18H10T steel (steel 302 being US analog) in the mode of weak evaporation of the surface layer ($\sim 6 \times 10^{-2} \mu$m per pulse) efficiently cleans the surface from undesirable impurities and results in the formation of a fast-quenched structure with a smoothed microrelief. The increased degree of chemical homogeneity of the surface leads to a shift of the stationary potential to the positive region and to a significant decrease in dissolving current (Fig. 17) [30].

A favorable effect on the corrosion properties of this steel is played by alloying with tantalum being a strong carbide-producing element that prevents a reduction of the chromium concentration in the solid solution. Experiments have shown that an optimal irradiation mode is the single-pulse mode that ensures initial melting of the coating-substrate system. With increasing energy density and number of pulses, the corrosion resistance of coated specimen decreases, as distinct from uncoated specimens. Model experiments with a Ta–Fe system have shown [31] that as the energy density is increased, the tantalum concentration at the surface decreases because of its diffusion deep into the specimen and partial evaporation. This reduces the corrosion resistance of specimens with a coating.

3.9. Enhancement of the electric strength of vacuum insulation

The electric strength of vacuum insulation largely depends on the quality of the preliminary treatment of the electrodes, aimed at suppressing the activity of the emission centers on the cathode and reducing the gas release from the electrodes. It has been established [32] that the LEHCEB irradiation of electrodes efficiently smooths the working surface due to its melting and cleans the near-surface layers from impurities and dissolved gases. This treatment followed by conditioning of the vacuum gap with low-current pulsed discharges reduces substantially the prebreakdown currents and enhances the electric strength of the vacuum insulation (Fig. 18). The best effect has been achieved for stainless-steel electrodes.

4. Summary

The principle of operation and characteristics of the sources of wide LEHCEBs based on an electron gun with an explosive-emission cathode and a plasma anode are described. It has been shown that the use of these sources makes it possible to develop new efficient techniques for surface treatment of materials.

We anticipate that the LEHCEB sources can be refined by using low-pressure discharges in crossed electric and magnetic fields to produce anode plasmas. Our preliminary experiments have demonstrated that this improves the beam uniformity and stability. In combination with the use of other cathode materials, this allows minimization of the pollution of workpieces with carbon.

In our opinion, promising lines of use of LEHCEBs are treatment of pieces made of heat resistant titanium and nickel alloys, hardening of hard-alloy tools, enhancement of the corrosion resistance of alloys, removal of worked-out protective coatings, enhancement of the electric strength of vacuum insulation, and production of highly concentrated surface alloys.

5. Acknowledgments

References

[1] Surface Modification and Alloying by Laser, Ion and Electron Beams, edited by J.M. Poate, G. Fotti, and D.C. Jacobson, Plenum Press, New York, 1983.

[2] Yu.A. Bykovsky, V.N. Nevolin, V.Yu. Fominsky. Ion and Laser Implantation of Metallic Materials, Moscow, Energoatomizdat, 1991.

[3] A.D. Pogrebnyak and D.I. Proskurovsky, Phys. Stat. Sol. (A), 145 (1994) 9-49.

[4] B.A. Kalin, V.L. Yakushin, and V.I. Pol'sky, Izv. Vyssh. Uchebn. Zaved. Fizika, No. 5 (1994) 109-126.

[5] A.C. Greenwald, A.R. Kirkpatrick, R.G. Little, and J.A. Minnucci, J. Applied Physics, 50 (1979) 783-787.

[6] B.A. Koval', G.A. Mesyats, G.E. Ozur, D.I. Proskurovsky, and E.B. Yankelevich, Proc. IVth Intern. Topic Conf. on High Power Electron and Ion Beams, Paris, July 1981, p. 512-519.

[7] G. Leggieri, A. Luches, V. Nassisi, A. Perrone, and M.R. Perrone, Vacuum, 32 (1982) 9-10.

[8] A.S. El'chaninov, B.A. Koval', G.A. Mesyats, D.I. Proskurovsky, and E.B. Yankelevich, Prib. Tekh. Exper., No. 5 (1987) 122-125.

[9] G.A. Mesyats and D.I. Proskurovsky, Pulsed Electrical Discharge in Vacuum, Springer-Verlag, Berlin, 1989.

[10] D.V. Iremashvili, T.A. Osepashvili and P.I. Kakuchaya, Pis'ma v Zh. Tech. Fiz., 1 (1975) 508-511.

[11] D.V. Iremashvili, P.I. Kuznetsov, T.A. Osepashvili, A.P. Timoshenko, Zh. Tekhn. Fiziki, 49 (1979) 1485-1488.

[12] G.E. Ozur and D.I. Proskurovsky, Pis'ma v Zh. Tekhn. Fiz., 14 (1988) 413-416.

[13] G.E. Ozur and D.I.'Proskurovsky, Proc. XIVth Intern. Symp. on Discharges and Electrical Insulation in Vacuum, Santa Fe, USA, September, 1990, p. 665-670.

[14] M.Yu. Kreindel', E.A. Litvinov, G.E. Ozur, and D.I. Proskurovsky, Fizika Plasmy, 17 (1991) 1425-1439.

[15] M.Yu. Kreindel', E.A. Litvinov, G.E. Ozur, and D.I. Proskurovsky, Proc. XVth Symp. on Discharges and Electrical Insulation in Vacuum , Darmstadt, Germany, August 1992, p. 707-710.

[16] D.S. Nazarov, G.E. Ozur, and D.I. Proskurovsky, Ibid., p. 716-720.

[17] M.Yu. Kreindel', E.A. Litvinov, G.E. Ozur, and D.I. Proskurovsky, Proc. 9th Intern. Conf. on High-Power Particle Beams, Washington, USA, May 1992, p. 1111-1116.

[18] D.S. Nazarov, G.E. Ozur, and D.I. Proskurovsky, Proc. 10th Intern. Conf. on High-Power Particle Beams, San Diego, USA, June 1994, p. 653-655.

[19] D.S. Nazarov, G.E. Ozur, and D.I. Proskurovsky, Fizika Plasmy, 21 (1995) 173-179.

[20] D.S. Nazarov, G.E. Ozur, and D.I. Proskurovsky, Izv. Vyssh. Uchebn. Zaved. Fizika, No. 3 (1994) 100-114.

[21] D.S. Nazarov, G.E. Ozur, and D.I. Proskurovsky, Prib. Tekh. Exper., No. 2 (1996).

[22] Yu.F. Ivanov, V.I. Itin, S.V. Lykov, A.B. Markov, G.A. Mesyats, G.E. Ozur, D.I. Proskurovsky, V.P. Rotshtein, and A.A. Tukhfatullin, Izvestiya Akademii Nauk SSSR Seriya Metally, No. 3 (1993) 130-140.

[23] Yu.F. Ivanov, V.I. Itin, S.V. Lykov, A.B. Markov, V.P. Rotshtein, A.A. Tukhfatullin, and N.P. Dikii, Fizika Metallov i Metallovedenie, 75 (1993) 103-112.

[24] V.P. Rotshtein, Modification of structure and properties of metallic materials by intensive pulsed electron beams, D. Sc. thesis, Institute of High-Current Electronics, Tomsk, 1995.

[25] E.F. Dudarev, G.P. Pochivalova, D.I. Proskurovsky, V.P. Rotshtein, A.B. Markov, Izv. Vyssh. Uchebn. Zaved. Fizika, No. 3 (1996) 126-132.

[26] V.S. Kraposhin, Metallovedenie i Termicheskaya Obrabotka Metallov, No. 2 (1994) 2-4.

[27] I.M. Goncharenko, D.V. Lychagin, D.S. Nazarov, G.E. Ozur, P.V. Orlov, K.N. Poleshchenko, D.I. Proskurovsky, V.P. Rotshtein, and A.A. Tukhfatullin, Proc. 4th Intern. Conf. "Computer-aided Design of Advanced Materials and Technologies", Tomsk. 1995, p. 120.

[28] Yu.D. Yagodkin, K.M. Pastukhov, S.I. Kuznetsov, N.F. Ivanova, and E.Yu. Aristova, Fizika i Himija Obrabotki Materialov, No. 5 (1995) 111-119.

[29] Yu.D. Yagodkin, D. Sc. thesis, Moscow Aviation Institute, Moscow, 1995.

[30] I.M. Goncharenko, V.I. Itin, S.V. Isichenko, S.V. Lykov, A.B. Markov, O.I. Nalesnik, G.E. Ozur, D.I. Proskurovsky, and V.P. Rotshtein, Zashchita Metallov, 29 (1993) 932-937.

[31] Yu.F. Ivanov, Yu.Yu. Kryuchkov, A.B. Markov, D.S. Nazarov, G.E. Ozur, A.D. Pogrebnyak, D.I. Proskurovsky, and V.P. Rotshtein, Poverkhnost'. Fizika, Khimiya. Mekhanika, No. 10-11 (1994) 95-102.

[32] A.V. Batrakov, A.B. Markov, G.E. Ozur, D.I. Proskurovsky, V.P. Rotshtein, IEEE Trans. on Dielectrics and Electr. Insul., 2 (1995) 237-242.

Figure 1. Block diagram of the electron source. 1 — cathode; 2 — anode; 3 — plasma spark sources; 4 — collector; 5 — solenoid; 6 — vacuum chamber; 7 — control unit; 8 — solenoid power supply unit; 9 — trigger unit; 10 — pulse generator; 11 — cathode plasma; 12 — double layer; 13 — anode plasma; 14, 15 — Rogovsky coils; R1, R2 — voltage monitor; R_{sh} — current shunt.

Fig. 2. Typical waveforms of the diode voltage V_d, total diode current I_d, and beam current I_b for different storage capacitances C and different storage capacitor voltages V_1: (a) – $C = 0.4\mu F$, $V_1 = 25$ kV; (b) – $C = 3.6\mu F$, $V_1 = 40$ kV.

Fig. 3. Beam energy density variations w vs storage capacitor voltage V_1 (a) and drift channel length l (b).

Fig. 4. Beam energy density distribution *vs* beam radius r for the conditions pointed out on the Fig. 2a (a) and on the Fig. 2b (b).

Table 1. The parameters of three versions of the low-energy, high-current electron beam source for surface treatment.

Source parameters	Type 1	Type 2	Type 3
Electron energy, keV	10–30	10–30	20–45
Beam current, kA	up to 2	up to 15	up to 50
Beam pulse duration, μs	0.5–1.2	1–5	2–4
Beam energy density, J/cm^2	0.5–6	1–10	2–40
Beam cross section, cm^2	up to 3	up to 30	up to 50
Pulse repetition rate, Hz	up to 0.2	up to 0.2	up to 0.2
Operating pressure, Torr	$10^{-4} - 10^{-5}$	$10^{-4} - 10^{-5}$	$10^{-4} - 10^{-5}$
Power input, kW	1	3	5

Figure 5: Time dependence of the surface temperature for iron irradiated in the mode of melting $(0.8~\mu s, 3.2~\mathrm{J/cm^2})$ – (a) and evaporation $(2.5~\mu s, 25~\mathrm{J/cm^2})$ – (b).

Figure 6: Variation of the position of the melt-solid boundary for iron irradiated in the melting mode $(0.8~\mu s, 3.2~\mathrm{J/cm^2})$ – (a), the same (curve 1) and the variation of the surface coordinate (curve 2) for iron irradiated in the evaporation mode $(2.5~\mu s, 25~\mathrm{J/cm^2})$ – (b).

Figure 7: Depth variation of the crystallization front velocity for iron irradiated in the mode of melting (0.8 μs, 3.2 J/cm^2) – (a) and evaporation (2.5 μs, 25 J/cm^2) – (b).

Figure 8: Maximum temperature as a function of the distance from the surface for iron irradiated in the mode of melting (0.8 μs, 3.2 J/cm^2) – (a) and evaporation (2.5 μs, 25 J/cm^2) – (b).

Figure 9: Structure of the heat-affected zone in steel 45 treated with an LEHCEB of microsecond duration [22].

Figure 10: In-depth distribution of microhardness for a pre-hardened steel 45 specimen irradiated by an LEHCEB with $\tau = 0.7$ μs, $E_s = 2.5$ J/cm^2; number of pulses $N = 1$ (1), $N = 300$ (2) [22].

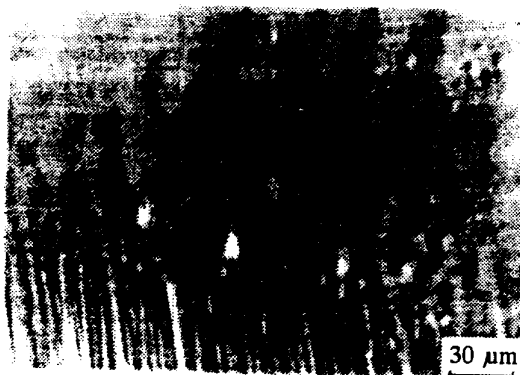Figure 11: Structure of the cross-section of a steel 60 specimen irradiated in the evaporation mode.

Figure 12: Scanned electron micrograph of the surface of a titanium alloy taken after irradiation by an LEHCEB with τ=0.7 μs, E_s=2 J/cm^2 , N=10. Seen below are marks of original mechanical processing near the beam edge.
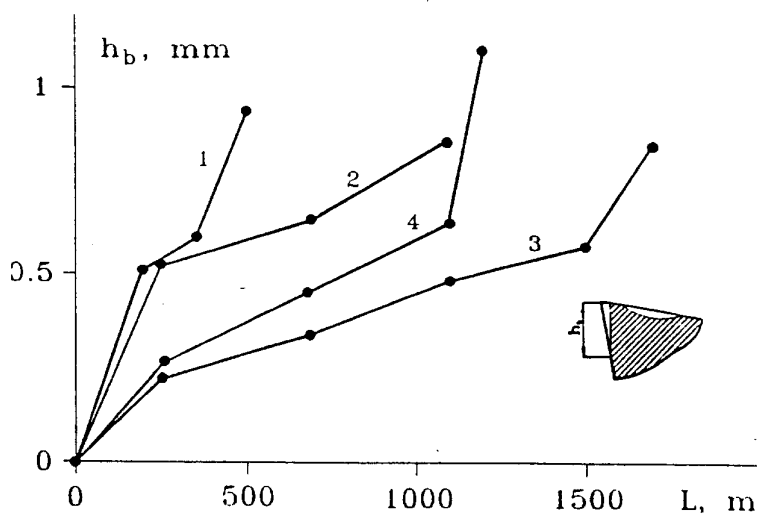

Figure 13: The width of wear area on the rear surface of a cutter made of T5K10 alloy as a function of cutting length before (1) and after (2, 3, 4) irradiation with E_s = 2.7, 4, and 7 J/cm^2, respectively. The material under treatment - a steel 40X. Conditions of cutting: S = 0.14 mm/rev, d = 1.5 mm; V = 300 m/min.
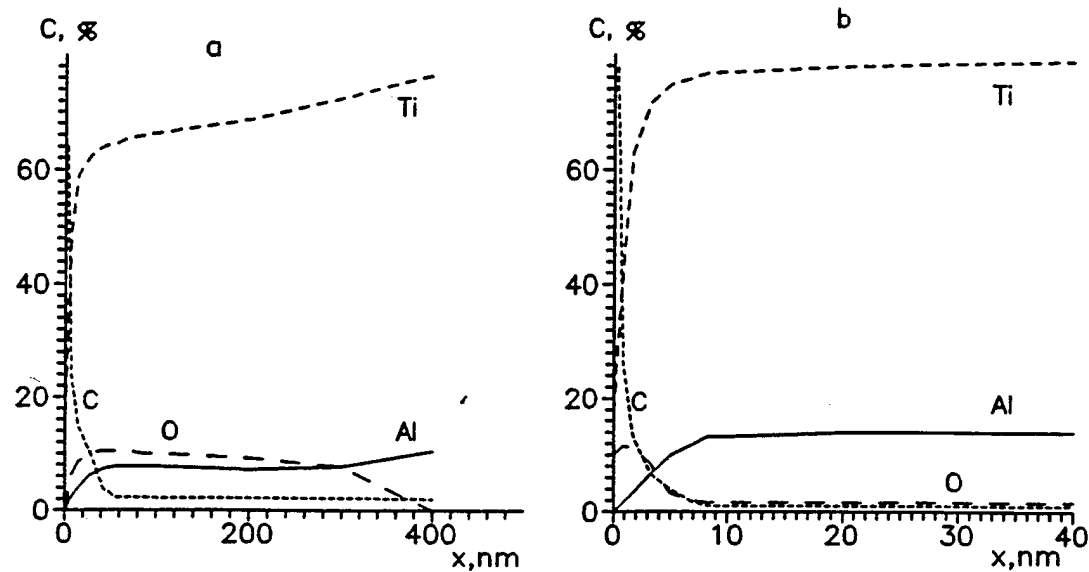
Figure 14: Concentration profiles of the elements in the surface layer of a BT9 titanium alloy specimen before (a) and after (b) LEHCEB action with $\tau = 2.5$ μs, $E_s = 5$ J/cm^2, $N = 100$.

Figure 15: Profilographs of surface of specimens with Ni-Cr-Al-Y coating in initial state (1) and after irradiation (2).
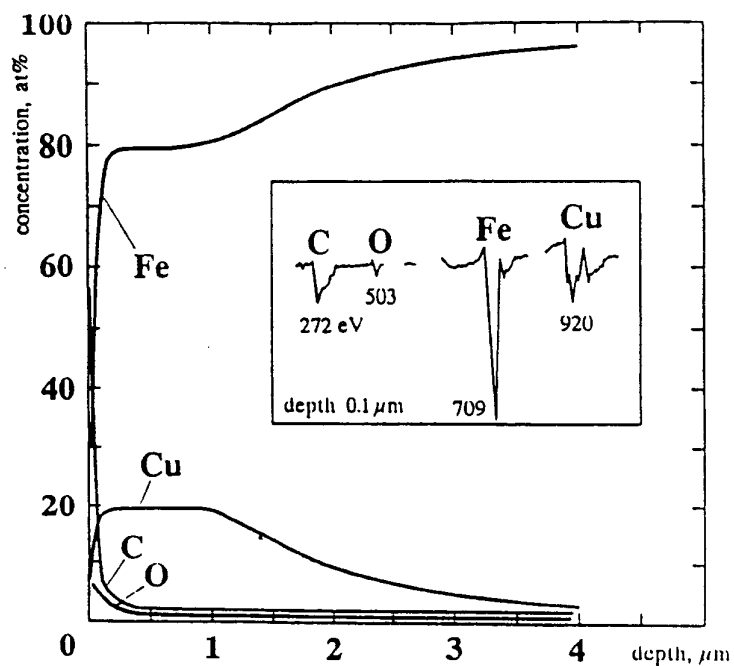
Figure 16: Concentration profiles of the elements in the surface Cu-Fe alloy formed with the use of an LEHCEB by Cu deposition on a Fe substrate and by surface melting.
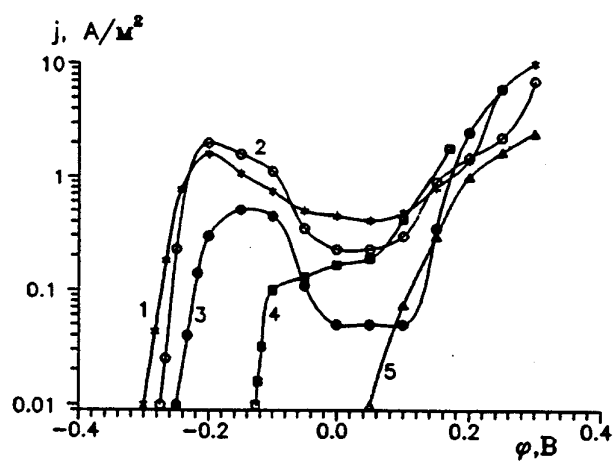

Figure 17: Anode polarization curves obtained for a stainless steel specimen in a 1% HCl solution under various irradiation conditions: 1 - original specimen; 2 - $E_s = 2$ J/cm^2, $N = 1$; 3 - $E_s = 5$ J/cm^2, $N = 1$; 4 - $E_s = 5$ J/cm^2, $N = 20$; 5 - $E_s = 5$ J/cm^2, $N = 100$. Pulse duration $\tau = 0.7$ μs.
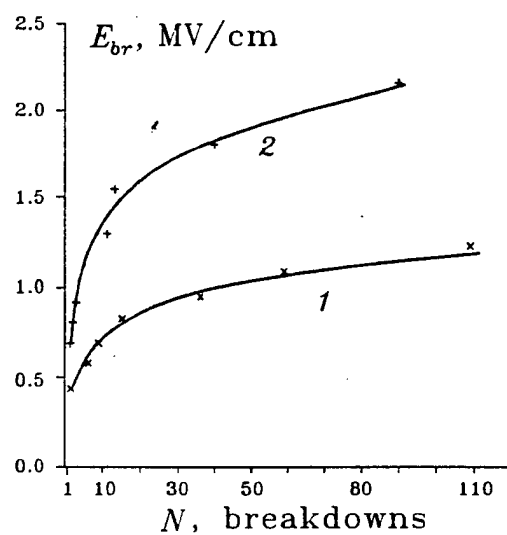
Figure 18: Conditioning curves for vacuum gaps with stainless-steel foil electrodes. (*1*) Preliminarily electrochemically polished electrodes; breakdown conditioning with high-voltage pulses of duration 40 ns. (*2*) Preliminarily LEHCEB-irradiated electrodes; breakdown conditioning with high-voltage pulses of duration 40 ns.

NUCLEAR PHYSICS INSTITUTE
ENGINEERING PHYSICAL CENTER
CHARGED PARTICLES ANALYTICAL LAB

The accelerated ion beams from Cyclotron U-120 and electrostatic generator EG-2.5 are used for:

- a certification of solid samples by destructive Charged Particle Activation Analysis (CPAA) trace determination of C, N and O in wide various of high-purity materials with the detection limits of 1, 3 and 10 ppb, respectively;

- a certification of solid samples by nondestructive Charged Particle Activation Analysis (CPAA) and Heavy Ion Activation Analysis (HIAA) trace determination of light elements and isotopes with the detection limits of 0.1 ppm for ^{2}H, Li, Be, B, F, Na, P, S, and 1 ppm for K and Ca, and 10 ppm for C, N, O;

- a nondestructive CPAA , HIAA / Heavy Ion Induced Gamma Emission (HIIGE) determination of stoichiometric ratio of the chemical compounds and of isotopic ratio of elements with the relative standard deviation of 0.001-0.005;

- a nondestructive concentration depth profiling of light elements by Proton Induced Gamma Emission (PIGE) and of other elements by Rutherford Backscattering Spectrometry (RBS) with the depth resolution about n(10-100)A and the detection limits 10^{16}-10^{18} at/cm^3;

- a certification of mineral raw materials by CPAA-technique for direct isotopic analysis of ^{187}Os in 0.5 gram-samples: the determination limit of ^{187}Os in MoS$_2$ is 0.1 ppm and relative standard deviation is 0,05-0,1 for n(1-0,1) ppm ^{187}Os contents;

- a study of mass transfer processes in solids by radio-labeling with radionuclides of ^{11}C, ^{15}O, ^{13}N, ^{18}F and ^{24}Na implanted in sample under investigation via recoil from the nuclear reactions following on heavy ions: the intensities of the radioactive ion beams are 10^7-10^8 s^{-1};

- the HIAA/HIIGE complemented by Elastic Recoil Determination Analysis (ERDA) are used for the determination of hydrogen isotopes H and D for study of hydrogen isotopic ratio in biological and environmental microprobes: the detection limits are about 1 at.ppm D and n100 at. ppm H relative standard deviation is less than 0.02.

Nucl.Phys.Institute, 634050, Tomsk, Russia
Tel: (3822) 440097, 440621
Fax: (3822) 440812
E-mail: remnev@ifc.tiasur.tomsk.su

Dr. **Remnev** G.E., EPC director
Dr. **Ryzhkov** V.A., head of CPA Lab

TECHNOLOGY AND EGUIPMENT FOR ELECTRO-SPARCLE ALLOYING

The new equipment was developed for hardening of wood-cutting tools. It has extended the technological abilities and consists of movement of an electrode and processed article.
Parameters of the eguipment are following:
- length 700 mm;
- width 500 mm;
- height 400 mm
- weight < 40 kg;
- power 1.5 kwtt;
- power supply one-phase, 220w 50 Hz.

Any standard sharpening equipment or usual metal treatment machines may be used as a unit for mechanical movement. The rate of the processing os about 600 sm2 a day (5 round flat saws of 560 mm in diameter).
It is necessary to remove the corrosion and fats to prepare the saws for hardening. The coating may be carried out on air or in flowing atmosphere of innert gas.

For more information please contact:

634048, Tomsk, pr.Akademicheskii, 2/1
Russian Materials Science Center
Mrs.L.Kornienko
tel: (3822) 258 561

NT Ltd. ofRMSC
Mr. O.Kashin
(3822) 908 536
□И□□~□OF WOOD-CUTTING TOOLS
BY ELECTRO-SPARCLE ALLOYING

The list of tools may be hardened:

- FRAME SAWS

HARDENING OF WOOD-CUTTING TOOLS
BY ELECTRO-SPARCLE ALLOYING

The list of tools may be hardened:

- FRAME SAWS
- DISK SAWS
- ROUND FLAT SAWS
- TIPS FOR SHAPER CUTTING
- SHAPER CUTTERS

Hardening of wood-cutting tools made of instrumental steel of any type is realised by hard alloy coating.
- thickness of the coating may be varied in the range of 10-200 mc and defined by the application purpose;
- technology of the coating allows multy-shrpening of the tools keeping the hardenning effect;
- stanard sharpenning eguipment may be used;
- to resharp the edge of the hardened tool you may sharp out 1.5-2.0 times less mterial;
- there is self-sharpennig effect during the work;
- both set and unset of saws may be hardened by the coating;
- the coated saws may be set and the coating remains actual;
- the working resource of hardened tools is 4-10 times higher as to non hardened ones.

The hardened saws are delivered to wood and furniture plants.
The proposed technology is patenting.

RUSSIAN MATERIALS SCIENCE CENTER NT, LTD

CIRCULAR SAWS
with hardened edge for wood processing machines of industrial and domestic use

- processing of logs, boards, pressed wooden, plates;
- the working resource is 3 times higher as compares with non - hardened saws;
- sharpening is by abrasive tools;
- multiple sharpening and setting the teeth of a saw do not influence the hardening effect;
- saw diameters are of 200, 250, 315, 360 and 400 mm.

Russian Materials Science Center offers hardening, sharpening and setting the teeth of the saws as well as deliver of the saws in industrial volumes.

Address: 634021, Tomsk-21, Russia
2/1 Academicheskii av,
R. 218, tel (3822) 906-821